COMPUTATIONAL FOOT MODELING FOR CLINICAL ASSESSMENT

Enrique Morales Orcajo

Doctoral Degree in Computational Mechanics

Doctoral Degree in Mechanical Engineering

FACULTY ADVISORS:

Javier Bayod López

Estevam Barbosa de Las Casas

Universidad Zaragoza

UNIVERSIDADE FEDERAL DE MINAS GERAIS

UFMG

Computational foot modeling for clinical assessment

Dissertation submitted in Partial Fulfillment of the Requirements
for the Doctoral Degree in

Computational Mechanics at the University of Zaragoza
&
Mechanical Engineering at the Federal University of Minas Gerais
by

Enrique Morales Orcajo

Faculty Advisors
Dr. Javier Bayod López
University of Zaragoza, Spain
&
Dr. Estevam Barbosa de Las Casas
Federal University of Minas Gerais, Brazil

Zaragoza, October 2015

A mis padres
y a mi hermano

AGRADECIMIENTOS

En primer lugar me gustaría agradecer a Javier por la oportunidad que me dio de realizar la Tesis en el departamento de Ingeniería Mecánica, confiando en mí desde el principio y dándome libertad para disfrutar y desarrollar el trabajo durante estos años. *Também quero destacar a oportunidade que me deu Estevam para fazer uma proveitosa estadia na UFMG para conhecer outro jeito de fazer as coisas. Muito obrigado aos dois pela sua orientação e disponibilidade sempre para me ajudar em tudo o que foi preciso.*

También quiero agradecer a todos los coautores de los artículos producidos durante el desarrollo de este trabajo por haber participado de forma directa en la Tesis, a los sábios consejos de Manolo, a las colaboraciones y al punto de vista clínico de Ricardo y Marta *e as frutuosas discussões na sala de fisioterapia do professor Thales.* Gracias a los técnicos de laboratorio y personal administrativo de ambas universidades, especialmente a Roxana *e Marina pela ajuda com toda a papelada.*

No quiero olvidarme de todos los compañeros de sala que han compartido día a día las aventuras de un doctorando, a los que ya terminaron y a los que aún les queda. Con especial cariño quiero agradecer a esas compañeras de viaje que han hecho más valiosa esta etapa de mi vida: Sara, Marina, Reich y Andrea porque cada una a vuestra manera formáis parte de esta Tesis.

Quero lembrar também de todos aqueles amigos que fiz no Brasil, companheiros de festas e viagens a Michelle, Agnes, Herbert, Eduardo, Poliana, Sabrina os

amigos de Cool Trip, de Minas e BH Roller por ter compartilhado experiências únicas com vocês e ter-me acolhido com os braços abertos. Especialmente a Diana pelas fantásticas aventuras que vivemos e nos restam para viver.

Por último, dar las gracias a todos mis amigos de siempre, a los expatriados, a los patinadores y a mi familia por recordarme que hay vida fuera del doctorado. En particular gracias a mis padres y a mi hermano por haberme enseñado a tomar las decisiones necesarias para cumplir mis sueños.

Un abrazo muy grande a todos.

17 de octubre de 2015

ABSTRACT

In this Thesis, a complete detailed three-dimensional finite element model of the human foot is described to advance towards a more refined computational simulation which provides realistic and meaningful information for clinical practice. From an engineering perspective, the human foot is a complex structure of small bones supported by strong ligaments and controlled by a network of tendons and muscles that achieves a superb mechanical responsiveness. The current barrier in foot computational simulation is the inclusion of these musculotendinous structures in the models.

To advance in this direction, a complete detailed three-dimensional foot finite element model with actual geometry of the inner structure is created differentiating cortical and trabecular bone, tendon, muscle, cartilage and fat tissues. Experimental tests of foot tendons and plantar soles are performed to determine their structural and material properties and to characterize computationally their non-linear mechanical behavior. Those advances are oriented to refine the geometry and the tissue characterization of the internal foot components. The model developed in this Thesis can be used in the field of biomechanics, in the areas of orthopedics, injury, treatment, surgery and sports biomechanics.

The research is structured by chapters where small steps towards the main objective are developed and the potential of these advances are applied to particular cases. These partial contributions in the area of the experimental testing are: the determination of a complete dataset of the mechanical properties of the

balance foot tendons, the definition of a criteria to quantify the regions of the tendon stress-strain curve and the analysis of the compressive response of plantar soft tissue as function of the location. And, in the area of clinical biomechanics the contributions are: the investigation of a skeletal parameter as etiology factor of the hallux valgus, the tendon force sensitivity study of the five major stabilizer tendons, the quasi-static analysis of the midstance phase of walking and the study of the impact absorption mechanism of the foot during barefoot running at different strike patterns.

Keywords: Foot biomechanics; Finite element method; Computational simulation; 3D foot modeling; Hyperelastic material models; Tissue testing; In-vitro test; Tendon characterization; Plantar sole characterization; Hallux valgus; Midstance phase analysis; Tendon force sensitivity analysis; Barefoot running; Running-related-injuries

RESUMEN

Esta Tesis desarrolla un modelo de elementos finitos del pie humano completo y detallado en tres dimensiones para avanzar hacia una simulación computacional más precisa que proporcione información realista y relevante para la práctica clínica. Desde el punto de vista ingenieril, el pie humano es una compleja estructura de pequeños huesos, soportados por fuertes ligamentos y controlada por una red de músculos y tendones con una capacidad de respuesta mecánica excepcional. La barrera actual en la simulación computacional del pie es la inclusión de estas estructuras musculotendinosas en los modelos.

Para avanzar en esta dirección, se crea un modelo de elementos finitos del pie completo y detallado con geometría real de la estructura interna diferenciando hueso cortical y esponjoso, tendón, músculo, cartílago y grasa. Se realizan ensayos experimentales de los tendones del pie y la suela plantar para determinar sus propiedades materiales y estructurales y caracterizar computacionalmente su comportamiento mecánico no lineal. Estos avances están orientados hacia la mejora de la representación geométrica y caracterización del tejido de los componentes internos del pie. El modelo desarrollado en esta Tesis puede usarse en el campo de la biomecánica en áreas de ortopedia, lesiones, tratamiento, cirugía y deporte.

La investigación está estructurada por capítulos en los cuales se desarrollan pequeños avances hacia el objetivo principal de la Tesis al mismo tiempo que se aplica el potencial de estos avances a casos particulares. Estas contribuciones parciales en el área de los ensayos experimentales son: la determinación de un

completo conjunto de datos de las propiedades mecánicas de los tendones del pie, la definición de un criterio para cuantificar las regiones de la curva de tensión-deformación del tendón y el análisis de la respuesta a compresión de la suela plantar en función de la posición. Y, en el área de la biomecánica clínica las contribuciones son: la investigación de un parámetro del esqueleto como factor etiológico del hallux valgus, el estudio de sensibilidad de la fuerza de los cinco mayores tendones estabilizadores, el análisis cuasi-estático de la fase de apoyo de la marcha y el estudio del mecanismo de absorción de la fuerza de impacto del pie durante la carrera descalzo a diferentes ángulos de impacto.

Palabras clave: Biomecánica del pie; Método de los elementos finitos; Simulación computacional, Modelado 3D del pie; Modelos de materiales hyperelásticos; Ensayo de tejidos; Ensayo in-vitro; Caracterización del tendón; Caracterización de la suela plantar; Hallux Valgus; Análisis de la fase de apoyo de la marcha; Análisis de sensibilidad de la fuerza de los tendones; Carrera descalzo; Lesión por correr

RESUMO

Esta Tese desenvolve um modelo de elementos finitos do pé humano completo e detalhado em três dimensões para avançar na direção de uma simulação computacional mais precisa que proporcione informação realista e relevante para a prática clínica. Desde o ponto de vista da engenharia, o pé humano é uma estrutura complexa de pequenos ossos, suportados por fortes ligamentos e controlada por uma rede de músculos e tendões. A barreira atual na simulação computacional do pé é a inclusão destas estruturas musculotendinosas nos modelos.

Para avançar nesta direção, se cria um modelo de elementos finitos do pé completo e detalhado com geometria real da estrutura interna diferençando osso cortical e esponjoso, tendão, músculo, cartilagem e gordura. Se realizam ensaios experimentais dos tendões do pé e o solado plantar para determinar suas propriedades materiais e estruturais e caracterizar computacionalmente seu comportamento mecânico não lineal. Estes avanços estão orientados para a melhora da representação geométrica e caracterização do tecido dos componentes internos do pé. O modelo desenvolvido nesta Tese pode ser usado no campo da biomecânica, em áreas da ortopedia, lesões, tratamento, cirurgia e esporte.

A pesquisa está estruturada por capítulos nos quais se desenvolvem pequenos avanços em direção ao objetivo principal da Tese enquanto se aplica o potencial destes avanços a casos particulares. Estas contribuições parciais na área dos ensaios experimentais são: a determinação de um conjunto completo de dados das propriedades mecânicas dos tendões do pé, a definição de um critério para quan-

tificar as regiões da curva tensão-deformação do tendão e a análise da resposta à compressão do solado plantar em função da posição. E, na área da biomecânica clinica, as contribuições são: a investigação de um parâmetro do esqueleto como fator etiológico do hallux valgus, o estudo da sensibilidade da força dos cinco maiores tendões estabilizadores, o analise quase-estático da fase de apoio da marcha e o estudo do mecanismo de absorção da força de impacto do pé durante a corrida descalço a diferentes ângulos de impacto.

Palavras chave: Biomecânica do pé; Método dos elementos finitos; Simulação computacional; Modelagem 3D do pé; Modelos de materiais hiperelásticos; Ensaio de tecidos; Ensaio in-vitro; Caracterização do tendão; Caracterização do solado plantar; Hallux Valgus; Anàlise da fase de apoio da marcha; Anàlise de sensibilidade da força dos tendões; Corrida descalço; Lesão por correr

CONTENTS

LIST OF FIGURES

LIST OF TABLES

NOMENCLATURE

2D	Two Dimensional
3D	Three Dimensional
CoP	Center of Pressure
CT	Computer Tomography
DCA	Depth of the Concave Area at the base of the proximal phalanx of the hallux
EDB	Extensor Digitorum Brevis
EDL	Extensor Digitorum Longus
EHL	Extensor Hallucis Longus
FDB	Flexor Digitorum Brevis
FDL	Flexor Digitorum Longus
FE	Finite Element
FFS	Forefoot Strike
FHL	Flexor Hallucis Longus
H	Height of the base of the proximal phalanx of the hallux

LDC	Longitudinal Distance of the Central aspect
LDL	Longitudinal Distance of the Lateral aspect
LDM	Longitudinal Distance of the Medial aspect
MFS	Midfoot Strike
MRI	Magnetic Resonance Images
PB	Peroneus Brevis
PL	Peroneus Longus
PPH	Proximal Phalanx of the Hallux
RFS	Rearfoot Strike
TA	Tibialis Anterior
TP	Tibialis Postior
W	Width of the base of the proximal phalanx of the hallux

MODELADO COMPUTACIONAL DEL PIE PARA EVALUACIÓN CLÍNICA

RESUMEN EXTENDIDO EN ESPAÑOL

En este capítulo se incluye un resumen extendido en castellano del contenido de la Tesis en cumplimiento de la normativa relativa a la obtención del grado de Doctorado Europeo (art.15 RD 99/2011) y del convenio de cotutela internacional de Tesis entre la Universidad de Zaragoza y la Universidade Federal de Minas Gerais. El resumen incluye la motivación del trabajo, los objetivos propuestos, la estructural de la tesis y el contenido de cada uno de los capítulos. También se incluyen las conclusiones obtenidas en los ámbitos de la simulación computacional, los ensayos experimentales y en el ámbito clínico. Finalmente, se listan las contribuciones a revistas científicas y presentaciones en congresos realizadas durante la tesis así como las líneas futuras de investigación.

I Motivación

La principal motivación de esta Tesis es avanzar hacia una simulación computacional más precisa que proporcione información realista y relevante para la práctica clínica. La ciencia de la medicina ha evolucionado a lo largo de la historia por un proceso de prueba y error normalmente empujada por la necesidad de una solución en vez de evidencias en la mejora del tratamiento. En este sentido, la ingeniería mecánica puede ayudar en el proceso de perfeccionamiento de la técnica médica adaptando herramientas de la ingeniería a problemas clínicos.

Dentro de todas las ramas de la medicina, esta Tesis se centra en la biomecánica;

ortopedia, tratamiento y cirugía. Específicamente, se desarrolla un modelo computacional del pie para un mejor entendimiento de la biomecánica del pie, que ayude a predecir el comportamiento de nuevas terapias y estimar el valor de ciertos parámetros que no es posible medir con métodos experimentales. Los avances en el modelado del pie proporcionarán herramientas útiles para la evaluación clínica reduciendo los costes y los riesgos para la salud.

La medicina y la ingeniería son dos campos que están colaborando cada vez más para analizar sistemas biológicos. Esta nueva área interdisciplinaria es un campo prometedor para enfrentarse a futuros retos y resolver complejos problemas que están por venir. Uno de estos retos es la llamada medicina personalizada. Con avances en la capacidad computacional y mejoras en la creación de modelos específicos de pacientes, será posible crear modelos computacionales para cada paciente con la suficiente precisión y en un tiempo razonable para ayudar en el proceso de toma de decisión del tratamiento.

Aunque alcanzar este nivel de modelado parece lejano, el ritmo al que avanza la simulación computacional del pie desde que aparecieron los primeros modelos anima a creer que llegue a ser posible, como se muestra en el Capítulo 1. Por lo tanto, esta Tesis busca avanzar en la simulación computacional del pie humano, analizando los límites actuales y proporcionando mejoras a aplicar en problemas reales de la medicina.

II Objetivos

Basado en los argumentos anteriormente expuestos, el objetivo de esta Tesis es adaptar las herramientas de la ingeniería a la práctica clínica, siendo capaces de analizar la respuesta mecánica del pie y del tobillo y enfocando los resultados a casos prácticos. En particular, los pasos a seguir son los siguientes. Primero, identificar los límites actuales de la simulación computacional del pie para marcar una hoja de ruta de los próximos hitos para mejorar el modelado por elementos finitos del pie. Segundo, realizar una serie de experimentos para caracterizar los tejidos blandos del pie, tales como los tendones y la suela plantar. Tercero, reconstruir la geometría de la estructura interna del pie y generar una malla de

elementos finitos detallada. Y, por último, aplicar estas mejoras a problemas clínicos reales. Con este propósito, el trabajo principal y sus objetivos parciales presentados en esta Tesis son listados a continuación:

- Identificar los factores clave de la simulación biomecánica del pie. Basándose en una profunda revisión de la literatura de modelos computacionales de pie y analizando las limitaciones de un modelo previamente desarrollado, se van a definir las líneas de la próxima generación de modelos de elementos finitos.
- Determinar las propiedades materiales y estructurales de los tendones de los pies. Los tendones serán diseccionados y ensayados en una máquina de ensayos realizando ensayos de tracción uniaxial para obtener las curvas de fuerza-desplazamiento y las de tensión-deformación de todos los tendones de los pies excepto el tendón de Aquiles.
- Caracterización mecánica del tejido tendinoso del pie. Diferentes modelos constitutivos serán ajustados para elegir la simulación más adecuada de la respuesta a tracción de los tendones del pie.
- Diferenciación de la respuesta a compresión de la suela plantar en función de su posición. Varias suelas plantares serán indentadas en diferentes lugares para obtener su respuesta mecánica.
- Caracterización mecánica de la suela plantar bajo el calcáneo y bajo la cabeza de los metatarsos. Los parámetros de diferentes modelos de materiales serán ajustados para simular el comportamiento del tejido blando del antepié y del retropié.
- Desarrollo de un modelo de elementos finitos del pie con geometría detallada de los componentes internos. Tomografías computacionales y resonancias magnéticas serán usadas para reconstruir la estructura interna y externa del pie. A continuación, una refinada malla será creada para incluir todas las singularidades de los componentes internos.
- Inclusión de propiedades no lineales a todos los tejidos blandos del pie. Propiedades no lineales serán aplicadas a tendones, músculos y grasa, basán-

dose en los parámetros previamente ajustados y parámetros optimizados de la literatura.

- Aplicación de todas las mejoras a problemas clínicos prácticos. Al mismo tiempo que el modelo se va mejorado, los avances se van a aplicar a casos particulares en diferentes campos. Las aplicaciones cubren áreas como patologías clínicas, tratamientos fisioterapéuticos y lesiones deportivas como ejemplo de las posibilidades del modelo.

III Estructura de la Tesis

La tesis está organizada en siete capítulos. En la Figura 1.18 se esquematiza un resumen gráfico del contenido de la Tesis. Cada capítulo individual tiene una meta que persigue el objetivo principal de la Tesis y se enfoca a una aplicación clínica-práctica incorporando los avances descritos en dicho capítulo. Más específicamente el trabajo se estructura como sigue:

- En el Capítulo 1 se presenta una revisión exhaustiva del uso actual de los modelos de elementos finitos para el estudio de la biomecánica del pie. La revisión incluye modelos en dos y tres dimensiones con geometrías detalladas y simplificadas, del total o de una parte de la extremidad inferior, el tobillo o el pie. Son extensamente debatidos temas prácticos del modelado computacional, diferentes modelos constitutivos de tejidos y aplicaciones pioneras. Por último se perfilan los retos más recientes en el campo de la simulación computacional del pie.

- En el Capítulo 2 un modelo esquelético del pie es explotado para explorar sus límites. El modelo se usa para analizar la influencia de la falange proximal del primer dedo como un potencial parámetro esquelético de la etiología del Hallux Valgus. Se configuran diez modelos diferentes correspondientes a cinco percentiles de hombre (0, 25, 50, 75, 100%) y cinco de mujer. Después de la discusión clínica se explican las características del modelo. Este trabajo se usa para destacar las líneas a seguir en el futuro modelo mejorado.

- En el Capítulo 3 se realizan ensayos de tracción uniaxial para obtener la curva de tensión-deformación de los principales tendones intrínsecos y extrínsecos del pie humano. Se informa de la sección, la carga y deformación de rotura, el módulo de elasticidad y la tensión ultima para diferentes aplicaciones clínicas e ingenieriles.

- En el Capítulo 4 se desarrolla un modelo de elementos finitos completo y detallado en tres dimensiones con geometría real y comportamiento no lineal de los tendones diferenciando hueso cortical, esponjoso, tendones, músculos, cartílagos y grasa. La respuesta del modelo es evaluada con medidas *in-vivo* e *in-vitro*. Dos aplicaciones son desarrolladas; un análisis de sensibilidad de la fuerza de los cinco principales tendones estabilizadores y una análisis cuasi-estático de la fase de apoyo de la marcha.

- En el Capítulo 5 se caracteriza por regiones la suela plantar (tejido adiposo y piel). Se realizan quince indentaciones a lo largo de la suela plantar para comparar la curva de tensión-deformación, de las cuatro regiones de la suela plantar: retropié, mediopié, antepié y dedos. Las respuestas mecánicas medias del tejido bajo el talón y la cabeza de los metatarsos son caracterizadas mediante un modelo de material no lineal.

- En el Capítulo 6 el modelo del pie con geometría detallada de los tejidos blandos desarrollado en el Capítulo 4 es actualizado con los modelos de materiales no lineales de la suela plantar ajustados en el Capítulo 5 y con parámetros optimizados encontrados en la literatura. El modelo es configurado para estudiar el mecanismo de absorción de la fuerza de impacto del pie a diferentes ángulos de impacto.

- En el Capítulo 7 se presentan las principales conclusiones de la Tesis divididas por áreas de conocimiento, junto con un pequeño resumen de las contribuciones originales y las futuras líneas de investigación.

IV Conclusiones

Las conclusiones más importantes del trabajo recogido en esta Tesis, se clasifican en tres secciones. La primera sección incluye los aspectos de la simulación computacional de la biomecánica del pie. La segunda sección cubre los aspectos experimentales de los ensayos de tendones y suela plantar. Por último, en la tercera sección se detallan las principales conclusiones en el ámbito clínico extraídos de las aplicaciones de cada uno de los modelos de pie.

IV.i Aspectos computacionales

- La sofisticada estructura ósea del pie en forma de arco hace que el modelado de su respuesta mecánica sea extremadamente desafiante. Esta simulación es más compleja cuando se considera la función de los músculos.

- El análisis por elementos finitos es una tarea compleja con posibilidad de que se produzcan errores. Por lo tanto, debe hacerse todo el esfuerzo posible por crear modelos que simulen el tema a un nivel lo suficientemente preciso, especialmente en aplicaciones médicas. Las suposiciones y simplificaciones son necesarias a algún nivel y dependen del objetivo del estudio. Las razones para el uso de estas y su impacto en los resultados tienen que ser explicadas claramente.

- Los modelos del esqueleto del pie son aproximaciones prácticas para el estudio de temas relacionados con los huesos a un coste computacional bajo y con un nivel de precisión suficiente. Debido a la mayor rigidez de los huesos comparado con el tejido blando, no incluir los tejidos blandos en el modelo del pie puede ser una forma práctica de producir buenas soluciones en tiempos mucho menores.

- El modelo de Ogden de primer orden empleado para ajustar el tejido tendinoso recoge un comportamiento más preciso de la respuesta de los tendones sometidos a cargas de tracción que los modelos lineales y el modelo de Mooney-Rivlin usados en la literatura.

- La caracterización independiente de la parte anterior y posterior de la suela plantar permite analizar de forma precisa la presión plantar y la deformación de la suela plantar a diferentes ángulos de contacto inicial con el suelo.

- El modelo de elementos finitos completo del pie desarrollado en esta Tesis puede ser usado en un amplio rango de aplicaciones en el campo de la biomecánica y bajo todos los ratios de carga: en pie, andando y corriendo.

- La simulación computacional del pie expande el conocimiento de la biomecánica del pie, proporcionando información significativa para la práctica clínica. Especialmente, el modelo desarrollado en esta Tesis puede ser usado en el campo de la biomecánica en áreas de ortopedia, lesiones, tratamientos, cirugía y deporte.

IV.ii Aspectos experimentales

- Se ha encontrado que los tendones de los pies que trabajan en distintos planos tienen respuestas mecánicas diferentes. Los tendones flexores y extensores de los dedos tienen mayor módulo de elasticidad y tensión última mientras que los tendones inversores y eversores tienen una deformación de rotura mayor.

- El criterio propuesto para cuantificar las regiones de la curva de tensión-deformación de los tendones basado en el módulo de Young permite una definición precisa de la deformación inicial, del inicio de la región lineal y del punto de fluencia.

- Las curvas de tensión-deformación de los tendones muestran proporcionalidad entre regiones, siendo la deformación inicial el 15%, el comienzo de la región lineal el 30% y el punto de fluencia el 70% de la deformación de rotura.

- Las propiedades estructurales son relevantes en cirugías de reconstrucción ortopédica y estimación de lesiones en tendones. Las propiedades materiales junto con la descripción cuantitativa de la curva de tensión-deformación

ayudan en el diseño de materiales sintéticos y en el desarrollo de modelos constitutivos más depurados.

- La medición de la sección y el método de anclaje de las muestras a la máquina de ensayos se han identificado como factores claves para calcular las propiedades de los tejidos en ensayos de tracción.

- El tejido bajo el calcáneo muestra una respuesta más rígida que el tejido bajo la cabeza de los metatarsos, mientras que la suela plantar del antepié es más rígida que la del medio pie. Esta diferenciación de la respuesta mecánica a compresión es particularmente relevante cuando se estudia la distribución de presiones en el pie durante la carrera descalzo a diferentes ángulos de impacto.

IV.iii Aspectos clínicos

- La geometría de la falange proximal del primer dedo tiene la característica de un lado medial mayor que el lado lateral sometiéndola a una tensión que puede provocar la rotación de la falange proximal del primer dedo hacia una posición más relajada. Esta potencial posición de equilibrio produce una tendencia hacia la separación del primer metatarso relativa a su posición anatómica original que constituye el inicio de la deformidad del hallux valgos.

- La geometría de la falange proximal del primer dedo es un factor significativo en el desarrollo del hallux valgus, siendo igual de influyente que resto de parámetros del esqueleto reportados en la literatura y debe considerarse durante la evaluación preoperatoria. La evaluación clínica del hallux valgus debe tener en cuenta el primer radio completo y no cada factor por separado.

- Se predice un trabajo sinérgico entre los tendones de inversión y eversión. Tirando de un tibial o de un peroneo se tensa el antagonista mientras que se destensa el agonista. Esta acción conjunta se predice también para el tendón de Aquiles con el tibial posterior. Este comportamiento explica el complejo control de movimiento que realiza el pie.

- Al final de la posición de apoyo de la marcha, el pie esta solicitado a mayores esfuerzos. La suela plantar, la fascia, el cartílago de la articulación del tobillo y los tendones están más tensionados en esta posición que al inicio de la fase de apoyo.
- Basándose en el nivel de tensión de los componentes internos del pie durante la carrera descalzo con el patrón talón-antepie es más probable que se produzca una fractura del calcáneo por estrés, daño en los cartílagos, tendinitis en el tibial y ulceraciones en el talón.
- Fractura de los metatarsos por estrés, plantar fascitis, tendinitis del tendón de Aquilles y ulceraciones en el antepie son lesiones relacionadas con el impacto que son más probables de ocurrir en corredores descalzos que impactan inicialmente con toda la planta o con el antepie. Los resultados muestran niveles de tensión más altos en estos componentes cuando se aterriza con la parte delantera del pie.

V Contribuciones originales

La principal contribución de esta Tesis es la creación de un detallado modelo de elementos finitos del pie que supone un paso adelante en la simulación de la biomecánica del pie desde la mecánica de medios continuos. A continuación se expone una lista con todas las contribuciones originales llevadas a cabo durante el desarrollo de esta Tesis.

- Un modelo de elementos finitos en tres dimensiones completo del pie humano con una detallada representación de los componentes internos y propiedades no lineales de todos los tejidos blandos. El modelo se ha creado de la segmentación independiente de cada componente interno con un tamaño de malla optimizado incluyendo la geometría detallada de cada tendón, musculo, cartílago y hueso del pie distinguiendo entre las propiedades de hueso cortical y esponjoso. Toda la estructura está rodeada del tejido conectivo (grasa). Este detallado modelo permite el estudio de la biomecánica de los tejidos blandos y duros.

- La caracterización del tejido tendinoso del pie con un modelo hiperelástico. El modelo de material de Ogden de primer orden se ha ajustado para simular el comportamiento a tracción de los tendones. Esta caracterización proporciona una respuesta más precisa que las propuestas anteriormente.

- La caracterización mecánica de la suela plantar por regiones. Se han ajustado los coeficientes del modelo de Ogden con las curvas de tensión-deformación de la suela plantar del retropié y el antepie.

- Un completo conjunto de datos de las propiedades mecánicas de los tendones del pie. Se han determinado las propiedades estructurales y materiales de los tendones de los pies bajo la misma metodología. Se han diferenciado las respuestas mecánicas de los tendones inversores/eversores y flexores/extensores de los dedos.

- Un criterio para cuantificar las regiones de la curva de tensión-deformación de los tendones. El criterio toma como referencia el módulo de Young, habiendo definido la deformación inicial como la parte de la curva desde el comienzo hasta una desviación mayor del 20% del módulo de Young y la región lineal se ha definido como la parte de la curva con una curvatura menor del 20% del módulo de Young.

- El análisis de la respuesta a compresión de la suela plantar en función de su localización. Se han comparado las curvas de tensión-deformación del tejido blando bajo el calcáneo, el puente, la cabeza de los metatarsos y los dedos.

- La investigación de un parámetro del esqueleto como factor etiológico del hallux valgus. El tamaño y la forma de la falange proximal del primer dedo se ha identificado como un factor etiológico del hallux valgus y debe ser tenido en cuenta durante la evaluación clínica.

- Un análisis de sensibilidad de la fuerza de los cinco mayores tendones de estabilización. Se ha predicho un trabajo conjunto entre los tendones peroneos y los tibiales y entre el tibial anterior y el tendón de Aquiles lo que explica la compleja respuesta del control de movimiento del pie.

- Un análisis cuasi-estático de la fase de apoyo de la marcha. Se han estimado una mayor solicitación mecánica al final de la fase de apoyo que al inicio de la misma.

- Un estudio del mecanismo de absorción de la fuerza de impacto durante la carrera descalzo a diferentes ángulos de aterrizaje. Se han identificado las lesiones de impacto más propensas a sufrir por los corredores descalzos o con calzado minimalista en función del patrón de impacto.

V.i Publicaciones

Los siguientes artículos escritos durante el desarrollo de esta Tesis han sido ya publicados o serán publicados en revistas científicas revisadas por pares:

1. **Morales-Orcajo, E.**, Bayod, J., and Las Casas, E.B. (2015). Computational Foot Modeling: Scope and Applications. *Archives of Computational Methods in Engineering*, Publicado online.

2. **Morales-Orcajo, E.**, Bayod, J., Becerro-de Bengoa-Vallejo, R., Losa-Iglesias, M., and Doblare, M. (2015). Influence of first proximal phalanx geometry on hallux valgus deformity: a finite element analysis. *Medical & Biological Engineering & Computing*, 53(7):645-653.

3. **Morales-Orcajo, E.**, Becerro de Bengoa Vallejo, R., Losa Iglesias, M., and Bayod, J. Structural and material properties of human foot tendons. *Clinical Biomechanics*, En revisión.

4. **Morales-Orcajo, E.**, Souza, T.R., Bayod, J., and Las Casas, E.B. Non-Linear finite element model to assess the effect of tendon forces on the foot-ankle complex. *Journal of Biomechanics*, En revisión.

5. **Morales-Orcajo, E.**, Becerro de Bengoa Vallejo, R., Losa Iglesias, M., Bayod, J., and Las Casas, E.B. Foot injuries in barefoot running as function of strike pattern - A finite element study. *Journal of Sport Science*, En revisión.

V.ii Conferencias

Las siguientes ponencias han sido presentadas durante el desarrollo de esta Tesis:

1. **Morales-Orcajo, E.**, 3D Muscle detailed ankle-foot model for finite element analysis. *II Reunión Jóvenes Investiagadores del Instituto de Investigación en Ingeniería de Aragón*, Zaragoza, (España), 2013.

2. **Morales-Orcajo, E.**, Bayod, J., Becerro-de Bengoa-Vallejo, R., Losa-Iglesias, M., and Doblare, M., Influencia de la geometría de la falange proximal del primer dedo del pie en la formación de juanetes. *Congress on Numerical Methods in Engineering (CMN 2013)*, Bilbao, (España), 2013.

3. **Morales-Orcajo, E.**, Becerro de Bengoa Vallejo, R., Losa Iglesias, M., and Bayod, J., Mechanical properties of foot tendons - In vitro study. 1^st *Pan American Congress on Computational Mechanics (PANACM 2015)*, Buenos Aires, (Argentina), 2015.

4. **Morales-Orcajo, E.**, Bayod, J., and Las Casas, E.B., Developing a proper biomechanical computational model. *VI International Conference on Computational Bioengineering (ICCB 2015)*, Barcelona, (España), 2015.

VI Trabajo futuro

Las aplicaciones de los modelos de elementos finitos continuarán aumentando con el aumento de la potencia informática, que dobla su capacidad computacional cada 18 meses desde que se inventaron los microprocesadores, reduciendo los costes a la mitad (ley de Moore). Sin embargo, la potencia informática nunca será suficiente considerando que el número de geometrías detalladas, de formulaciones complejas y de exigentes condiciones de contorno también aumentará. La búsqueda de mejores soluciones y más rápidas es un campo prometedor con un amplio potencial de mejora.

Teniendo en mente que el principal objetivo de la Tesis es el avance hacia una simulación computacional del pie más precisa para evaluación clínica, los progresos

conseguidos durante esta Tesis han sido orientados a refinar la representación geométrica y la caracterización tisular de los componentes internos del pie. Por lo tanto, los futuros avances deben orientarse hacia la mejor determinación de cargas y condiciones de contorno. Los trabajos futuros en esta dirección son listados aquí:

- Incluir contacto entre los componentes internos del pie. Dentro del pie hay muchos componentes solapados, limitando el desplazamiento de un componente respecto a su alrededor. Una interacción deslizante entre estos componentes cuando una fuerza es aplicada a un tendón proporcionará una transmisión de fuerzas más realista dentro del pie. También se debería definir contacto entre las articulaciones.

- Simular el comportamiento activo de los músculos. El modelo creado en esta Tesis se alimenta de datos cinéticos, los cuales son difíciles de medir experimentalmente y suelen ser estimados a partir de modelos matemáticos o cinemáticos. Por lo tanto, introducir cargas en el modelo por medio del comportamiento activo de los músculos aumentará las posibilidades del modelo.

- Realizar simulaciones dinámicas. Médicos y fisioterapeutas están mostrando interés en explorar la simulación dinámica del ciclo de la marcha completo en vez de posiciones discretas. Las simulaciones dinámicas incluyen la variable del tiempo y los efectos dinámicos, lo que permite el estudio del movimiento completo.

- Combinar modelos de elementos finitos con modelos multicuerpo. La integración de los dos tipos de modelos puede ser una buena aproximación de cara a enfrentarse a las simulaciones dinámicas movidas a partir de la activación de los músculos.

- Simulación de procesos mecano-químicos. La detallada geometría del modelo puede ser explotada con la formulación de procesos químicos gobernados por estímulos mecánicos como en el caso de las ulceraciones o la regeneración ósea.

- Reducir el tiempo de generación del modelo. Crear modelos de elementos finitos del pie específicos de un sujeto es una tarea que requiere mucho tiempo. Investigaciones en la automatización de este proceso serán decisivas en la implementación de estudios específicos de pacientes.
- Reducir el tiempo de cálculo. Para orientar las predicciones del modelo a la ayuda en el proceso de toma de decisión de un tratamiento clínico para un paciente específico el tiempo de computación deberá ser mucho más rápido.

MODELAGEM COMPUTACIONAL DO PÉ PARA AVALIAÇÃO CLÍNICA

RESUMO ESTENDIDO EM PORTUGUÊS

Neste capítulo inclui-se um resumo em português do conteúdo da Tese em cumprimento do convênio de co-tutela internacional de Tese entre a Universidad de Zaragoza e a Universidade Federal de Minas Gerais. O resumo inclui a motivação do trabalho, os objetivos propostos, a estrutura de tese e o conteúdo de cada um dos capítulos. Também se incluem as conclusões obtidas nos âmbitos da simulação computacional, dos ensaios experimentais e no âmbito clínico. Finalmente, listam-se as contribuições em revistas científicas e apresentações em congressos realizadas durante a Tese assim como as línhas futuras de pesquisa.

I Motivação

A principal motivação desta Tese é avançar em direção de uma simulação computacional mais precisa que proporcione informação realista e relevante para a prática clínica. A ciência da medicina tem evoluído ao longo da história num processo de tentativa e erro normalmente empurrada pela necessidade de uma solução em vez de evidência na melhora do tratamento. Neste sentido, a engenharia mecânica pode ajudar no processo de aperfeiçoamento da técnica medica adaptando ferramentas de engenharia a problemas clínicos.

Dentro de todas os ramos da medicina, esta Tese se centra na biomecânica, ortopedia, tratamento e cirurgia. Especificamente, se desenvolve um modelo computacional do pé para um melhor entendimento da biomecânica do pé, para predi-

zer o comportamento de novas terapias e para estimar o valor de certos parâmetros que não é possível medir com métodos experimentais. Os avanços na modelagem do pé proporcionarão ferramentas úteis para a avaliação clínica reduzindo os custos e os riscos para a saúde.

A medicina e a engenharia são dois campos que estão colaborando cada vez mais para analisar sistemas biológicos. Esta nova área interdisciplinar é um campo promissor para enfrentar-se futuros desafios e resolver complexos problemas que estão por vir. Um destes desafios é a chamada Medicina Personalizada. Com avances na capacidade computacional e melhoras na criação de modelos específicos de pacientes, será possível de criar modelos computacionais para cada paciente com a suficiente precisão e em um tempo razoável para ajudar no processo de toma de decisão do tratamento.

Ainda que alcançar este nível de modelagem pareça distante, o ritmo ao que avança a simulação computacional do pé desde que apareceram os primeiros modelos anima a acreditar que chegue a ser possível, como se mostra no Capítulo 1. Portanto, esta Tese procura avançar na simulação computacional do pé humano, analisando os limites atuais e proporcionando melhoras a aplicar em problemas reais da medicina.

II Objetivos

Baseado nos argumentos anteriormente expostos, o objetivo da tese é adaptar as ferramentas da engenharia aplicadas à prática clínica, sendo capazes de analisar a resposta mecânica do pé e do tornozelo e enfocar os resultados a casos práticos. Os passos a seguir são: (a) identificar os limites atuais da simulação computacional do pé para marcar um roteiro dos próximos marcos para melhorar a modelagem por elementos finitos do pé; (b) realizar uma serie de experimentos para caracterizar os tecidos moles do pé, tais como os tendões e o solado plantar (c) reconstruir a geometria da estrutura interna do pé e gerar uma malha de elementos finitos detalhada, (d) por último, aplicar estas melhoras a problemas clínicos reais. Com este propósito, o trabalho principal e seus objetivos específicos apresentados nesta Tese são listados a seguir:

- Identificação dos fatores chave da simulação biomecânica do pé. Baseando-se em uma revisão aprofundada da literatura de modelos computacionais de pé e analisando as limitações de um modelo previamente definido, vão-se definir as línhas da próxima geração de modelos de elementos finitos de pé.
- Determinar as propriedades materiais e estruturais dos tendões dos pés. Os tendões serão dissecados e ensaiados numa maquina de ensaios realizando ensaios tração uniaxial para obter as curvas de força-deslocamento e tensão-deformação de todos os tendões dos pés exceto o tendão de Aquiles.
- Caracterização mecânica do tecido tendinoso do pé. Diferentes modelos constitutivos serão ajustados para escolher a simulação mais adequada da resposta à tração dos tendões do pé.
- Diferenciação da resposta à compressão do solado plantar em função da posição. Vários solados plantares serão endentados em diferentes lugares para obter sua resposta mecânica.
- Caracterização mecânica do solado plantar abaixo do calcâneo e abaixo da cabeça dos metatarsos. Os parâmetros de diferentes modelos materiais serão ajustados para simular o comportamento do tecido mole do antepé e do retropé.
- Desenvolvimento de um modelo de elementos finitos do pé com geometria detalhada dos componentes internos. Tomografias computacionais e ressonâncias magnéticas serão utilizadas para reconstruir a estrutura interna e externa do pé. Em seguida, uma malha refinada será criada para incluir todas as singularidades dos componentes internos.
- Inclusão de propriedades não lineares em todos os tecidos mole do pé. Propriedades não lineares serão aplicadas a tendões, músculos e gordura baseando-se em os parâmetros previamente ajustados e em parâmetros otimizados da literatura.
- Aplicação de todas as melhoras a problemas práticos clínicos. Ao mesmo tempo que modelo vai melhorando, os avanços vão se aplicar a casos partic-

ulares em diferentes campos. As aplicações cobrem áreas como patologias clinicas, tratamentos fisioterapêuticos e lesões esportivas como exemplo das possibilidades do modelo.

III Estrutura da Tese

A Tese está organizada em sete capítulos. Em a Figura 1.18 se esquematiza um resumo gráfico do conteúdo da Tese. Cada capítulo individual tem-se uma meta que persegue o objetivo principal da Tese e enfoca-se em uma aplicação clínica prática incorporando os avanços desse capítulo. Mais especificamente o trabalho estrutura-se como se segue:

- No Capítulo 1, apresenta-se uma revisão exaustiva do uso atual dos modelos de elementos finitos para o estudo da biomecânica do pé. A revisão inclui modelos em duas e três dimensões com geometrias detalhadas e simplificadas, do total ou duma parte da extremidade inferior, o tornozelo e o pé. São extensamente debatidos temas práticos da modelagem computacional, diferentes modelos constitutivos de tecidos e aplicações pioneiras. Recentes desafios no campo da simulação computacional do pé são elencados.

- No Capítulo 2, um modelo esquelético do pé é edesenvolvido para explorar seus limites. Se usa o modelo para analisar a influência da falange proximal do primeiro dedo como um potencial parâmetro esquelético da etiologia do hallux valgus. Configuram-se dez modelos diferentes correspondentes a cinco percentis de homem (0, 25, 50, 75, 100%) e cinco de mulher. Depois da discussão clínica explicam-se as características do modelo. Este trabalho se usa para destacar as línhas a seguir nos passos seguintes.

- No Capítulo 3, descreve-se ensaios de tração uniaxial para obter a curva de tensão-deformação dos principais tendões intrínsecos e extrínsecos do pé humano. Reportam-se a seção, a carga e deformação de rotura, o módulo de elasticidade e a tensão ultima para diferentes aplicações da clínica e da engenharia.

- No Capítulo 4, desenvolve-se um modelo de elementos finitos completo e detalhado em três dimensões com geometria real e comportamento não lineal dos tendões diferenciando osso cortical, esponjoso, tendões, músculos, cartilagens e gordura. A resposta do modelo é avaliada com medidas *in-vivo* e *in-vitro*. Duas aplicações são desenvolvidas: um análise de sensibilidade da força dos cinco principais tendões estabilizadores e um análise quase-estático da fase de apoio da marcha.

- No Capítulo 5, caracteriza-se por regiões o solado plantar (tecido adiposo e pele). Realizam-se quinze endentações ao longo do solado plantar para comparar a curva de tensão-deformação, de las quatro regiões do solado plantar: retropé, meiopé, antepé, e dedos. As respostas mecânicas meias do tecido baixo o calcanhar e a cabeça dos metatarsos são caracterizadas com um modelo de material não lineal.

- No Capítulo 6, o modelo de pé com geometria detalhada dos tecidos moles do desenvolvida no Capítulo 4 é actualizado como os modelos de materiais não lineais do solado plantar ajustados no Capítulo 5 e com parâmetros optimizados encontrados na literatura. O modelo é configurado para estudar o mecanismo de absorção da força de impacto do pé a diferentes ângulos de impacto.

- No Capítulo 7, apresentam-se as principais conclusões da Tese divididas por áreas de conhecimento, junto com um pequeno resumo das contribuições originais e as futura líneas de pesquisa.

IV Conclusões

As conclusões mais importantes do trabalho recolhido nesta Tese, classifica-se em três secções. A primeira secção inclui os aspectos da simulação computacional da biomecânica do pé. A segunda secção cobre os aspectos experimentais dos ensaios de tendões e solado plantar. Por último, na terceira secção se detalham as principais conclusões no âmbito clínico extraídos das aplicações de cada um dos modelos de pé.

IV.i Aspectos computacionais

- A sofisticada estrutura óssea do pé em forma de arco faz que a modelagem da sua resposta mecânica seja extremadamente desafiante. Esta simulação é mais complexa quando se considera a função dos músculos.

- O análise por elementos finitos e uma tarefa complexa com possibilidade de que se produzam erros. Por tanto, deve fazer-se todo o esforço possível por criar modelos que simulem o tema a um nível o suficientemente preciso, especialmente em aplicações médicas. As suposições e simplificações são necessárias a algum nível e dependem do objetivo do estudo. As rações para o uso destas e seu impacto nos resultados tem que ser claramente explicadas.

- Os modelos de esqueleto do pé são aproximações práticas para o estudo de temas relacionados com os ossos a um custo computacional baixo e com um nível de precisão suficiente. Devido à maior rigidez dos ossos comparado com o tecido mole, não incluir os tecidos moles no modelo do pé pode ser uma forma prática de produzir boas soluções em tempos muito minores.

- O modelo de Ogden de primeira ordem empregado para ajustar o tecido tendinoso recolhe um comportamento mais preciso da resposta dos tendões submetidos a cargas de tração que os modelos lineais e o modelo de Mooney-Rivlin usados na literatura.

- A caracterização independente da parte anterior e posterior do solado plantar permite analisar de forma precisa a pressão plantar e a deformação do solado plantar a diferentes ângulos de contato inicial com o chão.

- O modelo de elementos finitos completo do pé desarrolhado nesta Tese pode ser usado num amplio rango de aplicações no campo da biomecânica e baixo todos os rácios de carga: em pé, caminhando e correndo.

- A simulação computacional do pé expande o conhecimento da biomecânica do pé, proporcionando informação significativa para a prática clínica. Es-

pecialmente, o modelo desenvolvido nesta Tese pode ser usado no capo da biomecânica em áreas de ortopedia, lesões, tratamentos, cirurgia e esporte.

IV.ii Aspectos experimentais

- Tem se encontrado que os tendões dos pés que trabalham em distintos planos tem respostas mecânicas diferentes. Os tendões flexores e extensores dos dedos tem maior modulo de elasticidade e tensão última enquanto que os tendões inversores e eversores tem uma deformação de rotura maior.

- O critério proposto para quantificar as regiões da curva de tensão-deformação dos tendões baseado no modulo de Young permite uma definição precisa da deformação inicial, do início da região lineal e do ponto de fluência.

- As curvas de tensão-deformação dos tendões mostram proporcionalidade entre regiões sendo a deformação inicial o 15%, o começo da região lineal o 30% e o ponto de fluência o 70% da deformação de rotura.

- As propriedades estruturais são relevantes em cirurgias de reconstrução ortopédica e estimação de lesões em tendões. As propriedades materiais junto como a descrição quantitativa da curva de tensão-deformação ajudam no desenho de materiais sintéticos e no desenvolvimento de modelos constitutivos mais depurados.

- A medição da secção e o método de fixação das mostras a máquina de ensaio tem se identificado como fatores chaves para calcular as propriedades dos tecidos em ensaios de tração.

- O tecido baixo o calcâneo mostra uma resposta mais rígida que o tecido baixo a cabeça de metatarsos, enquanto que o solado plantar do antepé é mais rígido que a do meio pé. Esta diferenciação da resposta mecânica a compressão é particularmente relevante quando se estuda a distribuição de pressões no pé durante a carreira descalço a diferentes ângulos de impacto.

IV.iii Aspectos clínicos

- A geometria da falange proximal do primeiro dedo tem a característica do lado medial maior que o lado lateral sometendo a falange a um estres que pode provocar a rotação da falange proximal do primeiro dedo para uma posição mais relaxada. Esta potencial posição de equilíbrio produze uma tendência para a separação do primeiro metatarso relativa à sua posição anatômica original que constitui o início da deformidade do hallux valgus.

- A geometria da falange proximal do primeiro dedo é um fator significativo no desenvolvimento do hallux valgus, sendo igual de influente que o resto de parâmetros do esqueleto reportados na literatura e devem se considerar durante a avaliação pré-operatória. A avaliação clínica do hallux valgus deve ter em conta o primeiro radio completo e não cada fator por separado.

- Predisse-se um trabalho sinérgico entre os tendões de inversão e eversão. Puxando dum tibial ou dum fíbular estica-se o antagonista enquanto que se afrouxa o agonista. Esta ação conjunta predisse-se também para o tendão de Aquiles com o tibial posterior. Este comportamento explica o complexo controle de movimento que realiza o pé.

- Ao final da posição de apoio da marcha o pé esta solicitado a maiores esforços. O solado plantar, a fáscia, a cartilagem do tornozelo e os tendões estão mais estressados em esta posição que ao início da fase de apoio.

- Baseando-se no nível de estes dos componentes internos do pé durante a carreira descalço com padrão calcanhar-antepé é mais provável que se produza uma fratura do calcâneo por estres, dano nas cartilagens, tendinites no tibial e ulcerações no calcanhar.

- Fratura dos metatarsos por estres, plantar fascitis, tendinites do tendão de Aquiles e ulcerações no antepé são lesões relacionadas com o impacto que são mais prováveis de acontecer em corredores descalços que impactam inicialmente com todo a planta o com o antepé. Os resultados mostram

níveis de estres mais altos nestes componentes quando se aterrissa com a parte dianteira do pé.

V Contribuições originais

A principal contribuição desta Tese é a criação dum refinado modelo de elementos finitos do pé que supõe um passo à frente na simulação da biomecânica do pé desde a mecânica de meios contínuos. A continuação expõe-se a lista com todas as contribuições originais levadas a cabo durante o desenvolvimento desta Tese.

- Um modelo de elementos finitos em três dimensões completo do pé humano com uma representação detalhada dos componentes internos e propriedades não lineais de todos os tecidos moles. O modelo tem-se criado da segmentação independente de cada componente interno com um tamanho de malha otimizado incluindo a geometria detalhada de cada tendão, músculo, cartilagem e osso do pé distinguindo entre as propriedades de osso cortical e esponjoso. Toda a estrutura está rodeada do tecido conectivo (gordura). Este refinado modelo permite o estudo da biomecânica dos tecidos moles e duros.

- A caracterização do tecido tendinoso do pé com um modelo hiperelástico. O modelo de material de Ogden de primeiro ordem tem-se ajustado para simular o comportamento a tração dos tendões. Esta caracterização proporciona uma resposta mais precisa que as propostas anteriormente.

- A caracterização mecânica do solado plantar por regiões. Tem-se ajustado os coeficientes do modelo de Ogden com as curvas de tensão-deformação do solado plantar do retropé e o antepé.

- Um completo conjunto de dados das propriedades mecânica dos tendões do pé. Tem-se determinado as propriedades estruturais e materiais dos tendões do pé baixo a mesma metodologia. Tem-se diferenciado as respostas mecânicas dos tendões inversões/eversões e flexores/extensores dos dedos.

- Um critério para quantificar as regiões da curva de tensão-deformação dos tendões. O critério toma como referência o modulo de Young, tendo definido a deformação inicial como a parte da curva desde o começo até um desvio maior do 20% do modulo de Young e a região lineal tem se definido como parte da curva com uma curvatura menor do 20% do modulo de Young.

- A análise da resposta a compressão do solado plantar em função de sua localização. Tem-se comparado as curvas de tensão-deformação do tecido mole baixo o calcâneo, a ponte, a cabeça dos metatarsos e os dedos.

- A investigação de um parâmetro do esqueleto como fator etiológico do hallux valgus. O tamanho e a forma da falange proximal do primeiro dedo tem-se identificado como um fator etiológico do hallux valgus e deve ser tido em conta durante a avaliação clínica.

- Um análise de sensibilidade da força dos cinco maiores tendões de estabilização. Tem-se predito um trabalho conjunto entre os tendões fibulares e tibiais e entre o tibial anterior e o tendão de Aquiles o que explica a complexa resposta do controle de movimento do pé.

- Um análise quase-estático da fase de apoio da marcha. Tem-se estimado uma maior solicitação mecânica ao final da fase de apoio que ao início da mesma.

- Um estudo do mecanismo de absorção da força de impacto durante a carreira descalço a diferentes ângulos de aterragem. Tem-se identificado as lesões de impacto mais propensas a sofrer pelos corredores descalços ou com calçado minimalista em função do padrão de impacto.

V.i Publicações

Os seguintes artículos escritos durante o desenvolvimento desta Tese foram já publicados ou serão publicados em jornais científicos com revisão por pares:

1. **Morales-Orcajo, E.**, Bayod, J., and Las Casas, E.B. (2015).

Computational Foot Modeling: Scope and Applications. *Archives of Computational Methods in Engineering*, Publicado online.

2. **Morales-Orcajo, E.**, Bayod, J., Becerro-de Bengoa-Vallejo, R., Losa-Iglesias, M., and Doblare, M. (2015). Influence of first proximal phalanx geometry on hallux valgus deformity: a finite element analysis. *Medical & Biological Engineering & Computing*, 53(7):645-653.

3. **Morales-Orcajo, E.**, Becerro de Bengoa Vallejo, R., Losa Iglesias, M., and Bayod, J. Structural and material properties of human foot tendons. *Clinical Biomechanics*, Em revisão.

4. **Morales-Orcajo, E.**, Souza, T.R., Bayod, J., and Las Casas, E.B. Non-Linear finite element model to assess the effect of tendon forces on the foot-ankle complex. *Journal of Biomechanics*, Em revisão.

5. **Morales-Orcajo, E.**, Becerro de Bengoa Vallejo, R., Losa Iglesias, M., Bayod, J., and Las Casas, E.B. Foot injuries in barefoot running as function of strike pattern - A finite element study. *Journal of Sport Science*, Em revisão.

V.ii Conferências

As seguintes palestras foram apresentadas durante o desenvolvimento desta Tese:

1. **Morales-Orcajo, E.**, 3D Muscle detailed ankle-foot model for finite element analysis. *II Reunión Jóvenes Investiagadores del Instituto de Investigación en Ingeniería de Aragón*, Zaragoza, (España), 2013.

2. **Morales-Orcajo, E.**, Bayod, J., Becerro-de Bengoa-Vallejo, R., Losa-Iglesias, M., and Doblare, M., Influencia de la geometría de la falange proximal del primer dedo del pie en la formación de juanetes. *Congress on Numerical Methods in Engineering (CMN 2013)*, Bilbao, (España), 2013.

3. **Morales-Orcajo, E.**, Becerro de Bengoa Vallejo, R., Losa Iglesias, M., and Bayod, J., Mechanical properties of foot tendons - In vitro study. 1^st *Pan American Congress on Computational Mechanics (PANACM 2015)*, Buenos Aires, (Argentina), 2015.

4. **Morales-Orcajo, E.**, Bayod, J., and Las Casas, E.B., Developing a proper biomechanical computational model. *VI International Conference on Computational Bioengineering (ICCB 2015)*, Barcelona, (España), 2015.

VI Trabalho futuro

As aplicações dos modelos de elementos finitos continuarão crescendo com o aumento da potência informática, que dobra sua capacidade computacional cada 18 meses desde que se inventaram os microprocessadores, reduzindo os custos a metade (lei de Moore). Contudo, a potência informática nunca será suficiente considerando que o número de geometrias detalhadas, de formulações complexas e de exigentes condições de contorno também aumentará. A busca de melhores soluções e mais rápidas é um campo promissor com um amplo potencial de melhora.

Tendo em mente que o principal objetivo da Tese é o avanço em direção a uma simulação computacional do pé mais precisa para avaliação clínica, os progressos conseguidos durante esta Tese têm sido orientados a refinar a representação geométrica e a caracterização tissular dos componentes internos do pé. Portanto, os futuros avanços devem ser orientados para a melhor determinação das cargas e condições de contorno. Os trabalhos futuros nesta direção são listados aqui.

- Incluir contato entre os componentes internos do pé. Dentro do pé há muitos componentes sobrepostos, limitando o deslocamento dum componente em relação ao redor. Uma interação deslizante entre estes componentes quando uma força é aplicada a um tendão proporcionará uma transmissão de forças mais realista dentro do pé. Também deveria se definir contato entre articulações.

- Simular o comportamento ativo dos músculos. O modelo criado nesta Tese alimenta-se de dados cinéticos, os quais são difíceis de medir experimentalmente e costumam ser estimados a partir de modelos matemáticos ou cinemáticos. Portanto, introduzir cargas no modelo por meio do comportamento ativo dos músculos aumentará as possibilidades do modelo.

- Realizar simulações dinâmicas. Médicos e fisioterapeutas estão mostrando interesse em explorar a simulação dinâmica do ciclo da marcha completo em vez de posições discretas. As simulações dinâmicas incluem a variável do tempo e os efeitos dinâmicos, o que permite o estudo do movimento completo.

- Combinar modelos de elementos finitos com modelos multicorpos. A integração dos dois tipos de modelos pode ser uma boa aproximação para enfrentar-se a simulações dinâmicas movidas pela ativação dos músculos.

- Simulação de processos mecâno-químicos. A detalhada geometria do modelo pode ser explorada com a formulação de processos químicos governados por estímulos mecânicos como no caso das ulcerações ou a regeneração óssea.

- Reduzir o tempo de geração do modelo. Criar modelos de elementos finitos do pé específicos de um sujeito é uma tarefa que requer muito tempo. Pesquisas na automatização deste processo serão decisivas na implementação de estudos específicos de pacientes.

- Reduzir o tempo de cálculo. Para orientar as predições do modelo à ajuda no processo de toma de decisão dum tratamento clinico para um paciente especifico o tempo de computação deverá ser muito menor.

COMPUTATIONAL FOOT MODELING FOR CLINICAL ASSESSMENT

CHAPTER

ONE

INTRODUCTION

In this chapter the state of the art of the computational foot modeling is presented in form of in-depth review providing a general view of the scope and applications of the computational models of the human foot. The field of computational simulation in biomechanics has significantly advanced in the last three decades. Medicine and engineering fields increasingly collaborate to analyze biological systems. This work seeks a link between two areas of knowledge to achieve a better understanding between clinicians and researchers. The review includes two-dimensional (2D) and three-dimensional (3D), detailed and simplified, partial- and full-shape models of the lower limb, ankle and foot. Practical issues in computational modeling, tissue constitutive model approaches and pioneering applications are extensively discussed. Recent challenges in the field of foot computational simulation are delineated. At the end of the chapter, the motivation, objectives and outline of the Thesis are manifested. The in-depth review of the foot computational simulation presented in this chapter has been published in "Archives of Computational Methods in Engineering" (Section 7.2.1 — Publication 1).

1.1 Introduction

Feet are some of the most complex structures in the human body; they consist of small bones connected by cartilages and ligaments, which maintain structural integrity, several muscles, which conduct movements, and fat tissue and heel pads, which absorb impacts. They are responsible for supporting the weight of the entire body and balancing forces during human locomotion (Saltzman and Nawoczenski, 1995). Due to their arched structure, they respond to an extensive range of activities, such as walking, running, jumping, and climbing. However, human feet are often neglected when the lower limb or entire body is analyzed and are treated as a single body while disregarding the complex structure that achieves superior mechanical responsiveness.

Due to this complexity, feet must be simulated to understand how they function. Medical imaging, external measurements and cadaveric dissections are insufficient for understanding the role of each internal structure during gait. In this regard, computational simulations and, in particular, the finite element (FE) method is the most popular and accepted method for predicting the behavior of structural and mechanical systems for performance analysis (Prendergast, 1997; Mackerle, 2006). The significant progress in computational simulation and computing power of current computers constitutes a successful tool for biomechanical research to analyze irregular geometries with complex boundary conditions and advanced material properties. These simulations provide important clinical information, which is difficult to measure with experimental procedures. From a podiatric point of view, models of the human foot and lower extremity have already been pointed out as one of the most important directions for predicting structural behavior of their components (Kirby, 2001). The knowledge obtained from simulations aids in the diagnosis, treatment and prevention of foot pathologies.

The challenge of computational simulation of the foot/ankle complex began in 1981. Nakamura et al. (1981) presented a simplified and idealized model of the foot and shoe during midstance. The next model that appeared in the literature was a 2D foot skeleton, which was employed to analyze the stresses during three

walking phases (Patil et al., 1996). Although the model by Patil et al. did not simulate the soft tissue compared with the model by Nakamura et al., it considered the properties of cartilages and ligaments. In 1997, Lemmon et al. (1997) published an investigation of the alterations in pressure under the second metatarsal head as a function of insole thickness and tissue thickness. Although this model only represented a sagittal section through the second metatarsal bone, their approach considered hyperelastic properties of the foot soft tissue; it was significant and extensively cited. Gefen's studies provided significant advances in the description of the stress distribution for several subphases of stance, which established the groundwork in material properties, loads and constraints of foot FE models (Gefen et al., 2000; Gefen, 2002, 2003).

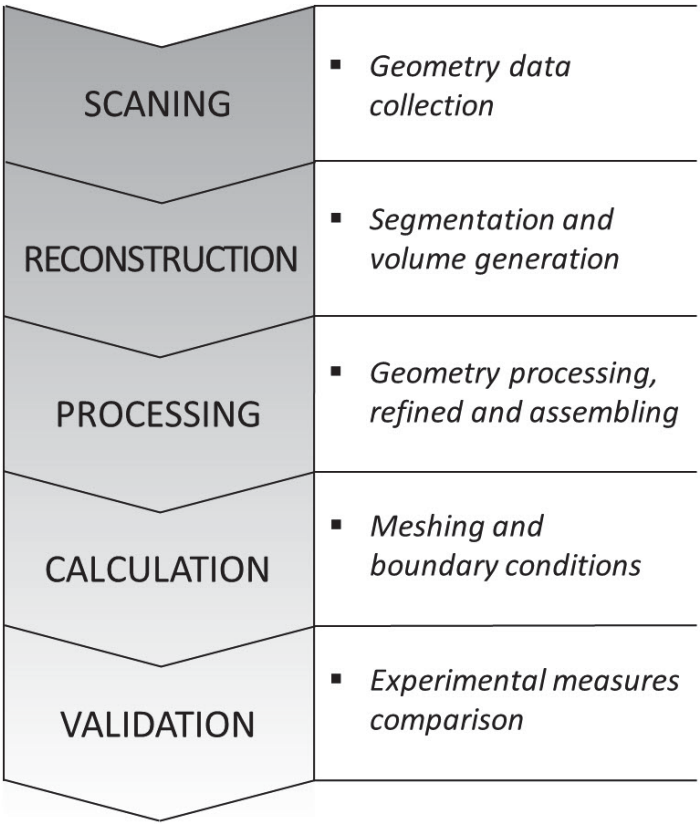

Figure 1.1: Computer model developing process diagram.

In the early 2000s, 3D foot models were developed with important simplifications. Jacob's oversimplified model, which treated the lateral metatarsals and the medial metatarsals as single bodies (Jacob and Patil, 1999) was one such model. Other authors simplified the geometry by affixing the midfoot and forefoot joints (Bandak et al., 2001; Chen et al., 2001). Cheung's studies (Cheung et al., 2004, 2005) facilitated the use of 3D foot models for analyzing internal stress and strain distributions of the foot structure. Based on the boundary conditions and material properties proposed by these researchers, a large number of foot models with more accurate geometries were used in many different applications in recent years.

1.2 Foot model development

Model reconstruction, the characterization of tissues and the determination of boundary conditions are the most complex steps in FE analysis. To address these problems, a methodology should be followed, as outlined in Figure 1.1 and described in the next section.

1.2.1 Geometry and mesh reconstruction

The geometry of the foot in a FE model is generally obtained from 3D reconstruction of computer tomography (CT) or magnetic resonance imaging (MRI), which can be obtained from dataset libraries (Gefen et al., 2000; Qiu et al., 2011; Sopher et al., 2011) or scanned patients (Cheung and Zhang, 2006; Antunes et al., 2007; Bayod et al., 2012). In the literature, CT and MRI are equally cited. Both techniques are painless and noninvasive; the main difference between the two techniques is that CT accurately outlines bone inside the body, whereas MRI provides much finer soft tissue detail, as shown in Figure 1.2. For the patient, CT scanning can pose a small risk of irradiation, especially by prolonged exposure; however, no biological hazards have been reported with the use of MRI. From a practical viewpoint, less time is required for total testing in CT whereas MRI can change the imaging plane without moving the patient.

The individual volumes of each compound are created by the segmentation

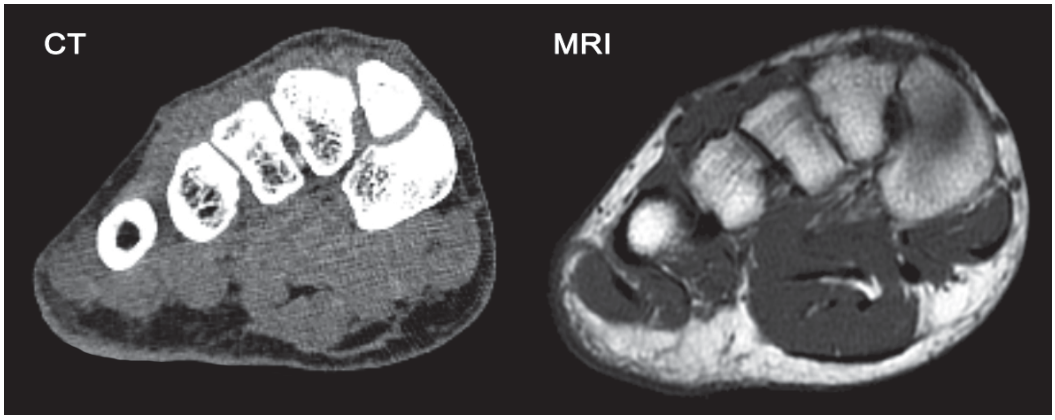

Figure 1.2: Left: Computer tomography image of midfoot. Right: Magnetic resonance image of midfoot.

process, 2D slice information is retrieved for 3D reconstruction. The volumes generated from the segmentation are frequently refined in a CAD program to accomplish a good fit between hard and soft tissue; small gaps, sharp edges or other disruptions that may unnecessarily complicate the mesh are prevented. It is also used to add objects such as insoles, implants and ground blocks for specific applications. These volumes are exported to a FE program to perform the analysis. In this step, the geometry is meshed and loads, constraints and material properties are defined.

A large variety of software for image reconstruction, geometry processing and FE calculation are available. The most popular medical image processing software for 3D generation from DICOM files are MIMICS (Materialise, Leuven, Belgium) (Flavin et al., 2008; Chen et al., 2010a), SIMPLEWARE (Simpleware Ltd., Exeter, UK) (Fontanella et al., 2012) and AMIRA (Mercury Computer Systems, Germany) (Cheng et al., 2008); the segmentation process is occasionally performed with custom-made codes (Budhabhatti et al., 2007; García-González et al., 2009; Isvilanonda et al., 2012). The models that require extra editing to improve model accuracy or to smooth surfaces were processed by SOLIDWORKS (Dassault Systemes, SolidWorks Corp., USA) (Yu et al., 2008; Qian et al., 2010b). Regarding FE packages, ABAQUS (ABAQUS Inc., Pawtucket, RI, USA) and ANSYS (ANSYS Inc., Canonsburg, PA, USA) are the most cited software. They

Table 1.1: Percentage of papers that employed each finite element package on the literature of computational analyses of the foot.

ABAQUS	45%
ANSYS	17%
PATRAN	6%
LS-DYNA	6%
MARC	6%
OTHERS	20%

are employed in more than 60% of the papers published on FE analyses of the foot; LS-DYNA (LSTC, Livermore, CA, USA), PATRAN (MSC., Santa Ana, CA, USA) and MSC.MARC (MSC.software corporation, Santa Ana, CA, USA) are also commonly reported [Table 1.1].

1.2.2 Verification and validation

The ultimate objective of a biomechanical simulation is to obtain reliable results that can be used to develop clinically relevant recommendations. The opinions about the limits of these simulations and their conclusions significantly differ. Some researchers consider computational simulation to be acceptable from a practical engineering perspective because it provides statistically meaningful predictions (Babuska and Oden, 2004). Other researchers suggest that numerical models are inherently false (Oreskes et al., 1994). Despite the diverse viewpoints, models have exponentially increased in the last three decades (Erdemir et al., 2012) due to the potential applications of this tool and the fact that modeling reduces complicated clinical testing. To raise the credibility of their predictions, models must be verified and validated and all relevant aspects must be discussed (Roache, 1998).

Verification measures how close a result is to the exact solution. Validity evaluates whether mathematical descriptions of structural aspects mimic a real problem. In the field of solid biomechanics, verification usually consists of implementing constitutive equations and geometry simplifications and assessing resulting errors. This verification is probably due to the fact that most biomechanics

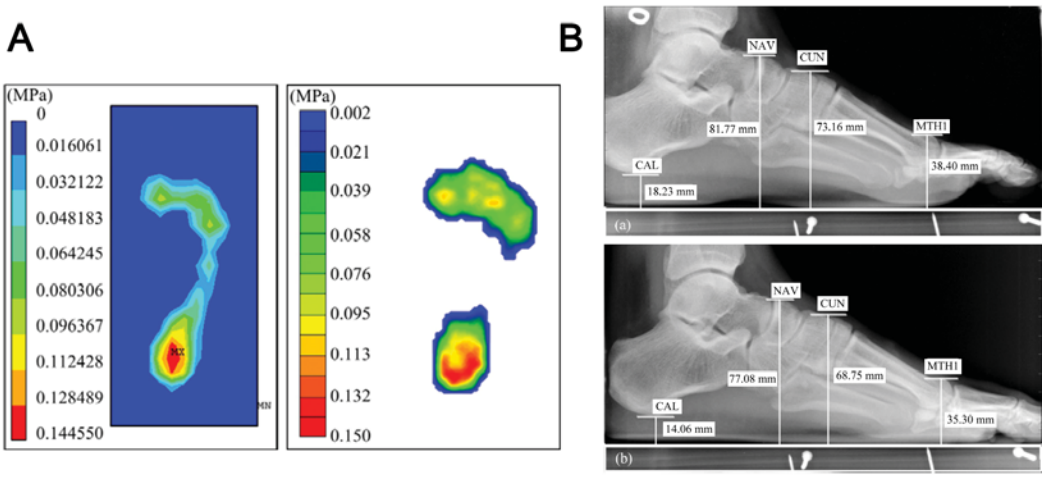

Figure 1.3: Common measurements employed to validate foot finite element models. A) Plantar pressure distribution. B) Bone vertical displacement. (Tao et al., 2009)

studies use established and/or commercially available computational software for which code verification has already been completed (Anderson et al., 2007). However, validation must be assessed by experimental tests and requires a long process that involves the entire scientific community (scientists, engineers and clinicians) (Viceconti et al., 2005). Henninger et al. (2010) described two predominant types of validation: direct validation and indirect validation. In direct validation, the experiment is specifically designed for the validation of the proposed model. In indirect validation, a comparison of the model predictions with previous studies, in which the settings of the experiment cannot be controlled by the user, is performed. Both processes appear in the literature of FE analyses of the foot.

Regarding the validation of foot models, the most common process to validate FE results is the comparison between predicted plantar pressure and measured plantar pressure (Figure 1.3A). The most prevalent plantar pressure measurement systems are platform systems and in-shoe systems (Razak et al., 2012; Chockalingam et al., 2013). In this process, the matching parameters include the entire plantar pressure distribution (Chen et al., 2010a), the peak plantar pressure of each region (Guiotto et al., 2014), the total contact area (Isvilanonda et al., 2012) or the ground reaction force along the stance phase (Lin et al., 2014). The peak

plantar pressure that is predicted by FE models is generally higher than the measured peak pressure (Cheung et al., 2005; Liu and Zhang, 2013; Yu et al., 2013). This deviation is primarily attributed to different resolutions between the scan system and the model. The measuring system reports an average pressure for the area of the sensor; a minimum average pressure of 25 mm^2 has been suggested to prevent underestimations (Razak et al., 2012). The FE model provided values for an area between 1 to 5 mm^2 depending on the mesh size. The maximum plantar pressure predicted by the FE model is expected to exceed the pressure measurements with the platform. This discrepancy may be influenced by the fact that some authors compared the measured plantar pressure with the von Mises stress predicted by FE model. These values do not apply the same concept because the von Mises stresses include hydrostatic and deviatoric stresses. Thus, the comparison with the plantar pressure prediction reduces this overestimation.

When the comparison with the plantar pressure is not feasible because the model does not include fat tissue, the validation parameters consist of bone displacement and arch deformation (Figure 1.3B). The validation can be performed using radiographic images (Cheng et al., 2008) or by cadaveric experiment (Liang et al., 2011). Post-surgery studies or treatment simulations can be compared with cadaveric studies or clinical reports (Gefen, 2002; Liu and Zhang, 2013; Chen et al., 2012). Computational values have also been validated by measuring soft tissue deformation (Petre et al., 2013). Another method used to assess the model involves computationally replicating the experiments and comparing the results, for example, the impact test (Tannous et al., 1996; Shin et al., 2012) or kicking a ball (Ishii et al., 2014). A good practice for ensuring the reliability of model predictions is a comparison of the results with different measurements for different load conditions (Natali et al., 2010b; Tao et al., 2009) and the use of different FE models for different patient/donor experiments (Trabelsi et al., 2014). This practice is especially important for clinical applications, in which the validation process should be much more exhaustive, because the predictions enable direct application in patients. Any parameter that can be used for computational predictions and experimental measurements is suitable for validating a FE model.

Although the validation must be performed by authors, detailed information

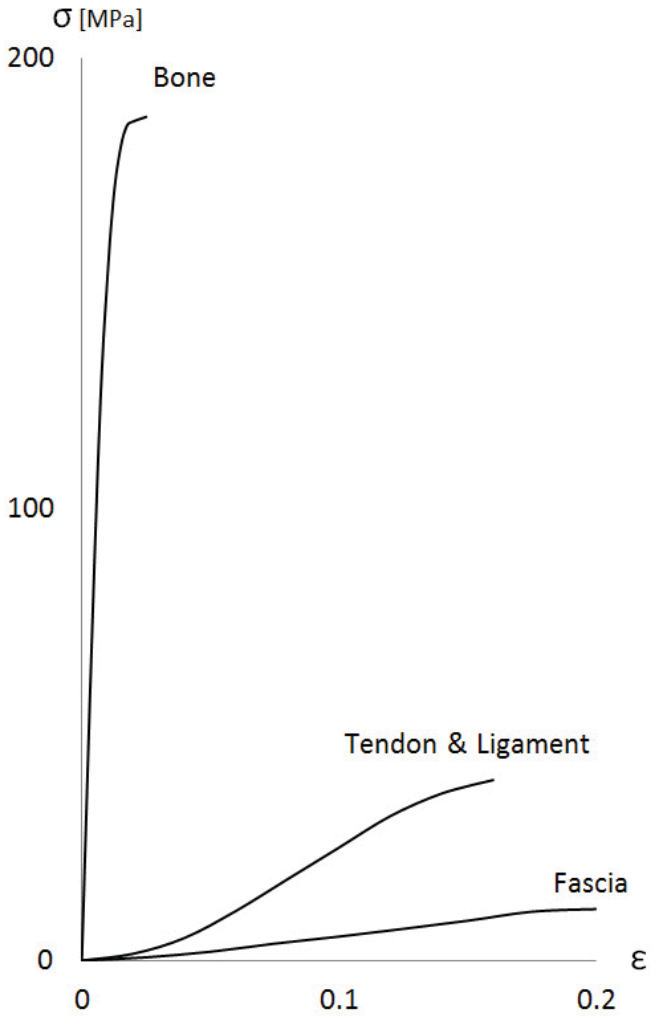

Figure 1.4: Stress-strain curves of the foot tissues that function under traction loads.

about the quality of the mesh (Burkhart et al., 2013) and the characteristics of the model (Erdemir et al., 2012) should be provided when a study is based on a FE analysis to ensure that the reader will be able to assess and eventually replicate the value of the results and accept its predictions. According to Oberkampf et al. (2002), engineering does not require the "absolute truth" but a statistically meaningful comparison of computational and experimental results, which are designed to assess random (statistical) and bias (systematic) errors. Computational mod-

els in biomechanics are habitually developed to simulate phenomena that cannot be experimentally measured and require model inputs that are unknown or may vary by several orders of magnitude. Although the predictions cannot be directly compared, computational models may provide valuable insight into the mechanical behaviors of complex biological systems, such as feet, if the verification is properly performed.

1.3 Foot tissue properties

The simulation of biological tissues is a fascinating challenge because they exhibit complex characteristics. They have a fibrous structure with a specific spatial orientation and an anisotropic mechanical response. Biological tissues are multiphasic with a fluid phase and a solid matrix. Many biological tissues experience a strong nonlinear behavior, such as large deformations (hyperelastic behavior) and a time-dependent nature (viscoelastic behavior). Generally, they display patterns of hysteresis and their responses vary with load application speed. As living tissue, they experience intersubject variability, sexual differentiation, age-dependency; they evolve according to solicitations, diseases or different types of cell activities (Currey, 2003). Fortunately, engineers employ tools, such as arrangements, assumptions and simplifications, which help them to address these complexities.

In the sequence, a brief summary of the main numerical approaches and the approved parameters of foot tissues that are used in computational studies are provided.

At the foot level and from a biomechanical perspective, only the connective and muscular tissues are included in the models. Connective tissues give shape to organs and hold them in place, whereas muscular tissue actively produces force and causes motion within internal organs. Epithelial tissue and nervous tissue are not considered for mechanical analysis. Biological tissues contain two types of tissues: hard and soft tissues. The main difference is the existence of the inorganic phase. This mineral component makes hard tissue stiffer and more resistant than soft tissue, as shown in Figure 1.4. Figure 1.4 depicts the behaviors of the tissues in

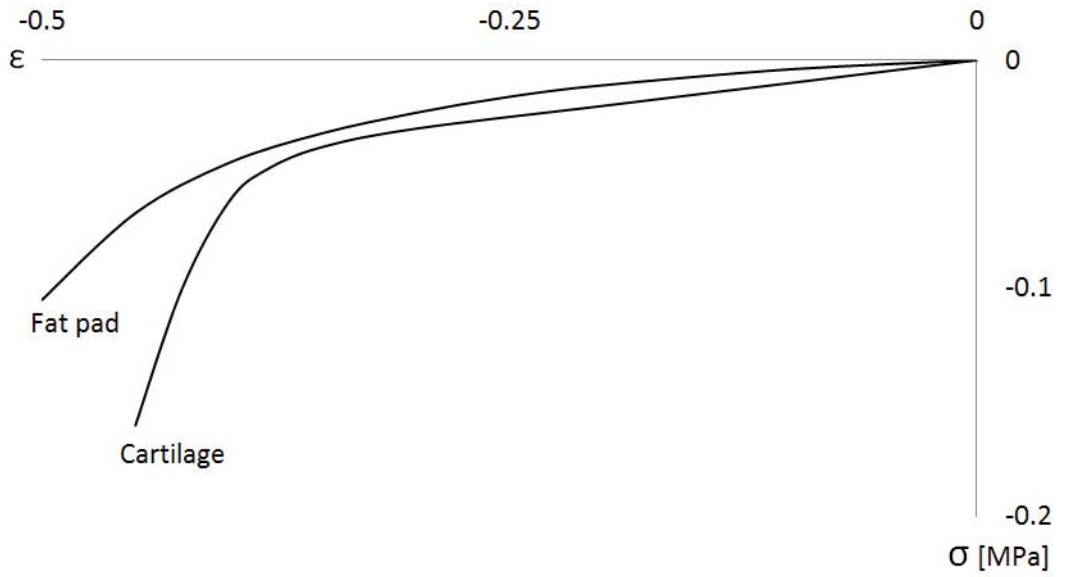

Figure 1.5: Stress-strain curves of the foot tissues that function under compressive loads.

a uniaxial traction test until the failure point. During physiological performance, tissues are expected to function in the lower half of their curves. Figure 1.5 shows the stress-strain curve of the foot tissues that function under compression loads. These graphs are presented as a qualitative comparison between the mechanical behaviors of the different healthy tissues that are involved in foot computational analysis; however, these curves can quantitatively vary depending on the speed load application.

1.3.1 Hard tissues

The biological tissue that incorporates minerals into soft matrices, which generally form a protective shield or structural support, is classified as hard tissue. This group includes bones, horns and shells. The foot only contains osseous material. Bony tissue is one of the stronger and most rigid structures of the body due to its combination of inorganic and organic elements. It achieves very high mechanical

performance because the minerals, calcium and phosphate confer stiffness and stretch in compression and soft organic materials, such a collagen, proteoglycans and proteins, contribute to traction properties. Bone is an anisotropic material that exhibits different behaviors under tension and compression (Cowin, 1979). It is composed of cortical bone and trabecular bone; the latter has the lower elastic modulus (Wirtz et al., 2000).

1.3.1.1 Bone

Dense compact bone is referred to as cortical bone, is located on the cortex, which is the outer shell of bone (Figure 1.6). It is harder, stronger and stiffer than cancellous bone and contributes to approximately 80% of the weight of a human skeleton. The mechanical properties of the cortical tissue vary depending on the orientation of the specimen (longitudinal, medial-lateral, and anterior-posterior) (Cowin et al., 1987). Due to the complexity of this material in computational simulations, it is frequently assumed to be homogeneous, isotropic and linear elastic. These assumptions were investigated by Huiskes (1982), who reported that cortical and trabecular bones may be considered to exhibit linearly elastic behaviors in the quasi-static loading case. The most predominant value of Young's modulus for cortical bone is 17GPa (Bayod et al., 2012; Shin et al., 2012; Wu et al., 2007). The literature contains limited data regarding the mechanical properties of foot bones; thus, the properties that are utilized in foot models are estimated with mean values of leg bones (Evans, 1973). This comparison is reasonable because the modulus of elasticity measurements for both the leg and the arm fall within the same range (Yamada, 1970).

Generally, biological material are discontinuous to any level but cancellous bone are also discontinuous on a macroscopic level; thus, it resembles a structure instead of a material (Figure 1.6). The orientation and density of the trabecular structure are important factors in the mechanical behavior of spongy bone (Cowin, 1985). A dependence of the mechanical properties of cancellous bone on the anatomic location and function of the tested bony region is observed (Goldstein, 1987; Morgan et al., 2003), that is, bones adapt to their mechanical environment (Currey, 1984). Keaveny et al. (1994) reported that trabecular bone exhibits a

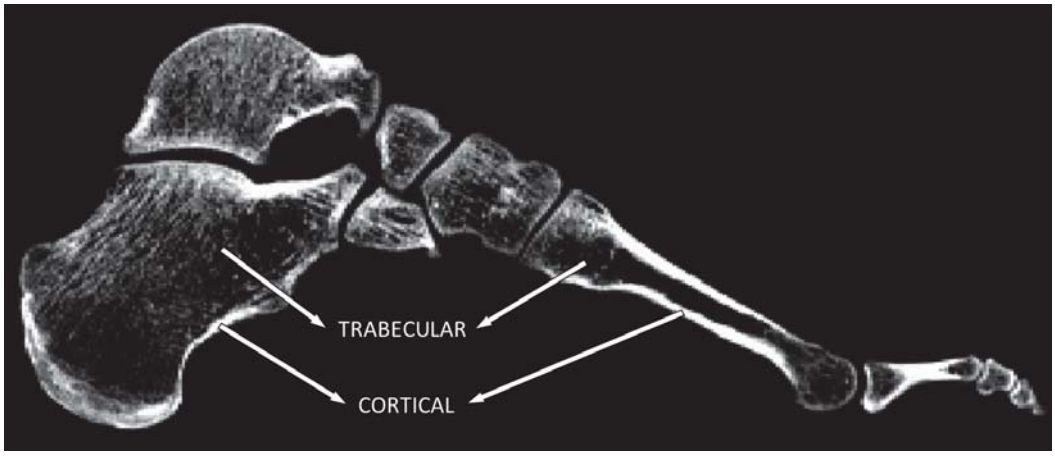

Figure 1.6: Cortical and trabecular bone in the foot skeleton (Computer tomography image).

completely linear elastic behavior and yields at low strains. Due to these features, the estimated values for the Young's modulus of trabecular bone material range from 0.1 to 20GPa (Rho et al., 1993; Novitskaya et al., 2011). Current studies have indicated considerably lower values for Young's modulus. Regarding foot models, the few authors who consider the properties of the trabecular bone use these lower values, which range from 0.4 to 0.7 GPa (Bandak et al., 2001; Shin et al., 2012; García-Aznar et al., 2009), with 5.5GPa as the highest value (Wu, 2007). A Poisson's ratio of 0.3 has been reported for both cortical and trabecular bone in all tests.

The elastic properties of bone can also be defined by the mathematical relationship with bone density using gray scale values of computer topographies. In the scientific literature, a large number of mathematical relationships between the densitometric measurements and Young's modulus with extensive scatter are identified (Helgason et al., 2008). This finding may be attributed to the difficulty of measuring the properties of trabecular bone. In any case, this procedure has not been applied to subject-specific FE foot models. Bandak et al. (2001) utilized one of these formulas to determine the elastic modulus of spongy bone but they did not use it to apply a progressive transition of the Young modulus between both types of bone. A recently published metatarsal FE study employed an inho-

mogeneous (density dependent) Young's modulus for bone (Trabelsi et al., 2014). They postulated that the distribution of the different material properties of the metatarsal significantly affected the mechanical response. They also compared the mean difference in the strains between the FE models with inhomogeneous properties with three distinct constant values that are commonly found in the literature. The authors conclude that a specific constant Young's modulus may adequately represent a particular metatarsal, whereas the same constant Young's modulus may result in poor agreement with other metatarsal bones.

The most common simplification of the simulation of the foot osseous structure involves treating it as a homogeneous, isotropic, and linear elastic material. The elastic modulus and Poisson's ratio of this equivalent material is assumed to be 7.3 GPa and 0.3, respectively. This value was obtained by Nakamura et al. (1981), who justified it as a frequent value in the literature; however, they did not provide any source or justification for this value. The most cited authors in foot FE modeling (Gefen, 2002; Cheung and Zhang, 2005) defended this value as a weighted average of cortical and trabecular elasticity properties. Despite the apparent lack of validation, this idealization is accepted by the majority of authors who continue to use these properties. A slightly higher value of 10 GPa for the Young's modulus of 10 GPa for the bone block was employed by some authors (Lemmon et al., 1997; Chen et al., 2003) based on Van Buskirk and Ashman (1981) studies; however, this value has not been recently utilized. A recent study of the effect of Young's modulus on the simulation of a foot FE model consisted of a comparison between a computer simulation and an in-vitro experiment, which yielded values that were four times higher than the traditional Young's modulus. The value of 29.2 GPa for the Young modulus of foot and ankle bones showed better agreement with the measurements of surface strain in an in-vitro experiment of six cadaveric feet (Niu et al., 2013).

Some studies assume foot bones as rigid bodies (Shin et al., 2012). In these studies, the internal stress is not considered to be a variable and the objective of the study is the motion of the bones (joint kinetics). This approximation is even more simplistic than the homogenous bone; it is justified by the fact that the bone has a much greater stiffness than soft tissues (Figure 1.4). This assumption can

only be accepted in particular cases, when the objective of the study is the stress of the surrounding tissues due to the motion of the foot joints.

Shoulder (Wakabayashi et al., 2003), elbow (Willing et al., 2013), finger (Butz et al., 2012), pelvis (Kim et al., 2009) and knee (Beillas et al., 2004) FE models tend to distinguish both materials because the complexity of the bony structure and the size and number of bones in these parts is simpler compared with the foot, where achieving the convergence of the model and computer time are significant problems. As a result, uniform mechanical properties are used to analyze the mechanical behavior of the foot skeleton.

In 2009, García-Aznar et al. (2009) compared the displacement and stresses of a foot skeleton FE model using two different methodologies. They noted that the deformed shape in both models was similar; however, they detected an important underestimation of the maximum stress level when homogeneous bone was considered. Therefore, this assumption may be suitable for foot applications that focus on the adipose tissue surrounding a foot skeleton, such as plantar pressure estimation and footwear design problems. However, for an analysis of bone functions, it is inaccurate.

The current trend, which is aided by continuous advancements in numerical techniques and computer technology, features the use of refined models that not only distinguish between cortical and trabecular bone but also include more complex simulations that consider anisotropic and hyperelastic behaviors.

1.3.2 Soft tissues

Soft tissue connects, supports, or surrounds other structures and organs of the body. It is a composite that consists of a very flexible organic matrix that is strengthened by collagen and elastin fibers. Soft tissues in the feet include cartilage, ligament, fascia, tendon, muscle, skin, artery and vein. Blood vessels are not considered in the mechanical analysis.

The behavior of soft tissue is dependent on its composition and structure, particularly with regard to the percentage of fibers, its features, the directionality and the type of grouping. Thus, the tissues that are specialized in tensile stresses,

such as tendons and ligaments, are rich in fibers that are oriented in the direction of the stress, whereas the tissues that can withstand compressive forces, such as cartilage rich in proteoglycans with fiber, are randomly distributed. They regularly support large deformations and are highly anisotropic. They are quasi-incompressible in an extensive range of deformations.

1.3.2.1 Cartilage

Cartilage is a relatively soft tissue that is present in many parts of the body, such as nose, ear, and joints; this review focuses on articular cartilage. Specifically, articular cartilage covers the ends of bones to facilitate load carriage and lubrication (Figure 1.7). Its structure can withstand enormous compressive forces and it is capable of creating a low friction surface on which joints glide (Nguyen, 2005). This tissue can be considered to be highly heterogeneous, anisotropic and multiphasic and primarily consists of water, collagen fibrils and a dense skein of negatively charged proteins — the proteoglycans.

Similar to other biological tissues, an extensive variety of numerical approaches exist to represent the constitutive behavior of articular cartilage, which includes elastic, viscoelastic, poroelastic, electro-mechanic, fibril-reinforced, bi-component, biphasic, and three-phased behaviors (Nguyen, 2005). However, the complete spectrum of the tissue's complex responses is not recovered in a unique model. The appropriateness of each approach is dependent on the specific case to analyze. In foot modeling, which includes many joints, articular cartilage tissue is considered to be an isotropic linear elastic material with no interstitial fluid flow during the steady-state phase. Clift (1992) noted that, under short-term or instantaneous loading, cartilage should be modeled as a linear elastic material. This approach reduces the complexity of the calculations without losing accuracy because the volume of cartilage and its influence in the final result is almost negligible when compared with other tissues of the foot.

Two basic pathways can be followed to simulate the articular behavior: (a) to fill the articular gap with a solid to simulate the flexibility of the connection between bony structures (Gefen et al., 2000; Thomas et al., 2004; Tao et al., 2005) or (b) to consider the surface-surface interaction with frictionless contact elements.

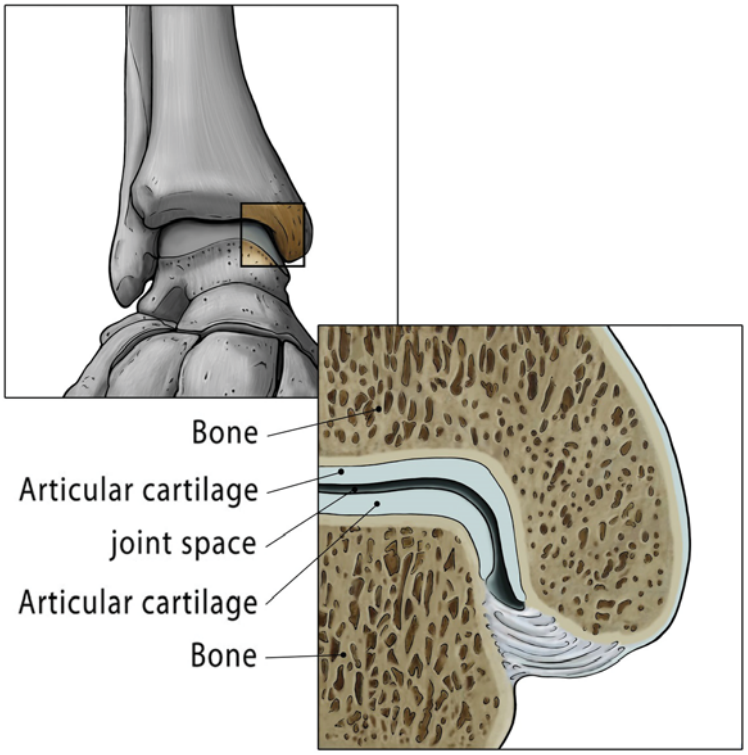

Figure 1.7: Scheme of the articular cartilage at the talocrural joint. Source <http://myankle.co.uk>.

In this case, bones are allowed to slide over each other with the constraints governed by the congruent facets and ligamentous structures (Liu et al., 2013; Chen et al., 2012; Cheung and Zhang, 2005). Regarding the accuracy of the approximation, the second pathway is slightly better because it enables a real articulating movement. However, from the perspective of small strains, both models exhibit a reasonable approximation. A unified phalanx for removing the cartilage between phalanges (single toe), which is frequently utilized by some authors (Cheung et al., 2005; Actis et al., 2006), is a more serious simplification. Some authors explain that the contact stresses applied to the forefoot do not flex the interphalangeal joints at a moderate velocity in a normal gait; therefore, significant inaccuracies in the predicted stress distributions are not expected (Gefen et al., 2000). This simplification is only suitable when the objective is kept away from the forefoot.

Regarding linear elastic properties, cartilage is defined as an incompressible

material for an instantaneous response (Mak et al., 1987); a Poisson's ratio of 0.4 is common to the literature. The Young's modulus value is more controversial with two different values — 1 and 10 MPa. The first value was derived in a study about cartilage biomechanical properties in the human cadaveric first metatarsophangeal joint by Athanasiou et al. (1998). The value of 10 MPa was identified in previous literature based on the linear elastic properties of the knee FE model suggested by Schreppers et al. (1990). The selection of both values may be appropriate because higher values are frequently applied to larger joints, such as knee (Moglo and Shirazi-Adl, 2003) and lower values are frequently applied to smaller joints, such as finger joints (Butz et al., 2012). A value of 10 MPa may be more suitable for tarsus, whereas a value of 1 MPa may be suitable for phalanges.

1.3.2.2 Ligaments

Ligaments consist of the fibrous connective tissue that maintains contact with the bones across joints (Figure 1.8). They are a biological composite that consists of a ground substance matrix reinforced by closely packed collagen and elastin fiber bundles. The ground substance matrix is composed of proteoglycans, glycolipids, fibroblasts and water (Weiss and Gardiner, 2001). Cartilage enables free slipping among bones, ligaments guide joints in a normal motion, which provides stability for the joints.

The main purpose of including ligaments in a foot model is to simulate the articulation function of providing guides to maintain touch with the head bones and provide stability for the hindfoot. For this purpose, ligaments in the foot simulation are represented by truss elements or springs. Both elements are one-dimensional and only support tensile forces, whereas the compression forces are withstood by cartilage. Thus, the difference between the options is that springs are independent of the cross-section and employ stiffness as the input property. An accurate geometry of the ligament is only used for studies of injuries to specific ligaments, such as the anterior cruciate ligament in the knee (Peña et al., 2006; Guo et al., 2009). The same situation applies to material properties. Despite the fact that ligaments exhibit a viscoelastic behavior (Provenzano et al., 2001; Peña et al., 2008), a linear elastic approach is usually applied to ligaments in foot

Figure 1.8: Scheme of the ligaments within the foot-ankle complex. Source <http://www.solesee.com>.

models, with the exception of special applications in which the ligaments are the focus (Forestiero et al., 2014). These arrangements are distinct in the knee-ankle-foot model presented by Liu and Zhang (2013), in which the knee ligaments were defined as hyperelastic properties with an accurate geometry and the foot and ankle ligaments were simulated as tension-only truss elements with linear elastic properties.

Due to the functional nature of these components in foot simulation, the literature contains minimal discussion on this topic. The majority of the models use a Young's modulus of 260 MPa and a Poisson's ratio of 0.4. These values were extracted from a study of the mechanical characteristics of the collateral ligaments of the human ankle joint by Siegler et al. (1988). Due to advancements in computer science, recent models have begun to use nonlinear approaches for foot-ankle complex studies (Isvilanonda et al., 2012; Forestiero et al., 2013), which may provide insight on future foot models.

1.3.2.3 Tendon and muscle

Tendon is the tissue that connects bone and muscles at their ends and transmits the forces generated by muscles to the bony structure. They have a multi-unit hierarchical structure that is composed of collagen molecules, fibrils, fiber bun-

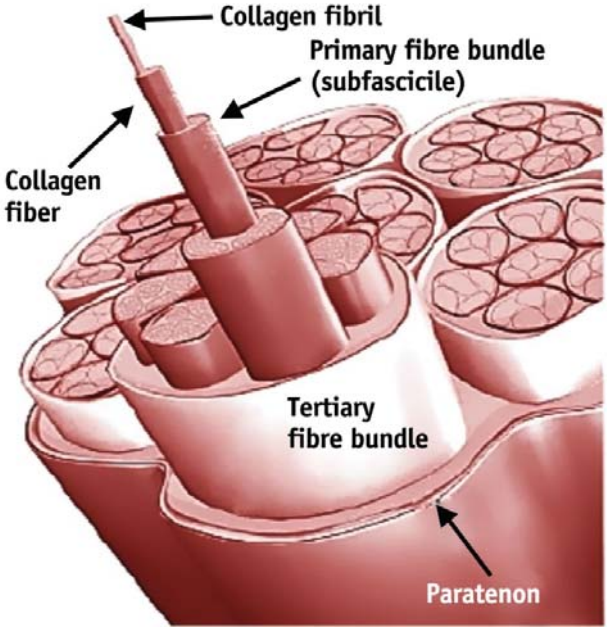

Figure 1.9: Scheme of the multi-unit hierarchical structure of the tendon. Source <http://www.medicalsportsnetwork.com>.

dles, fascicles and tendon units (Figure 1.9). These fiber bundles are aligned with the long axis of the tendon and provide the tendon's tensile strength. Tendons exhibit fiber patterns and viscoelastic characteristics; their typical stress-strain curve (Figure 1.10) has an initial maximum strain of 2% followed by a linear region until the ultimate strain with macroscopic failure (Wang, 2006). Unlike muscle fibers, which exhibit passive and active behaviors, tendon fibers only exhibit passive behaviors where the stress is dependent on the strain.

Within foot tendons, the Achilles tendon is the most important because it is one of the strongest in the human body; it bears large forces (Komi, 1990) and frequently fails by rupture (Kongsgaard and Aagaard, 2005). Its importance is evidenced by the substantial amount of literature dedicated to this tendon compared with any other tendon in the lower limb. The majority of the properties of the remaining tendons of the foot are extrapolated from the Achilles tendon. The mechanical properties of the Achilles tendon have been examined *in vivo* (Lichtwark and Wilson, 2005; Peltonen et al., 2012; Kongsgaard et al., 2011), by

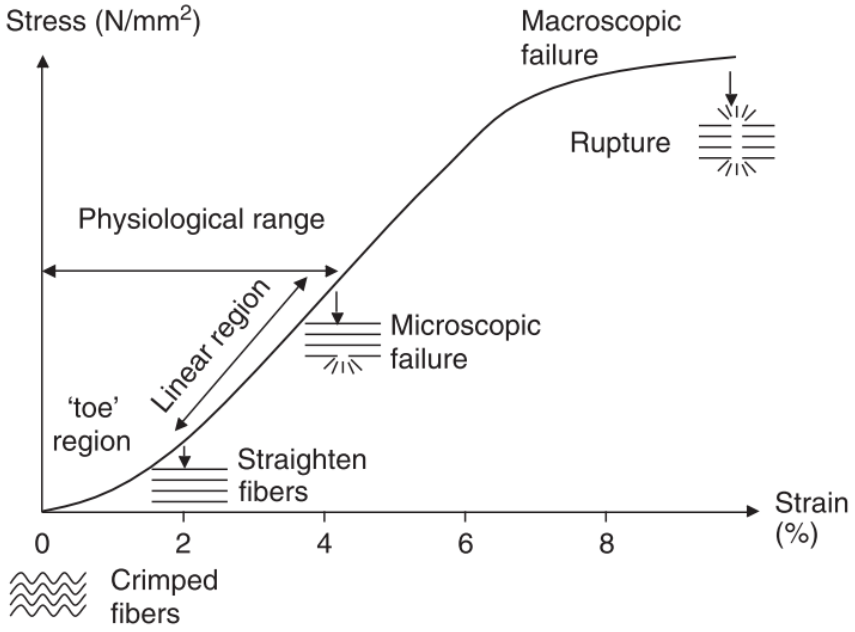

Figure 1.10: Typical stress-strain curve of tendon tissue (Wang, 2006).

the cadaveric tensile test (Louis-Ugbo et al., 2004; Wren et al., 2001), and by the microtensile test (Hansen et al., 2013); the Young's modulus generally varies from 0.2 to 2 GPa. The information about other foot tendons is incomplete, the majority of the tests provide data on structural parameters, stiffness (Datta et al., 2006; Sebastian et al., 2007) or cross-sectional areas (Severinsen and Andersen, 2007; Hing et al., 2009; Mickle et al., 2013) of different tendons. Few studies discuss the material properties of the extrinsic foot tendon (Schechtman and Bader, 1997; Maganaris and Paul, 1999, 2002), for which the data is similar.

Despite their analogous mechanical response to ligaments, which is dominated by the collagen fibers, the majority of the proposed models focus on predicting the ligament response; few simulations of foot tendons have been performed. In complete foot models, feeble attempts have been made in which tendons were simplified by truss/bar elements that approximate the actual tendon trajectory (Qian et al., 2010b; Chen et al., 2012; Bayod et al., 2010). The tendon activity is only introduced in the model to directly transmit the forces to the bone insertions. A more accurate numerical approach was proposed by Gu et al. (2008), who

presented an incompressible, hyperelastic, two-parameter Mooney-Rivlin formulation to investigate the mechanical response of the Achilles tendon for different types of sports.

Few models have considered muscle tissue. The majority of the authors define a bulk fat connective tissue with weighted material properties, as for trabecular and cortical bone. The 2D foot model proposed by Wu (2007) distinguishes the passive properties of the muscle from the fat tissue. Note the study by Spyrou (2009) and his group , who defined a constitutive model for muscle-tendon coupled behavior with active and passive responses and his application to the simulation of human foot movements (Spyrou and Aravas, 2012).

1.3.2.4 Plantar fascia

Fascia is a type of tendon with a similar histologic but a flattened layer shape. Its main function is to join the muscles and the body parts that the muscles act upon. In particular, plantar fascia serves an important role in absorbing foot-ground impact, storing and returning strain energy, transmitting Achilles tendon forces and maintaining arch stability (Figure 1.11) (Erdemir et al., 2004; Kim and Voloshin, 1995; Sarrafian, 1987).

Similar to ligaments, plantar fascia is modeled for its mechanical function in the foot structure to maintain stability in the medial longitudinal arch; however, its morphology and mechanical behavior is not refined. Plantar aponeurosis is only modeled when the entire foot is involved and is neglected in partial geometry models. It is typically simulated with truss elements — one per ray — that join the calcaneal tuberosity with the base of each proximal phalange (Luximon et al., 2012; Hsu et al., 2008). The properties applied to these tension-only elements are usually linear elastic models with a Young's modulus of 350 MPa and a Poisson's ratio of 0.4. These parameters are based on the experimental test of the elastic properties of plantar fascia, which was performed by Wright and Rennels (1964). Because of the important role of plantar fascia in human locomotion, some authors employed more accurate nonlinear approaches (Cheng et al., 2008; Isvilanonda et al., 2012). The data for adjusting the terms of the functions were obtained from clinical research results (Kitaoka et al., 1994).

Figure 1.11: Plantar fascia is placed under the intrinsic muscles of the foot. It is inserted in the base of the calcaneus conected with the metatarsal heads. Source <http://www.webmd.com>.

Recent investigations have expanded the nonlinear mechanical properties of this tissue as a basis to develop suitable numerical models (Pavan et al., 2011, 2014). A dynamic simulation of the plantar fascia during the entire stance phase of a gait has been performed using transversely isotropic properties (Lin et al., 2014). Those approaches comprise an important step for future simulation.

1.3.2.5 Fat and skin

In foot modeling, fat tissue is referred to as the fat pad; it is located under the calcaneal and metatarsal heads. However, fat tissue is also found in other parts of the foot. For mechanical purposes, the properties of the fat pad are considered. This tissue is commonly referred to as plantar soft tissue. The heel pad is a highly specialized structure that is designed to resist compressive loads; it consists of packed fat cells that are enclosed by elastic fibrous connective tissue (Rome, 1998). This soft tissue is characterized by nonlinear and time-dependent behaviors, that is, the level and the rate at which the tissue is loaded influence its instantaneous stiffness (Miller-Young et al., 2002).

This viscoelastic tissue provokes substantial interest in the development of a more refined characterization of its mechanical properties due to its strong relationship with diabetic ulcerations and the complexity of measuring its internal

stresses. In this regard, many numerical approaches have been provided based on *in vivo* and ex vivo test data: the viscoelastic Voight-Kelvin model (Gefen et al., 2001), the hyperelastic Mooney-Rivlin model (Miller-Young et al., 2002; Spears and Miller-Young, 2006), the hyperelastic first-order Ogden model (Erdemir et al., 2006; Chokhandre et al., 2012), the quasi-linear viscoelastic theory (Ledoux and Blevins, 2007) and the visco-hyperelastic formulation (Natali et al., 2010a). These approaches were based on the stress-strain curve under compressive load of the heel pad, with the exception of the fitting of coefficients provided by Ledoux and Blevins (2007), which were adapted from stress relaxation experiments of six different regions of the plantar soft tissue.

These approaches have not been run in 3D complete foot FE models. Viscoelastic formulations have only been applied in partial geometrical models (Sopher et al., 2011; Petre et al., 2013; Chen and Lee, 2015). In complete 3D foot simulations, a hyperelastic formulation is applied to an encapsulated bulk soft tissue, in which the skeleton is embedded. This volume includes fatty tissue, muscles, tendons and the skin layer; it is frequently characterized with the parameters calculated by Lemmon et al. (1997) and Erdemir et al. (2006). For simplicity and to reduce the computational cost, this bulk tissue was also assumed to be linear elastic (Brilakis et al., 2012; Takahashi et al., 2012; Sun et al., 2012). The most detailed representation of heel pad geometry was the FE model that considered fat cells and their septa fiber structure; they were modeled separately using different material properties (Qian et al., 2010a).

In the last few years, numerical models have been gradually developed to separately simulate skin behavior from fatty tissue behavior. These studies primarily focused on the influence of this fibrous tissue on the internal stress of the fat pad. The hyperelastic Ogden formulation was initially proposed to describe skin behavior (Spears et al., 2007; Gu et al., 2010a). A recent approach based on a fiber-reinforced hyperelastic model has been provided by the research group led by Natali at the University of Padova (Fontanella et al., 2012; Natali et al., 2012). In their latest study, they analyzed the mechanics of foot skin with a special focus on the orientation and distribution of the fibers that characterize the anisotropic response of the skin (Fontanella et al., 2014).

1.4 Foot model applications

FE foot models provide a vast amount of data, which can be useful in different fields. These applications can be grouped into two main areas: (1) biological and clinical applications and (2) orthosis and footwear design. The former includes physiological analysis, pathological and foot disorder studies and surgical and healing treatment evaluations. The latter involves the design and optimization of orthotic devices, shoe soles and other shoe components. In this section, existing studies are sorted and exposed in a compressive manner to demonstrate the extensive range of studies that have been performed with FE foot models. The type of model and the validation method are discussed.

1.4.1 Clinical applications

Some recurrent topics in clinical applications are as follows: the study of the stress distribution in a gait, the relevance of each structure in the foot arch function, ankle ligaments injuries, car crash impacts, the plantar stress distribution on the diabetic foot, hallux pathologies, plantar fasciitis surgery and the comparison of different procedures for claw toe. Computer foot models that consider partial, total, simplified or geometrically detailed foot structures, which were intended for clinical applications, are reviewed.

1.4.1.1 Physiological studies

Because direct measurements of the stress distribution within the human foot *in vivo* are not feasible, the use of models became necessary. First, studies that discussed and proved the potential of the FE method in the simulation of the mechanical behavior of the human foot are presented.

In 1993, the medial arch of a human foot was modeled to investigate the internal stress pattern. The 2D single bone model presented by Patil et al. (1993a)(Patil et al., 1993b) was intended to calculate the physiological state as a reference to examine and improve the comprehension of foot disorders. The same authors subsequently performed a similar study with an oversimplified 3D two-arch model of a normal foot (Jacob et al., 1996). With a similar purpose, Andrea

et al. (1999) explored the strain distribution of the calcaneus in a 2D sagittal view as guidance for more complex models. Unlike the bony model presented by Patil et al. (1993b), Andrea et al. (1999) included nonlinear properties of the soft tissue. Calcaneal loading was also assessed by Giddings et al. (2000) for walking and running conditions. Their scalable subject-specific calcaneus/foot 2D model was capable of predicting normalized peak forces for the Achilles tendon, plantar fascia and plantar ligament, which exhibited quantitative agreement with the *in vivo* measurements.

Consistent with understanding the biomechanics associated with the normal foot, (Chen et al., 2001) established a preliminary 3D FE model to estimate the stress distribution in the foot from the midstance phase to the push-off phase in a barefoot gait. To simulate the relative movement of the floor with respect to the foot, they constructed a rigid plane to apply a constant linear velocity and an angular velocity that moves toward the foot. Using this floor movement and by immobilizing the upper tibial nodes, they set the loading and boundary conditions from the midstance phase to the push-off phase. A similar objective was achieved by Gefen et al. (2000) in a different manner. They analyzed the biomechanics of the foot structure in discrete events during the stance phase of a gait. They performed an experimental analysis to gather information about both the kinematic and dynamic forces of the foot in a gait, which helped to define the boundary conditions in all phases of a gait by trial and error. Their 3D model considered the nonlinear behavior of the soft tissue. The objective of these studies was to define the stress reference state (baseline case) of the normal foot for both pattern (qualitative) and range (quantitative), which facilitates the identification of high stresses when compare with the stress state of a pathological foot.

After a significant improvement in computational power and tools, geometrically detailed models for exploring the role of the main lower leg muscles in a human gait were developed. Takahashi et al. (2012) investigated the importance of considering the spontaneous plantar flexion of a gait. They performed an experimental measurement of the motion, the reaction force and the contact area of the human foot. Information about the position of the ankle and the displacement of the heel for simulating the Achilles tendon force was given as boundary

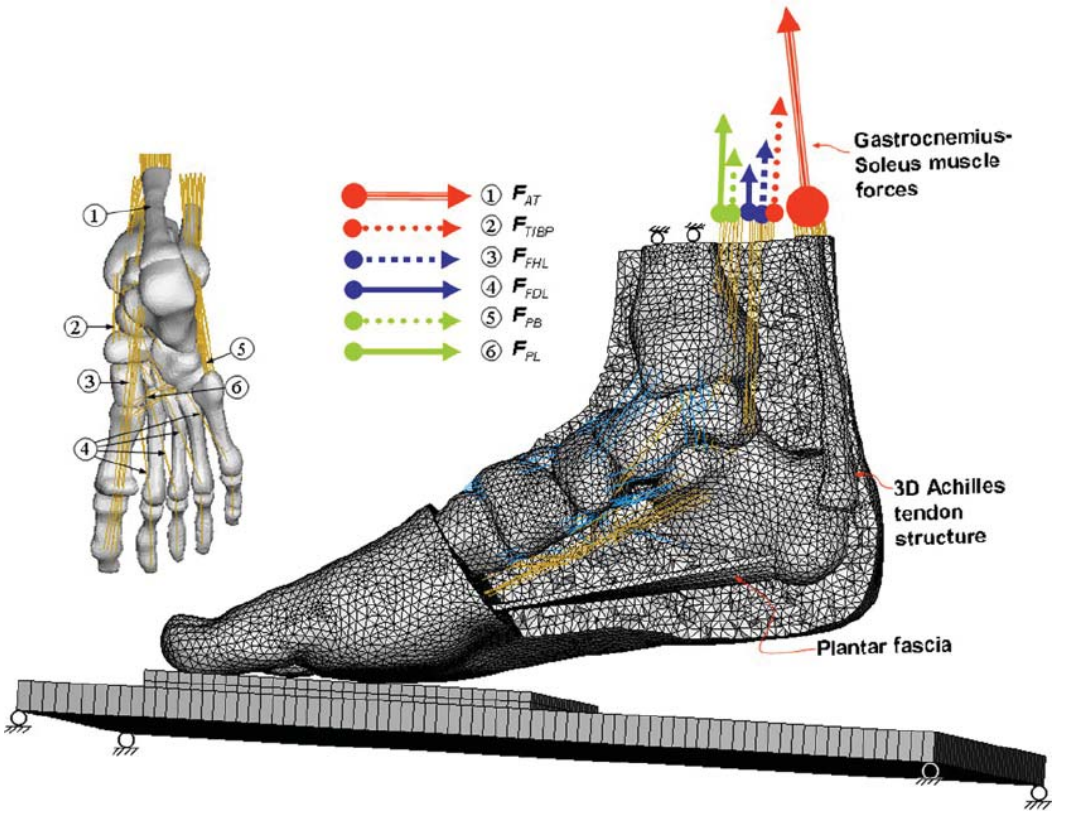

Figure 1.12: Complete foot finite element model including muscle forces with real geometry of Achilles tendon and plantar fascia (Chen et al., 2012).

conditions in their 3D FE foot model. Chen et al. (2012) analyzed the contribution of the gastrocnemius-soleus and other plantar flexor muscles during heel rise. This analysis was performed using a sophisticated FE musculoskeletal model with hyperelastic material properties and real Achilles tendon geometry, as shown in Figure 1.12. The values of the muscle forces and local plantar pressure peaks were compared with *in vivo* experiments, and strains in the second metatarsal were compared with the cadaveric measurements. Another model that addresses the high degree of complexity of the musculoskeletal system of the human foot was proposed by Qian et al. (2010b). A 3D FE foot model that comprises 29 bones, 85 ligaments and the plantar soft tissues was used to study the foot arch and plantar fascia deformations in the midstance phase. In this model, only mus-

cle forces and ankle joint forces acting on the talus bone were utilized to drive the model. A subsequent study that employs this model and a FE hell pad model, which consists of fat cells and a reticular fiber structure, was introduced with the biological coupling theory (Qian et al., 2010a). They examined the biomechanical response of the coupling mechanism of the heel pad (impact attenuation function) and the foot arch (energy absorption function). They suggested that the impact attenuation and energy absorption function of the foot is the coupled result of both subsystems. The muscle-driven simulation was also applied by Spyrou and Aravas (2012). They described a FE scheme for realistic muscle-driven simulation of human foot movements. Their lower leg model was used to estimate internal stresses and strains and shape changes of the deformed tissues during plantar flexion of the ankle.

The dynamic foot response over the entire stance phase was analyzed by Qian et al. (2013). A 2D subject-specific dynamic FE foot model was developed and validated with gait measurements. A sensitivity analysis of the material properties and frictional and damping coefficients was also performed. They suggested the use of dynamic analysis over the quasi-static step analysis to simulate dynamic motions. The greatest challenge in dynamic studies is the computational time. With the intention of reducing the computational cost, Halloran et al. (2009) presented a musculoskeletal model coupled to a FE model of the foot using an adaptive surrogate modeling scheme. The FE model and the musculoskeletal model were directly coupled by sharing boundary conditions at a point in the talocrural joint. With this technique, they were able to study the peak pressure and ankle vertical load as a function of time for the optimal solution to maximum height jumping. In a subsequent study with the same procedure, they predicted a substantial reduction in peak strain energy density in plantar tissue under metatarsal heads, which alters gait patterns (Halloran et al., 2010).Chen and Lee (2015) also employed the technique of combining two models to perform a dynamic study. In this case, a visco-hyperelastic heel and shoe FE model was combined with a spring-dumper-body model to analyze the heel/shoe dynamics during running.

In addition to a gait analysis, the foot arch stability and windlass mechanism

of the Achilles tendon is a frequent topic in the literature. A computational study by Cheung et al. (2006b) explored the relationship between plantar fascia and the Achilles tendon; they determined that an increase in the Achilles tendon load resulted in a reduced arch height and increases in plantar fascia stresses. They also present the fascia as an important arch-supporting structure. This idea was expanded by Wu (2007), who demonstrated that plantar longitudinal arch function is supported not only by plantar fascia and ligaments but also by intrinsic muscles. The FE estimations were validated with plantar pressure measurements, electromyography activity and anatomical experiments. The connection between plantar fascia strain and the Achilles tendon force, which is known as the windlass mechanism, was also computational simulated by Cheng et al. (2008). Their results corresponded with the results of previous studies, which indicated that the plantar fascia strain increased as the dorsiflexion and Achilles tendon force increased. The fascia stress underneath the first foot ray gradually decreased as it moved toward the fifth foot ray. Recently, Lin et al. (2014) developed a 3D dynamic foot model to estimate the stresses in the plantar fascia during the entire stance phase. Kinematic data and ground reaction forces were measured from a healthy subject to validate the model. Sun et al. (2012) analyzed the relationship between different foot arches and stress variations inside the foot. From a standard FE foot model, four models were generated, in which the original arch height varied from a low-arched configuration to a high-arched configuration. In the low-arched foot, high stresses were detected in the rear and midbones, whereas high stresses in the forefoot and fascia were detected in the high-arched foot. The predicted strains and stresses in these studies contributed to an enhanced understanding of the complex foot arch function and may have practical implications in plantar fascia and ligament release interventions.

1.4.1.2 Injuries

For clinicians, understanding the risk of foot injury due to mechanical loading is essential. Biomechanical measurements can provide important information about the total reaction forces but cannot directly assess the internal stress state of the foot. In these cases, the FE method becomes a very useful tool, which can be

used to better understand the mechanical responses of biological systems. This information is valuable not only for clinicians but also for other professionals. For example, in the area of car crash injury, a better understanding of injury mechanisms helps in the design of safety devices. In this context, the study by Beaugonin et al. (1996) (Beaugonin et al., 1997) was framed. The model was initially validated against inversion/eversion and dorsiflexion responses and subsequently applied by Kitagawa et al. (1998) to study tibial pylon fractures in frontal crashes. They studied the combined effect of muscle preloading and external force by applying the Achilles tendon force to the calcaneus while an external impact force was applied to the forefoot. The results were compared with the results from the dynamic impact test in cadaveric specimens. This model was subsequently revised to examine the dynamic response after adding plantar aponeurosis and modeling metatarsal joints (Kitagawa et al., 2000). Ankle skeletal injury under high-energy compressive force was evaluated by Iwamoto et al. (2005). They implemented an anisotropic inelastic constitutive model of cortical bone by considering damage evolution in a lower limb FE model. A parametric study on ankle skeletal injury was performed in terms of footwell intrusion and pedal impact. Beillas et al. (1999), who specifically noted the importance of properly setting (stiffness and position) the ligaments and fat pad, presented a baseline model to investigate car crash injury.

The injury tolerance of the ankle ligaments was examined by Shin et al. (2012). They developed a complete foot and leg FE model to analyze the failure of the ligaments and focused on a range of experimental forces in vehicle crashes. Several simulations for different loading conditions, including forefoot impact, axial rotation, dorsiflexion, and combined loadings, were performed based on previous tests to validate the model. Internal and external ankle rotated postures under brake pedal loading were simulated. Ligament failures were predicted as the main source of injury. Regarding ankle ligament injury, some models were specifically developed and validated with experimental cadaver studies. Such as the case of the computational model developed by Liacouras and Wayne (2007) to assess syndesmotic injury and ankle inversion stability. In addition, the model was also capable of predicting joint kinematics, which were not easily obtained via exper-

iments. The focus of this study was the changes in joint function after repair of a syndesmotic injury by insertion of a fracture staple and the increase in force experienced by other ligaments after transection of the calcaneofibular ligament. Similarly, Liu et al. (2013) evaluated the treatment of inferior tibiofibular syndesmosis injury using a transverse syndesmotic screw. Although that treatment effectively stabilizes syndesmotic diastasis, it decreases the joint's range of motion, and therefore, fixation should not be performed for an extended period of time. Wei et al. (2011a)(Wei et al., 2011b) measured the normal dorsiflexion, eversion, and external rotation of some subjects to drive a 3D multibody computational ankle model, which was employed to study the mechanism of high ankle sprain. The model predicted the strain of the anterior tibiofibular ligament in the motion sequence and a peak strain in the anterior deltoid ligament, which parallel the cadaver studies. They suggested that the posterior talofibular ligament injury caused by excessive levels of external foot rotation is a function of foot constraint and proposed additional studies to design shoes to minimize the injury risk.

Tannous et al. (1996) presented a preliminary study that characterized the foot-ankle complex for axial impact loadings by calibrating it against data tests. This model was used as a basis for developing a 3D lower limb model to investigate impact injury (Bandak et al., 2001). To evaluate the model, they conducted a series of experiments on the impact of a pendulum on a cadaveric lower extremity at various initial velocities. The results indicate that the calcaneus, the tibia and the talus experience the largest amounts of stress. Significant stress was detected in the lateral-collateral ligaments. Instead of ankle ligament injuries, the simulation performed by Gu et al. (2010b) changed the study focus to metatarsal injuries for landing impact. The deformation and stresses in the metatarsals at different inversion landing angles were comparatively evaluated. The results showed that stresses increased in the lateral metatarsals, whereas stresses decreased in the medial metatarsals with increasing inversion angles. It was found that the stiffness of the slip fascia is an important factor in the fifth metatarsal fracture. The stresses in the deep heel (calcaneal tuberosity) during walking were estimated by Spears et al. (2005). They suggested that the plantar heel pain is generally higher when the heel is loaded in an inclined position. Peak internal compressive stresses were

larger than the external plantar pressure. This estimation was calculated with a lower heel FE model with viscoelastic behavior and validated *in vivo* against mean and peak external plantar pressures. A different visco-hyperelastic constitutive model was formulated by Fontanella et al. (2012) to simulate the mechanical response of the heel tissues for different strain rates. Their 3D subject-specific heel pad model also included a fiber-reinforced hyperelastic formulation for the skin, which was a limitation of the Spears' model. Stresses in this region were also dynamically analyzed by Qian et al. (2010a) during barefoot walking and by Chen and Lee (2015) during shod running as previously mentioned.

1.4.1.3 Pathomechanics

A reasonable understanding of feet pathologies and disorders is crucial to determine the best treatment. The plantar stress distribution of a diabetic foot has been extensively and computationally investigated. Patil et al. (1996) simulated muscle paralysis from accidents or diseases such as leprosy or diabetes and its effect on the distribution of principal stresses. A 2D FE model was used to analyze three quasi-static walking phases. The results demonstrated that both the shape of the foot and the type of muscle paralysis contribute to the development of large stresses in different regions of the foot, which may be an important factor in the process of tarsal disintegration in leprosy. A similar study with a 3D two-arch model of muscle paralysis, which is associated with Hansen's diseases, was performed (Jacob and Patil, 1999). Their model predicted areas of the bone that disintegrated due to decreased mechanical strength of the bone in this region. This model was subsequently improved and characterized in a push-off position and performed to evaluate the effect of foot sole stresses on plantar ulcer development (Thomas et al., 2004) by simulating three decreasing thicknesses of foot sole soft tissue in the forefoot region with increasing hardness. FE analyses for the diabetic subject foot models showed that the normal and shear stresses at the foot sole-ground interface increased compared with corresponding values for the control subject with increased hardness and decreased thickness in the foot sole soft tissue in the forefoot region. The authors suggested that these high stresses in the foot soft tissue might be responsible for the development of plantar

ulcers in diabetic subjects. This idea was also supported by Gefen (2003). His results suggested that the process of injury in diabetic feet is likely to initiate in deeper tissue layers especially in the plantar pad underlying the metatarsal heads. The model comprised five planar longitudinal cross-sections through the foot. The total load and muscle forces were distributed by weight in the first ray through the fifth ray. The same hypothesis was analyzed in another study (Cavanagh et al., 2008). The results confirmed the clinical findings: bony prominences, such as the metatarsal heads, served as stress risers. In subsequent years, Chen et al. (2010a)(Chen et al., 2010b) also computationally analyzed this feature of the disease. Their 3D foot model indicated that large stresses occur where plantar soft tissue contacts geometrically irregular bony structures. Thus, the internal stress distribution within the plantar soft tissue was significantly influenced by bony prominences due to the stress concentration, as shown in Figure 1.13. The subject-specific model was validated by comparing the experimental measurements of the plantar pressure distribution and internal plantar tissue deformation. The idea that the internal stress is higher than the surface pressure was explored by Fernandez et al. (2012). They developed an anatomically-based subject-specific foot model that separately considered muscles, bones and soft tissue layers. Using anisotropic properties, they detected maximum internal stress values that were 1.6 times higher than the surface pressure values, which is consistent with the hypothesis that injuries may initiate in the deep tissue structures and may not be detected during in a clinical evaluation.

The effect of the increasing severity of diabetes was investigated by Cheung et al. (2005). They simulated the increasing stages of diabetic neuropathy, in which the soft tissue stiffness increases by 2 to 5 times the normal values. The 3D foot model predicted an increase in peak pressure in the forefoot, midfoot and rearfoot regions and a decrease in the contact area between the plantar foot and the support in the entire foot, which caused an increase in the gravity of the disease (increased soft tissue stiffening). The relationship between soft tissue stiffness and ulceration was also analyzed by Sopher et al. (2011) with a focus on the heel region. The risk of heel ulceration associated with foot posture during bedrest was investigated. Based on the results of the posterior heel FE model, a higher risk of

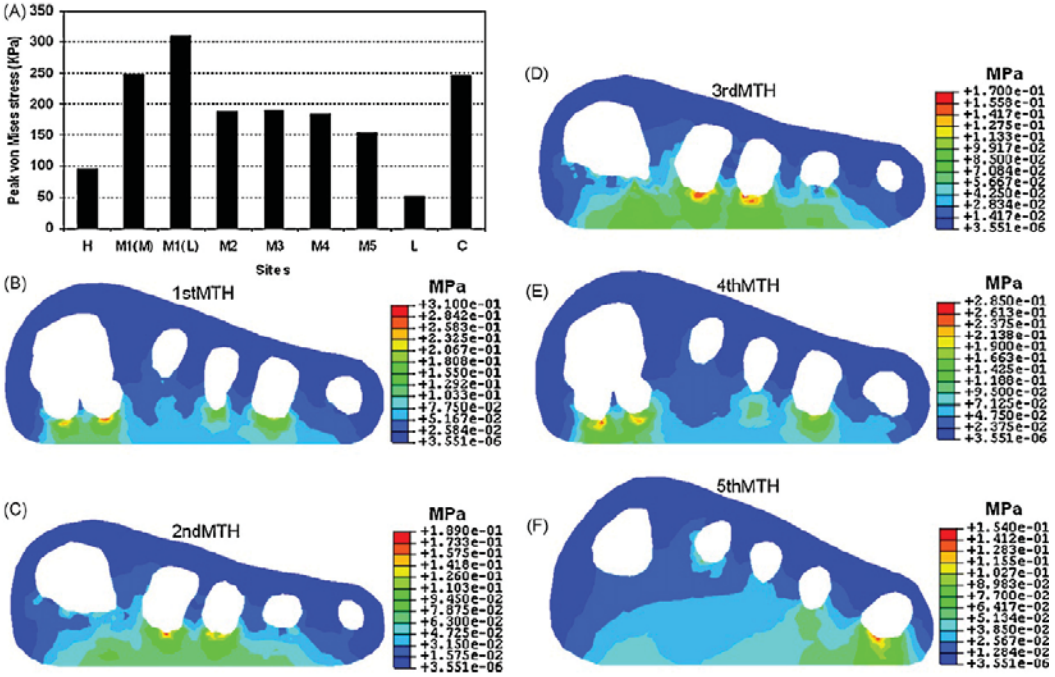

Figure 1.13: Internal von Mises stress at plantar soft tissue under each metatarsal head (Chen et al., 2010a).

heel ulceration was discovered for abducted foot posture compared with upright foot posture. With regard to foot posture, Brilakis et al. (2012) analyzed the effect of foot posture on fifth metatarsal fracture healing. Thirty 3D FE models were compared by considering fracture type, foot posture, and healing stage. No statistically significant differences were observed for different foot postures. An ulcer formation mathematical model was proposed to better understand the bio-chemo-mechanical process of foot ulceration and its progression. In this first step, a two-phase model of soft plantar tissue was applied to a 2D foot FE model to simulate several gait cycles of a healthy foot (Sciumè et al., 2014).

In addition to leprosy and diabetes, other pathologies have also been examined. Budhabhatti et al. (2007) presented a realistic FE model of the first ray used to perform a kinematical study of the late-stance phase of walking. This study focused on plantar pressures underneath the first ray in three different cases: pathology (hallux limitus), surgery (arthrodesis), and conservatory treat-

ment (therapeutic footwear). A metatarsophalangeal joint FE model was also employed by Flavin et al. (2008) to challenge the many etiological theories of hallux rigidus. They postulated an increase in stress of the plantar fascia as the cause of abnormal stress on the articular cartilage instead of a mismatch of the articular surfaces or subclinical muscle contractures. This finding may influence the treatment of early stages of hallux rigidus. Tao et al. (2005) investigated the relationship between hallux valgus and hypermobility of the first metatarsocuneiform joint. Their skeleton FE foot model predicted the plantar and medial displacement of the first metatarsal, which can affect the normal function of the first ray under repeated weight loading of the gait cycle. The same hypothesis was used in a computational study with a more detailed model (Wong et al., 2014). The joint forces at the metatarsocuneiform and metatarsophalangeal joints of two FE foot models (a normal foot and a foot with a hypermobile first ray) were compared. The results suggested that the hypermobility of the first ray increased the loading of both joints and caused them to be predisposed to the risk of joint problems.

1.4.1.4 Surgical treatments

The experimental verification of clinical procedures is frequently lacking. As a supporting tool in experimental cadaveric studies, computational modeling approaches can provide the means to explore different interventional procedures. As in product design, in which the product is modeled after initial trials to save money and time spent on prototyping, these approaches are also applicable in clinical procedures. Surgical interventions can be simulated as a step toward additional analysis to reduce the number of trials required to obtain an effective procedure and to shed light on pre- and post-surgery evaluations that are frequently difficult to quantify.

Several studies about plantar fascia release intervention have been published. This treatment was initially modeled by Gefen et al. (1998). Their five rays FE model estimated a large sagging of the arch and a significant increase in the long plantar ligament. These results were similar to the results of a subsequent study, in which the authors applied more accurate material properties in the model and suggested that surgery may reduce the dynamic shock-absorbing abilities of the

foot and cause additional musculoskeletal damage (Gefen, 2002). This finding is consistent with the predictions of a 3D foot model developed by Cheung et al. (2004). In their study, the biomechanical responses of the foot-ankle complex with different plantar fascia stiffness were quantified. The results indicated that significant stresses are induced in the ligamentous and bony structures when plantar fascia stiffness decreases; non-operative treatment was recommended. In the case of surgery intervention, a partial release of less than 40% of the fascia was recommended to minimize the effect on arch instability (Cheung et al., 2006a). This recommendation was also suggested by Liang et al. (2011); their 3D foot model did not predict total collapse of the foot arch until all four major plantar ligaments were simultaneously sectioned. Unlike the previously mentioned models that validated and compared predictions with plantar pressure distributions and radiologic measurements, Liang and coauthors tested seven fresh adult cadaveric feet to measure the displacement of the four major bone segments and stabilizers of the foot arch and to compare with the FE results. Similarly, Tao et al. (2010) simulated four cases after individual release of the plantar fascia and three major ankle ligaments. Although arch collapse was not predicted after each structure sectioning, a significant increase in tension in the remaining ligaments was predicted. According to these studies, the model proposed by Iaquinto and Wayne (2010) predicted high strains after plantar fasciotomy and identified plantar fascia as the greatest contributor to arch stability.

Several FE studies have been performed to investigate the biomechanics of toe interventions, such the case of the previously mentioned first toe models of Budhabhatti et al. (2007) and Flavin et al. (2008). The first study defined different dorsiflexion fixation angles and compared them with conventional angles to reduce plantar pressures in first ray arthrodesis surgery. Flavin & colleagues addressed the surgical procedure for the treatment of early stages of hallux rigidus. Osteotomy in the first ray for correction of hallux valgus deformity was analyzed by Matzaroglou et al. (2010). Unlike the majority of computational studies, this simulation was performed to confirm the positive long-term clinical results of the 90-degree Chevron osteotomy.

Other toe surgeries that were computationally evaluated entailed the correc-

tion of claw toe. Studies by García-González et al. (2009) and Bayod et al. (2010)(Bayod et al., 2013) presented an alternative technique to the proximal interphalangeal joint arthrodesis for the correction of hammer toe and claw toe deformities. They compared the effectiveness and risks of two recent techniques against the traditional procedure in a complete foot skeleton FE model in the push-off position. Similarly, Isvilanonda et al. (2012) compared the modified Jones procedure with the Flexor Hallucis Longus tendon transfer for the correction of clawed hallux deformity and determined that the most suitable procedure varies depending on the presence or absence of Flexor Hallucis Longus overpull.

FE simulations not only aid in the evaluation of clinical procedures but also quantitatively define guidelines for surgical treatment. For example, Bayod et al. (2012) estimated 1.30 cm^3 as the maximum of harvested calcaneus to prevent the risk of calcaneus fracture after surgery. The estimation was based on a series of calculus where the depth of bone excision and the Achilles tendon force gradually increase, as shown in Figure 1.14. A previously mentioned study recommended a maximum of 40% of plantar fascia release to minimize the arch instability Cheung et al. (2006a). The post-surgical effects of tarsometatarsal joint fusion was evaluated by simulating a normal foot and an operated foot (Wang et al., 2014a). The results that were validated with plantar pressure distribution during three instants of gait showed an increase in the stresses in the second metatarsal bone, which made it susceptible to fracture. García-Aznar et al. (2009) developed a 3D foot skeleton model to evaluate the stress distribution of four different metatarsal configurations, which helped physicians to perform metatarsal osteotomies to adjust the incorrect geometry of the metatarsal bones. Trabelsi et al. (2014) focused their study on the fracture of metatarsal bones to investigate the influence of a distally located drilled hole in the second metatarsal bones, which is a common Hallux Valgus surgical correction procedure. The single metatarsal bone model predictions were validated on a large number of experiments performed on metatarsals bones from different donors.

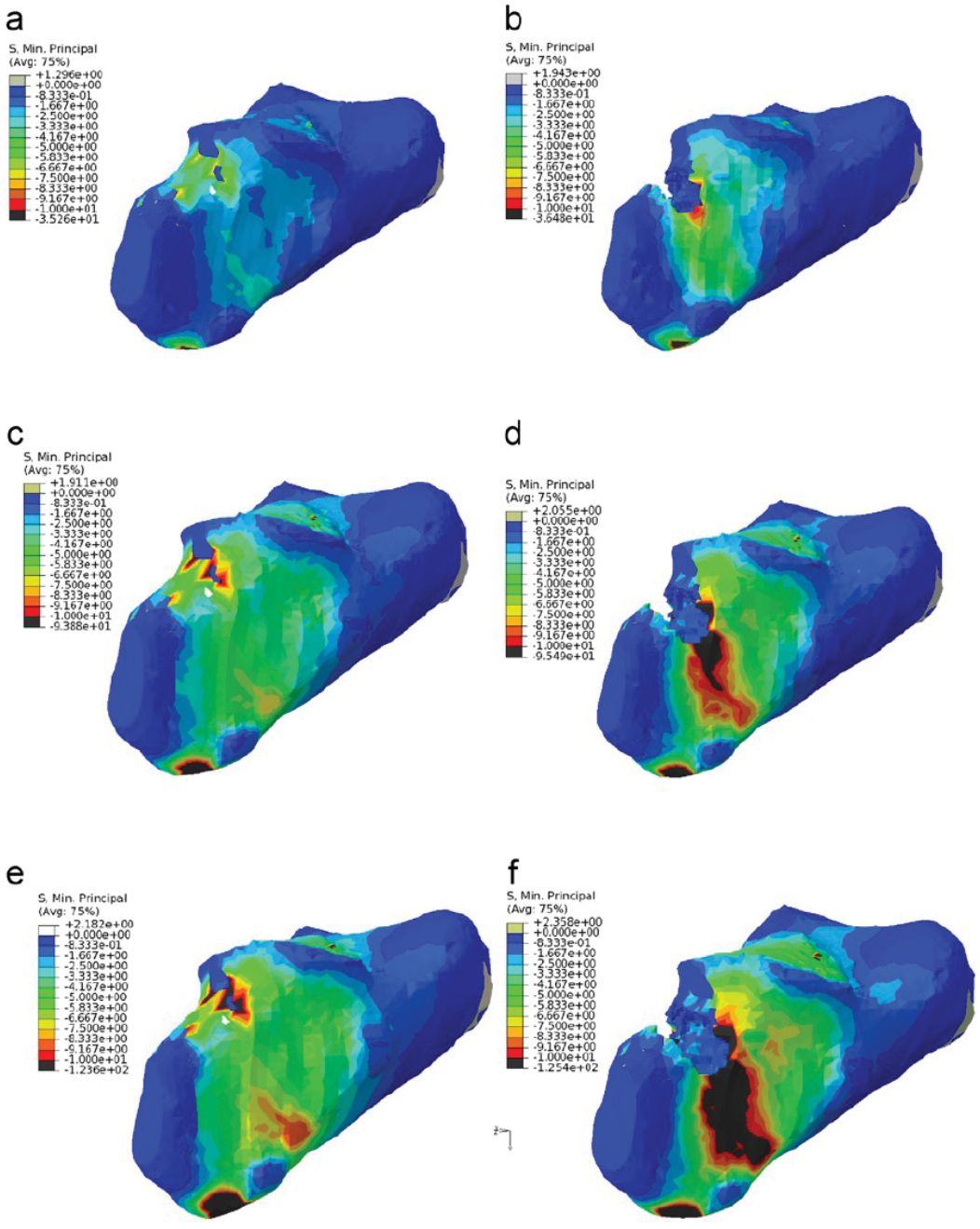

Figure 1.14: Compressive stress in the calcaneus increasing gradually size of bone excision and Achilles tendon force (Bayod et al., 2012).

1.4.2 Orthosis and footwear design

Orthosis design, material and shape, have been extensively explored by FE method as alternative treatments for many foot pathologies; orthosis are preferred to invasive methods such as surgery. The parameters for footwear design are of significant interest to the footwear industry. There is an extensive range of applications, including therapeutic orthosis, insole design, sport footwear, military boots and high-heeled shoes, focused on reducing plantar pressure because pressure on the plantar foot has been associated with perceived comfort and pain generation (Jordan and Bartlett, 1995; Witana et al., 2009).

1.4.2.1 Therapeutic orthosis

Diabetic and Hansen's disease patients are frequently prescribed therapeutic orthosis to relieve elevated plantar pressure and to prevent plantar ulceration. The design of these types of orthosis is based on the experience of the practitioner and adheres to a trial and error process. Numerous studies have been conducted to help researchers to design optimal orthosis for a desirable plantar pressure distribution.

To reduce plantar pressure, some authors focused their research on material properties of the therapeutic orthosis. Despite its limitations, the pioneer FE analysis presented by Nakamura et al. (1981), established the basis for posterior studies. Their 2D idealized foot was designed to estimate the range of elastic properties of the shoe sole that minimized peak stresses within the soft tissue. They performed a simple material test to define nonlinear behavior of the heel soft tissue and a convergence study to establish the method of calculus. Lemmon et al. (1997) also performed a uniaxial *in vivo* test of the heel soft tissue. Data on five subjects were collected using an ultrasound device to measure tissue displacement and a load cell to measure force. The data were introduced in a 2D second metatarsal head model to investigate alterations in pressure under the metatarsal head as a function of insole and tissue thickness. The results predicted that peak pressure in the soft tissue decreases as the insole thickness increases; this effect intensifies with thin soft tissue. Erdemir et al. (2005) also presented a 2D FE model

of the second metatarsal bone to analysis plugs located in the midsole. Thirty-six plug designs were investigated: a combination of three materials, six geometries, and two placements. The results suggested that the placement of plugs based on plantar pressure measurements are more effective for reducing peak plantar pressure. A similar study was performed by Actis et al. (2008). With a 2D second ray FE model, several design variations were examined, with variations such as changes in the number of plugs, plug diameter, distance between plugs, plug height and material properties located in the insole under the metatarsal head. The results demonstrated that customized inserts with softer plugs distributed throughout the regions of high plantar pressure are more effective for decreasing peak plantar pressure than total contact inserts. Unlike these studies, which were focused on the stresses under the metatarsal heads using 2D sagital models, Gu et al. (2011) investigated the properties of the midsole plugs under the calcaneus with a 3D complete foot model. The effect of material properties and the thicknesses and dimensions of the plugs on the plantar pressure distribution during the heel strike phase was systematically analyzed to optimize the design. Another study that evaluates the influence of different material characteristics on the mechanical response of the heel pad region was the computational analysis by Fontanella et al. (2013). A 3D heel FE model with linear orthotropic formulation for bone, visco-hyperelastic formulation for fat, fiber-reinforced hyperelastic formulation for skin and hyperfoam formulation for insole was employed. Different combinations of materials for midsole and insole layers were considered to evaluate the mechanical behaviors of the heel pad tissues at the heel strike in bare and shod conditions.

Other authors, such as Chen et al. (2003), assessed the reduction in peak plantar pressure via stress redistribution using total contact insoles. The results of their FE analysis of total contact insoles against flat insoles showed that the total contact insole redistributes the stresses and decreases the peak pressure in the heel and metatarsal regions. A similar study by Lin et al. (2007) obtained the same conclusion. Total contact insole can significantly offer pressure relief compared with flat insoles in forefoot and rearfoot regions. Lin & colleagues also measured this distinction in experimental tests. Consistent with these results,

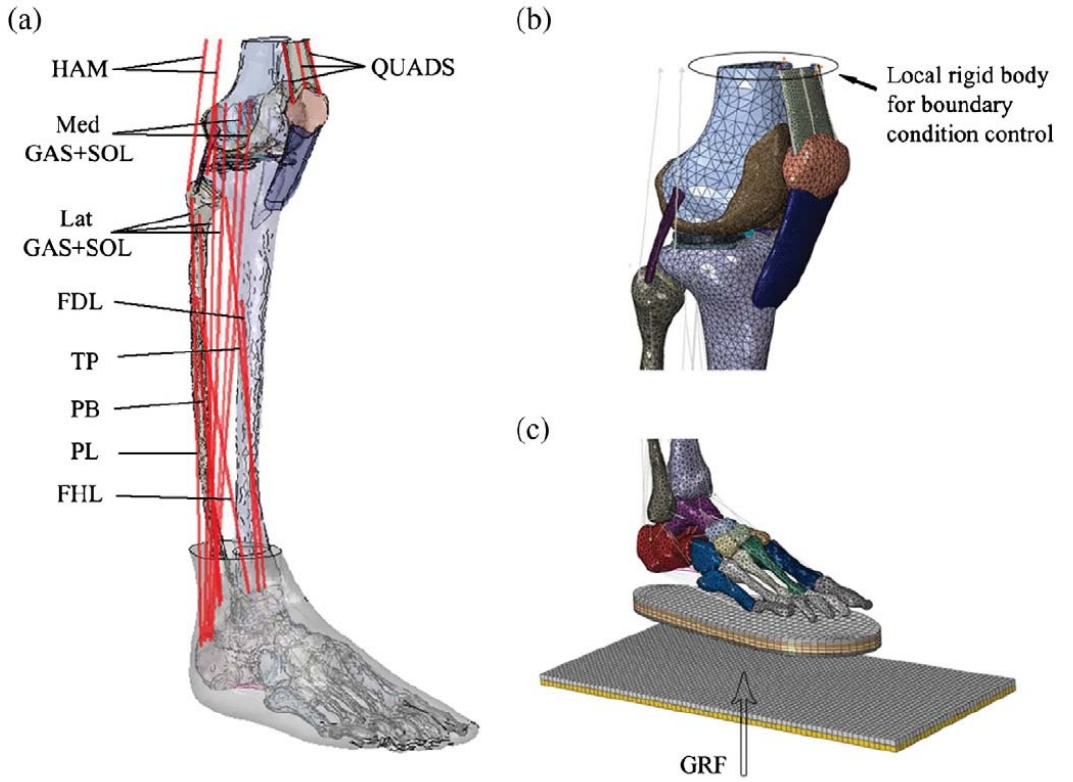

Figure 1.15: Finite element model of the human lower limb to investigate the effects of wedged insoles in femur cartilage and meniscus (Liu and Zhang, 2013).

Cheung and Zhang (2005) specifically focused their investigation on the effect of the custom-modeled shape vs stiffness of the material insole for peak plantar pressure reduction. The 3D FE analysis indicated that the insole's custom-molded shape is more important for reducing peak plantar pressure than the stiffness of the material from which it is constructed.

Liu and Zhang (2013) recently developed a 3D FE model of the human knee-ankle-foot complex with orthosis to investigate the effect of lateral wedged insoles on the internal loading distributions in the knee joint, as shown in Figure 1.15. The results of this lower extremity model suggest that the lateral wedged insoles can redistribute the knee internal loadings and relieve stress at the medial compartment of the knee. Other types of therapeutic orthosis have also been

examined. A simple 3D model of a foot coupled with ankle foot orthosis was developed by Chu et al. (1995). This early 3D model was intended to confirm the peak stress position in ankle foot orthosis. They concluded that the stress distribution in the orthosis is dependent on patient body build and is distinctly asymmetric. They also confirmed the hypothesis that high stress concentration occurs in the neck and heel regions of the ankle foot orthosis, which is a common fracture point (Chu and Reddy, 1995).

1.4.2.2 Insole design parameters

Therapeutic footwear has been proven to be effective in plantar pressure relief. Goske et al. (2006) focused their research on the parameters of insole design. A plane strain heel-pad FE model was created to investigate the effect of three insole design variables (conformity, thickness, and material). The comparison of the 27 designs (combination of three levels for each variable) indicated that the full-conforming insole design provided the largest reduction in heel pressure, whereas material selection had a minimal effect. A sensitivity analysis of five design factors of foot orthosis was subsequently performed by Cheung and Zhang (2008). Their statistics-based FE analysis revealed arch-conforming foot orthosis and softer insole material as the most important factors for peak pressure reduction. Other design factors, such as insole and midsole thickness and midsole stiffness, played less important roles. To assess these effects, FE foot models with 16 different orthosis configurations were constructed. Regarding the insole shape, Hsu et al. (2008) implemented an optimization analysis to determine the optimal insole that minimized the junction stress between the plantar fascia and the calcaneus. They defined the von Mises stresses between the plantar fascia and the calcaneus as the objective function. The optimal resulting insole did not make complete contact with the foot plantar surface compared with the total contact insoles that were previously proposed. The symmetric heel FE model presented by Luo et al. (2011) was developed to compute the stresses on the surface and within the plantar soft tissue under the calcaneus. They concluded that, the peak pressure near the calcaneus and on the skin surface should be reduced in the design of optimal insoles. These four cited studies were validated by comparing the plantar pres-

sure predicted by the FE analysis with the plantar pressure measurements of the volunteers.

FE models of foot and footwear were also developed to evaluate the design of the soles. Using reverse engineering to construct the actual rocker sole, Lin et al. (2013) estimated the effectiveness of the sole design to transfer the high pressure from rearfoot and forefoot to the arch region of the foot. These simulations are very useful for footwear companies, which can assess the biomechanical effect of their products without prefabricating samples and repeating subject trials. A review of footwear models for industrial applications was presented by Cheung et al. (2009). They summarized in a table the FE software, the geometry and number of elements, the material properties and boundary conditions, the parameters of interest and the type of validation process in numerous FE models that were published in the scientific literature until 2008.

1.4.2.3 Footwear for impact attenuation

Another interesting area in which FE models have been employed is the analysis of foot impact attenuation caused by the heel and the shoe for different activities. The most common impact on the human foot occurs during running. Verdejo and Mills (2004) conducted a study to evaluate the fatigue of the foam used in running-shoes midsoles and the possible cause of running injuries. They developed a 2D heel/shoe model to analyze the synergy response. Both materials were simulated with Ogden hyperelastic properties. Pressure distribution experiments on runners were performed to validate the analysis and to monitor changes in shoe cushioning. The peak plantar pressure was doubled after a 500 km run. A similar study also analyzed this overuse of sport shoe foam. Even-Tzur et al. (2006) used a lumped system and FE models to evaluate heel pad stresses and strains during running. In this case, a 3D half heel model considered the viscoelastic behavior of the heel pad and foam. The results showed that peak heel pad stresses were more sensitive to loss of foam thickness than to degradation in its viscoelastic properties. Peak heel pad stresses were consistently lower for running with shoes versus bare feet, even when properties of the foam were degraded. Cho et al. (2009) introduced a 3D foot-shoe FE to evaluate the requirements of court sports shoes. They

described the problem as the landing impact attenuation that accompanies every sport. The proposed model involved a detailed footwear simulation with complete contact interaction between the internal face of the shoe and the foot, at the expense of disregarding the majority of the singularities of the complex internal structure of the foot. These two independent meshes facilitated the individual prediction of the dynamic response of the foot and the sport shoe . The same concept was presented by Qiu et al. (2011). They developed a 3D coupled foot-boot FE model that focused on parachute landing impact; however, this model requires complete validation under static and dynamic loading conditions. The combination of the five rays as a whole for the sake of simplification was applied by Dai et al. (2006) to investigate the effect of socks during walking. A foot-sock-insole contact FE model was employed to perform three dynamic simulations: a barefoot condition and two sock-wearing conditions. They concluded that shear force can be reduced by wearing the sock due to low friction against the foot skin and high friction against the insole compared with the opposite combination. This simplification of the foot without any detail of its inner structure has also been applied in other simulations with a highly demanding interaction of the outer layer, such as kicking a ball (Ishii et al., 2014) or walking on mud substrate (Bates et al., 2013).

To investigate the effect of the confinement of the heel on internal fat pad stress, Spears et al. (2007) performed a 2D FE model of the heel pad using either homogeneous or composite material properties (fat pad and skin). Based on the results, they suggested that the external confinement due to the heel counter of the shoe functions similar to skin walls by providing external pressure to the heel pad. They also noted that the natural load dissipation mechanism of the skin is sufficiently effective for reducing fat pad stress and that the confinement may be undesirable.

1.4.2.4 High-heel studies

In addition to the design of sport footwear for high-performance athletes or military boots, current female trends of wearing high-heeled shoes, which affect the biomechanics of the foot, also concern researchers. Gu and Li (2005) were the

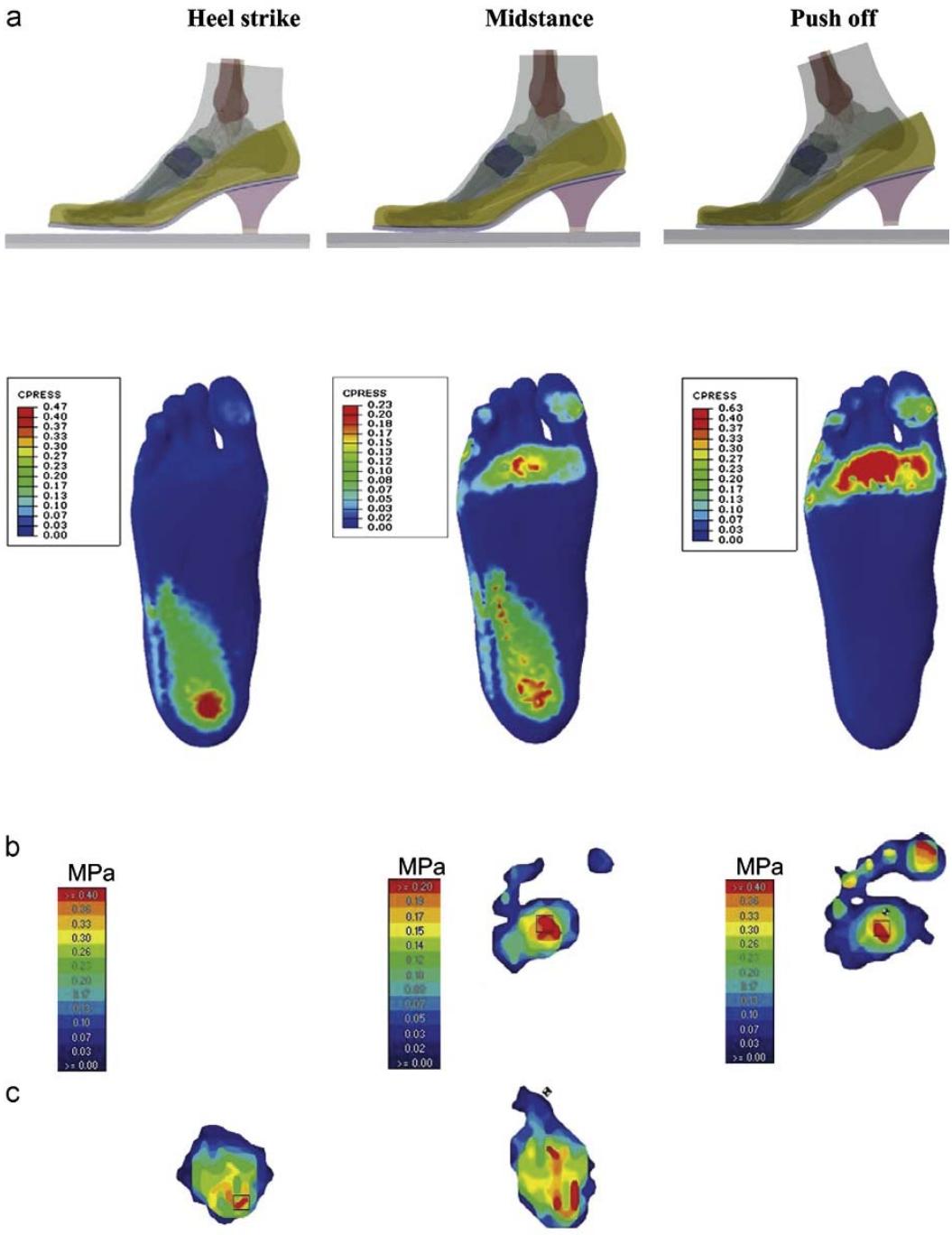

Figure 1.16: Plantar pressure distribution predicted and measured from a female wearing high-heeled shoes (Yu et al., 2013).

first authors to analyze the biomechanical effect of walking with high-heeled shoes by the FE method. They simulated the high-heeled gait and the flat-shoe gait with a 2D sagital model; the results showed larger stresses in the metatarsus and plantar aponeurosis for the high-heel case. A more elaborated model was subsequently presented by Yu et al. (2008). They developed a 3D anatomically detailed model of the female foot with a high-heeled support. In this preliminary study, they compared experimental measurements with FE predictions of plantar pressure for flat- and high-heeled conditions for the same volunteer. In a subsequent study, they measured the plantar pressures of twenty-four female volunteers for three heel elevations by applying four different weight-bearing conditions. The average pressure in these measurements was calculated and compared with four different heel elevation FE models (Luximon et al., 2012). In both studies, the pattern of load transfer from heel to forefoot was predicted; however, the point-to-point correspondence in the pressure distribution was not achieved. Both the experiment and the model indicated a nonlinear relationship from flat support to high-heeled support. A better match was accomplished when the model was donned with a real high-heeled shoe. This recent coupled foot-high-heeled-shoe FE model was employed to simulate the three major stance instances, as shown in Figure 1.16, which enable the prediction of not only the bone and joint stresses during shod walking but also the confinement foot pressure (Yu et al., 2013).

1.5 Topic interest over the years

The objective of foot FE studies has evolved over the years. This evolution is depicted in Figure 1.17. The first studies in the 1990s were focused on the physiological behavior of the foot. Estimations of the stress distribution in a normal foot during gait in different stance phases were habitual objectives of 2D models with strong simplifications. These papers attempted to establish the basis of foot simulations; although the majority of the results were not compared with experimental measurements, the potential application of foot FE models was recognized. In subsequent years, a number of papers about car crash injuries in the foot and ankle were published. These models were validated by comparing the

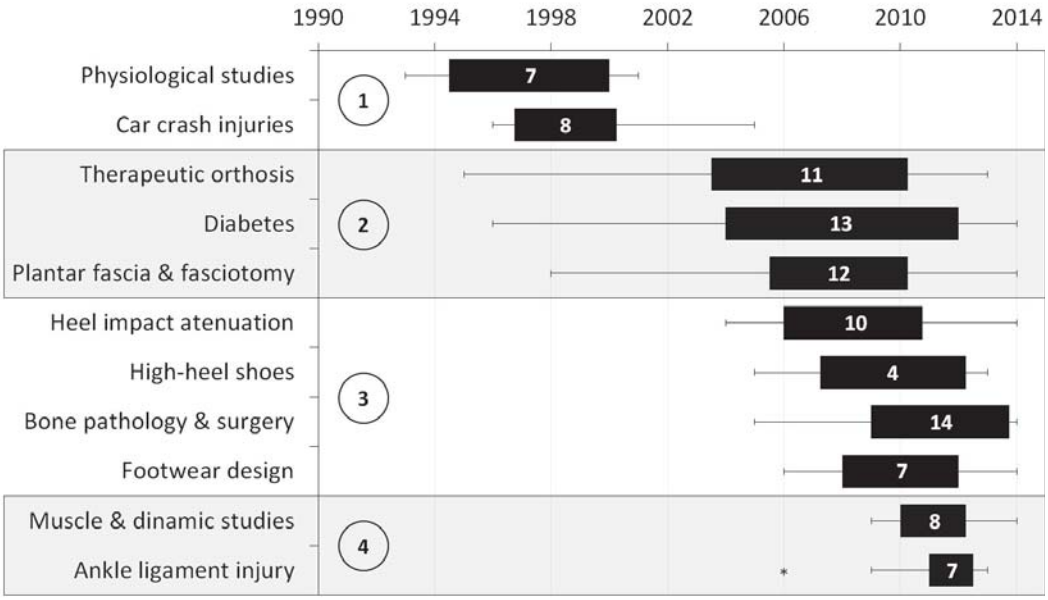

Figure 1.17: Boxplot of the years of publication of computational foot models in different topics. Four different periods are distinguished: (1) first studies, (2) recurrent topics, (3) new topics boom 2005, (4) latest topics. The numbers over the boxes means number of papers published in that topic. Asterisk represents an outlier.

FE predictions with the results of impact tests. Studies of specific topics, such as therapeutic orthosis and clinical application studies about diabetic foot and plantar fascia became prevalent. The three topics are directly related to plantar pressure under metatarsals heads and heel regions and have been continuously analyzed via modeling over the last 14 years. In these cases, the plantar pressure predicted by the FE models was compared with the experimental measurements of plantar pressure. With this background and the maturity of the computational simulation field, new topics emerged. In 2005, researchers began to focus on more concrete applications. New branches within the following main areas were developed: clinical applications and footwear applications. In the first field, many studies of the pre- and post-surgery evaluation of bone and fascia surgeries were reported. The impact absorbing function of the heel pad were completely explored, in bare feet and coupled with footwear. The new branches of footwear

focused on the biomechanics of the high-heeled gait and insole design, which were particularly oriented to sport footwear and military boots. These models are characterized by 3D detailed geometries of complete feet or partial and/or 2D models with nonlinear properties. The conclusions of these studies were much more practical with better validation processes. A better understanding of other soft tissues, in addition to fat (muscle/tendons and ligaments), was the objective of recent studies. Features of these components have been introduced in the models using more refined approaches. Dynamic studies of the foot have also been performed in recent years.

1.6 Computational challenges in foot modeling

No model is capable of realistic simulation without simplifications. Even with advances in computational simulation, assumptions at some level are necessary. These simplifications have evolved with advances in technology, such as computational capacity and numerical techniques, with the need to balance the geometry with the material properties and boundary conditions. In current foot FE models, some common simplifications are frequent. Simplifications in the geometry, such the fusion of phalanges joints, the representation of tendons and ligaments as truss elements and the simulation of the cartilage as a connecting tissue and disregarding its contact feature, are common in extremely demanding boundary condition models. When many nonlinear formulations are included in the model, simplified or partial foot shape 3D and 2D models are employed. When an accurately detailed full foot is modeled, cortical and trabecular bones are not differentiated and all tissues are simulated as linear elastic, with the exception of soft tissue that surrounds the skeleton, which is defined as bulk fat tissue with hyperelastic properties.

Regarding the discretization in foot FE simulation, the majority of the models employed a tetrahedral mesh, which is easier to automatically generate. The creation of an alternative hexahedral mesh is significantly more laborious in complex geometries, such as the foot structure, which requires user intervention. Although advances in automatic hexahedral meshing can reduce this time-intensive task

(Lievers and Kent, 2013), the tetrahedral mesh fits better in irregular geometries, where hexahedral mesh cannot be detailed with a reasonable element size. Models composed of hexahedral meshes are generally preferred; however, the literature about numerical modeling in biomechanics is inconsistent in this regard. A comparative study of tetrahedral and hexahedral FE meshes of a femur bone concluded that tetrahedral elements enabled results that are similar to the theoretical results and the use of second-order elements did not produce significant differences (Ramos and Simões, 2006). Conversely, a similar study that compared soft tissue contact with hyperelastic properties yielded better performance with linear hexahedral elements; however, quadratic tetrahedral mesh was qualitatively similar and may be a reasonable alternative because tetrahedral mesh generation is a highly automated process (Tadepalli et al., 2011).

Based on the analyzed subject, some studies were unable to obtain reliable experimental data to compare the results of the simulation. In these cases, a comparison of the results with other computational models may help to determine whether the results fall within a reasonable range. This comparison is a controversial issue. Unlike comparisons with experimental data, the comparison of computational results is highly dependent on the assumptions and conditions imposed in each model. Therefore, this information should be considered in the comparison of FE results. Instead, a discussion of the conclusions from the simulations is highly recommended.

To assess stresses in foot tissues, the values of von Mises stresses are frequently listed in the literature. The von Mises stress is a criterion of failure for isotropic and ductile materials. In tissue engineering, this criterion can be useful to predict pain in a component in total terms; however, maximum principal strain criterion is preferred to predict fracture (Schileo et al., 2008). The use of von Mises stress is also inaccurate for the comparison with experimental measurements because this criterion converts the complex stress state to a single scalar numerical value. For tissues, the maximum and minimum principal stress values enable computational and experimental comparisons.

1.7 Motivation

The main motivation of this Thesis is to advance towards a more refined computational simulation of the foot in order to provide realistic and meaningful information for clinical practice. The science of medicine has evolved through history by the trial-error process usually pushed by the necessity of a solution rather than evidence of improvement of the treatment. In that way, the mechanical engineering can help in the process of refinement of the medical technique adapting the engineering tools to clinical problems.

Within all branches of medicine, this Thesis is focused on foot biomechanics; orthopedic, treatment and surgery. Specifically, a computational foot model is developed to better understand foot biomechanics, to predict the performance of new therapies and to estimate the value of certain parameters that are not feasible to measure with experimental methods. Advances in foot modeling will provide useful tools for clinical assessment reducing cost and held hazards.

Medicine and engineering fields increasingly collaborate to analyze biological systems. This new interdisciplinary area is a promising field to face future challenges and solve complex problems that are to come. One of these challenges is the so-called personalized medicine. With advances in computational capacity and improvements in patient-specific model generation, it will be possible to create computational models for each patient with sufficient precision and in a reasonable time to help in the decision making process of the treatment.

Although reaching this level of modeling seems to be distant, the pace of advances in foot computational modeling since the first models appeared encourage to believe that could be possible, as has been shown in this chapter. Therefore, this Thesis seeks for advance in the computational simulation of human foot, analyzing the current limits and achieving improvements to apply in actual medical problems.

1.8 Objectives

Based on the arguments above, the objective of this Thesis is to adapt the engineering tools to the clinical practice, being able to analyze the 3D mechanical response of the foot-ankle complex and orient the result to practical cases. In particular, the steps to be taken are as follow. Firstly, identify the current boundaries of the computational foot simulation to draft a roadmap of next milestones to improve foot FE modeling. Secondly, conduct a series of experiments to characterize foot soft tissues, such as tendons and plantar sole. Thirdly, reconstruct the geometry of the internal foot structure and generate a detailed FE mesh. And, finally, apply such improvements to actual clinical problems. With this purpose, the main work and their partial objectives presented in this Thesis are itemized below:

- Identification of the key factors of foot biomechanical simulation. Based on an in-depth review the foot computational modeling and analyzing the limitations of a previous developed foot model, the guidelines for next generation of foot FE models will be draft.
- Determination of the structural and material properties of foot tendons. Tendons will be dissected and tested in a material testing machine performing uniaxial tensile tests to obtain the load-displacement and stress-strain curves of all tendons within the foot except Achilles tendon.
- Mechanical characterization of foot tendon tissue. Different constitutive models will be adjusted to chose the most appropriate simulation of foot tendon tensile response.
- Differentiation of the compressive response of the plantar sole as function of the location. Foot plantar soles will be indented in different locations to obtain its mechanical response.
- Mechanical characterization of the subcalcaneal and submetatarsal plantar soft tissue. The parameters of different material models will be fitted to simulate the rear and forefoot plantar soft tissue behavior.

- Development of a foot FE model with detailed geometry of the internal components. Foot CT and MRI will be used to reconstruct the internal and external structure of the foot. Then, a refined mesh will be created to include all the singularities of the inner foot structure.
- Inclusion of non-linear properties for all soft tissues. Non-linear properties will be applied to tendon, muscle and plantar sole, based on the parameters previously fitted and parameters optimized found in the literature.
- Application of all the improvements to practical clinical problems. At the time that the model is refined, the advances will be applied to particular cases in different fields. The applications reach clinical pathologies, physiotherapeutic treatments and sports injuries as example of the possibilities of the model.

1.9 Thesis outline

The Thesis is organized in seven chapters. A graphical summary of the Thesis content is schemed in Figure 1.18. Each individual chapter has an objective, which follows the primary goal of the Thesis and is focus on a practical-medical application incorporating the advances described in the chapter. More specifically the work is structured as follows:

- In chapter 1, an in-depth review of the current use of FE models to study of foot biomechanics is presented. The review includes 2D and 3D, detailed and simplified, partial- and full-shape models of the lower limb, ankle and foot. Practical issues in computational modeling, tissue constitutive model approaches and pioneering applications are extensively discussed. Recent challenges in the field of foot computational simulation are outlined.
- In chapter 2, an skeletal foot model is exploited to explore its limits. The model is used to analyzed the influence of the proximal phalanx of the hallux as a potential skeletal parameter of the etiology of the hallux valgus. Ten different models are configured corresponding to five percentiles for males

(0, 25, 50, 75, and 100 %) and five for females. After the clinical discussion the features of the model are explained. This work is used to highlight the guidelines of the future improved model.

- In chapter 3, uniaxial tensile tests are performed to obtain the stress-strain curve of the main intrinsic and extrinsic human foot tendons. Cross-sectional area, load and strain failure, Young's modulus and ultimate tensile stress are reported for different clinical and engineering applications. The data obtain from the experiments is used to fit the parameters of a hyperelastic constitutive model for foot tendon tissue.

- In chapter 4, a complete detailed 3D foot FE model with actual geometry and non-linear behavior of tendons is developed from CT and MRI differentiating cortical, trabecular, tendon, muscle, cartilage and fat tissues. The model performance is evaluated against *in vivo* and *in vitro* measurements. Two applications are developed; a tendon force sensitivity analysis of the five major stabilizer tendons and a quasi-static analysis of walking midstance phase.

- In chapter 5, the compressive response of the bilayer plantar sole (adipose tissue and skin) is characterized by regions. Fifteen indentations along the plantar sole are performed to compare the stress-strain curve of the four regions of the plantar sole: rearfoot, midfoot, forefoot and toes. The average mechanical response of the subcalcaneal and submetatarsal soft tissue is characterized with a non-linear material model.

- In chapter 6, the foot model with detailed soft tissue geometry developed in chapter 4 is updated with the non-linear material models of the plantar sole fitted in chapter 5 and with optimized parameters found in the literature. The model is configured to study the impact absorption mechanism of the foot at different strike patterns.

- In chapter 7, the main conclusions of the Thesis sorted by areas of knowledge, together with a brief summary of the original contributions and future research lines are presented.

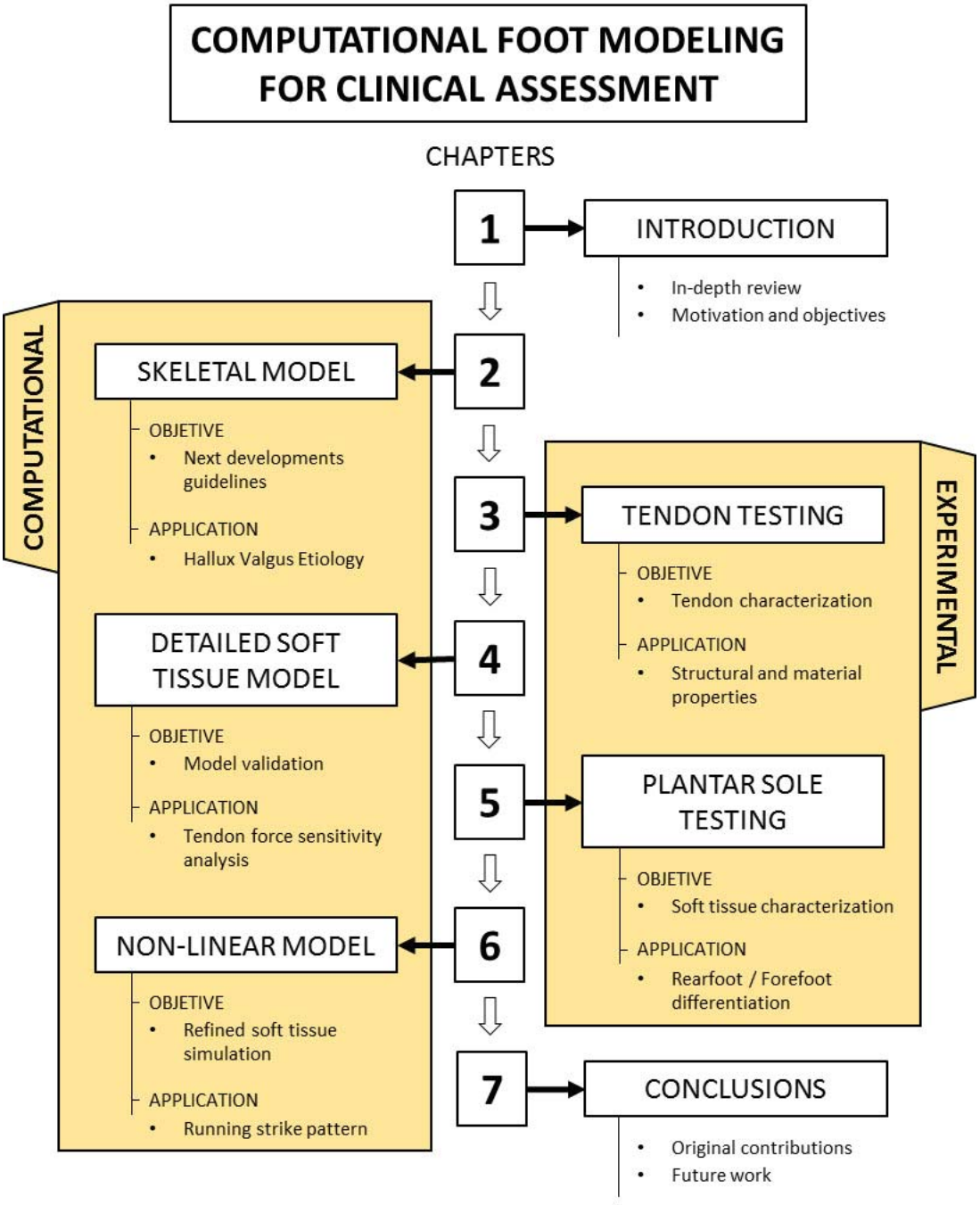

Figure 1.18: Thesis outline.

CHAPTER

TWO

SKELETAL FOOT FINITE ELEMENT MODEL FOR BONE RELATED STUDIES

In this chapter the limits of a skeletal FE model are explored and the potential improvements for future models drafted. In order to do that the model is used to study a bone related pathology. Particularly, the influence of the proximal phalanx of the hallux (PPH) is analyzed as a potential skeletal parameter of the etiology of the hallux valgus. Hallux valgus is one of the most common forefoot deformities which occurs primarily in elderly women. It is a complex disease without a clearly identifiable reason for its higher prevalence in women compared with men. With the geometric data of the PPH provided by surgeons ten representative PPHs for both genders are selected, corresponding to five percentiles for males (0, 25, 50, 75, and 100 %) and five for females. These ten different PPHs are modeled and inserted in ten foot models. Stress distribution patterns within these ten PPH models were qualitatively compared. In the ten cases analyzed, tensile stresses are larger on the lateral side, whereas compressive stresses are larger on the medial side. The bones of males are larger than female bones for each of the parameters examined; however, the mean difference between lateral and medial sides of the PPH (mean $\pm$SD) is larger in women. Also the shallower the concavity at the base of the PPH, the larger the compressive stresses predicted.

Internal forces on the PPH, due to differences in length between its medial and lateral sides, may force the PPH into a less-stressful position. The geometry of the PPH is a significant factor in hallux valgus development influencing the other reported skeletal parameters and, thus, should be considered during preoperative evaluation. Clinical assessment should evaluate the first ray as a whole and not as isolated factors. After the clinical discussion the features of the model and the further developments are explained. The study of the hallux valgus presented in this chapter has been published in "Medical & Biological Engineering & Computing" (Section 7.2.1 — Publication 2).

2.1 Introduction

As it has been shown bone orthopedics is the area in which more computational studies have been focused. This is due to the similarities with the origin of the method. FE method was originated to study structural performance of human made designs, specifically at the beginning, civil and aeronautical engineering. Nowadays the method has been extended to much wider applications such as biomechanics.

Within the biological tissues, bone is the tissue more similar to the engineering materials, given its structural function. Its inorganic base provides higher stiffness and lesser nonlinearity than the rest of the biological tissues. First attempts in the area of biomechanics using FE method were related to the bony structure. Big bones performance were simulated during seventies and it was not until eighties when appeared the first foot model (Nakamura et al., 1981). Those models were characterized by the absence of soft tissue. Later, with the development of constitutive models for rubber-like materials soft tissues were included.

It is reasonable, therefore, beginning the analysis of the features of foot FE modeling with a foot skeletal model. A previously developed foot FE model is initially used to evaluate the capacities of this kind of models and to pinpoint the important factors of foot simulation for future developments. The model consisted of 28 bones (talus, calcaneus, cuboid, navicular, three cuneiforms, five metatarsals, five proximal phalanges, four middle phalanges, five distal phalanges

and two sesamoids), the respective intraarticular cartilages, nine ligaments (posterior talo-calcaneal, calcaneus, navicular, tarsometatarsal, and intermetatarsal, lisfranc, calcaneal cuboid-calcaneus-navicular, plantar), the flexor tendons and the plantar fascia (Figure 2.1).

This model has been previously employed to study bone internal stresses of different pathologies and surgeries in midstance and toe-off position. In the first study, the model was developed to compare the biomechanical response of different metatarsal geometries. The stress-strain distributions during the stance posture of four different cases were evaluated (García-Aznar et al., 2009). In a subsequent study, the model was adapted to toe-off position and it was focus in the surgery of claw toe deformity. Three FE models were developed to compare the biomechanical outcome of each method (García-González et al., 2009). After that, a comparative analysis of three clinical techniques and the pathological case was performed with the aim of extracting advantages and drawbacks of each procedure (Bayod et al., 2010). In midstance position, six different cases were developed to investigate the effect of progressive bone removal from the calcaneus onto the mechanical stress redistribution of the foot, and therefore, on the increase in fracture risk (Bayod et al., 2012). Finally, the most recent study carried out with this model was focused on the potential risks of metatarsalgia or stress fracture for patients after surgery of hammer and claw toe correction (Bayod et al., 2013). In all those studies, comparison of different bone stresses scenarios were investigated.

The main features of the current skeletal model are: the independent cortical and trabecular bone segments, differentiating their material properties and the detailed mesh of phalanges and forefoot joints. To explore the limits of the model and draft the potential improvements, the model was adapted to study a case of clinical interest. Considering the characteristic of the model, a bone related pathology is studied, particularly the hallux valgus deformity. This pathology is chosen for two reasons. Firstly because hallux valgus is a forefoot deformity with high incidence in the adult population which arose interest for clinicians and secondly, because exploit the model features, the refined mesh of the forefoot.

Three studies have studied previously the hallux valgus pathology with the

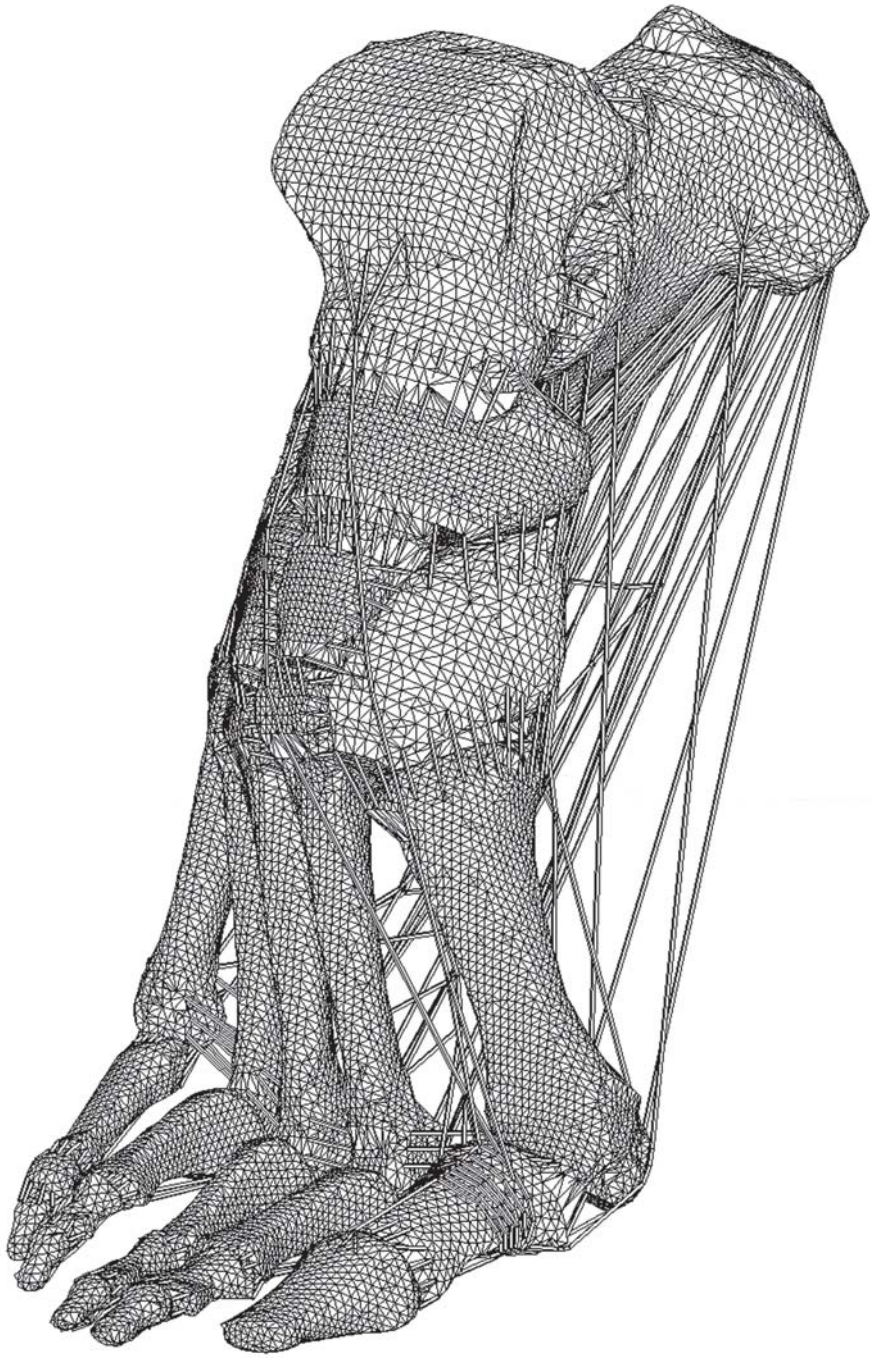

Figure 2.1: Lateral view of the finite element model of a human skeleton right foot. The model was reproduced in toe-off position, forming a 90^o angle between the metatarsals and phalanges.

FE method. The first study analyzed the influence of ligament laxity on the metatarso-cuneiform joint of the first radius in the development of the pathology (Tao et al., 2005). Then, Matzaroglou et al. (2010) compared the Chevron osteotomy at 60^o and 90^o as a treatment for hallux valgus. Finally, Wai-Chi Wong et al. (2015) recently explored the functional restoration and the risk of non-union after first metatarsocuneiform arthrodesis which is one of the surgical interventions to correct hallux valgus.

This chapter explores the limits of the current foot skeletal model examining a skeletal parameter as a potential etiologic factor in the hallux valgus. From data of the geometry characteristics of the PPH, obtained by cadaveric dissection, ten different PPHs are modeled and inserted in the model creating ten different models. The stress distribution of each configuration is compared and the clinical consequences are discussed. This work permits to identify the limits of the current skeletal model and helps in the definition of guidelines for next improvements of the model.

2.2 Hallux valgus deformity

Hallux valgus is one of the most common forefoot deformities, occurring more frequently in elderly women (Nix et al., 2010). The symptoms associated with hallux valgus are well known (Figure 2.2) and can be summarized as (Coughlin, 1984):

- Lateral deviation of the big toe: Deviations greater than 15^o are considered pathological.
- Increased angle between the first and second metatarsal: the anatomical angle is 10^o in a pathological foot can reach 30^o.
- Bunion: It is the bony bump formed at the metatarsophalangeal joint.
- Dislocation of the sesamoids: This occurs as consequence of the first metatarsal deviation.

Figure 2.2: Forefoot anterior-posterior radiography of an hallux valgus patient.

- Muscle dysfunction: The hallux adductor becomes flexor and the flexors becomes abductors.

These changes do not always correlate with each other, nor do they have the same intensity, rendering hallux valgus a complex disease. In fact, there are more than 130 surgical procedures for the treatment of hallux valgus which can be divided into soft tissue procedures, osteotomies, arthrodesis, arthroplasties, and combined procedures (Helal, 1981).

Hallux valgus is considered a deformity of multifactorial origin, primarily attributed to the use of footwear (Sim-Fook and Hodgson, 1958; Kato and Watanabe, 1981), genetic conditions (Johnston, 1959), and gender (Wu, 1987). Additional factors also include metatarsus varus (Hardy and Clapham, 1951), ab-

normal length of the metatarsus (Lundberg and Sulja, 1972) or abnormal shape of the metatarsal head (Mann and Coughlin, 1981), action of the foot muscles (Shimazaki and Takebe, 1981) and foot pronation (Root et al., 1977).

Despite a large number of studies on this subject, the underlying cause of this deformity remains unclear. Even the use of footwear (commonly regarded as the primary suspect in hallux valgus pathology) has not been confirmed as a cause. Barnicott and Hardy (1955) measured the angle of the first metatarsophalangeal joint in Nigerians who had never worn shoes and compared it with age-matched Nigerian soldiers who wore army boots. They found no significant differences in the angle of the metatarsophalangeal joint between the shod vs. barefoot population. However, a significant difference was observed between men and women.

Using radiographs from pathologic vs. non-pathologic male and female patients, several studies have focused on the skeletal parameters influencing hallux valgus. Excessive length of the first metatarsal with respect to the second (Heden and Sorto, 1981; Tanaka et al., 1995; Munuera et al., 2008), also called protusion (Hardy and Clapham, 1951; Lundberg and Sulja, 1972; Bryant et al., 2000; Mancuso et al., 2003), has been associated with hallux valgus, but a short first metatarsal relative to the second (Viladot, 1973) has also been suggested as an etiologic factor in hallux valgus. Other reported etiologic factors include the shape of the metatarsal head (Mann and Coughlin, 1981; Mancuso et al., 2003), a high intermetatarsal angle (Hardy and Clapham, 1951; Heden and Sorto, 1981), and hypermobility (Root et al., 1977; Laporta et al., 1974). Such a divergence of opinions regarding the etiology of hallux valgus underscores the need for a new perspective in order to elucidate the underlying cause of this deformity.

Unlike previous studies, this chapter proposes the size and shape of the PPH as a skeletal parameter involved in hallux valgus development. The underlying hypothesis involves abnormal stress on the PPH due to its shape (characterized by a larger length on the medial side compared with the lateral side) causing a tendency for the PPH to rotate. The effect of sexual dimorphism on the PPH is also evaluated to determine if this factor predisposed women to suffer hallux valgus pathology to a greater extent compared with men. The geometry of the

PPH is examined by cadaveric dissection and the stress state is predicted by FE analysis. In addition to providing a better understanding of this deformity, it is hoped that PPH geometry may provide an additional criterion by which physicians may gauge potential hallux valgus severity.

2.3 Model base configuration

The FE geometry was obtained from a 3D reconstruction of CT images of the right foot of a healthy male in his mid-thirties. CT images were acquired using a slice thickness of 2 mm. The FE meshes were constructed using commercial software HARPOON (Harpoon r1.4.5, CEI, Manchester, England). The mesh consisted of 797,753 linear tetrahedrons with an average size of 1 mm which were determined after a mesh sensitivity analysis to ensure the convergence of the model.

Seven different tissues are considered in the model, all idealized as homogeneous, isotropic and linearly elastic materials (Table 2.1). Each bone is differentiated into cortical and trabecular bone (García-Aznar et al., 2009; Duda et al., 2001). Ligaments are modeled using a tension-only one-dimensional truss element that transmitted only axial forces, distinguishing between two types of material, i.e., stiffer ligaments (such as plantar fascia and superficial and deep plantar ligaments) and the remaining, more compliant ligaments (Cheung et al., 2005). Cartilage properties are selected from the literature (Gefen, 2002). The muscles are simulated with one-dimensional beam elements. In order to prevent moments at elements representing tendons, connections between muscles and bones are characterized as tension only, one-dimensional elements, similar to ligaments (Maganaris and Paul, 1999; Bayod et al., 2010). Joints are simulated by ligaments and cartilage which enabled free movement between bones during simulations (Bayod et al., 2010). Node to surface contact is used to prevent penetration between tendons and bones. The external face of the bone elements is defined as the master surface whereas the slave surface is modeled with the nodes between the beams that represented the muscle.

The position of the model is very important, since loads on the foot change in both direction and amplitude with each position. With this aim, Gefen et al.

Table 2.1: Material properties and element types used in the 3D skeletal finite element models.

Component	Young's modulus [MPa]	Poisson ratio	Type of element
Cortical bone	17000	0,3	Tetrahedral
Trabecular bone	700	0,3	Tetrahedral
Ligaments	260	0,3	Tension only truss
Plantar fascia	350	0,3	Tension only truss
Cartilage	10	0,4	Tetrahedral
Muscles	450	0.3	Beam
Tendons	450	0.3	Tension only truss

(2000) proposed dividing the stance phase of gait into six different stages (initial-contact, heel-strike, midstance, forefoot-contact, push-off, and toe-off), defining loads for each of these stages.

The best position to analyze the initial development stage of the hallux valgus deformity is the position where the metatarsals heads support their self-weight. According to the stance phases suggested by Gefen et al. (2000), the model is positioned in the toe-off stage, forming an angle of 90 degrees between the metatarsals and phalanges.

In this position, the insertion of the Achilles tendon is considered as a fixed support, since this tendon generates most of the reaction force balancing the body weight. First and second phalanges are also considered as fixed support. For the remaining phalanges (third, fourth and fifth toes) only the vertical movement is restricted (Gefen et al., 2000). In this position, the PPH displacement is fully restrained due to the position of the PPH in the foot structure at the particular stage of the gait cycle analyzed (Gefen et al., 2000). Furthermore, a load of 1805N is applied to the joint surface formed by contact between tibia and fibula with the talus. This is the load that roughly corresponds to a subject with a body mass of 60Kg at this phase of gait. Also, at this stance phase, tendons are subjected to an initial pre-tension of 2% to sustain the position in a resting state.

2.4 Model adaptation

2.4.1 PPHs data acquisition

As the objective of the study is to analyze the influence of the PPHs geometry in the development of the hallux valgus pathology, before configuring the case of study it is necessary gather information about the actual geometry of the PPHs. That information is requested to surgeons who examined a total of 43 cadaver feet (22 males and 21 females) by means of cadaveric dissection. Data obtained from cadaveric dissection is common among surgeons as it allows quicker and easier collection of patient data, thereby obtaining a sufficient quantity of data (Lamur et al., 1996). Parameters that defined PPH geometry included: longitudinal distance of the medial aspect (LDM), longitudinal distance of the central aspect (LDC), longitudinal distance of the lateral aspect (LDL), depth of the concave area at the base of the PPH (DCA), height of the base of the PPH (H), and width of the base of the PPH (W) (Figure 2.3).

2.4.2 PPHs modeling

The dataset provided by surgeons is tabulated and divided by percentiles. Five representative PPHs are selected for each gender, corresponding to five percentiles for males (0%, 25%, 50%, 75%, and 100%) and five for females (Table 2.2).

These ten representative PPHs of the whole population dissected are modeled to configure ten different foot models which shared the same bony structure, differentiated only by PPH geometry. The new phalanges are generated grounded on the volume of the current PPH. This volume is imported to a software of 3D image edition, SOFTIMAGE. In this software an adaptive cage is generate around the volume associating the dimensions of the cage to the geometry. This cuboid cage can be divided as many sections as necessary. Therefore, dividing the width in three sections, corresponding to the parameters LDM, LDC and LDL, is possible to adjust the initial volume to the new dimensions. The same process is employed in the transversal axis to adjust the other dimensions. Subsequently, the new volumes are imported to MIMICS to adjust the parameters of the concavity.

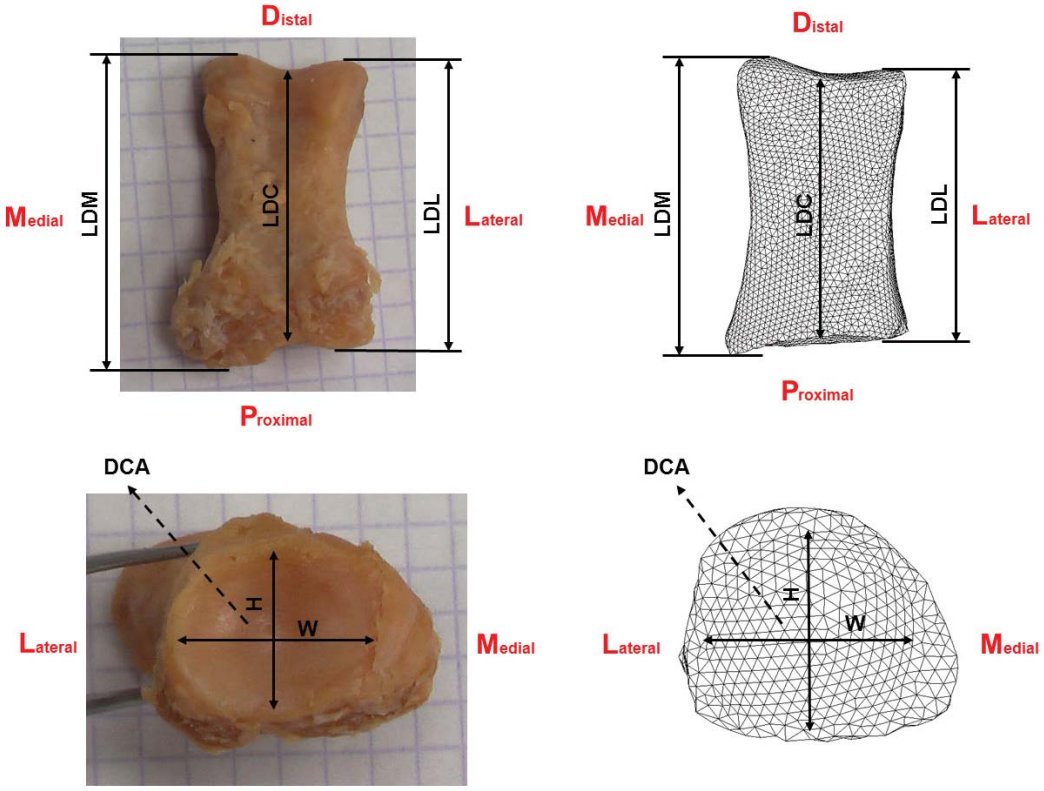

Figure 2.3: Clinically significant parameters of the proximal phalanx of the hallux.

Due to the way in which this software treats the 3D images it is easier measure DCA. The concavity is generated by a Boolean operation removing the negative volume of concavity. The key point in that operation is to control the ellipsoidal shape of the volume at the intersection with the base of the PPHs. The new geometry is meshed and includes in the base model by removing the current PPH. To connect the new PPH to the model, cartilages and ligaments are reconstructed. This process is followed to generate the ten representative PPHs.

Taking into account the importance of the muscle forces in the development of the hallux valgus, a gross approximation of the tendons that control first ray movement is considered. The tendons are simulated with one-dimensional links elements and includes the flexor, extensor, adductor and abductor of the hallux. These elements provide a more realistic load environment to the PPH.

Table 2.2: Parameters used to model the new proximal phalanges sorted by percentiles of the dissected population.

	LDM	LDC	LDL	DCA	H	W
M_0	30.52	28.76	29.04	3.57	16.51	20.93
M_25	31.18	31.54	31.33	1.56	16.39	22.39
M_50	36.5	35.39	35.04	3.08	23.21	24.53
M_75	40.31	33.01	36.51	1.25	17.78	21.35
M_100	38.51	37.91	38.4	2.21	15.56	20.72
W_0	31.23	29.00	29.5	1.27	14.08	17.51
W_25	31.71	30.48	30.86	0.72	13.23	17.66
W_50	34.45	30.15	32.63	0.66	12.33	19.04
W_75	38.64	34.24	35.34	2.32	17.26	17.72
W_100	40.16	39.35	42.78	2.42	18.7	20.00

2.5 Results

2.5.1 Model predictions

For proper comparison, all models are ordered by size and gender. Gender is defined by a letter (M for males, W for females) and the percentile of the dissected population is characterized by a number (0 for the smallest phalanx and 100 for the largest one). Figure 2.4a depicts the tensile stress distributions in the PPH while Figure 2.4b depicts the compressive stress distributions. The stress distributions are similar for both men and women with a larger loaded area (appearing primarily in the larger phalanges) found in women compared with men. The tensile stresses (maximum principal) are mainly located in the lateral zone and the head of the PPH, whereas the compressive stresses (minimum principal) appear mainly in the base and medial aspect of the PPH. Figure 2.5 shows the average tensile and compressive stress on both sides of PPH for each case analyzed. In all cases, tensile stresses are larger on the lateral side whereas compressive stresses are larger on the medial side.

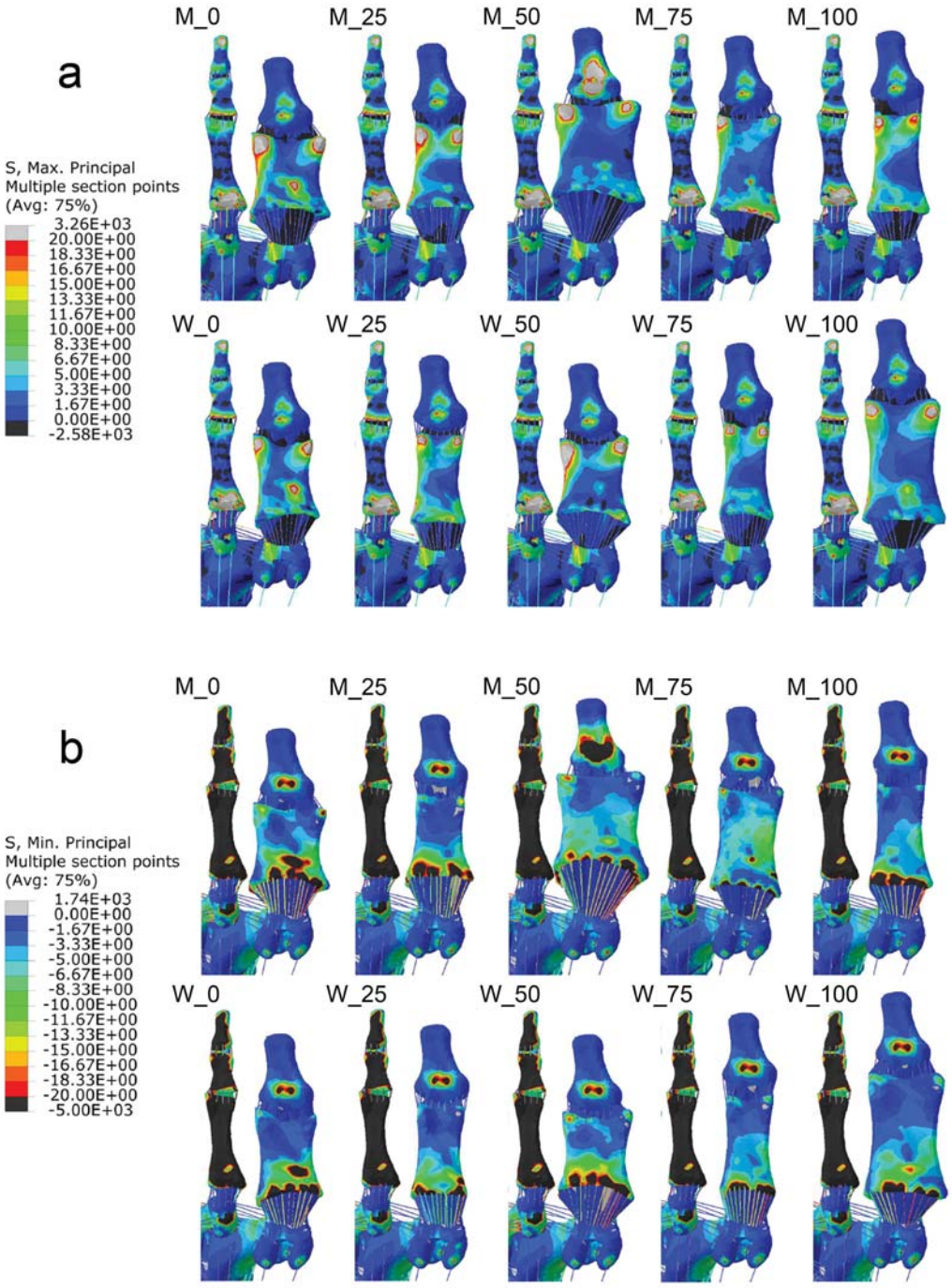

Figure 2.4: Stress in MPa on the plantar area of the first and second radii of undeformed shape. **a** Tensile stress. **b** Compressive stress. The letter corresponds to the gender and the number corresponds to the percentile.

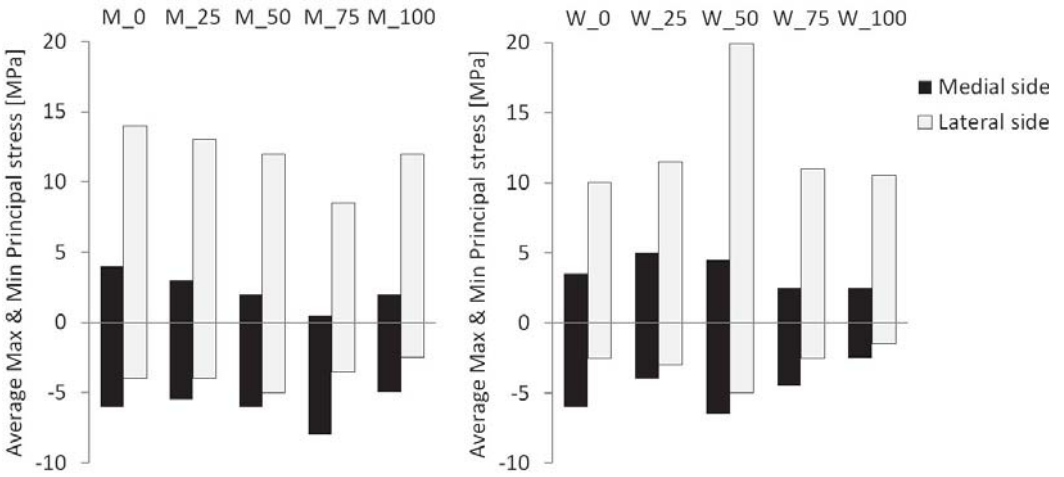

Figure 2.5: Average of the tensile and compressive stresses at the medial and lateral sides of the proximal phalanx of the hallux. The letter corresponds to the gender and the number corresponds to the percentile.

2.5.2 Phalanx measurements

The measurements for the 43 PPH dissected are summarized in Table 2.3. Male bones are larger than female bones for each of the parameters examined in this study. However, the mean difference between the length of the lateral and medial sides of the large PPH (Mean + SD) in men is 1.87 mm, while this value was 2.40 mm in women, with the medial side being longer in both cases. In relative values, this difference is also proportionally larger in female phalanges. In large PPHs, the LDM compared with the LDL is 7% larger in women whereas it is only 5% larger in men.

$$1.051 = \frac{38.80}{36.93} < \frac{36.95}{34.55} = 1.070 \tag{2.1}$$

According with the stress distribution, the medial side of the PPH in each model is compressed which appears to be because of its length whereas the lateral area is tensioned because it is shorter.

Stress differences are also found in the concavity at the base of the PPH where the metatarsal joint is located. In this area, a correlation between stress and DCA is observed, where the shallower the concave area, the larger the compressive

Table 2.3: Summary of data gathered from dissection.

Variable	Male (n=22)					Female (n=21)				
(mm)	Min	Mean -SD	Mean	Mean +SD	Max	Min	Mean -SD	Mean	Mean +SD	Max
LDM	30.52	33.84	36.32	38.80	40.31	31.23	31.71	34.33	36.95	42.78
LDC	28.76	31.08	33.38	35.68	37.91	29.00	29.11	31.47	33.83	39.35
LDL	29.04	32.05	34.18	36.93	38.40	29.50	29.79	32.17	34.55	40.16
DCA	0.87	1.26	2.04	2.82	3.90	0.66	1.04	1.63	2.22	2.83
H	13.79	14.66	16.88	19.10	23.21	12.33	13.56	15.33	17.10	19.35
W	17.88	19.73	21.48	23.23	25.34	17.51	17.86	20.05	22.24	25.45

stresses predicted (Figure 2.6). It should be noted that compressive stresses in this area are doubled in magnitude and extent when compared with tensile stresses and are higher than the compressive stresses on the plantar face.

2.6 Clinical discussion

It is very common to use the FE method to study foot pathology (Cheung and Nigg, 2008). This technique provides an estimate of the mechanical stresses within the internal structures of the body that is often not directly measurable. In addition, the calculated stress distributions suggest where injury is likely to occur before it actually occurs. Three FE studies related to hallux valgus have been reported in the literature (Tao et al., 2005; Matzaroglou et al., 2010; Wai-Chi Wong et al., 2015), however, any of these two studies took into account the geometry of the PPH as etiological factor.

In this chapter, a new approach to understand the hallux valgus etiology is described from the perspective of the shape of the PPH. Prior research measured the length of the bones of first ray at the initial stage of hallux valgus pathology for both male and female feet. Munuera et al. (2008) concluded that the length of the metatarsal and the PPH in patients with hallux valgus was higher than in non-pathological cases. Using 98 non-pathological feet, they reported an absolute mean PPH length of 32.70 $\pm$3.2mm very similar to the 32.43 $\pm$2.3mm measured in our population. Furthermore, in the figure they used to explain their method of measuring PPH length, they showed a representative PPH geometry. In that

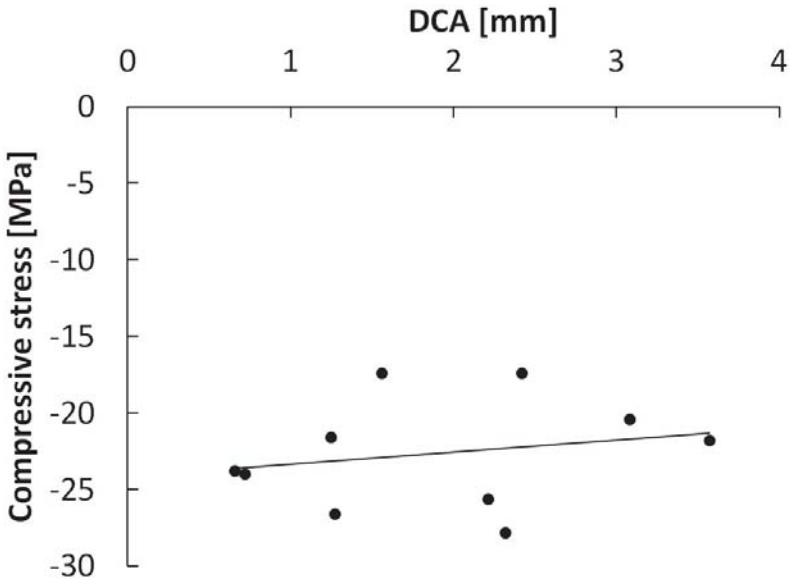

Figure 2.6: Scatterplot and the trend line showing compressive stress at the proximal phalanx of the hallux base versus depth of the concave area (DCA).

figure, it was easy to see the different lengths between medial and lateral sides of the PPH (Munuera et al., 2008). They also mentioned that the values of the variables between males and females were higher for male feet compared with female feet, which is consistent with the results of this study. Measurements reported by Ferrari et al. (2004) similarly noted that size was the main difference between male and female bones of the feet.

From earlier research, the shape of the first metatarsal head has also been considered an important anatomical feature of hallux valgus. Mann and Coughlin (1981) postulated that the shape of the first metatarsal head could be either square or rounded. A flattened metatarsophalangeal articulation would resist deforming forces much better than a rounded metatarsal head, which was thought to be highly prone to hallux valgus development. This idea was also expressed by Mancuso et al. (2003) in their study of the protrusion of the first metatarsal. They found a preponderance of rounded heads in their hallux valgus population. The results from the simulations presented in this chapter support this hypothesis. The stresses in the concavity at the base of the PPH are larger for smaller depths

(flatter heads) where opposition to rotation occurred. However, in deeper PPHs (rounded heads), lower stress levels are predicted (Figure 2.6).

The current results suggest that the geometry of the PPH influence its own stress pattern. The stresses estimated using the FE models are due to the difference in length between the medial and lateral sides. Stresses are tensile on the medial aspect of the PPH and compressive on the lateral aspect (Figure 2.4). This stress pattern indicated an imbalance in the first ray. The internal forces within the PPH could then force a rotation of the PPH towards a more balanced position. Such a potentially less-stressful position involves rotation of the PPH laterally, so that the new configuration offsets the difference in lengths, thus, relieving the stress. This rotation also causes separation of the metatarsals (Figure 2.7).

A similar idea was proposed by Ferrari et al. (2004), but was expressed using angles to explain the differences in the angulation of the metatarso-cuneiform joint between genders. They identified a significant difference in the angle of the facet on the metatarsal base with the medial cuneiform between men and women. Women had a greater angle, which caused a greater adduction of the metatarsal on the cuneiform compared with men (Ferrari et al., 2004). In the case of the PPH base, the larger the differences in length between sides, the greater would be the abduction.

The rotation of the phalanx may be compounded by muscle function. No muscle inserts on the distal zone or head of the first metatarsal, nor on its middle area or diaphysis. The peroneus longus tendon is the only tendon that inserts on the proximal plantar area or on the base of the first metatarsal. In addition, the tibialis anterior tendon inserts on the medial and plantar area. By contrast, several tendons insert on the base of the PPH, as follows: at its dorsal base, the tendon of the pedal muscle and tendon capsularis; at its plantar zone, two tendons from the short plantar flexor muscle; at its medial area, the adductor hallucis tendon; and at its lateral area, the tendon of the abductor hallucis muscle. Two tendons insert on the distal phalanx, one at the dorsal base (the extensor hallucis longus) and another at the plantar base (the flexor hallucis longus).

The electromyographic investigations performed by Iida and Basmajian (1974)

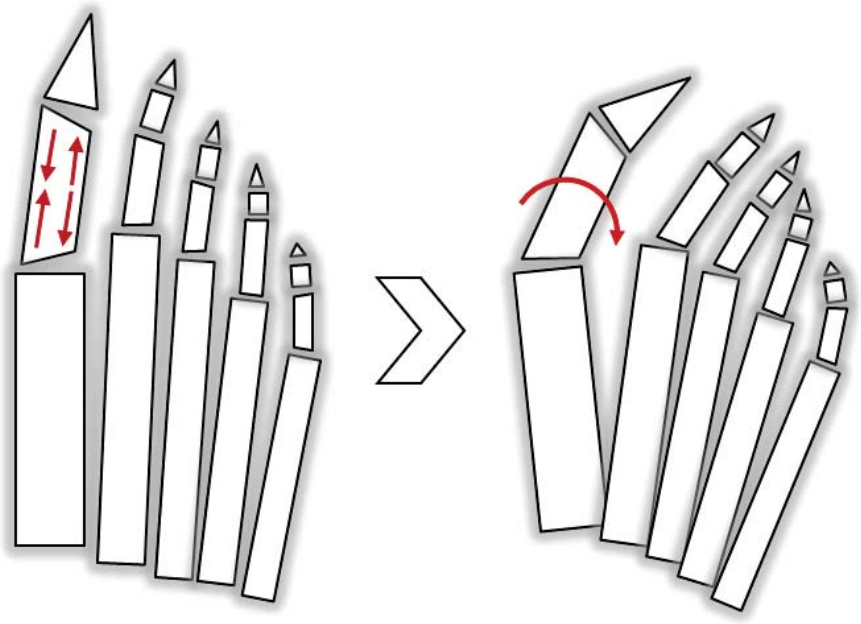

Figure 2.7: Diagram of how the proximal phalanx rotates to reduce the stress.

and Shimazaki and Takebe (1981) found a weak medial flexion force against a stronger lateral flexion force in mild and severe hallux valgus. Forces that markedly decreased abduction activity compared with adduction were also reported in a much more recent electromyographic study (Arinci Incel et al., 2003), but none of these studies clarified whether this was a cause or a consequence of hallux valgus. Thus, although is still unclear if muscle imbalance in first ray is the cause or just an aggravating factor in hallux valgus development, there is evidence that muscle imbalance is related to the development hallux valgus and could have a strong influence if other factors triggered rotation of the PPH.

Therefore, there must be some intrinsic predisposing factors (such as protrusion of the first metatarsal, shape of the head of the first metatarsal, metatarsocuneiform angulation, intermetatarsal angle or the geometry of the PPH) that make some feet more vulnerable to hallux valgus deformity than others. In addition, these factors are also affected by confinement forces exerted by footwear and the imbalanced forces of the muscular activity at the metatarsophalangeal joint. Future studies which investigate all these factors together, instead of examining

each factor individually, are needed. Also, the influence of each factor on hallux valgus development would be very useful for clinical evaluation.

Concerning the parameters used in this study, it should be noted that for all simulated cases, differences in the stress state are due solely to differences in the geometry of the PPH, since the materials used, the boundary conditions, and the geometry and position of the rest of foot skeleton are the same for all simulated cases. This assumption is adopted in order to isolate the influence of PPH geometry from other factors. On this basis, the same load condition was estimated for the female skeletons as was used for the male skeletons. As bone density is lower in women compared to men (Berntsen et al., 2001), in the same way that women's feet are smaller (Wunderlich and Cavanagh, 2001) and support lower body weight, the value of the load for women should be increased to match these factors, in a way that maintains the rate of load vs. the degree to which the female foot is able to withstand the load. That configuration is reasonable considering that the results of the simulation were limited to a qualitative comparison between the cases analyzed. Such assumptions had no influence on the stress distribution pattern of the model, where tensile stresses predominate on the lateral side while compressive stresses predominate on the medial side of the PPH.

It is important advise caution when comparing the results obtained from the current simulation with other studies. The current technology is not able to measure the stress within bone, so the results cannot be compared directly with experimental measures. Another option involves comparison with other FE models of the foot. In this regard, however, the reader should beware of comparing stress values between different FE models. This is not a trivial matter. The simplifications, assumptions, and boundary conditions influence the values predicted which makes direct comparison of the results from different FE models almost impossible. Furthermore, there is no previous FE model which has reported values of bone stress in the toe-off position. Most prior studies only measured values of plantar pressure (Cheung et al., 2005; Chen et al., 2010a; Takahashi et al., 2012) and rarely in toe-off position (Gefen et al., 2000; Actis et al., 2006; Budhabhatti et al., 2007). In addition, usually only Von Mises stresses were reported, but for the purpose of analysis of bone, maximum and minimum stresses are more mean-

ingful than Von Mises stresses, particularly in this study where is attempted to distinguish between tensile and compressive stresses.

The present study proposes a new skeletal parameter involved in hallux valgus. The geometry of the PPH has the feature of a larger medial compared with lateral side, subjecting it to stresses that could provoke rotation of the PPH toward a more relaxed position. That potential balanced position produces a tendency toward separation of the first metatarsal relative to the original anatomical position, which constitutes the beginning of the hallux valgus deformity. The data gathers from the dissection shows that the difference in length between the medial and proximal side is greater in women. This suggests that sexual dimorphism of the PPH could be an influential factor in the formation of bunions, with women more prone to suffers this pathology.

The geometry of the PPH is a significant factor in the development of hallux valgus, with as much influence as the other reported skeletal parameters, and should be considered during preoperative evaluation. Therefore, the clinical assessment of hallux valgus should involve evaluation of the first ray as a whole and not as isolated factors.

2.7 Features of the model

The skeletal model has some advantages and drawbacks depends on the objective pursuit. One of the advantages of the absence of surrounding tissue is the easier modification of the geometry. Within all the variables that can be controled in a FE model, the modification of the geometry is the higher time-consuming task. This is because geometry definition is the first step of the process, as shown in Figure 1.1. Then, when the geometry of the model is modify it is necessary to generate a new mesh and define new boundary conditions. That process can be avoided when the modified volumes have few elements connected, which allows alter a part of the model just reconstructing the elements in contact. That advantage is exploited in the hallux valgus study carries out in this chapter, interchanging PPHs and reconstructing the cartilages of the extremes. Similarly, in the particular case of foot modeling, the skeletal model allows to simulate all the

positions of the foot during the stance phase, which only flex the phalanges with respect to the hindfoot. Other possibilities are the easy inclusion of implants or any kind of surgical device. All these alterations in a 3D foot FE model surrounding by soft tissue require not only remeshes the whole geometry, if not defines the loads and boundary condition again.

The computational time is other factor to take into account. The soft tissue that embedded the foot skeleton is a large volume, greater than the own skeleton. This means that a high number of elements is needed to mesh such a volume. The computational time varies exponentially with the number of elements. Therefore, with the same mesh size skeletal models yield computational times much lower than complete foot geometries. This reduction of the computational time is also influenced by the fact that when soft tissue is included in the simulations contact between the plantar foot and the ground is considered and this interaction has a high computer cost. The skeletal models runs in this chapter take less than one hour to conclude (Intel core i5 3.2GHz processor and 4GB of RAM).

However, the current skeletal model has several limitations for a proper simulation of the foot pathologies. The fat was not simulated and other soft tissues that interact with the skeleton such ligaments and tendons were introduced in a gross representation. This was considered to create a more realistic environment for the bone structure, although that approximation does not allows studying the stress in those tissues. This assumption is considered adequate as bone is much harder than soft tissue, and the goal of the study is focused in the bony structure. Therefore, the current model is limited to bone related studies; such as bone pathologies, bone fractures, bone surgeries and intraarticular pressures. The study of any other issue that involves foot soft tissues require further developments.

2.8 Further improvements

The general goal of the Thesis is to improve the computational foot modeling for more accurate clinical assessment. With that in mind, considering the features of the current model, detailed in section 2.7, and the in-depth review presented in

chapter 1, the alterations in the model with major impact in the outcomes and greater advance for the field are proposed. The steps forwards are oriented in two directions. On one side, the refinement of the geometry including all components within the foot and on the other side, setting non-linear properties for soft tissue components.

Generally, in foot simulation, complete 3D models are composed by a homogenous bone structure embedded in a homogenous bulk soft tissue. This configuration limited the sort of pathologies than can be studied. To really step forward in computational foot modeling it is necessary to go deeper in the representation of the inner components of the foot, particularly relevant in clinical applications. Then, it is proposed to maintain the differentiation between cortical and trabecular bone of the skeletal structure and to add soft tissue components. That is, within bulk soft tissue that surrounds the skeleton differentiates tendons, muscles and fat tissue. This new foot-ankle complex will open new possibilities in the study of foot biomechanics.

Identifying these new components, a new challenge arises. As soft tissue have a strong non-linear behavior, it become necessary to refine the current linear properties employed fitting the parameters of non-linear models. Special importance has the tendon tissue, which plays a relevant role in control motion and stress distribution in the foot. With a refined formulation of the fat layer it will be interesting taking into account that the current non-linear models for this tissue are based in heel pad test which have different properties than the rest of the plantar sole.

This updated foot model will be very useful set in real environment including contact interaction with the ground. This will help in the validation process and will permit study actual performance of the foot. Finally, configure all the complex to allow simulations in all range of loads such standing, walking an running will definitely provide a wide range of applications with refined outcomes.

CHAPTER

THREE

MECHANICAL CHARACTERIZATION OF HUMAN FOOT TENDONS

In this chapter the mechanical properties of the main intrinsic and extrinsic human foot tendons *in vitro* are investigated. Structural and material properties of tendons are relevant in fields such as orthopedic reconstruction surgery and computational biomechanics. One hundred and ten uniaxial tensile tests are performed to obtain the stress-strain curve of different foot tendons. The specimens are harvested from five frozen cadaver feet including: Extensor and Flexor tendons of all toes, Tibialis Anterior and Posterior tendons and Peroneus Brevis and Longus tendons. Two different behaviors can be differentiated. Tibialis and Peroneus tendons exhibit higher values of strain failure compared to Flexor and Extensor tendons which have higher Young's modulus and ultimate tensile stress. Stress-strain tendon curves exhibit proportionality between regions. The initial strain, the toe region and the yield point correspond to the 15, 30 and 70% of the strain failure respectively. The data obtained from the experiments is used to fit the parameters of a hyperplastic constitutive model for foot tendon tissue. The study of the mechanical properties of the foot tendons presented in this chapter has been submitted for publication in "Clinical Biomechanics" (Section 7.2.1 — Publication 3).

3.1 Introduction

Tendon is a white fibrous tissue that connects the extremes of the muscles to the bones. Its biomechanical role is to transmit the contraction of the muscles to the skeleton in order to produce force or movement of the body. This tissue is evolutionary mechanoadapted to work axially, analogous to a string, with a large length compared which its section.

Mechanical properties of tendons have been studied previously, particularly the Achilles tendon. It is one of the biggest tendon of the human body and very relevant clinically due to its high incidence of injury. Furthermore, its location and structure facilitate the measures *in vivo*. There is an extensive bibliography about this tendon which in certain situations is extrapolated to estimate the properties of other tendons, as in the case of other foot tendons where the information available is scarce and incomplete (Thordarson et al., 1995; Sharkey and Hamel, 1998).

The material properties reported for the Achilles tendon have a great variability. For example, the Young's modulus vary in an order of magnitude from 0.2 to 2GPa (Wren et al., 2001; Maganaris and Paul, 2002; Lichtwark and Wilson, 2005; Maganaris et al., 2008; Zhao et al., 2009; Arya and Kulig, 2010; Peltonen et al., 2010; Kongsgaard et al., 2011; Hansen et al., 2013). There are two main reasons for this disparity of results: one is the natural biological variation and the other is the different procedures used to assess the properties. To reduce the influence of the first factor some authors prefer to test animal specimens where the history of the subject can be controlled, although for clinical applications human material is frequently required. The second factor could be compensated applying the same methodology to calculate the properties, but there is no agreement about a proper method to evaluate mechanical tendon properties yet. Furthermore, different methodologies are needed depending on the objective pursued. For instance, in the field of simulation, the characterization of a tissue can be approximated by linear, hyperelastic or viscoelastic models, which require different mechanical parameters. The positive aspect of the use of different techniques to assess the mechanical properties is that it prevent bias.

Figure 3.1: Foot tendon dissection (Extensor Digitorum Longus).

The mechanical properties of human foot tendons is a valuable information in different fields. In orthopedic reconstruction surgery, the use of tendon grafts is common to repair tendons and ligaments (Sebastian et al., 2007; Giannini et al., 2008; Zhao and Huangfu, 2012). Among other characteristics, the structural properties of the potential graft is one of the prerequisites that surgeons evaluate in the election of a suitable replacement. Detailed information of structural properties of every foot tendon would help surgeons in the decision making process. Computational biomechanics is another field in which experimental data of actual behavior of human foot tendons would provide a significant advance. From the engineering perspective, the human foot is a complex structure of small bones supported by strong ligaments and controlled by a network of tendons and muscles. The current barrier in foot computational simulation is the inclusion of these musculotendinous structures in the models (Morales-Orcajo et al., 2015a).

The purpose of these experiments are to assess the mechanical properties of

the human foot tendons responsible for the stabilization and control motion. One hundred and ten samples of these lesser-studied foot tendons were tested *in vitro*. Particular effort is made to proportionate a refined description of their hyperelastic feature. As outcome, a complete dataset of experimental values for engineering and clinical applications is provided. Subsequently, the material properties are used to characterize the foot tendon tissue fitting hyperelastic constitutive models to the experimental curves.

3.2 Mechanical testing

The tendons included in the experiments are sorted in two groups: the long tendons involved in flexion and extension of the toes, on the one hand and the thick tendons intervening on the inversion and eversion of the ankle, on the other hand. The former includes the Extensor Digitorum Brevis (EDB) and the Extensor Digitorum Longus (EDL) which extent lesser toes, the Extensor Hallucis Longus (EHL) which extends the great toe, the Flexor Digitorum Brevis (FDB) and the Flexor Digitorum Longus (FDL) which flex the four lateral toes and the Flexor Hallucis Longus (FHL) which flexes the hallux. The latter involves the Tibialis Anterior (TA) and the Tibialis Postior (TP) which invert the foot, and the Peroneus Brevis (PB) and Peroneus Longus (PL) which evert the foot. Those muscles and, by extension, their tendons enable us to stay balanced in upright position.

A total of 110 tendons samples are taken from five male elder donors (Figure 3.1), with the approval of the Bioethical Research Committee of the Hospital Clinico San Carlos at Complutense University (n^o 12/210-E). A sample of each tendon is cut from the most relative uniform cross-sectional area (CSA) removing all the soft tissue around the tendon (Figure 3.2). After the dissection, the samples are frozen and kept at a temperature of -20^{o}C (Schechtman and Bader, 1997; Devkota and Weinhold, 2003; Sebastian et al., 2007; Zhao and Huangfu, 2012) until the day of testing (8-12 months) (Vergari et al., 2011). Specimens are gradually thawed and kept hydrated until the time of testing at room temperature ($\sim$25^{o}C). The CSA is measured right before testing. Three measures

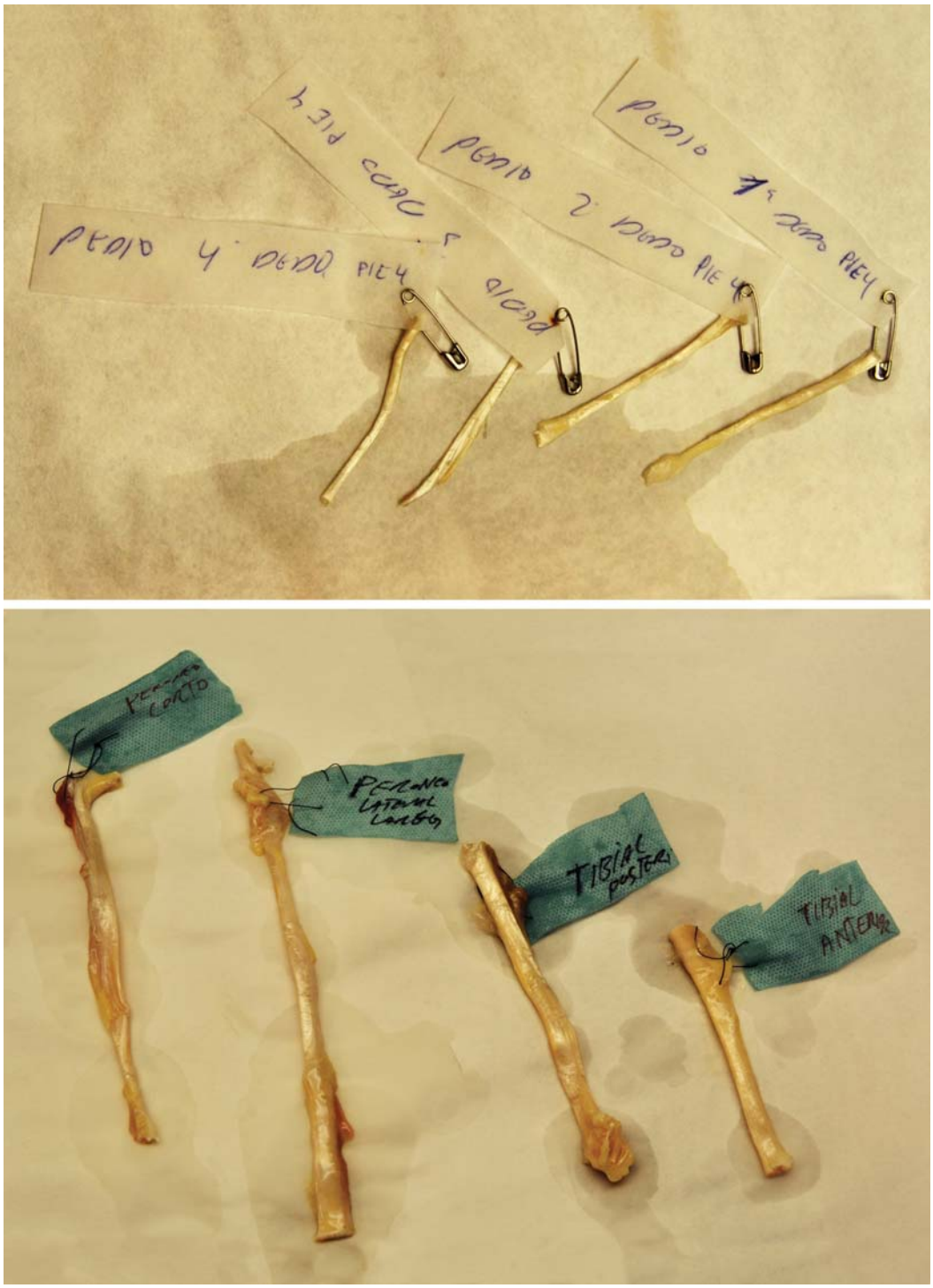

Figure 3.2: Samples labeled after dissection ready for cross-sectional area measure.

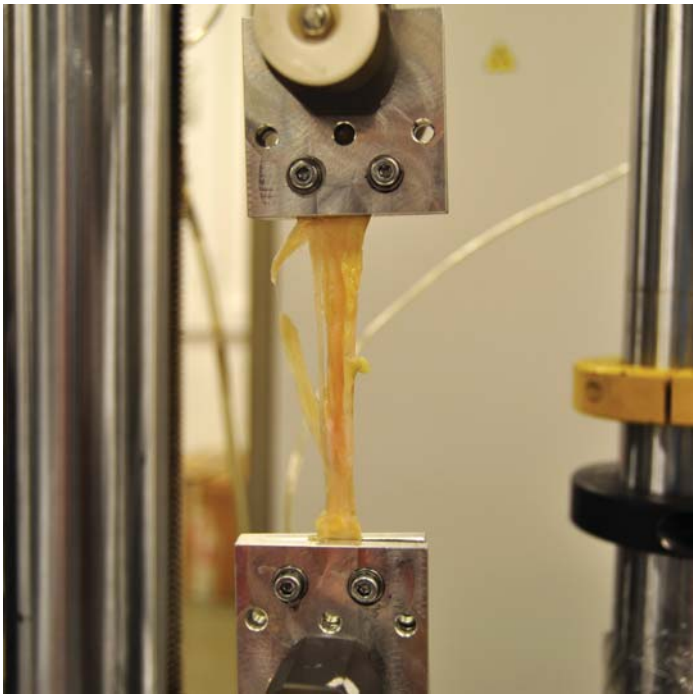

Figure 3.3: Tibialis Anterior sample in the universal testing machine during test.

along the longitudinal axis of the sample are taken and the average of the three measurements is selected. The maximal and minimal diameters of the tendon are measured with a digital caliper to calculate CSA by approximating it as an ellipse (Giannini et al., 2008; Vergari et al., 2010). No cycle of tissue preconditioning is apply to the samples (Butler et al., 1984; Schechtman and Bader, 1997; Giannini et al., 2008; Zhao and Huangfu, 2012).

Tendons function in longitudinal tension only, which simplify the measurements required to assess their behavior. Hence, uniaxial tensile test proportionate sufficient information for its full mechanical characterization. A universal testing machine (Instron Ltd., U.K., model 5548) is used to perform the tests (Figure 3.3). An initial stretch of 1MPa is applied to remove any slack in the samples. Then, a displacement is applied at a rate of 0.1 mm/s to failure. This rate correspond with approximate 10$\sim$20% s^{-1} depending on length sample. Strain is measured using clamp-to-clamp displacement. The trials with evidences of slipping or initial damage are discarded.

Table 3.1: Structural properties of each tendon included in the study. Mean ± standard deviation (range). *These measures correspond to the toe-branches of distal part of the tendon and not to the common proximal part.

Tendon	Cross-sectional Area [mm2]		Failure load [N]	
EDB*	3.09 ±0,95	(1.53 - 4.56)	37 ±14	(12 - 62)
EDL*	4.81 ±1,25	(2.83 - 7.34)	127 ±84	(52 - 237)
FDB*	2.72 ±1,02	(1.48 - 5.18)	65 ±48	(13 - 179)
FDL*	4.87 ±2,12	(1.54 - 9.03)	74 ±30	(37 - 138)
EHL	8.53 ±1,35	(6.91 - 10.41)	316 ±88	(247 - 443)
FHL	15.77 ±2,64	(12.53 - 18.69)	525 ±200	(356 - 770)
TA	26.40 ±2,85	(23.75 - 29.85)	458 ±155	(306 - 669)
TP	24.02 ±3,69	(20.29 - 33.18)	475 ±60	(397 - 528)
PB	11.87 ±2,01	(10.13 - 15.22)	239 ±99	(138 - 392)
PL	16.59 ±3,38	(13.22 - 21.17)	346 ±196	(130 - 629)

3.3 Results

3.3.1 Tendon structural properties

Structural parameters are the mechanical properties of a singular sample tested meaning that are dependent of its geometric characteristics (CSA and length). This reliance causes that structural parameters present a high dispersion and mean value might be an ambiguous value on account of is non-robustness to outliers which are common due to the intersubject variability. For that reason, in Table 3.1 ranges are reported together with mean and standard deviation in order to facilitate comparison with other works. Note that values reported of extensor and flexor digitorum correspond to the toe-branches of the tendons. Hence, to estimate the failure load of the whole tendon, the maximal load measured in these experiments should be multiplied by the number of branches of the tendon.

Tendon specimens show relatively uniform CSA along their long axis. As previously mentioned three measures were taken at different heights of each sample. The reported values correspond to the values employed to calculate the stress. Failure load values shown in Table 3.1 are the maximum load recorded by the load cell of the testing machine. After that value, the loads decreased drastically.

The ultimate load is directly related to the CSA. Tendons with bigger CSA are

expected to withstand higher loads. Other structural parameters such as stiffness and energy to failure cannot be calculated in the present study because the length of the samples tested no corresponded to the total length of the tendons.

3.3.2 Stress-strain curve

The stress-strain curve is the normalized curve of the load-displacement graph provided by the test machine. Normal stress was calculated dividing the load by the initial CSA (engineering stress) and the strain was calculated dividing the displacement by the initial length of the sample.

All trials had the characteristic stress-strain curve of tendon tissue. Three distinct regions are identified: the toe region characterized by a non-linear strain with small tension, the linear region where the stress increase linearly with the strain and the yield region or the region where starts the macroscopic failure. The toe region, in turn, is possible to divide in two parts: the noteworthy initial strain and the non-linear transition previous to the linear region (Figure 3.4).

The criterion to determine these regions never had been stipulated and it is subjected to the visual perception of the slope of the curve. This demarcation although is qualitatively worthy could be misleading in quantifying accurately the actual range of each region. Therefore, we propose a criterion to quantify those regions taking as reference the Young's modulus of each test. Hence, the initial strain is defined as the part of the curve from its beginning to a deviation greater than 20% of the Young's modulus and the linear region is defined as the part of the curve with the curvature less than 20% of the Young's modulus. The resulting regions visually fit with the description in the literature (Abrahams, 1967).

As it is possible to calculate the Young's modulus for each point of the curve, with this criterion, it is possible to quantify accurately the regions of the stress-strain curve. In Table 3.2 are presented the mean strain values of the four points that delimit the regions. Inversion/eversion tendons show strain values nearly twice that of flexor/extensor toes tendons for each region.

Based on these values, strain proportionality is detected within regions when normalized to strain failure, understanding failure point as the point of the curve

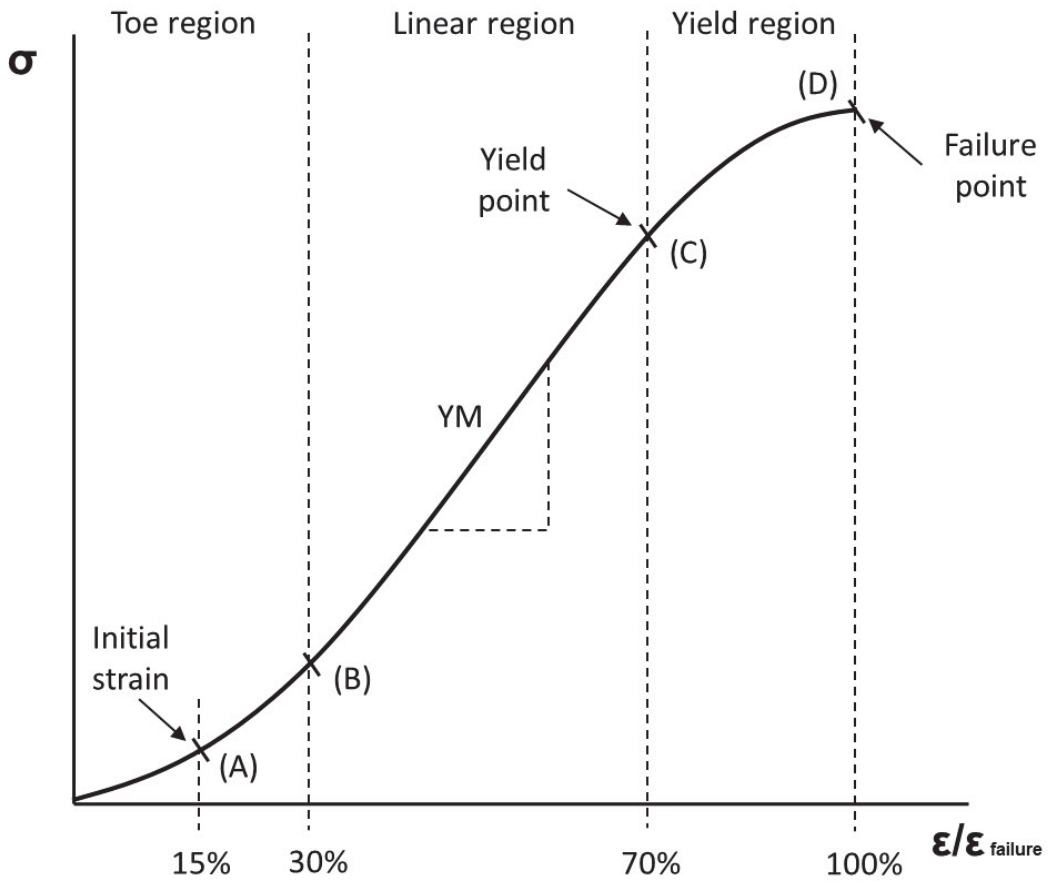

Figure 3.4: Scheme of the typical stress-strain curve for tendon tissue normalized to strain failure, identifying regions and proportionality ratios.

that supports the maximum stress. The initial strain, the toe region and the yield point correspond to 15, 30 and 70% of the strain failure respectively. These delimiting points and the region proportionality are shown schematically in Figure 3.4.

3.3.3 Material properties

The summary of all trial curves is depicted in Figure 3.5. The points represent the failure point of the stress-strain curve of each sample tested. They are connected to the origin with the characteristic S-shaped tendon curve although most of the curves have been removed in order to clarify the visualization. In this figure are

Table 3.2: Strain values of the points that delimit each region of the stress-strain curve.

		EDB	EDL	FDB	FDL	Average
Initial strain	(A)	1.0%	1.4%	1.4%	1.6%	1.4%
Toe region	(B)	1.4%	2.9%	2.5%	1.9%	2.2%
Yield point	(C)	4.3%	6.2%	5.2%	5.0%	5.2%
Failure point	(D)	6.0%	8.7%	7.1%	7.2%	7.2%

		TA	TP	PB	PL	Average
Initial strain	(A)	2.5%	3.6%	1.5%	2.1%	2.4%
Toe region	(B)	6.4%	6.4%	2.6%	4.5%	5.0%
Yield point	(C)	12.1%	12.9%	9.2%	9.5%	10.9%
Failure point	(D)	17.0%	16.3%	14.2%	13.7%	15.3%

		EHL	FHL	Average
Initial strain	(A)	1.6%	2.0%	1.8%
Toe region	(B)	3.9%	4.3%	4.1%
Yield point	(C)	9.8%	8.8%	9.3%
Failure point	(D)	11.7%	12.3%	12.0%

represented the main material parameters. The x coordinate indicates the strain failure, the y coordinate indicates the ultimate tensile stress and the Young's modulus is the slope of the linear region of the curve. The strain failures are summarized by tendon in Table 3.2. Young's modulus and ultimate tensile stress are sorted by tendon in Table 3.3.

Two different behaviors are distinguished. On the one hand, flexor/extensor tendons characterized by lower strain failure and higher Young's modulus. The median curve of these tendons is graphed with a black solid line (Figure 3.5). On the other hand, inversion/eversion tendons presented larger strain limits and lower Young's modulus. The median stress-strain curve of these tendons is graphed with a red solid line (Figure 3.5). The flexor/extensor tendons presented an average Young's modulus of 390±175MPa against 195±83MPa for inversion/eversion tendons.

There was no significant difference in any parameter analyzed between toe tendons, neither between flexor and extensor tendons nor interdonor variability.

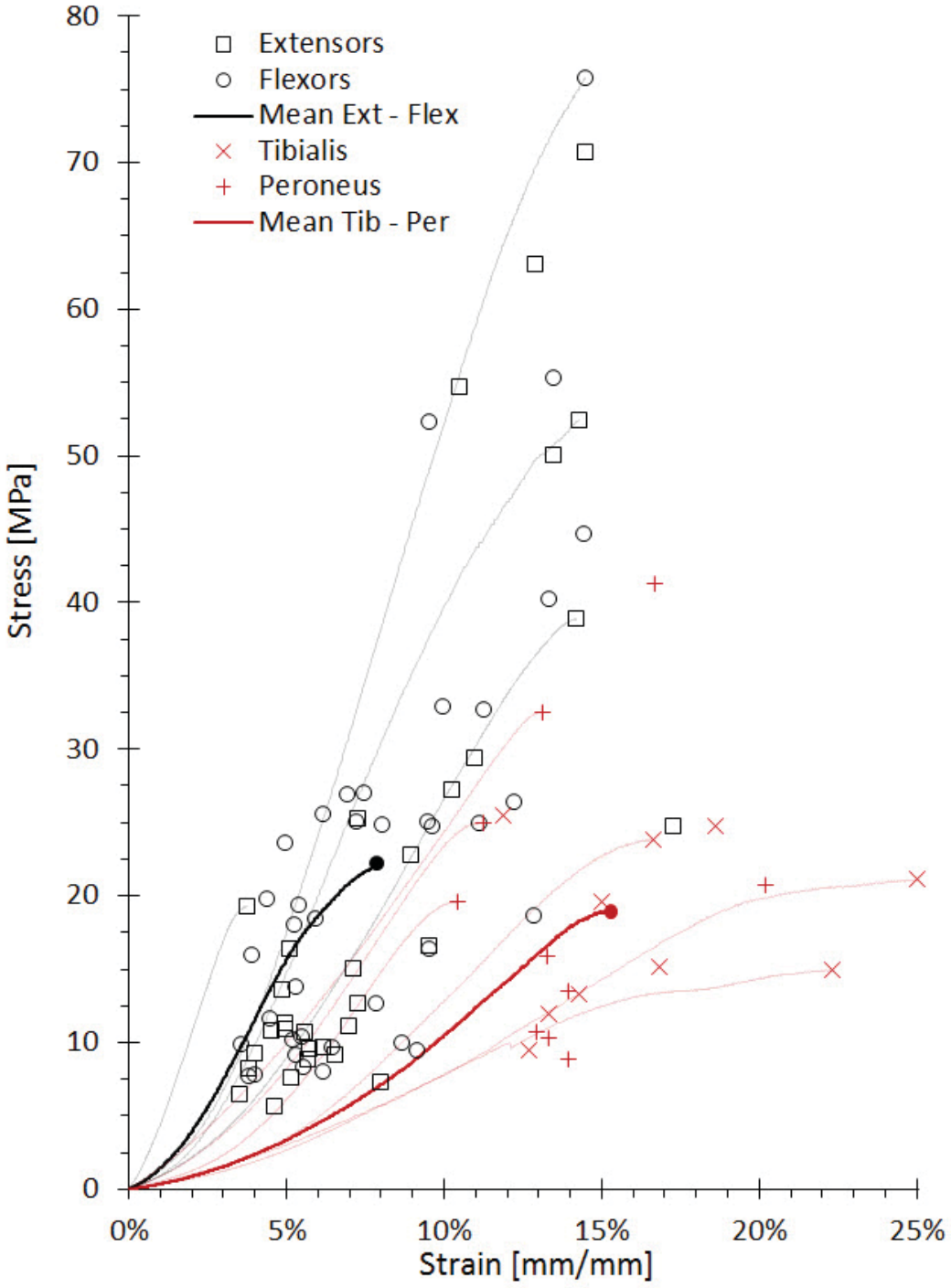

Figure 3.5: Stress-strain graph including all samples tested sorted by muscle function. The points are the failure point of each sample tested. Most of the curves have been removed in order to clarify the visualization.

Table 3.3: Material properties sorted by tendon. Mean ± standard deviation.

Tendon	Young's Modulus [MPa]	Ultimate Tensile Stress [MPa]
EDB	294±137	14±9
EDL	395±180	26±21
FDB	505±172	28±19
FDL	337±138	16±7
EHL	448±183	39±18
FHL	440±119	26±10
TA	165±73	17±6
TP	187±54	19±5
PB	203±94	20±10
PL	227±116	20±12

3.4 Discussion

Mechanical properties of human tissues are relevant for many practical issues. Frequently, the measurement of these properties are concentrated in a particular component with high clinical interest disregarding others less critical. This leads to the estimation of properties of those other components by extrapolation. That is the case of tendon tissue where most of the studies measure the properties of the Achilles tendon, the patellar tendon or the suprapinatus tendon. In this chapter, the tensile response of the lesser-studied foot tendons are tested *in vitro*. Structural and material properties are reported as a complete reference under the same test protocol. Moreover, a criterion for quantitative description of the stress-strain curve is defined for the first time.

The major finding of the experiments is found a significant difference ($p<0.001$) between tendons which work at different planes. Flexor/extensor toe tendons show twice the Young's modulus than inversion/eversion tendons. In practical terms, this means that tibialis and peroneus tendons undergo higher deformation for the same tensile stress. In computational simulation for linear models, the Young's modulus is the main parameter to describe the mechanical behavior of the material. In the case of tendon tissue the description of the fully mechanical behavior by a linear model is simplistic. Tendon tissue performs a hyperelastic

behavior, thus, the typical material parameters of Young's modulus, ultimate tensile stress and strain failure are not sufficient. The quantitative description of the stress-strain curve provides a more refined characterization.

A qualitative description of the stress-strain curve have been defined previously (Schechtman and Bader, 1997; Wang, 2006; Spyrou and Aravas, 2011). Generally three regions are identified: toe region, linear region and yield region. These regions are described based on the visual observation of a representative typical stress-strain curve, but do not consider the wide variability of each specimen. Analyzing the result of the present work, it is realized that the description do not well-fit the curves and the delimitation of the regions is subjective to the perception of the analyst. In order to standardize this division the criterion describe in Section 3.3.2 is proposed. Furthermore, another subdivision to characterize the transition between the initial strain and the beginning of the linear region is found important to include. This region was also identified by Abrahams (1967). The histological studies describe this second region at the stage where the collagen fibers reach the final parallel orientation that governs the linear behavior after the stretch out of the wave-pattern that occurs initially (Abrahams, 1967).

During testing process some experimental difficulties are found. First of all, the tendons tested are considerably small compared with the rest of the tendons in the human body. Measure the CSA of these small tendons is critical because of the sensibility of the measurement. Little variations in the CSA have high impact in the calculus of the material properties. Caliper is chosen because of its ease of use and its sufficient level of accuracy and repeatability. This method is acceptable to measure tendons with sections greater than $1.5mm^2$ and constant along the longitudinal axis. Lumbrical tendon tests are discarded for their tiny CSA. Vergari et al. (2010) found comparable results of the elliptical approximation against more sophisticated techniques. In the literature, only one study that report CSA of this smaller tendons are found. Blanton and Biggs (1970) used a planimeter over a thirty magnifications projected area to determine tendon CSA and the values reported are similar (Figure 3.6).

Clamping the samples at the testing machine is also a common difficulty testing soft tissues. The firmness with which the sample is fastened has to balance

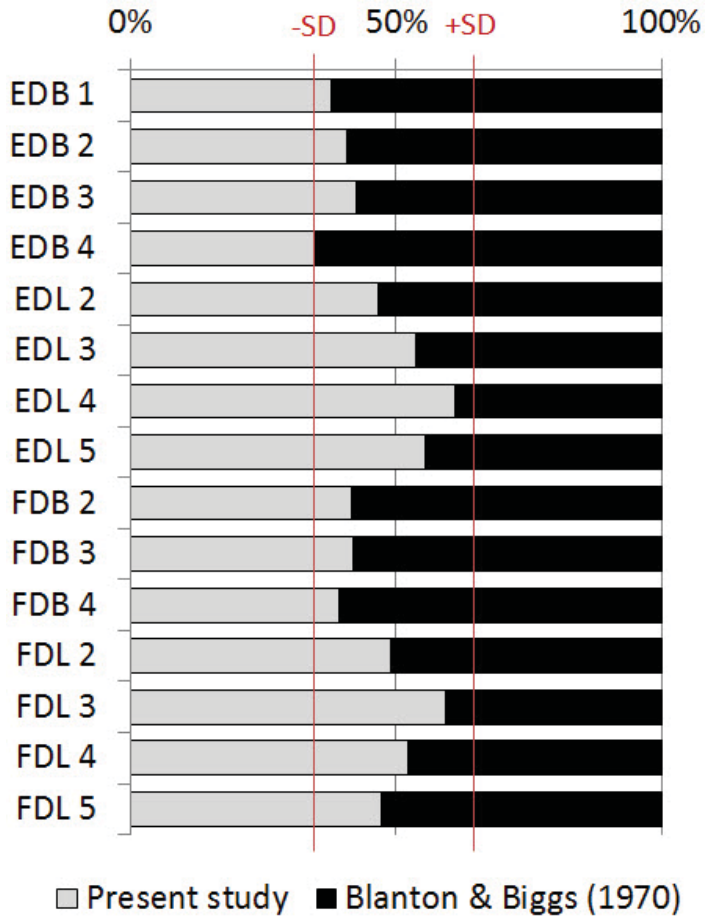

Figure 3.6: Comparison of the cross-sectional areas measured in the present study with the cross-sectional areas reported by Blanton and Biggs (1970).

the sufficient strength to avoid the slip out of the sample, but not too much to brake collagen fibrils. A pair of screw lock clamps are specifically designed to perform the tests. The inner sides of the stainless steel clamps are milled with small holes to improve the grip. Similar clamping systems have been employed in previous uniaxial tensile tests of tendon tissue (Schechtman and Bader, 1997; Abrahams, 1967). Due to the impact of the clamping system, stress concentrations are expected in the samples. Therefore, in physiological condition, values of tendon failure may be underestimated (Maganaris and Paul, 2002; Ker, 2007). This underestimation could be accentuated by the fact of reporting engineering

stress instead of true stress. Engineering stress at tendon failure have been found around 10% smaller than the corresponding true stress (Vergari et al., 2011). From a clinical point of view the failure values reported can be considered as conservative.

Other parameter of the testing process, which may have an impact in the results, is the storage method, but the literature is inconsistent in this regard. Different studies conclude in conflicting resolutions about the influence of freezing storage in the mechanical properties. Giannini et al. (2008) found important changes in frozen-thawed tendons compared to controls in a histological and mechanical analysis. Similarly, Smith et al. (1996) found significant differences in mechanical properties comparing distinct freezing methods. However, Huang et al. (2011) did not register mechanical differences until the fifth freezing-thawing cycle. No alterations in the tensile properties in other human and animal tendon studies have been also reported (Vanbrocklin and Ellis, 1965; Ho and Meng, 2002; Jung et al., 2011). These contradictory results are also present in ligament literature (Moon et al., 2006; Viidik and Lewin, 1966). Nevertheless, for comparison purposes the unconfirmed impact of storage method is counteracted by the fact that most of the *in vitro* studies of human tendon used freezing methods to preserve the samples until the testing day.

Conversely, it have observed in previous studies that tendons and ligaments exhibit strain rate sensibility (Wren et al., 2001; Abrahams, 1967; Vanbrocklin and Ellis, 1965; Noyes et al., 1974). As a viscoelastic tissue tendons became stiffer at higher strain rates. Therefore, the rate of strain has to be taken into account when comparing results of mechanical tests.

From the perspective of surgery reconstruction, the mechanical parameter used to evaluate a potential graft is the failure load. Previous studies in this matter have studied the structural properties of different foot tendons for reconstruction of Achilles tendon and knee ligaments. Zhao and Huangfu (2012) reported strength values of anterior half of the PL of 322.4N $\pm$63.2 comparable to the measurement of 346N $\pm$196. Other *in vitro* studies have informed a failure load of 333.1N $\pm$137.2 and 348.8N $\pm$124.9 for PB (Sebastian et al., 2007; Datta et al., 2006), somewhat higher than 239N $\pm$99 that now is measured. In the same stud-

ies, failure loads of FHL of 511N ±164.3 and 241.5N ±82.2 were also reported. In that case inferior to the 525N ±200 currently measured. Bigger differences are found with the TP failure loads reported by Giannini et al. (2008) which showed fourth times more strength than the samples tests in the current investigation.

Regarding material properties, the most complete dataset reported about these lesser-studied foot tendons is the investigation carried out by Blanton and Biggs (1970). They investigated the ultimate tensile stresses depending on the position and function of the muscle. They reported lower extremity extensor and flexor tendon values separately. The stress failure ranged between 9-55MPa for both groups being 26.2MPa the average for extensor tendons and 31.2MPa for flexor tendons. These results are similar to the range of 6-76MPa obtained in the present study and the mean values of 22.3MPa and 22.1MPa for extensor and flexor tendons respectively. These results do not represent a significant difference between extensor and flexor tendons in accordance with Cronkite (1936) findings. However, Benedict et al. (1968) found a slightly higher difference between extensor and flexor tendons. Extensor tendons failed at an average stress of 92.3MPa while flexors only reached 75.4MPa. Schechtman and Bader (1997) obtained a similar range, around 100MPa of ultimate tensile stress for EDL tendons. In that study Young's modulus were not reported, but it can be inferred from their typical stress-strain curve, mean ultimate tensile stresses and mean strain failure results that they obtained values that double the current measurements as happens with the Young's modulus reported by Benedict et al. (1968) and Giannini et al. (2008).

The disparity of results between experiments is likely caused by methodological differences such as storage method, criteria of exclusion, clamping system, preconditioning, preload configuration or strain rate coupled with the natural variability of living tissues (Cook et al., 2014). Maganaris et al. (2008) argued that this discrepancy is substantially reduced when comparing mechanical properties using the same methodology. The properties assess in this study constituted a complete reference of the mechanical properties of the balance foot tendons calculated on the basis of the same methodology.

As anecdotal note, during testing in the laboratory room was possible to hear

Figure 3.7: Fiber breakage of a fourth toe Extensor Digitorum Brevis (EDB4) specimen during test.

the soft sound of the tendon fiber breakage which reminds the guitar strings break noise (Figure 3.7). Benedict et al. (1968) pointed out this sound as rapidly break apart of fiber bundles.

This study assesses *in vitro* the mechanical properties of the main balance tendons of the human foot reporting structural and material properties sorted by tendon. Detailed information of the methodology employed during experiments is provided in order to frame the results for future applications. Finally, the impact of experimental issues are discussed. The results obtained can be utilized in different engineering and clinical applications. The material properties together with the quantitative description of the stress-strain curve will help in the design of synthetic materials and in the development of refined constitutive models

for computational simulation. The structural properties provide worthy information to practitioners of eligible tendons for reconstruction surgeries and for the estimation of tendon injuries.

In conclusion, the *in vitro* study of the mechanical properties of the main balance foot tendons reveals that flexor/extensor toes tendons have higher Young's modulus and ultimate tensile stress while inversion/eversion tendons have larger strain failure. In other words, Tibialis and Peroneus tendons are more deformable at the same stress and strain rate. A criterion to quantify the regions of the stress-strain curve is defined. Stress-strain tendon curves exhibit proportionality between regions corresponding the initial strain, the toe region and the yield point to the 15, 30 and 70% of the strain failure respectively.

3.5 Foot tendon characterization

The stress-strain curves obtained from the tendon tests are used to fit the parameters of a non-linear model. This chapter is particularly focuses on characterize the tensile response of the tendon; then, hyperelastic material models are used to fit the experimental curves. The procedure is divided in two steps. In the first step, several constitutive models are used to fit the reference tendon stress-strain curve. From this setting only the constitute models that performs a real physiological behavior are selected; this is, fit the experimental curve during positive strains and give compressive response with negative strains. In the second step, the models that successfully meet the first requirement are used to replicate the uniaxial tendon tests. The material model that shows better agreement with the actual tests is chosen. ABAQUS software is employed to perform the analysis.

The reference tendon curve selected to characterize the foot tendon tissue is the average curve of the two main responses described previously, the mean extensor/flexor curve and mean tibialis/peroneus curve (Figure 3.5). A weighted average is rejected in order to weight equally both responses independently of the number of samples tested in each group. Within all hyperelastic formulations predefined in ABAQUS, the constitutive models with smaller number of material parameters are preferred because less experimental tests are required to determine

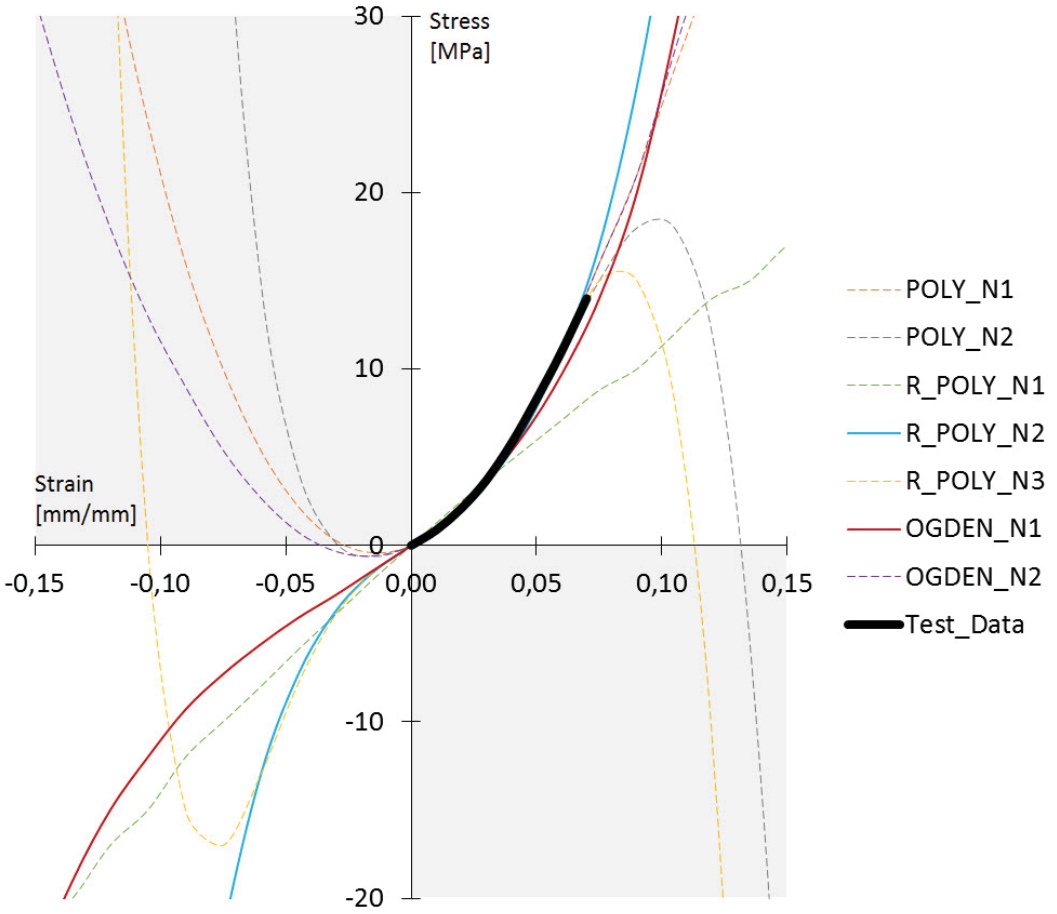

Figure 3.8: Constitutive models fitted to the experimental curve.

their parameters. The constitutive models included in the analysis are: Ogden first and second order, Polynomial n=1 and 2, and Polynomial reduced order 1, 2 and 3 formulations. Out of seven approaches, only first order Ogden formulation and polynomial reduced of second order fitted the experimental curve and performed a real physiological behavior (Figure 3.8).

In the second step, the uniaxial tendon tests are computationally replicated. Firstly, eight tests are randomly picked, one test for each sort of tendon (EDB, EDL, FDB, FDL, TA, TP, PB, and PL). A simple mesh with a one-dimensional truss element is created. An extreme of the element is fixed and the other extreme is configured with several steps increasing the axial load applied. This simple FE

model allows quick adjustment of the specimen structure defining the length and the CSA of the truss element. Running the eight cases with both constitutive models yield that Ogden model shows better agreement with load displacement curves of all sort of tendons. Moreover, the Ogden parameters determined for tendon tissue present stability for all ratios.

With this procedure, the material parameters are determined but remains undefined the compressibility parameter. Ogden model describes a hyperelastic behavior of rubber-like materials accounting for compressibility. Its strain energy density function U in terms of generalized strain is:

$$U = \frac{\mu}{\alpha^2}\left(\lambda_1^\alpha + \lambda_2^\alpha + \lambda_3^\alpha - 3\right) + \frac{1}{D}\left(J-1\right)^2 \tag{3.1}$$

where μ is the initial shear modulus, it has units of stress, α is the strain hardening exponent, it is unitless, and D is the compressibility parameter and it have units of 1/stress. It is commonly accepted that soft biological tissues because of their high water content are nearly incompressible, then a Poisson's ratio of 0.499 is defined (Vergari et al., 2011). The adopted coefficients of the hyperelastic model for foot tendon tissue are detailed in Table 3.4.

Table 3.4: Ogden parameters for foot tendon tissue. Units for the shear parameter (μ) is MPa and for the compressibility parameter (D) is mm^2N^{-1}

μ	α	D
33.1622	24.8987	0.0001207

To put the material model response into context, in Figure 3.9 is compared the stress-strain curve of the Ogden model with the stress-strain curves of the tendon samples tested.

3.6 Performance comparison

Once the parameters of the constitutive model for foot tendon tissue are defined, the model performance is compared with previous foot tendon material models employed in the literature. Particularly, in FE foot modeling, only three different

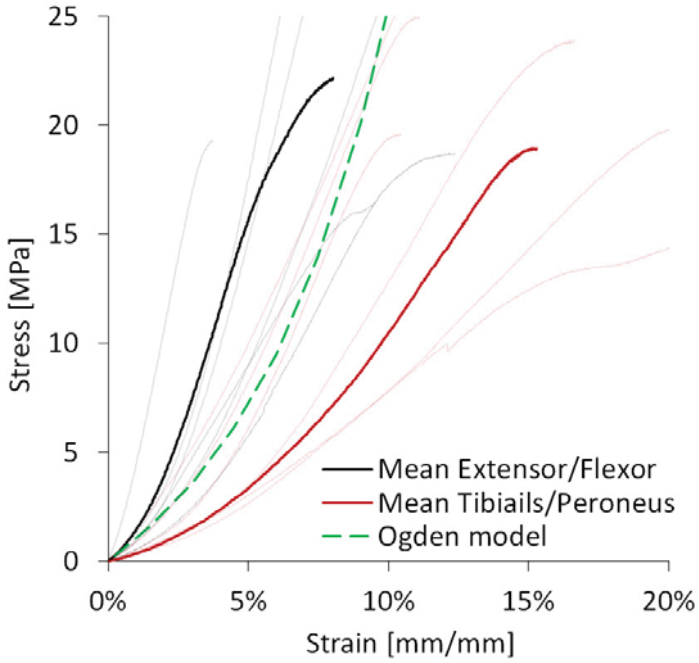

Figure 3.9: Comparison of the Ogden model fitted with the stress-strain response of the tendon samples tested.

approaches have been used for this tissue. The first approach was presented by Wu (2007) in a 2D foot FE model were the tendon tissue was configured linear elastic transverse isotropic using a Young's modulus of 1200MPa for the axial direction and a Poisson's ratio of 0.4. The second approach was given by Gu et al. (2008) in a 3D model of the Achilles tendon. They defined the Achilles tendon material using an incompressible hyperelastic two-parameter Mooney-Rivlin formulation. The third approach is the tendon properties used in the Chapter 2, firstly published by García-Aznar et al. (2009). This model is isotropic linear elastic with a Young's modulus of 450MPa and a Poisson's ratio of 0.3.

The performance comparison is made under the same procedure employed to assess the best constitutive model. The simple truss element model previously created to replicate tendon tests is now configured with the structural properties of two randomly selected samples tested in the universal testing machine. Each model is run four times, once for each different approach and the load-displacement curve obtained is compared with the original curve reported by the

testing machine. The comparative graphs are shown in Figure 3.10.

As is shown in the graphics (Figure 3.10), only the hyperelastic model configured in this chapter performs an actual non-linear behavior of tendon tissue in the toe region. The other hyperelastic approach, the two-parameter Mooney-Rivlin formulation, responds almost linear. Therefore, with this analysis is demonstrated that the Ogden parameters fitted in this chapter produces a more non-linear response and better agreement with the actual foot tendon tissue response than previous approaches.

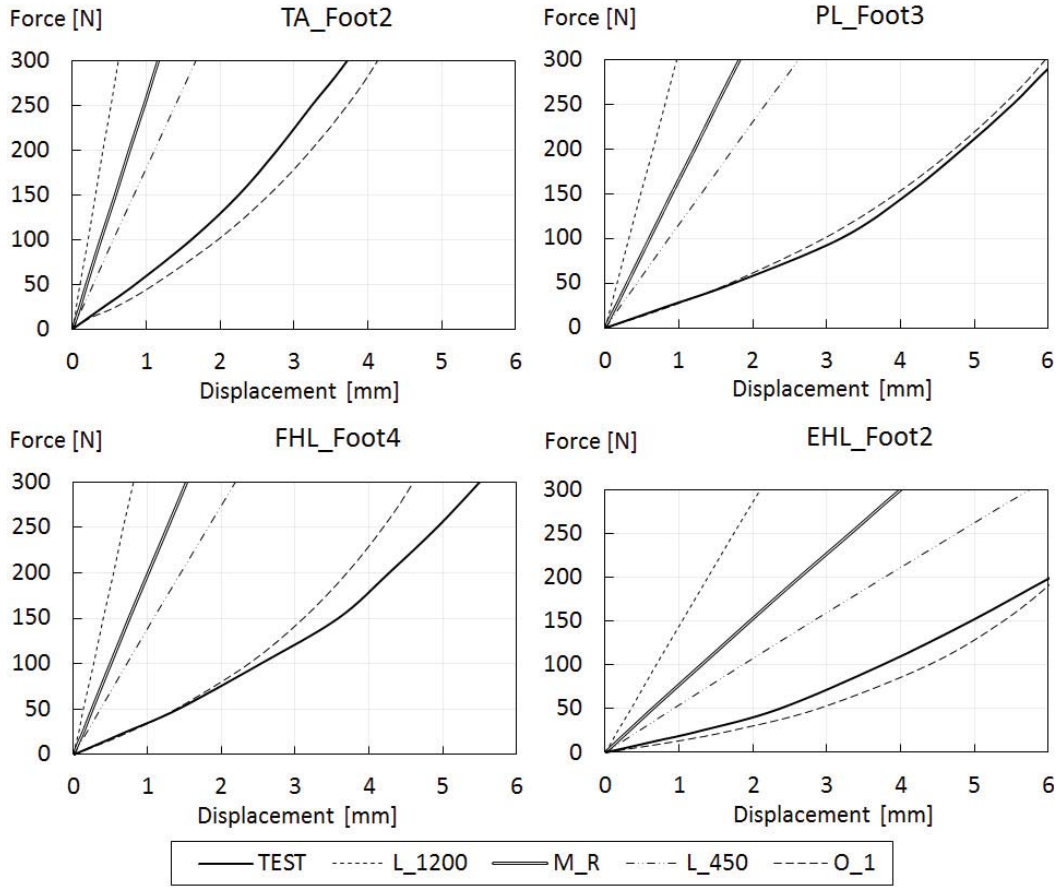

Figure 3.10: Comparative performance of the different foot tendon approaches employed to date. TEST – Experimental curve. L_1200 – Linear model used by Wu (2007). M_R – Mooney-Rivlin model used by Gu et al. (2008). L_450 – Linear model used by García-Aznar et al. (2009). O_1 – Ogden model fitted in this chapter.

CHAPTER

FOUR

COMPLETE DETAILED FOOT FINITE ELEMENT MODEL

In this chapter, a 3D foot FE model with actual geometry and non-linear behavior of tendons is developed and validated for analysis of the lower limb muscle forces effect in the inner foot structure. The geometry of the model is obtained from CT and MRI differentiating cortical, trabecular, tendon, muscle, cartilage and fat tissues. Tendon tissue is characterized with the Ogden model based on uniaxial foot tendon tests. Two applications are developed. In the first application, a force sensitivity study of the five major foot extrinsic tendons is conducted to evaluate the function of each tendon. A synergic work of the inversion/eversion tendons is predicted. Pulling from a peroneus or tibialis tendon stressed the antagonist tendons while reducing the stress in the agonist. This paired action is also predicted for the Achilles tendon with the tibialis anterior. In the second application, the functional role of the extrinsic muscle-tendon-units in foot pronation/supination and the stress state at the plantar fascia, the talocrural joint cartilage, the plantar soft tissue and the tendons are estimated in early and late-midstance phase of walking. The work presented in this chapter has been submitted for publication in the "Journal of Biomechanics" (Section 7.2.1 — Publication 4).

4.1 Introduction

Foot FE models have been developed during the last three decades improving their features as computational capacity and constitutive models for biological tissues were improving. Mechanical behavior of bone has been well addressed but soft tissues representation approaches are still evolving. Advances have been achieved in simulating non-linear behavior of foot plantar soft tissue and refined constitutive models with real geometries of ligaments are currently used in foot modeling. However, muscle and tendon components have not been appropriately addressed yet (Morales-Orcajo et al., 2015a).

In computational foot modelling, tendon representations have been limited to reaction forces in the tendon insertions (Cheung et al., 2006b; Chen et al., 2014b) or the use of one-dimensional link elements (Isvilanonda et al., 2012; Morales-Orcajo et al., 2015b). Recent approaches included realistic geometry of Achilles tendon, but the remaining tendons that control foot motion were represented by truss elements or neglected (Chen et al., 2012). Furthermore, linear properties were used to assess their non-linear behavior. In only one simulation of the AT performance an hyperelastic formulation was employed (Gu et al., 2008). The parameters were set through inverse dynamics; however, the resulting hyperelastic model did not accomplish the initial large strain characteristic of the tendon stress-strain curve, as shown in section 3.6.

Quantifying the forces exerted by each muscle during lower limb movements is another challenging task in foot biomechanics. Actual measurements on this matter are difficult to find in the literature because of measuring muscle forces *in vivo* is generally not feasible. Therefore, the use of optimization algorithms based on physiological parameters is a recurrent way to predict tendon pulling forces. Due to the nature of those estimations, proposed values are within a large range and variability increases by inter-subject differences, age and gender dependency. Previous computational foot models have estimated the magnitudes of muscle forces using equilibrium equations (Patil et al., 1996) or interpolating individual muscle forces proportional to physiological cross-sectional areas (Jacob et al., 1996; Chen et al., 2012). The initial reference value is taken from lower extremity mathe-

matical models, matching the prediction of the model with some experimental measurements (Gefen et al., 2000; Chen et al., 2012) or based on electromyography data (Liu and Zhang, 2013). Inverse dynamics is another common procedure to predict tendon forces exerted during movements (Erdemir et al., 2007; Gu et al., 2008). Within foot cadaver models physiological parameters such as physiological cross-sectional areas, electromyography values, maximum specific tension and location of the center of pressure were considered in different optimization algorithms (Thordarson et al., 1995; Sharkey and Hamel, 1998; Imhauser et al., 2004; Burg et al., 2013). Muscle activation patterns, kinematic and kinetic performance during lower limb movements have been deeply studied through those musculoskeletal and cadaver models, but the effect of muscle forces in the internal foot components is less known.

The purpose of this chapter is to establish a 3D foot FE model of the human foot using detailed and realistic geometry and non-linear behavior of tendons. The model performance is evaluated against *in vivo* and *in vitro* measurements. Through a force sensitivity analysis of ankle stabilizer tendons the model shed light on the role of each tendon in the mechanical response of the foot. Furthermore, the mechanical solicitations of the internal foot components are predicted at the beginning and the end of the midstance phase of walking.

4.2 Model creation

4.2.1 Geometry reconstruction

The right foot of a 49 years old male volunteer, with weight of 70kg and height of 170cm, was scanned to obtain the geometry of the FE model. Two different tomographies are performed to capture the geometry of all tissues in the foot. X-ray 0.6 mm slice distance CT images are used to define bone volumes (cortical and trabecular) and to sketch a primary distribution of tendons (Figure 4.1). The MRI, which provide a better definition of soft tissues, are subsequently used to refine the initial segmentation, especially the deeper layers of muscles.

MIMICS (Materialise, Leuven, Belgium) is employed to generate a 3D solid

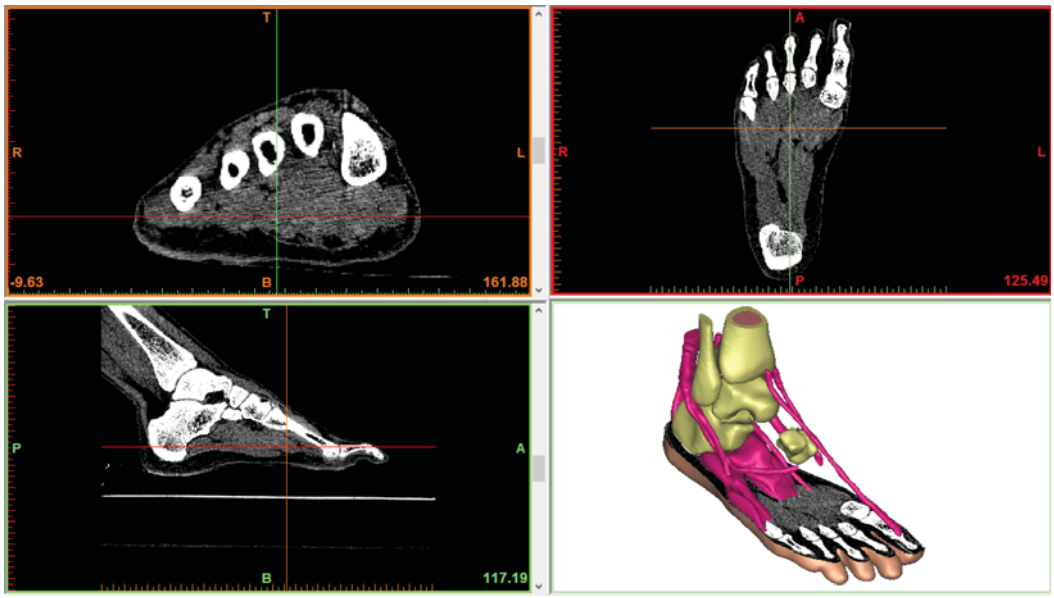

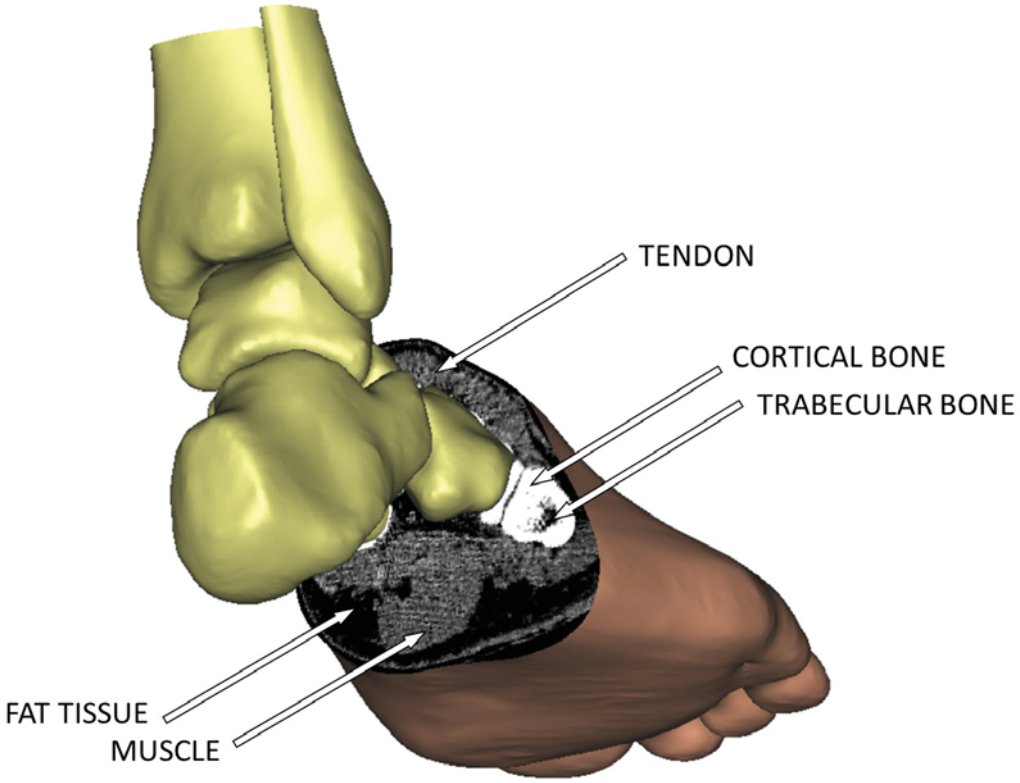

Figure 4.1: Geometry segmentation process from computer tomographic images in MIMICS.

model from 2D slices. Several anatomy references are additionally consulted to help in the identification and delimitation of each individual tendon geometry. Due to the complexity of the internal foot components, mostly the intrinsic muscles and tendons concentrated under the foot arch, the reconstructed geometry is processed to avoid volume intersection and other geometrical disruptions previous to meshing.

4.2.2 Meshing

At this step, 102 stl format files, representing the total of solid parts involved in the FE foot model, are imported to the meshing software. Those volumes correspond to 30 cortical bone segments, 18 trabecular bone segments, 22 cartilage segments, 29 tendon and muscle segments, 2 fascia segments and the soft tissue volume surrounding the complex (Figure 4.2). ANSYS ICEM CFD (ANSYS Inc., Canonsburg, PA, USA) is chosen because of its efficiency in meshing large and complex models and its extended mesh diagnosis. A trial-error approach is employed to optimize the mesh size of each segment. The conditions to achieve a reasonable mesh size without compromising the calculation time are:

- Minimum mesh size sufficiently small to fit into the tightest segments, particularly in the forefoot where many different minor components are concentrated such as proximal, medial and distal phalanges, toes joint cartilages and the thinnest tendons.
- Maximum mesh size consistent with the minimum to avoid large differences in element size between regions and to ensure that the results are independent of the mesh density.
- Mesh accuracy has to achieve more than 99% of the elements better than 0.2 mesh quality (Jacobians) and check that poor elements are located away from the region of highest interest.

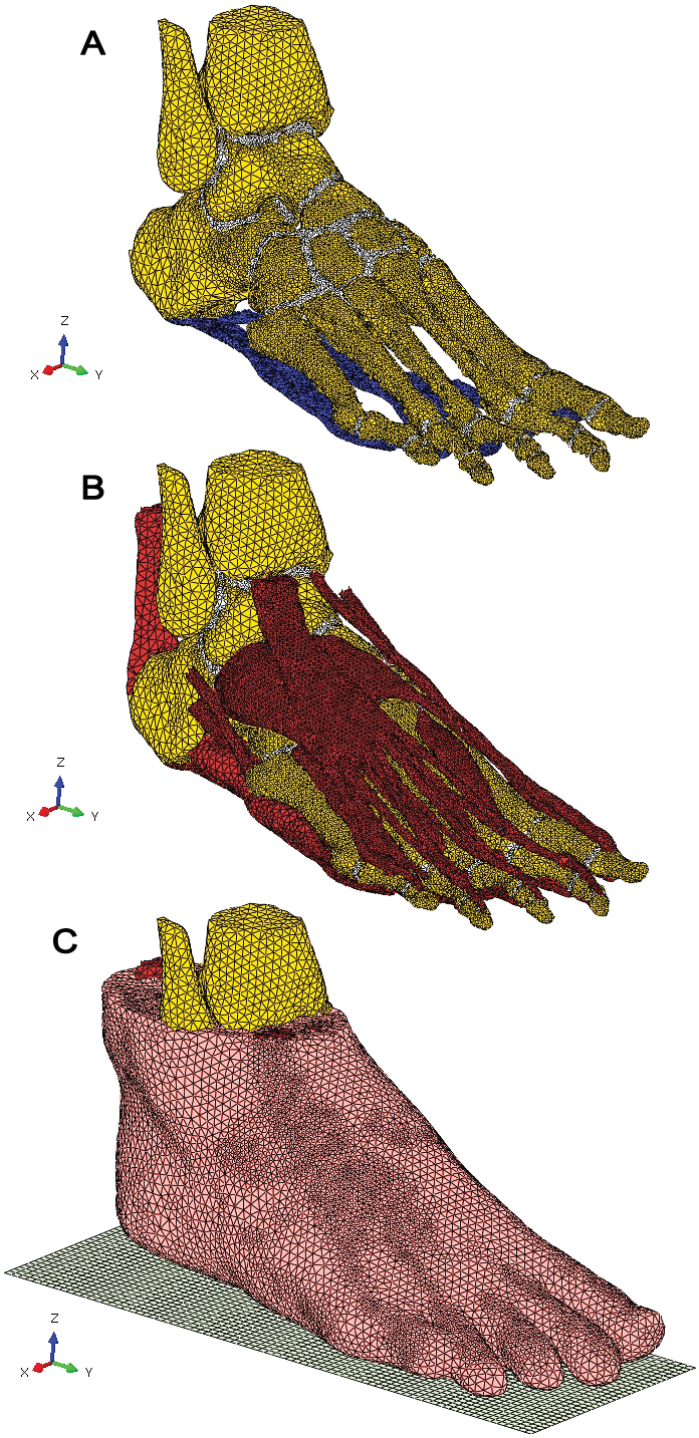

Figure 4.2: Tissue layers of the finite element model. (A) Skeleton + Fascia. (B) Skeleton + Muscle / Tendons. (C) Skeleton + Soft tissue + Ground.

- Number of elements below a million. With the current computational capacity, meshes higher than one million elements increase disproportionally the computational time.

The equilibrium is found with 806.475 linear tetrahedral elements with element sizes as follow: 1mm for smallest cartilages between phalanges, 2mm for phalanges, the thinnest tendons and the rest of the cartilages, 3mm for metatarsals and the rest of the tendons, 4mm for intrinsic muscles and AT and 5mm for the biggest bones in the hindfoot and the fat tissue. This configuration is similar to the 4mm element size reported by Isvilanonda et al. (2012), but optimized for geometry requirements. The quality of the mesh is checked taking as reference the recommendations of Burkhart et al. (2013). All parameters are within good mesh quality ratios (Table 4.1).

Table 4.1: Mesh quality metrics based on Burkhart et al. (2013) recommendations.

Mesh quality metric	Assessment criteria	Accurate elements	Inaccurate elements
Element Jacobians	>0.2	99.9%	0.1%
Aspect Ratio	<3	94.5%	5.5%
Min angles	$>30^o$	80.2%	19.8%
Max angles	$<120^o$	99.8%	0.2%

4.2.3 Model base configuration

The pre-processing of the mesh previous to calculus is conducted with the software I-DEAS (SDRC, Milford, CT, USA). A rigid plane under the foot is created in the model in order to calculate ground reaction forces. A surface-to-surface contact between the model and the rigid plane is defined with a friction coefficient of 0.6 (Cheung et al., 2006b). Loads, boundary conditions, calculus and post-processing are processed using ABAQUS (ABAQUS Inc., Pawtucket, RI, USA).

4.2.3.1 Material properties

The complete detailed 3D foot FE model differentiates seven tissues. Specially, highlight the hyperelastic approaches employed to simulate tendon and fat tissue. For tendon tissue the Ogden model parameters determined in the Chapter 3 are used (Table 3.4). The properties of the plantar soft tissue are taken from the literature. Particularly, the hyperelastic second-order polynomial parameters reported by Chen et al. (2010a) (Table 4.2).

Table 4.2: Coefficients of the hyperelastic second-order polynomial material model applied to the plantar soft tissue (Chen et al., 2010a). Units for the shear parameter (C_{ij}) are MPa and for the compressibility parameter(D_i) are mm^2N^{-1}.

C_{10}	C_{01}	C_{20}	C_{11}	C_{02}	D_1	D_2
0.08556	-0.05841	0.039	-0.02319	0.00851	3.65273	0

The remaining tissues, cortical, trabecular, fascia and muscle are determined with the same properties used in the skeletal model described in Chapter 2. Note that the skeleton is reconstructed from CT and MRI of a different patient. Fascia and muscle components, unlike in the skeleton model, in this case are modeled with real geometry. Cartilage properties are differentiated between the small joints between phalanges in the forefoot and the strong joints of the hindfoot. All these tissues are modeled with linear elastic isotropic properties. The elastic modulus and the Poisson's ratios are sumarized in Table 4.3.

Table 4.3: Elastic linear isotropic properties applied to the rest of the tissues. E= Young's Modulus in MPa. ν= Poisson's ratio, dimensionless

Component	E	ν	Reference
Cortical bone	17000	0.3	(García-Aznar et al., 2009)
Trabecular bone	700	0.3	(García-Aznar et al., 2009)
Hindfoot cartilages	10	0.4	(Gefen et al., 2000)
Forefoot cartilages	1	0.4	(Athanasiou et al., 1998)
Fascia	350	0.3	(Cheung et al., 2006b)
Muscle	450	0.3	(García-González et al., 2009)

4.2.3.2 Loads and boundary conditions

Input requirements of biomechanical models make it necessary to quantify the force applied by each muscle-tendon-unit during a specific movement. Since there are no actual measurements of those forces in the literature, kinetic estimations have to be used. In the present study, the muscle forces calculated by Salathe and Arangio (2002) are chosen as reference to set the different loading conditions. These values are consistent with the range of forces in which each tendon is expected to work. Considering that tendons work regularly below half of its capacity the values proposed for midstance positions are below 15% of the load failure (Table 3.1). These values have been adopted previously for the computational simulation of flatfoot (Pes Planus) (Wang et al., 2014b) and are similar to the values employed in other computational and cadaveric models predicted through different approaches (Imhauser et al., 2004; Liu and Zhang, 2013).

4.2.4 Validation

The biomechanical reliability of the model is evaluated by means of two different responses: plantar pressure distribution and vertical foot displacement. The plantar pressure distribution and location of the center of pressure (CoP) predicted by the model are matched with the measurements of the same subject who volunteered for scanning. The volunteer stand upright for 30 seconds on a pressure platform with $25mm^2$ resolution, model Footchecker (Loran Engineering S.R.L., Italy). Due to the slightly unbalanced standing of the volunteer during the record time, little variations are registered from one measure to another. Therefore, the most balanced distribution of three measurements is selected.

Good match of peak plantar pressure value and location are found (Figure 4.3). However, the CoP of the model is misaligned longitudinally and transversally with respect to the measured CoP. This deviation occurs because, in the simulation, the toes and the midfoot did not make ground contact, which displaced the predicted CoP medially and backwards.

The vertical displacement of the foot arch structure is evaluated with experimental measurements available in the literature. Cheung et al. (2006b) performed

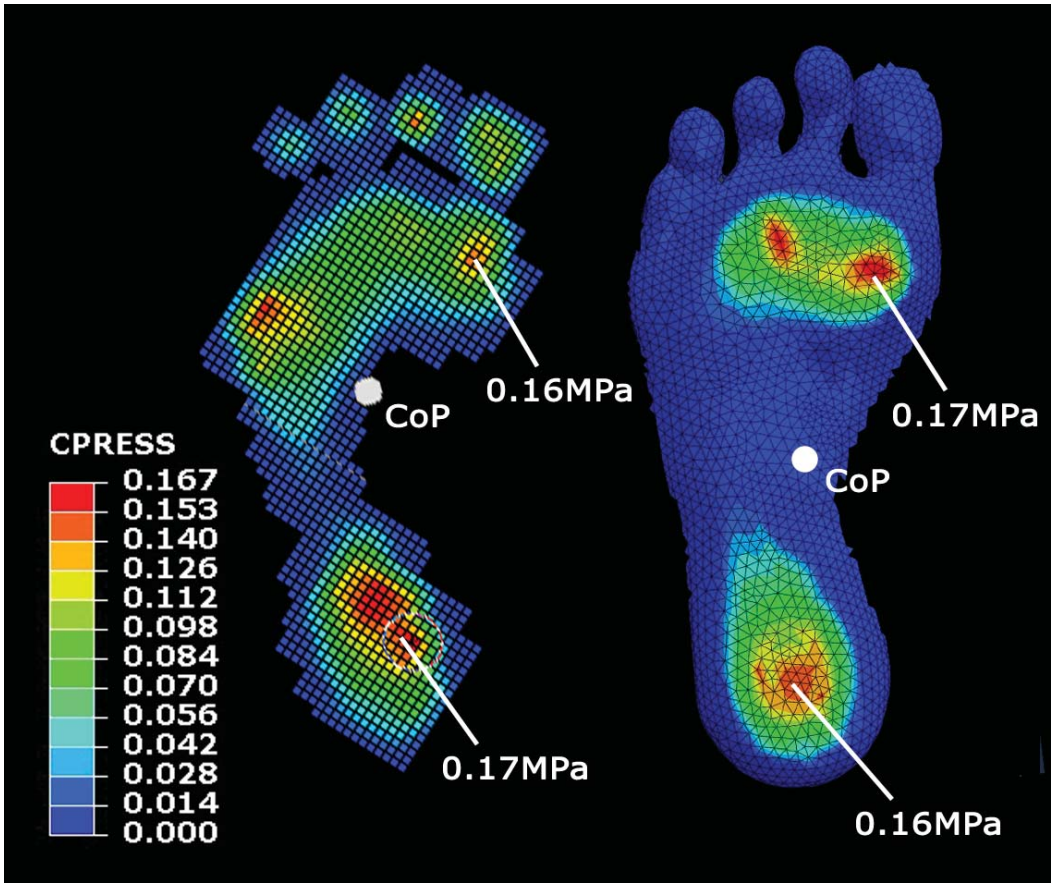

Figure 4.3: Comparison of the plantar pressure measured (left) and the plantar pressure predicted (right) in upright standing position. CoP–Center of Pressure.

a pure vertical compression test in six cadaveric feet and the average of the six curves reported are used for comparison. Tao et al. (2009) measured the vertical deformation of the foot *in vivo* under gradual increasing loads using a motion capture system. Both experimental measurements are compared with the vertical displacement of the navicular bone calculated by the FE model applying an increasing axial load from 0 to 500N.

In Figure 4.4 the vertical displacement are compared. The model reproduce accurately the non-linear response of the foot-ankle complex, becoming stiffer by increasing the axial load.

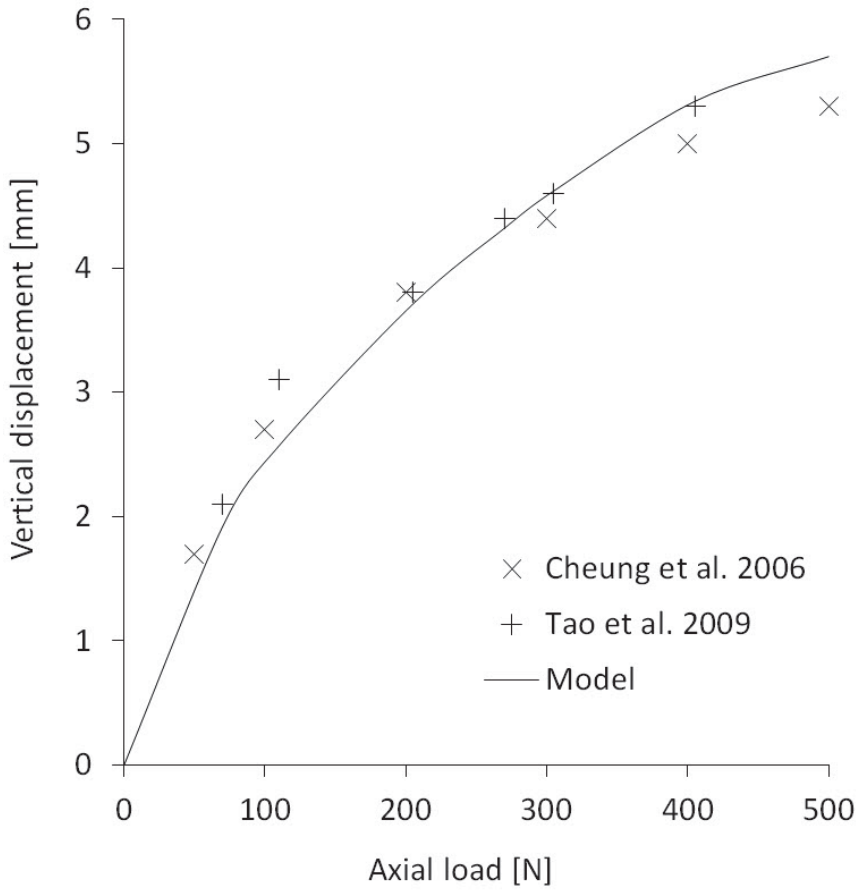

Figure 4.4: Comparison of the vertical displacement measured by Cheung et al. (2006b) and Tao et al. (2009) with the vertical displacement calculated by the model.

4.3 Applications

The complete detailed 3D foot FE model in total contact position is set in four different load conditions to perform two analysis (Table 4.4). First, a tendon force sensitivity analysis of the five major stabilizer tendons is perform to evaluate the function of each tendon and its effect on the inner structure of the foot. Second, quasi-static analysis of walking midstance phase is perform to evaluate the alteration in the internal components of the foot during this phase of gait. These applications are framed in the fields of physiotherapeutic treatments.

Table 4.4: Different load configurations applied to the model in total contact position. Ellipsis indicate the values that have been ranged in the sensitivity study keeping the rest of the tendon forces fixed.

[N]	Conf. 1	Conf. 2	Conf. 3	Conf. 4
Axial Load	350	630	630	630
AT	... 150 ...	... 300 ...	300	1300
TA	... - ...	... - ...	60	-
TP	... 30 ...	... 60 ...	60	60
PB	... 12 ...	... 24 ...	12	36
PL	... 24 ...	... 48 ...	24	72
EHL	15	30	60	30
FHL	15	30	30	120
EDL	7,5	15	30	15
FDL	7,5	15	15	60

4.3.1 Tendon force sensitivity analysis

The first configuration represented the load condition of the foot in standing position. Tendon forces are set as half the values for midstance position and the axial load is half of body weight. This setting is established to calculate the plantar pressure in standing position. Then, a sensitivity analysis of the five major stabilizer tendons is performed ranging their loads from 0 to 300N individually and keeping the rest of the forces in standing configuration. In the second configuration, the muscle forces were based on the estimation of Salathe and Arangio (2002) for the midstance walking phase and the axial load is fixed as 0.9 of the body weight (Barela et al., 2014). Again, a sensitivity study of the stabilizer tendons from 0 to 300N is performed. Tendon forces are sumarized in Table 4.4.

The results of the sensitivity analysis of the five major stabilizer tendons are similar in both configurations, standing position and midstance phase. All tendons except the tibialis anterior plantarflexed the foot, producing a load transfer from rearfoot to forefoot such that the Achilles tendon is the major contributor. The tibialis anterior dorsiflex the foot. The tibialis and peroneus tendons also produce load transference in the frontal plane. The peroneus tendons evert the foot (the peroneus longus contribute most), increasing the plantar pressure un-

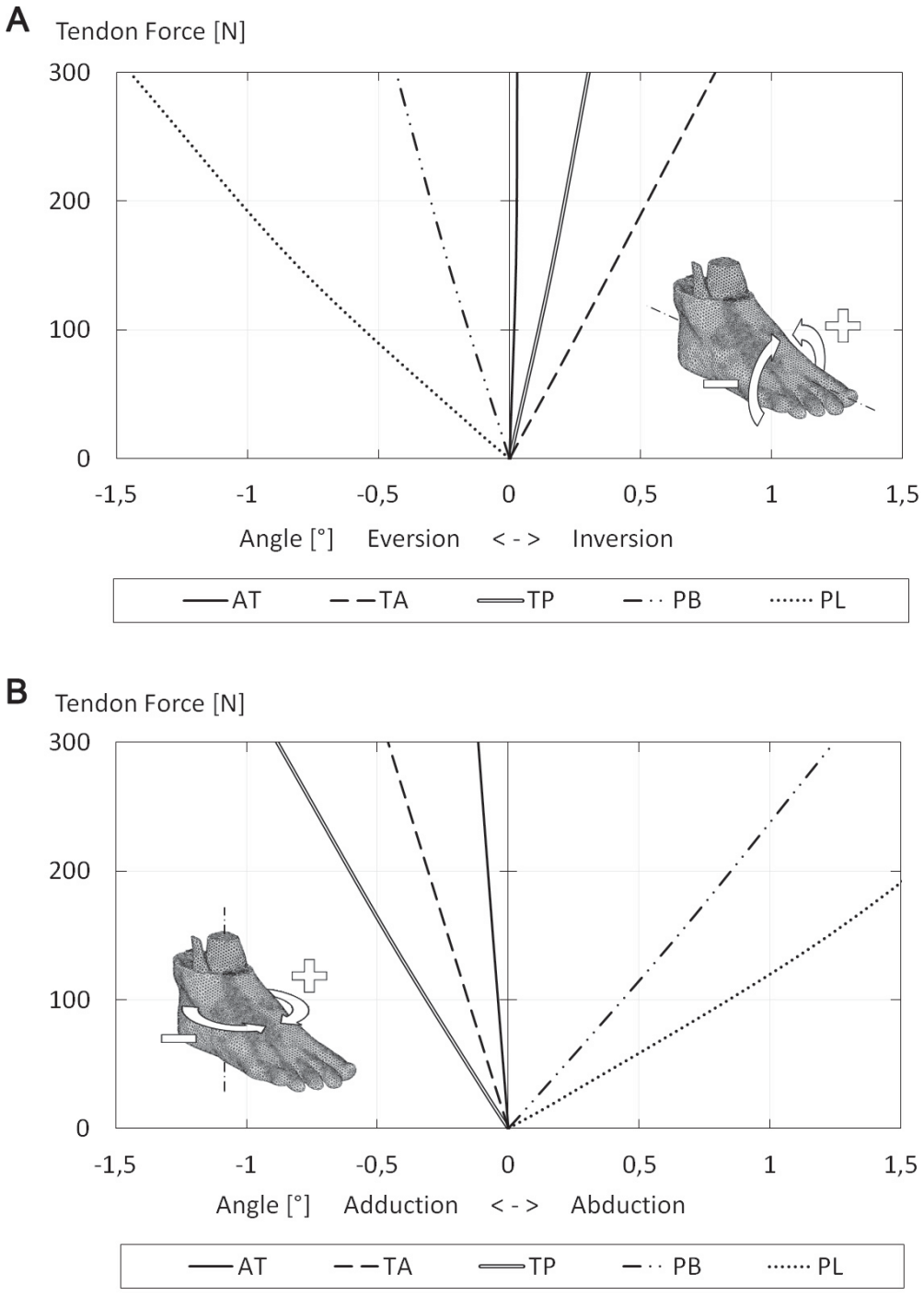

Figure 4.5: Rotation angles of the foot as function of force exerted by tendons. TA – Tibialis Anterior, TP – Tibialis Posterior, AT – Achilles Tendon, PB – Peroneus Brevis, PL – Peroneus Longus

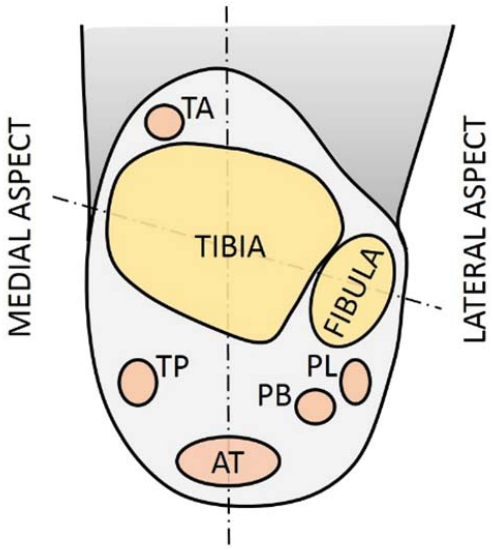

		TA	TP	PL	PB	AT
TA	▲	-	▼	▲	▲	▲
TP	▲	▼	-	▼	▲	▲
PL	▲	▲	▲	-	▼	▼
PB	▲	▼	▲	▲	-	▼
AT	▲	▲	▼	▼	▼	-

Figure 4.6: Left: Tendon location scheme in the cross-section of the ankle. Right: Tendon stress relationship observed in the sensitivity analysis. TA – Tibialis Anterior, TP – Tibialis Posterior, AT – Achilles Tendon, PB – Peroneus Brevis, PL – Peroneus Longus

der sesamoids, whereas the tibialis tendons relieve pressure under the first ray, inverting the foot (the tibialis anterior contribute most) (Figure 4.5A). In the transverse plane, similar response is observed. The peroneus tendons produce abduction while the tibialis tendons adducted the foot and the Achilles tendon keep the foot equilibrated (Figure 4.5B). The longitudinal arch is also influenced by muscular activity. The increase of Achilles tendon force stress the plantar fascia by increasing length and decreasing height of the arch. By contrary, the tibialis tendons reduce the stress in the plantar fascia by reducing length and increasing height of the arch. The tibialis posterior is more effective in this regard.

A coupled response of the eversion/inversion tendons is observed. When the force exerted in a peroneus or tibialis tendon is increased, the stress in the agonist tendon is reduced, while the stresses in the antagonists are increased. A similar response is perceived between Achilles tendon and tibialis anterior, such that pulling from one stressed the other one (Figure 4.6).

4.3.2 Quasi-static analysis of walking midstance phase

The last two configurations, 3 and 4, mimic the forces in early-midstance and late-midstance positions. The midstance phase comprehend about 50% of the stance phase of gait, from ∼15% to ∼65%, and within that period the muscular stimulus vary. Hence, the beginning and the end of this phase are configured in order to study the effect of these alterations. The load conditions for these cases are estimated considering the midstance configuration and muscle activation patterns during walking (Sharkey and Hamel, 1998). Tendon forces are sumarized in Table 4.4.

From early to late-midstance positions mechanical solicitations are predicted. At the beginning of midstance, a peak plantar pressure of 0.26MPa is estimated in the rearfoot. At the end, the contact area is reduced under the rearfoot and increased under the forefoot, reaching plantar pressure values of 0.6MPa. The plantar fascia during midstance is stressed up to 3MPa at 2cm of the calcaneus insertion. In the talocrural joint cartilage, compression stress values of -5.6MPa are predicted for late-midstance phase. With respect to the tendons, tibialis and peroneus tendons work in values of 1 to 3MPa during midstance cases and the Achilles tendon reaches 17.7MPa at late-midstance analysis. In late-midstance position, higher mechanical response of the foot structure is required.

4.4 Discussion

In the present study, a complete foot FE model is developed including a detailed representation of the actual geometry and behavior of tendons. Trabecular and cortical bone are differentiated and each cartilage, fascia, tendon and muscle that compounds the foot are included in the model, comprising 102 independent segments. Tendons are simulated with a non-linear first order Ogden constitutive model adjusting the parameters with uniaxial tendon testing curves. Finally, the model is validated and the effect in the foot-ankle complex produced by the extrinsic tendons is assessed.

The model predictions are validated in two different responses and showed

good agreement with *in-vivo* and *in-vitro* measurements. This model is a step further in the development of foot FE models, since it includes a more accurate simulation of the tendon tissue. This new feature opens new possibilities in the analysis of foot soft tissue function and pathology. In the literature there are abundant research studies related to the muscle-tendon activity during walking: capture motion measurements, electromyographic reports, musculoskeletal models estimations and dynamic cadaver performances, however none of these methods measured tissue stress. Stress information is relevant because it is the mechanical parameter closely related to pain, tissue damage and mechanical stimuli of biochemical processes. The FE model presented in this study, based upon kinetic parameters, estimates tissue stress, an important contribution to the production of trustworthy information of clinical relevance.

The model obtain the inversion/eversion movement of the foot relative to the tibia as function of tendon force. The peroneus tendons increase plantar pressure under the medial aspect and the tibialis tendons increase plantar pressure under the lateral aspect. At the ankle articular cartilage, the reverse is true, peroneus stressed lateral side while tibialis stress medial side. This pattern was noted by Potthast et al. (2008) measuring the effect of the muscle forces in the intraarticular pressure distribution of the talocrural joint. They concluded that the coupled activation of synergist tendons would intensify those changes. The FE model predicted cartilage peak stress values of this joint higher than the measurements reported for similar axial load ratios (Calhoun et al., 1994; Natsakis et al., 2015). This overestimation could be expected since the linear model applied to simulate the cartilage behavior is a gross approximation for this complex tissue. A refined formulation for these components will provide better results.

In the cadaveric simulation performed by Sharkey et al. (1995), a mirror effect was described with respect to the sagittal plane. Load settings that produced high medial strains tended to produce low strains in the lateral side. This effect is also noted in our simulations, but besides a combined work of the tendons to keep the ankle movement stable is predicted. This coupled activation pattern of tendons is understandable given the precise control motion requirements to reach the responsiveness of the foot-ankle complex.

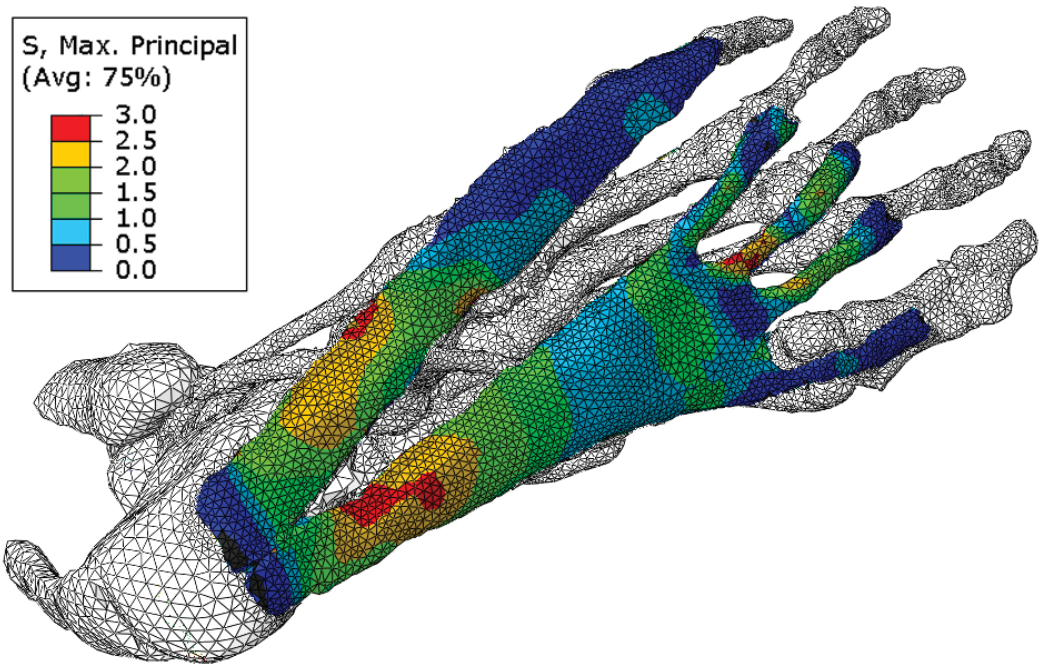

Figure 4.7: Stress (MPa) in the plantar fascia in late-midstance position.

The arch-supporting function of the tibialis posterior is a common discussion in the literature (Thordarson et al., 1995; Kitaoka et al., 1997; Watanabe et al., 2013). However, the capacity of tibialis anterior of avoiding excessive navicular drop has not been well studied yet. The model predicts similar functions for the tibialis anterior than for the tibialis posterior although in a lesser degree. Future research in this line could open new possibilities for the treatment or preservation of pes planus.

Regarding the midstance analysis, it was observed that the foot is subjected to higher mechanical stresses during late-midstance previous to the heel rise. Stress in the plantar fascia is predicted in the proximal portion where plantar fasciitis is more likely to occur (Figure 4.7). The Achilles tendon stress value predicted at late-midstance position is similar to the 19MPa maximal tension stress during walking measured by Finni et al. (1998). The stress levels estimated for the rest of the tendons constitute around 10% of their ultimate tensile stresses (Chapter 3). Considering that biological tissues, in their physiological performance, work below

half the failure stress, these levels of solicitation are reasonable for a relatively low mechanical demand activity such as walking.

From a clinical perspective, the model can be applied to many pathological or dysfunctional conditions, such as altered muscle activation patterns. The present model-based findings also provides clinically relevant information on the role of the ankle muscles on pronation-supination. Health professionals are frequently interested in walking mechanisms that may decrease excessive pronation during early stance and may produce supination during late stance, in order to treat or prevent pathological conditions such as plantar fasciitis and medial tibial stress syndrome (Neal et al., 2014; Chang et al., 2014). According to the present findings, at early-midstance the ankle muscles produce a total torque of inversion and adduction (i.e. supination) while it is known that the foot is pronating at this instant (Souza et al., 2010). Thus, these muscles decelerate pronation at early midstance and this function should be clinically optimized to avoid excessive pronation. The present results also show that, at late-midstance, the ankle muscles, mostly demanded to generate plantar flexion and gait propulsion, produce a total torque of eversion and abduction (i.e. pronation). At this instant, the foot is actually supinating (Souza et al., 2010), what would be decelerated by the ankle muscles. Therefore, to optimize supination at late-midstance, the role of tissues other than ankle muscles should be also regarded. Lower-limb external rotation produced at the hip and its role on increasing supination (Souza et al., 2014), through the mechanical coupling between shank external rotation and foot supination (Souza et al., 2010), should be then clinically considered.

In summary, a 3D FE model of the human foot, taking into account the real geometry and non-linear behavior of tendons, is developed and validated. Then, four tendon load conditions in total contact position are analyzed. From the tendon force sensitivity analysis, a paired work of the eversion (peroneus) and inversion (tibialis) muscle-tendon-units is observed and their functional role in foot pronation supination is discussed. From the analysis of midstance phase, higher stress values are predicted for the late-midstance position.

The model is fed by kinetic data and provided the mechanical response of the foot components. The model output is strongly related to the load tendon setting.

Therefore, advances in muscle control force quantification during different lower limb movements will significantly help for more reliable predictions of the model.

4.5 Model features

The foot FE model developed in this chapter is a clear step forward in the field of foot computational modeling. For first time have been introduce the actual geometry of all internal components of the foot. Latest models have included detailed geometry of fascia and Achilles tendon (Chen et al., 2015). In this case, every intrinsic muscle and all network of tendons that control foot movements are segmented independently. Also, central and lateral plantar fascia is distinguished and all complex embedded in fat tissue. Furthermore, the hyperelastic properties of foot tendon tissue determined in the Chapter 3 are applied to the tendons segments. Adding to this detailed geometry, the refined segmentation of the skeleton, distinguishing cortical and trabecular bone and identify the cartilage within each joint of the foot proportionate a very refined model for clinical assessment.

Note that the geometry is segmented entirely from a new scanning. Initially, it was intended to take advantage of the skeletal model previously developed, but it was not possible to put in place the soft tissue segmented from a different patient than the original. This option was definitely discarded and the model was created from the beginning.

It is remarkable that despite the fact that the volume meshed in this model is almost three times greater than the skeletal model, the number of elements is almost the same ($\sim$2% more elements). This is due to the optimization process performed during meshing. The previous skeletal model has a constant element size in the whole mesh. The small size element necessary to fit the small bones of the forefoot produced huge amount of elements in the big bones of the hindfoot. However, in the new model this feature has been taking into account to make practical the work with the model, optimizing the mesh size to the geometry requirements.

The great level detail of the new model influence computer time. Although the number of element almost not varies there is a high impact in the computing

time. The complete detailed 3D foot FE model created in this chapter takes more than 30 hours to converge (Intel core i5 3.2GHz processor and 4GB of RAM). This is a cost of computing 30 times higher than the skeletal model running under the same equipment.

Thus, if the number of element is almost the same, where the different of time of computing come from? This different is due to the material properties and the boundary conditions. In the new complete detailed 3D foot FE model almost a half of the elements have hyperelastic properties, witch require more time to compute than linear elastic approaches. The other factor that has a great impact is the contact interaction defined between the plantar sole and the ground.

Despite the cutting-edge features of the model, there are some limitations that need to be addressed in future developments. A better simulation of bone-to-bone contact is necessary. There are two main approaches to deal with this interaction. One is the use of frictionless contact elements, which allow free movement between bones. This approach produces higher displacements between bony structures than in the experimental measures (Cheung et al., 2006b). The other approach is to disregard contact properties of joints connecting one bone to another and use elements with low stiffness. The latter is used in this model and it has the limitation of stiffing joint movements. Because of this option, ligaments are not simulated.

Other features should also be improved to take full advantage of the model. Within the foot-ankle complex, many muscle and tendon components overlap, limiting the displacement of one component respect to its surrounding (Figure 4.8). A slipping interaction between these components when a force is applied to a tendon would be desirable, although this feature represents a difficult computational challenge.

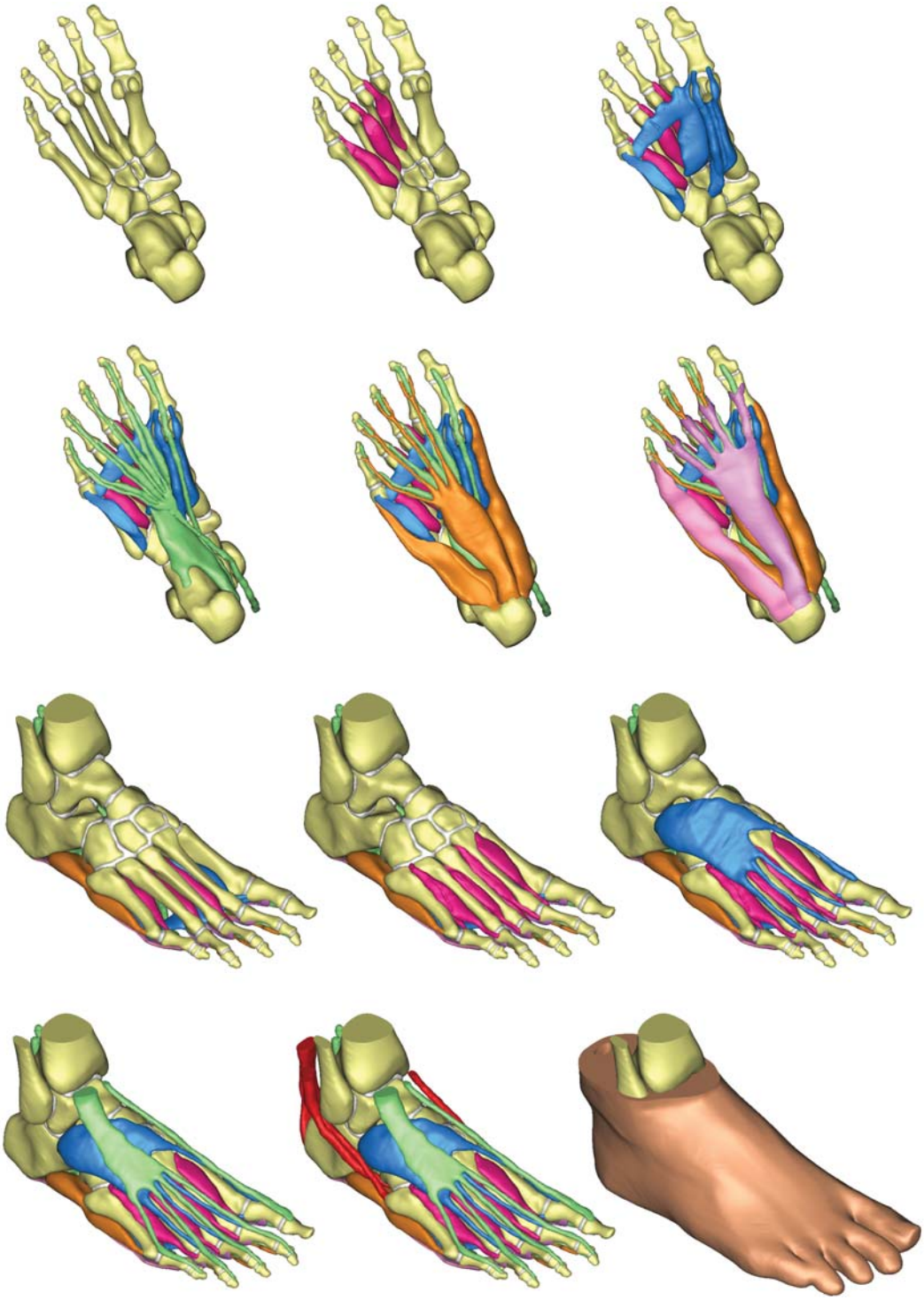

Figure 4.8: Muscle layers within the foot model.

CHAPTER

FIVE

MECHANICAL CHARACTERIZATION OF HUMAN PLANTAR SOLE

In this chapter, the compressive response of the bilayer plantar sole (adipose tissue and skin) is characterized by regions. Five human plantar soles are dissected and tested under compressive loads. Fifteen indentations along the plantar sole are performed to compare the stress-strain curve of the four regions of the plantar sole: rearfoot, midfoot, forefoot and toes. Three different mechanical responses are observed. Heel pad shows the stiffest response while the mid-arch region shows the softest. The indentations under metatarsal heads and toes exhibited very similar responses. Subsequently, two different plantar sole behavior results are parametrized: for rearfoot and forefoot. The former is based in heel pad tests and the latter on the average curve of submetatarsal heads and toes tests. The Ogden constitutive model is used to fit the experimental curves. The differentiation of the plantar soft tissue responses by regions will help in the understanding of the mechanical performance of this tissue, in the study of the energy absorption mechanism of the foot and in the refined characterization of human plantar sole. The study of the mechanical properties of the plantar sole presented in this chapter became part of the manuscript submitted for publication in the "Journal of Sport Science" (Section 7.2.1 — Publication 5).

5.1 Introduction

The plantar sole is the connective soft tissue located at the bottom of the foot. It is the part of the foot that makes contact with the ground providing perception and bearing the high local pressures under the heel and metatarsals heads. At macroscopic level, the structure of the plantar sole is composed of two layers, the adipose tissue and the thick skin layer. This region of the foot is highly vascularized contributing to the non-linear a time-dependent mechanical response.

In computational foot modeling the plantar sole is rarely treated as an independent part of the model. Usually, it is included in the bulk soft tissue that surrounds the foot skeleton including other tissues such muscles and tendons. Plantar soft tissue is also a recurrent expression used to refer to subcalcaneal and submetatarsal tissue. Another term related to the plantar sole is the heel pad. The heel pad is a highly specialized structure, located under the heel, designed to support highly compressive loads, which is composed of elastic fibrous chambers that enclose adipose tissue.

Despite the differences in structure between heel pad and the rest of the plantar sole, the bulk soft tissue embedding the foot skeleton is characterized with the compressive response of the heel pad and the mechanical behavior of other parts of the plantar sole have not been taken into account so far. Previous mechanical tests of the plantar soft tissue have centered on the heel pad (Bennett and Ker, 1990; Gefen et al., 2001; Rome et al., 2001; Miller-Young et al., 2002; Tong et al., 2003; Erdemir et al., 2006) and few studies investigated the response of the submetatarsal soft tissue (Chen et al., 2011). The comparison of results between regions in these cases is difficult due to the different test protocols employed in each study and because the studies are focused on structural properties instead of material properties.

Comparison between plantar soft tissue properties are related to diabetic and non-diabetic patients and aging rather than different locations. Young's Modulus has been shown to increase with diabetic condition (Kao et al., 1999; Zheng et al., 1999; Pai and Ledoux, 2010) and with age (Hsu et al., 2005; Chao et al., 2010; Kwan et al., 2010). Only one study investigated the material properties of the

plantar soft tissue in six different locations, and found differences between heel pad and other areas (Ledoux and Blevins, 2007). However, the results of this study cannot be employed for the purpose of this study because they removed the skin of the specimens and tested loads up to 20% of body weight.

In this chapter, the compressive response of the bilayer plantar sole (adipose tissue and skin) is investigated for loads greater than body weight in different plantar regions. Fifteen different locations on five cadaveric plantar soles are indented to obtain the stress-strain curves. The mechanical behavior of each region of the plantar sole is compared and the characteristic mechanical response of rearfoot and forefoot is used to adjust the parameters of a non-linear material model.

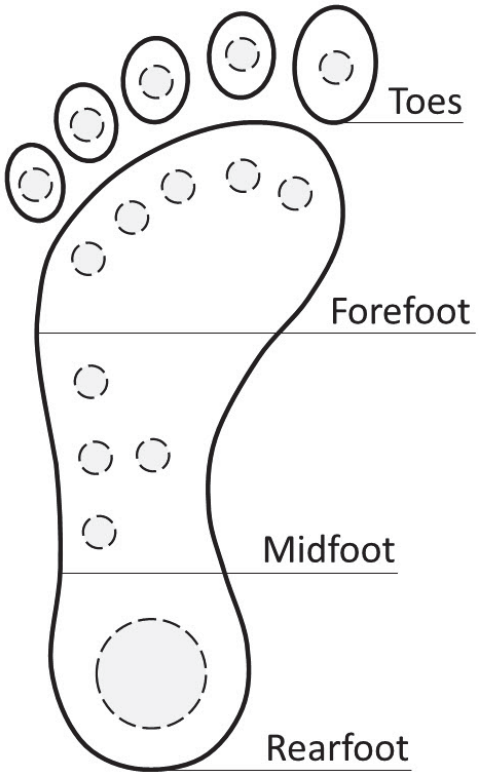

Figure 5.1: Size and location of the indentations performed in the plantar sole sorted by regions.

5.2 Mechanical testing

The soft tissue sole from five feet male elder donors are removed for testing. Each foot is stored frozen until 24h before testing. Plantar soft tissue are tested in compression in a universal material testing machine (Instron Ltd., U.K., model 5548) shortly after dissection. Each soft tissue sole is tested in fifteen different points as shown in Figure 5.1, so that fat tissues keep their natural confinement. A 40mm-diameter rounded stainless steel platen is used to test the heel pad and a 10mm-diameter cylindrical indenter is employed for the other points (Figure 5.2). Digital samples that present signs of frozen damage are excluded. The experiments has the approval of the Bioethical Research Committee of the Hospital Clinico San Carlos at Complutense University (n^o 12/210-E).

The testing machine scale is set to zero when the upper platen is in touch with the base plate. Thus, the undeformed thickness of the specimens is measured with the vertical position of the upper platen when the initial stress reach $\sim$1.25KPa (1.6N for Ø40 and 0.1N for Ø10) (Ledoux and Blevins, 2007). Compression tests are performed at 0.1mm/s of vertical displacement until load reaches 1KN at room temperature ($\sim 25^o$C). Soft tissues soles are kept hydrated during testing. For each test, a load-displacement curve is recorded by the testing machine.

The recorded curves are normalized to stress-strain curves and sorted in four groups: rearfoot, midfoot, forefoot and toes (Figure 5.1). The average curve of each of the four groups is used to compare mechanical behavior among different plantar sole regions.

Figure 5.2: Above: Heel pad indentation. Below: Forefoot indentations on metatarsal heads marks.

5.3 Mechanical properties of plantar soft tissue

The stress-strain curves of the heel pad indentations are graphed in Figure 5.3A. The indentation curves of the midfoot are shown in Figure 5.3B. The indentations curves of the forefoot are in Figure 5.4A and the indentation curves of the toes in Figure 5.4B. All graphs exhibit a strong non-linear response up to a limit of 0.1MPa, after which the stiffening ratio softens. The forefoot tests show the wider dispersion, while heel pad the narrower. This is likely because the indentations of the forefoot are performed on the metatarsals heads marks where higher singularities can be found, whereas the heel pad are indented on a more homogenous substance and with a greater indenter, which reduce the sensitivity to this particularities.

The average responses of the four regions are compared in Figure 5.5. Three different mechanical responses are observed. Heel pad showed the stiffest response while the mid-arch region showed the softest. The indentations under metatarsal heads and toes exhibited very similar responses. In Table 5.1 are listed the Young's modulus of the stress-strain curves of each plantar sole region as function of the stress level. The slopes of the four curves are similar for stress levels higher than 0.1MPa.

Plantar sole thickness decreases from rear to forefoot. The average thickness measured for heel pad samples is 16.8 $\pm$1.2mm. For midfoot, the average thickness is 10.5 $\pm$2.8mm, 6.7 $\pm$2.1mm under metatarsal heads and 6.7 $\pm$0.8mm in the toes.

Table 5.1: Young's modulus as function of stress level for each plantar sole region. Compression tests performed at 0.1mm/s.

Stress	Young's modulus [MPa]			
[MPa]	Heel Pad	Midfoot	Forefoot	Toes
0.010	0.113	0.070	0.083	0.086
0.025	0.385	0.239	0.267	0.304
0.050	0.806	0.524	0.558	0.589
0.100	1.496	1.057	1.120	1.037
0.250	3.022	2.593	2.447	2.362
0.500	4.763	4.602	4.969	4.965
0.750	6.170	7.102	7.789	8.802

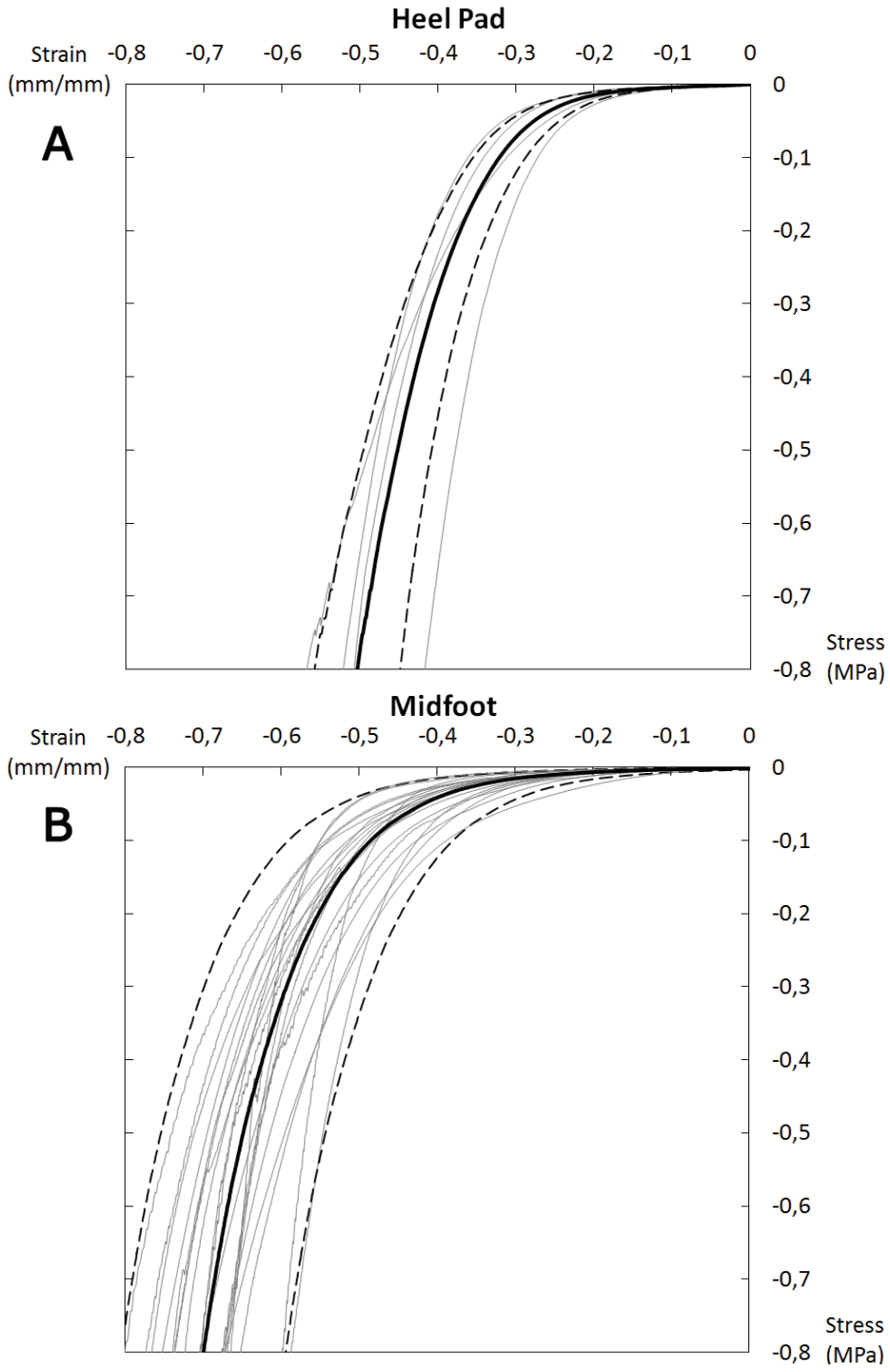

Figure 5.3: Stress-strain curves of the heel pad indentations (A) and midfoot indentations(B). Mean (solid line) and standard deviation (dashed lines).

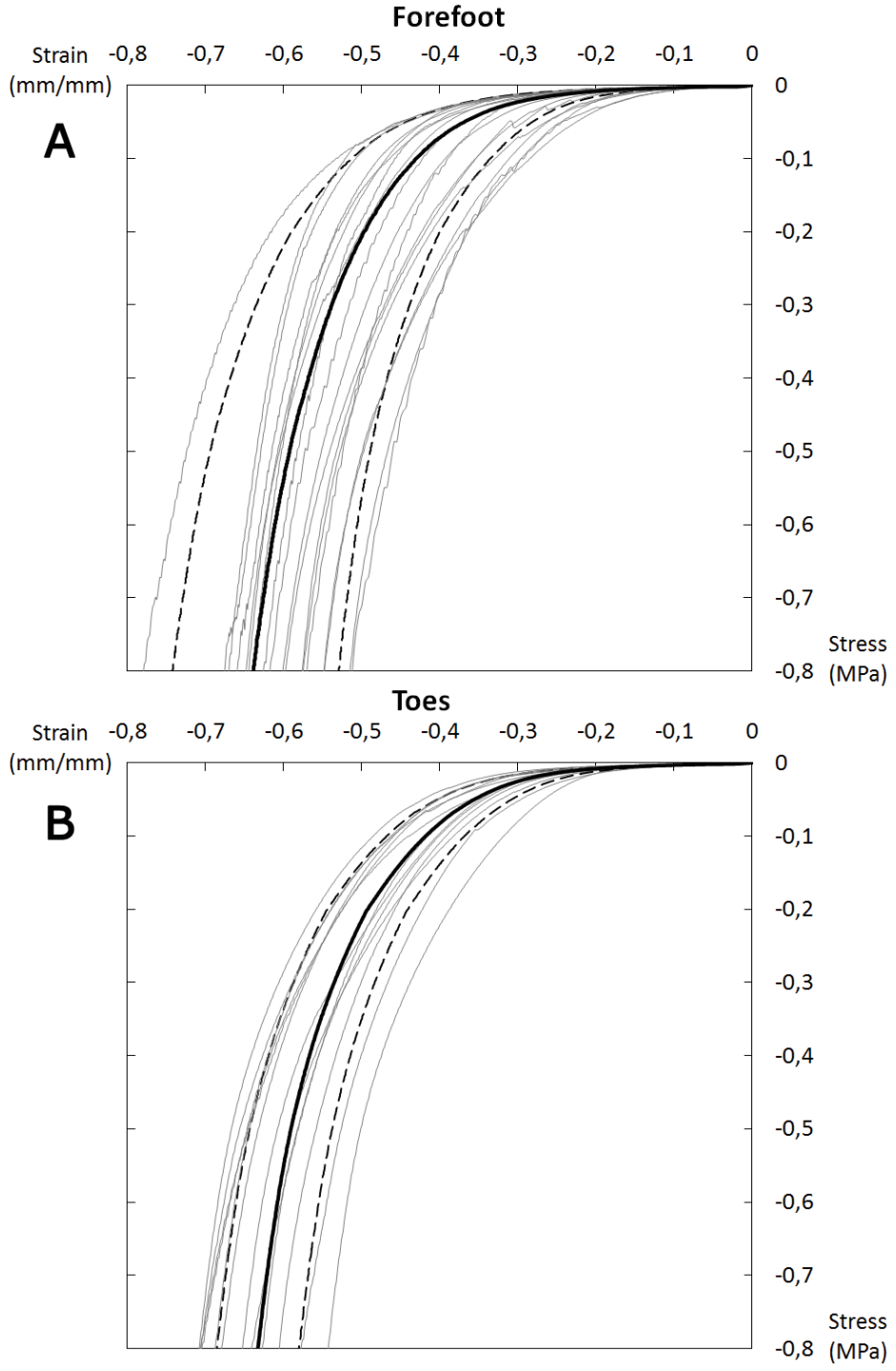

Figure 5.4: Stress-strain curves of the forefoot indentations (A) and toes indentations(B). Mean (solid line) and standard deviation (dashed lines).

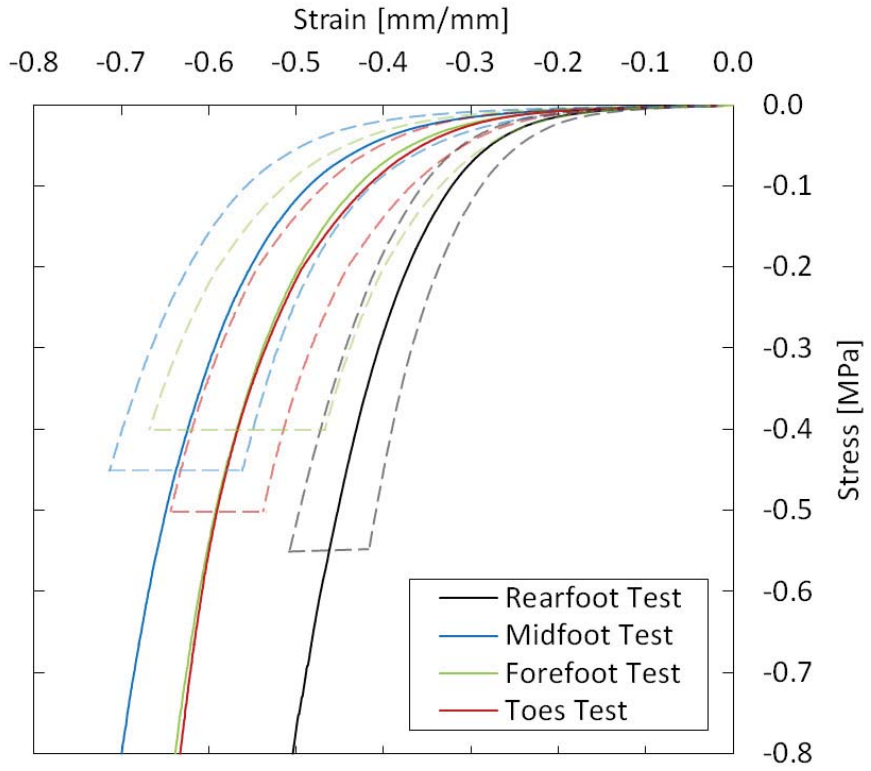

Figure 5.5: Average stress-strain curves of the four plantar sole regions. Mean (solid lines) and standard deviation (dashed lines). Standard deviations were cut to improve visualization.

5.4 Discussion

The plantar sole is the component of the foot with greater capacity of impact absorption. Its structure is mechanically adapted to work under compression. In this chapter the mechanical response of the plantar sole is assessed in four different region. To do so, fifteen locations of the plantar sole are indented to obtain the stress-strain curves. The subcalcaneal tissue shows a stiffer response than submetatarsal tissue, while the forefoot is stiffer than the soft tissue in the mid-arch. These differences seem to be due to the distinct structure and composition of the plantar sole in each location, as observed for diabetic foot (Kao et al., 1999; Tong et al., 2003). Chen et al. (2012) investigated differences in strength

at the plantar skin interface and found similar results. The strength in the heel region was significantly higher than in all other regions and forefoot higher than in mid-arch region. In the same line, Ledoux and Blevins (2007) determined in a stress relaxation study of the plantar soft tissue that the subcalcaneal tissue is different from other plantar soft tissue areas. Although tests are not performed in living subjects, it has been proven that plantar sole specimens stored frozen yield similar mechanical properties (Bennett and Ker, 1990).

The comparison of the mechanical behavior in this study is performed contrasting the whole stress-strain curves from zero to loads greater than body weight. This comparison provides a better image of the actual compressive response of the plantar sole than only contrasts Young's modulus. As shown in Table 5.1, the Young's modulus are similar in all curves because the curves run parallels at most of the stress levels. The comparison of Young's modulus between studies is also complicated, because the values reported depends on the stress level and the strain ratio at which the tissue was tested, making the comparison of results in most of the cases unworkable.

The differentiation of the plantar soft tissue responses by regions will help in the understanding of the mechanical performance of this tissue, in the study of the energy absorption mechanism of the foot and in the refined characterization of human plantar sole.

5.5 Plantar sole characterization

The stress-strain data collected from the tests are used to fit the parameters of a non-linear model. This study is particularly focused on characterize the compressive response of the plantar sole at different locations; then, hyperelastic material models are used to adjust the curves.

For contact simulation purposes, only two different plantar sole behavior results are parametrized: for rearfoot and forefoot. The former is based in heel pad tests and the latter on the average curve of submetatarsal heads and toes tests. The procedure to characterize the tissue is similar to the procedure used in the section 3.5 to characterize the tendon tissue. In the first step, several constitutive

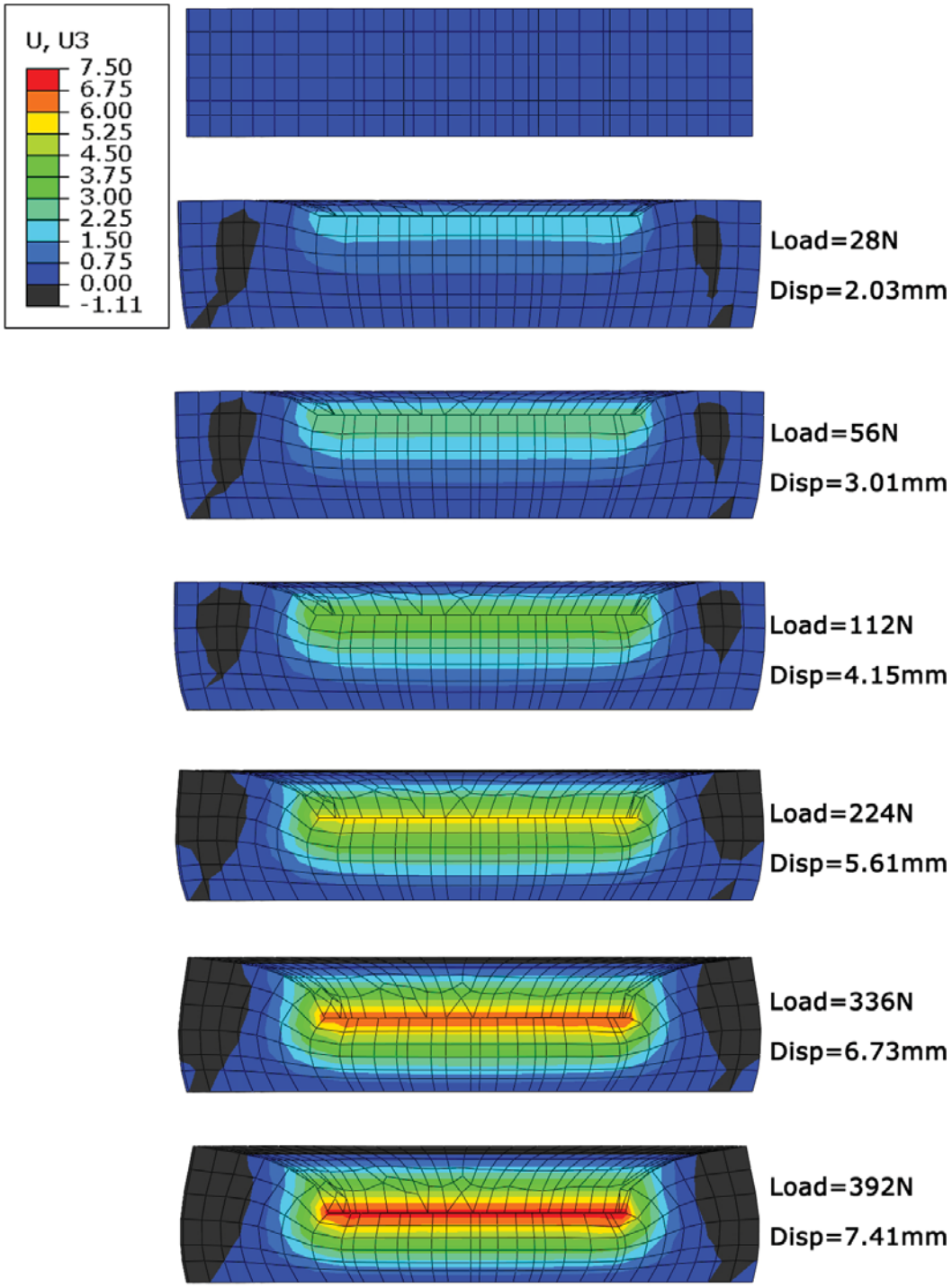

Figure 5.6: Computational replication of the heel pad indentation of the foot 5 .

models are used to fit the average rearfoot stress-strain curve. In the second step, the performance of material models are compared with the load-displacement curves of each heel pad tested to determine the most suitable model. Finally, the constitutive model selected for the rearfoot is adjusted for the forefoot response. ABAQUS software is employed to perform the analysis.

Three different hyperelastic constitutive models have been used previously for plantar soft tissue: Polinomial model (Lemmon et al., 1997), Yeoh model (Spears et al., 2005) and Ogden model (Erdemir et al., 2006; Chokhandre et al., 2012; Chen et al., 2012, 2014a; Telfer et al., 2015). Taking advantage of the fact that the three hyperelastic formulations are readily available in the FE package ABAQUS, the stress-strain curve obtained from the experiments is introduced in the software to calculate the parameters of the three material models that best fit the experimental curves. A Poisson's coefficient of 0.475 is defined to set the compressibility parameter (Chokhandre et al., 2012; Chen et al., 2014a).

The computational simulation of the indentations is subsequently performed to evaluate the structural response of the three constitutive models. A 3D FE model of an idealized heel pad is created to replicate the test computationally. The model consists in two cylinders, the big one of diameter 70mm represents the heel pad sample and the small one of diameter 40mm simulate the upper platen of the universal testing machine. The diameter of the sample is chosen in order to keep the lateral confinement of the tissue. The height of the sample is adjusted for each of the five specimens tested. The nodes of the base of the sample are fixed while a progressive load is applied to the upper plate (Figure 5.6). A contact frictionless interaction is defined between both cylinders.

Out of three material models, the Ogden model showed the closest response to the experimental values. Therefore, the first order Ogden constitutive model is chosen to simulate the non-linear response of the plantar sole tissue obtained from the experiments. This material model describes a hyperelastic behavior of rubber-like materials accounting for compressibility. Its strain energy density function U in terms of generalized strain is:

$$U = \frac{\mu}{\alpha^2}\left(\lambda_1^\alpha + \lambda_2^\alpha + \lambda_3^\alpha - 3\right) + \frac{1}{D}\left(J-1\right)^2 \tag{5.1}$$

Table 5.2: Ogden material model coefficients fitted for rear and forefoot human plantar sole.

Region	ν (MPa)	α	D (mm^2N^{-1})
Forefoot	0.01199	9.919	8.4822
Rearfoot	0.01995	15.011	5.0963

where ν is the initial shear modulus, α is the strain hardening exponent, and D is the compressibility parameter.

The same constitutive model is employed to characterized the forefoot response. The parameters of the first order Ogden constitutive model are calculated to fit the average curve of submetatarsal heads and toes tests. The parameters calculated for rear and forefoot are detailed in Table 5.2.

5.6 Performance comparison

Seven hyperelastic material models for plantar soft tissue are found in the literature. The coefficients of four of them were fitted with data of heel pad indentations (Lemmon et al., 1997; Spears et al., 2005; Erdemir et al., 2006; Chokhandre et al., 2012) and the remaining three were fitted with data of indentations under the second metatarsal (Chen et al., 2012, 2014a; Telfer et al., 2015). As shown in Figure 5.7 the curves are scattered in a wide range for both kinds of tissues (rearfoot and forefoot), making impossible a comparison of the responses between one region to the other. This is due to the methodological differences to obtain the experimental data and the procedure to calculate the coefficients.

Lemmon et al. (1997) calculated with ABAQUS the coefficients of a second-order polynomial material model based on uniaxial stress-strain data up to 300kPa obtained from *in vivo* tests of five heels. Spears et al. (2005) adjusted the elastic parameters of a Yeoh's material model with force-displacement data of the fat pad tested at different strain ratios, static and dynamic, and strained up to 0.35. Erdemir et al. (2006) adjusted the coefficients of the first order Ogden model iteratively by inverse FE analysis. The indentations used to fit the parameters were performed to a maximal pressure of 156kPa. The values reported by Chokhan-

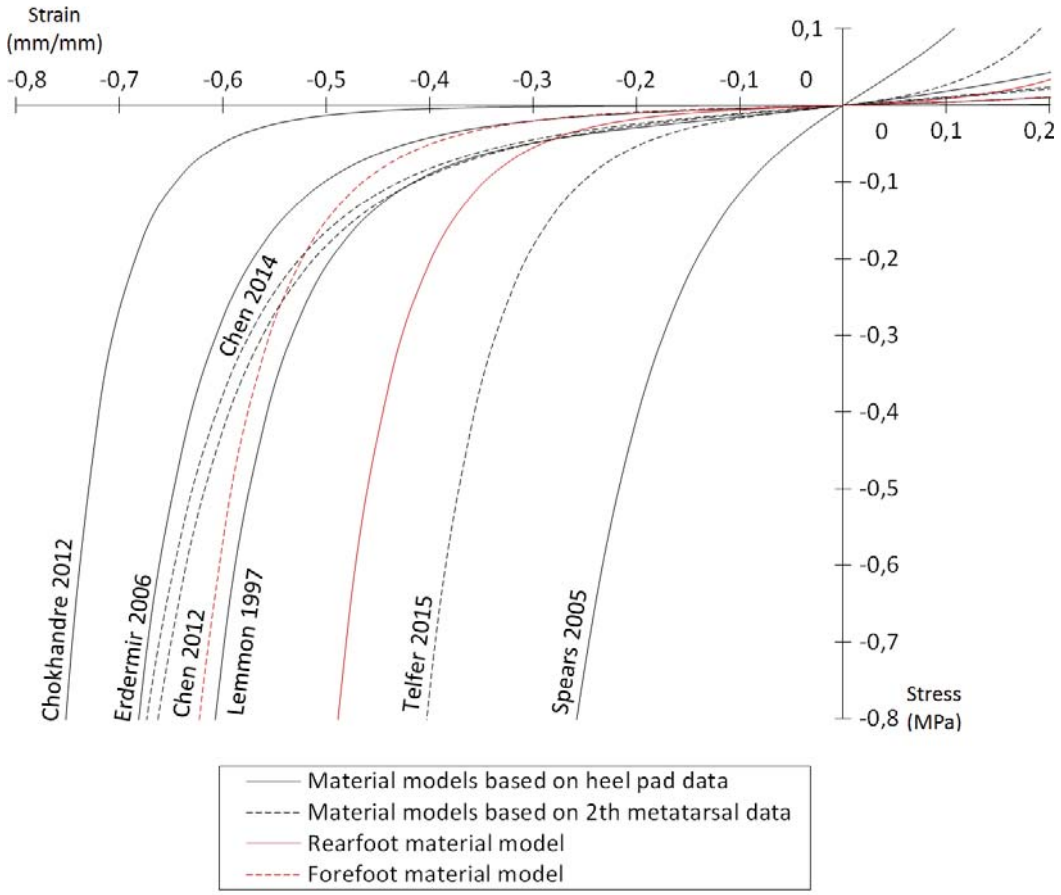

Figure 5.7: Comparison of hyperelastic material models of plantar soft tissue found in the literature (Lemmon et al., 1997; Spears et al., 2005; Erdemir et al., 2006; Chokhandre et al., 2012; Chen et al., 2012, 2014a; Telfer et al., 2015). The solid lines are models adjusted with heel pad data and dashed lines are model fitted with submetatarsal soft tissue data. Red lines are the material models fitted in this chapter.

dre et al. (2012) are the result of an improvement of the technique employed by Erdemir et al. (2006), using a 3D heel FE model for the inverse FE analysis rather than a 2D model and based on extended experimental data, varying strain rates and direction of indentation (multidimensional).

As respect to the material models based on second metatarsal indentations, Chen et al. (2012) determined the material constants of the Ogden material model

based on the indentations on a single subject. Chen et al. (2014a) presented an exhaustive investigation of joint angle-dependent plantar soft tissue properties. To calculate the material parameters they coupled the metatarsal-specific FE model with an optimization software. The experimental data employed to feed the inverse algorithm were performed to a maximum indentation depth of 5.6mm and a constant loading rate at 9.2mm/s. The curve included in the Figure 5.7 correspond to the optimal parameters for neutral position (metatarsophalangeal joint=0^o). Finally, the recent study of Telfer et al. (2015) determined the material coefficients of the plantar soft tissues under the forefoot through a iterative process where a series of static FE simulations were compared to the experimentally measured pressure.

CHAPTER

SIX

NON-LINEAR FOOT FINITE ELEMENT MODEL

In this chapter, the complete detailed 3D foot FE model created in the Chapter 4 is updated with the mechanical properties of the rear and forefoot soft tissue determined in the Chapter 5. The model is employed to estimate the stresses occurring in the foot at the impact during barefoot running with the aim of examining the impact absorption mechanism of the foot at different strike patterns from an engineering perspective. Rearfoot strike presents a stiffer response where only the heel pad absorbed the impact energy, producing high compressive stresses in the hindfoot bones and cartilaginous joints. However, the system gains compliance in midfoot and forefoot strike by the flexure of the metatarsals aided by the elastic response of the flexor muscles, which improved the absorption of the impact. It is found that the angle of impact has a greater effect in reducing peak plantar pressures than the stiffness of the surface. Understanding these two mechanisms to absorb impact forces allows predicting which foot anatomical structures are more susceptible to injury. The work presented in this chapter became part of the manuscript submitted for publication in the "Journal of Sport Science" (Section 7.2.1 — Publication 5).

6.1 Introduction

In recent years it is becoming trendy running barefoot or with minimalist footwear (Rixe et al., 2012) motivated by the belief in lower risk of injury (Rothschild, 2012) and by the absence of scientific evidence that heel-cushioning shoes reduce running-related injuries (Richards et al., 2009). Barefoot and minimalist running is a recent topic in the scientific literature. Some emerging topics are the study of preferred foot strike pattern in endurance runners, shod (Kasmer et al., 2013; de Almeida et al., 2014), barefoot (Larson, 2014), elite (Hasegawa et al., 2007) and recreational (Larson et al., 2011). Also comparative studies of mechanical performance in shod vs barefoot running such as energy efficiency (Divert et al., 2008) and collision forces (Lieberman et al., 2010) or as function of foot strike such as muscle activity (Yong et al., 2014) have been published in the last years. Other studies were focused on the capacity to convert foot strike pattern (Williams et al., 2000; Samaan et al., 2014), or on the capacity of mimicking barefoot running with minimalist footwear (Hein and Grau, 2014; Squadrone et al., 2015).

Recent in-depth reviews regarding running-related injuries in shod and barefoot running based on scientific studies (Rixe et al., 2012; Lohman et al., 2011; Jenkins and Cauthon, 2011; Altman and Davis, 2012; Daoud et al., 2012) concluded that:

1. Despite advances, runners continue to experience high injury rates.
2. Human beings are designed to run and we have ran barefoot throughout history until the last four decades.
3. There are no clinical evidences that shod or barefoot runners suffer fewer injuries.
4. There are biomechanical differences between both styles of running.
5. Because of this, there are certain benefits between running styles for particular injuries.
6. Many unknowns about the relationship between running style and injury remain to be answered.

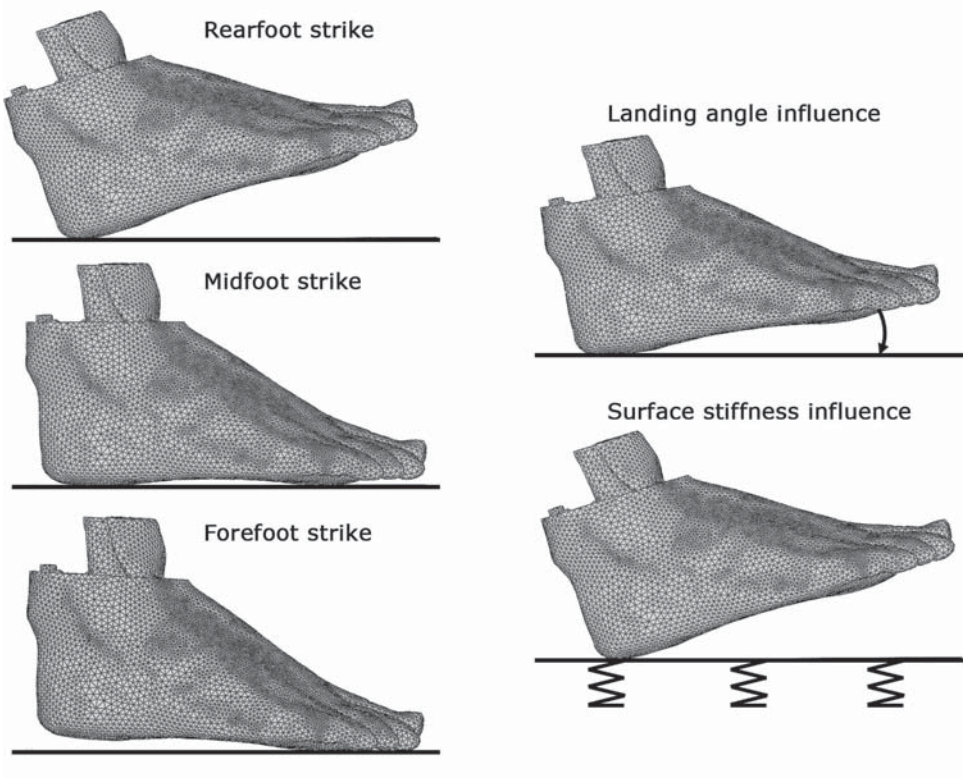

Figure 6.1: Running cases analyzed.

7. More large-scale studies are required.

8. There is no unique solution/advice for all runners.

In any case, it is undeniable that more and more runners are replacing their previous heel-cushioning shoes by the new minimalist, "more natural" trendy shoes (Squadrone et al., 2015). This change implies in alterations in several biomechanical aspects. Starting by the fact that running barefoot tends to strike forward, this modifies the stride length, which influences loading rate, plantar peak pressure, step frequency, muscular activity, leg compliance, ankle, knee and hip kinematics (Divert et al., 2008; Lieberman et al., 2010; Yong et al., 2014; De Wit et al., 2000). Despite this tendency to land flatter, there are still barefoot runners with heel-to-toe contact pattern. Kinematic studies showed that the strike patter have greater influence in the lower leg mechanics than the shod condition

(Shih et al., 2013). However no different approaches than kinematic and kinetic studies have been performed to study the relationship between strike pattern and running related injuries.

A computational simulation based on FE method can provide new information on this matter analyzing the internal stresses during impact at different strike patterns. This method allows estimating stresses on components under given loads and boundary conditions. Despite the large use of FE models in foot biomechanics and foot related injuries (Morales-Orcajo et al., 2015a), no previous simulation has analyzed foot running stresses. The closest simulations in this matter studied the cushioning sole response of modern footwear (Verdejo and Mills, 2004; Even-Tzur et al., 2006; Chen and Lee, 2015) and only one barefoot heel model analyzed how kinetic and kinematic differences affect stress during heel strike walking (Spears et al., 2005).

Therefore, the purpose of this study is to perform a biomechanical analysis of foot impact during barefoot running at different strike patterns. The complete detailed foot FE model created in Chapter 4 is used to compare the internal stress distribution in rearfoot strike (RFS), midfoot strike (MFS) and forefoot strike (FFS) and the influence of landing angle and surface stiffness in stress reduction (Figure 6.1). The study seeks a better understanding of the impact absorption mechanism of the foot to evidence risk of injury for new adopters of barefoot and minimalist running.

6.2 Updated finite element model

The complete detailed 3D human foot FE model developed in Chapter 4 is updated for this study. The model include every bone, intrinsic muscle and extrinsic tendon that form the foot-ankle-complex and is enveloped by a bulk soft tissue that represented fat and skin. The FE mesh contains 805792 tetrahedral elements with element size ranged from 1 to 5 mm as function of geometry requirements. The model is improved in this section incorporating the rearfoot and forefoot hyperelastic models configured in Chapter 5 and other non-linear models found in the literature.

Table 6.1: Material parameters of the tissues simulated with hyperelastic properties. The parameters correspond to the first order Ogden constitutive model.

Tissue	ν (MPa)	α	D (mm^2N^{-1})
Tendon	33.1622	24.899	0.0001207
Muscle	0.05737	28.820	1.1283
Forefoot sole	0.01199	9.919	8.4822
Rearfoot sole	0.01995	15.011	5.0963

Two isotropic linear material models are used to simulate bone tissue properties. Cortical bone properties, 17GPa for the Young's modulus and 0.3 for Poisson ratio, are applied to the external layer of elements while for the internal elements properties of trabecular bone are applied, 0.7GPa for the Young's modulus and 0.3 for the Poisson ratio (García-Aznar et al., 2009). The elements between bones are configured with linear properties of articular cartilage (0.01GPa of Young's modulus and 0.4 of Poisson ratio) (Gefen et al., 2000). The linear elastic properties of the plantar fascia are defined based on the experiment performed by Wright and Rennels (1964) with 0.35GPa and 0.3 for the Young's modulus and Poisson ratio respectively. The non-linear compressive response of the intrinsic muscles is simulated with the optimized parameters calculated by Petre et al. (2013) . The hyperelastic properties under tensile loads of extrinsic foot tendons are modeled with the parameters adjusted in Chapter 3. Finally, the tissue properties of the bilayer plantar sole (fat and skin) are defined in two regions, rearfoot and forefoot. The hyperelastic material model fitted in Chapter 5 is used for this tissues. The coefficients of each hyperelastic material model employed are summarized in Table 6.1.

6.3 Case studies

A solid block composed of hexahedral elements is created under the foot to simulate the different strikes patterns running over different sorts of grounds. Three barefoot running strikes are configured based on the running strike pattern study of Lieberman et al. (2010). The barefoot RFS running is configured with an im-

pact force of 1.89 of the body weight and an impact angle of θ=16.4^o. This angle corresponds to the impact angle of habitual shod adults running barefoot. The barefoot FFS running is set with 0.58 body weight of impact force with and impact angle of θ=-1.13^o. That configuration corresponds to barefoot runners than never were been shod. The barefoot MFS running is established with the average impact force of RFS and FFS and a landing parallel to the ground (θ=0^o). Additionally, a moment in the ankle is defined in order to include running dynamic forces. This moment is estimated according ankle moment measurements during running (Novacheck, 1998) and introduced in the model applying an axial force at the end of the Achilles tendon. The proximal extreme of the tibialis anterior is constrained to have zero displacement, to simulate the muscle tuning that occurs previously to impact (Nigg, 2001). A description of the boundary conditions is shown in Figure 6.2. A 700N of body weight is used for all cases.

Considering that RFS is the most unnatural landing in barefoot running, two additional scenarios are simulated to analyze their influence in the stress levels: RFS at lower angles of impact and RFS over softer surfaces. A moderate impact angle is set at θ=8.2^o keeping the rest of the parameters equal to the previously defined RFS settings. Running on different surfaces is represented by adjusting the elastic properties of the ground block. An elastic modulus of 30GPa is employed in all cases to simulate the hard surfaces of modern infrastructures such as roads or sidewalks (Demir, 2005). Softer elastic modulus are defined to emulate natural environments: 1GPa for compact soil, 0.2GPa for dense sand and 0.05GPa for loose sand (Bowles, 1996; Zhang et al., 2014).

6.4 Foot strike simulations

The impact forces in RFS are transmitted vertically through hindfoot bones, from heel to tibia. Figure 6.3 shows a sagittal section of the hindfoot where this vertical distribution of the compressive stress is observed. In the heel pad the stresses under the calcaneal tuberosity are higher than at the ground surface (i.e. internals stress are higher than at the external layers). Despite the cushioning properties of the heel pad, high stresses are predicted for the cortical layer of the calcaneal. This

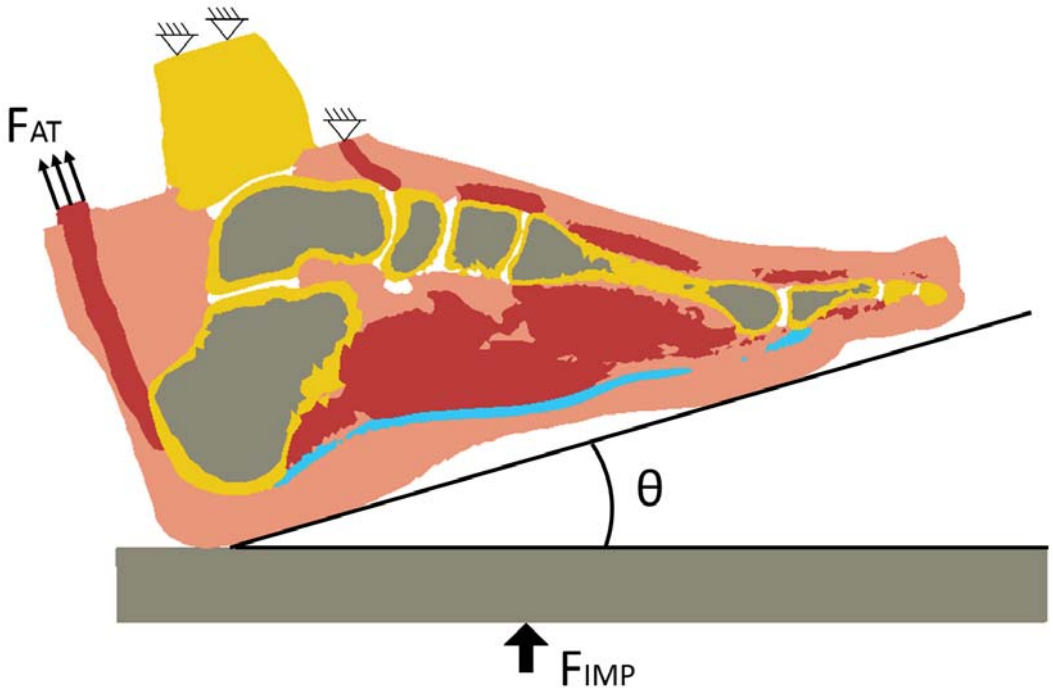

Figure 6.2: Boundary conditions of the model. The proximal end of the Tibia and tibialis anterior were encastred. F_{AT} = force applied at Achilles tendon to simulate ankle joint moment. F_{IMP} = impact force applied in each case. θ = strike angle.

effect is due to the cortical layer has a much greater stiffness than the plantar sole. Although the cortical bone supported most of the load, trabecular bone is also stressed. At the dorsal part of the calcaneus, high compressive stresses appeared due to the bending forces produced by the Achilles tendon. Due to the rigidity of the system in RFS, high pressures take place at the talocrural and subtalar joints. Heel pad is deformed up to 64.7% in the thinnest part just under calcaneal tuberosity. Maximum plantar pressures of 1.4MPa are predicted at the base of the heel (Figure 6.4A). The tibialis anterior presents high traction stresses in opposition to the ankle joint movement.

The impact force in FFS is distributed among the five rays. High stresses appear in the metatarsals due to the bending forces derived of the running advance and Achilles tendon force. This condition also produce the stretch of the plantar

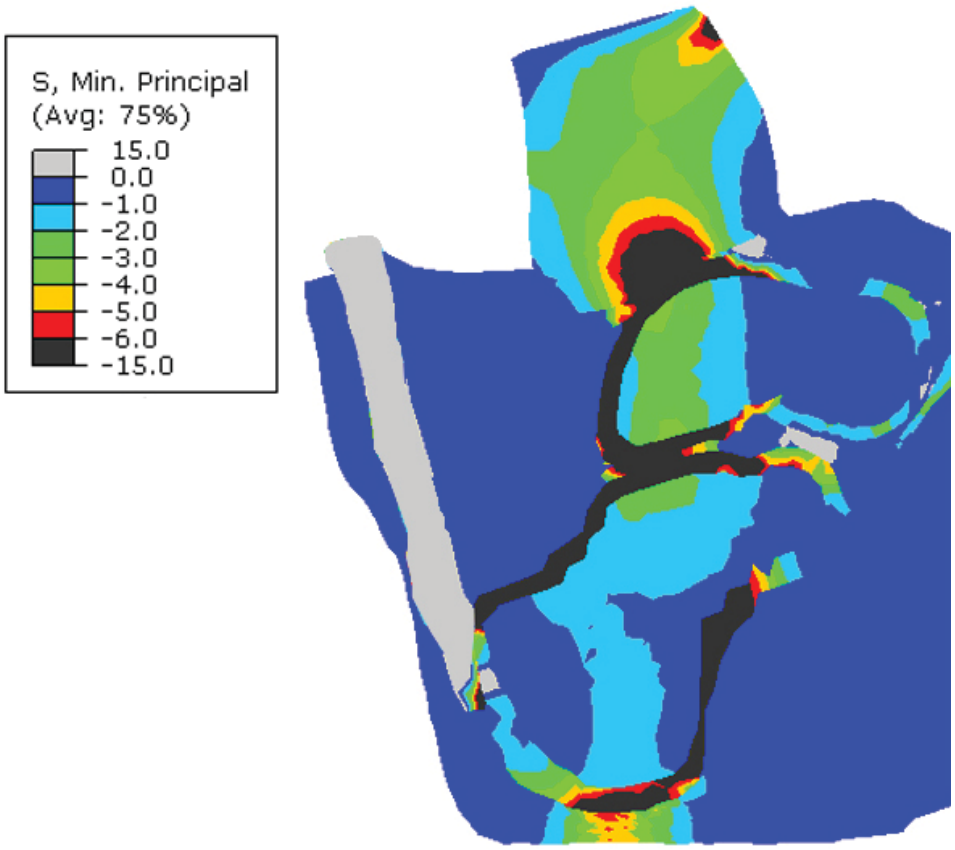

Figure 6.3: Compressive stress distribution of the hindfoot during rearfoot strike in barefoot running.

fascia. Plantar sole under metatarsal heads presents peak plantar pressures of 0.48MPa and strains up to 52.9% with a greater surface of contact than in RFS (Figure 6.4B). MFS analysis presented very similar stress distribution than FFS. In that case, the contact surface is twice that of FFS, which yielded maximal plantar pressure values similar to the FFS (Figure 6.4C). The deformation of the plantar sole is 55.6% under the calcaneus and 54.7% under the metatarsal heads. The remaining component of the foot are under analogous conditions to FFS.

Considering touchdown a repetitive event during running performance, the stress levels generated during strike can result in different physical ailments. Based on the stress level of the internal foot components during landing, Table 6.2 are summarizes the impact related injuries that are more prone to develop from each

Table 6.2: Stress related injuries with higher risk to suffer based on the internal stress levels of the foot components during impact in barefoot running for each foot strike pattern.

RFS	MFS/FFS
Calcaneal stress fracture	Metatarsal stress fracture
Cartilage damage	Plantar fasciitis
Tibialis anterior tendinitis	Achilles tendinitis
Heel ulceration	Submetatarsal ulceration

strike pattern.

The additional scenarios considered for RFS condition present a reduction of the maximal plantar pressure in 18% when halving the impact angle. However, the elastic properties of the ground show much lower influence. Running over compact soil does not reveal significant differences in peak plantar pressure and stress distribution comparing to landing over hard surfaces. Reduction of contact pressure similar to halving the landing angle are predicted for soil elastic modulus inferior to 0.2GPa (sand).

6.5 Discussion

Running barefoot is catching on in recent years, leading many runners to change heel-cushioning shoes to minimalist shoes. This transition requires adaptation of the running style in order to avoid possible injuries. The main difference between running shod and barefoot or minimalist is the midsole cushioning layer of modern running shoes. This layer provides an extra aid to absorb impact forces, which have modified the running technique to landing with high angles. Then, when this cushioning layer is removed, runners should return to the original flatter landing technique. If this transition is not well addressed, it can result in impact related injuries. In order to analyze impact absorption mechanisms of the foot, a number of simulations were performed at different strike patterns on barefoot condition.

The different behavior of the soft tissue under the heel and under the metatarsals heads studied in Chapter 5 is implemented in the updated FE model. The plantar sole strains predicted in RFS are in good agreement with the 60.5 $\pm$5.5%

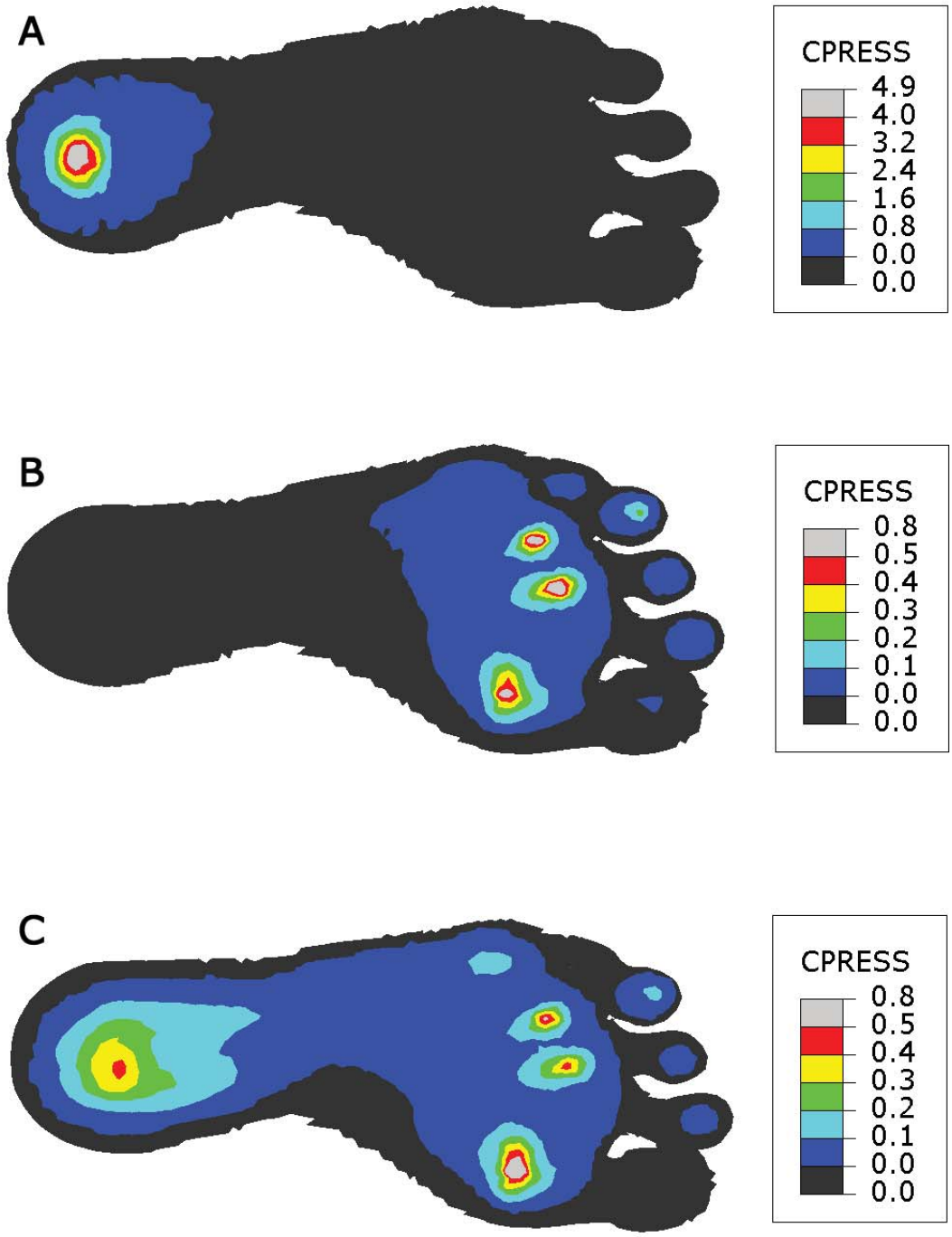

Figure 6.4: Plantar pressure distribution in Rearfoot strike (A), Midfoot strike (B), Forefoot strike (C).

in vivo heel pad deformation measured on an actual barefoot running step (De Clercq et al., 1994). In addition, plantar pressures estimation in RFS are in the range of the reported values. De Wit et al. (2000) measured an average maximal pressure of 0.97 $\pm$0.35MPa for seven volunteers running barefoot at 4.5 m/s with an average angle landing of 6.6 $\pm 5.6^o$. The contact pressure prediction of the model in RFS is similar for a strike angle of 8.2^o and in a standard deviation for striking at 16.4^o. The peak plantar pressures are calculated by averaging the contact pressure of the elements located under the calcaneus tuberosity and metatarsal heads as the measured local pressures in barefoot running (De Wit et al., 2000). Peak pressures predicted by the model are expected to be higher than actual measurements as heel impact is a quick event that rapidly increases and diminishes the pressure. Then, plantar pressure measurement during running will report higher peak pressure values as frequency of plantar pressure sensors improve (Urry, 1999; Gerlo et al., 2013). Only one study reported plantar pressure measurements in barefoot running as function of the strike pattern (Nunns et al., 2013). Their mean plantar pressure time histories of the whole stance phase yielded quite low values for all strikes at impact. The explanation may lie in the large group of study used to calculate the average values, which tend to smoothen sharp responses.

From the perspective of impact mechanics, MFS and FFS presented analogous response in the internal and external stress distribution. However, significant differences were found with RFS. Foot when landing rearfoot presented a stiffer response where only the heel pad absorbed the energy of the impact, producing high compressive stresses in the hindfoot bones and cartilaginous joints. However, for foot landing in a forward position, the system gained compliance through flexure of the metatarsals aided by the elastic response of the flexor muscles, which improve the absorption of the impact. Understanding these two mechanism to absorb impact forces allows predicting which foot anatomical structures are more prone to injury. Table 6.2 highlights the injuries that are more prone affect a runner according to its strike pattern based on the stresses level observed during barefoot impact.

A recent clinical report alerted to two cases of metatarsals stress fracture

in experienced runners who transitioned to minimalist footwear (Giuliani et al., 2011). It was proposed that the transition without specific training was a factor leading to injury. The model predicts higher stresses in RFS at the talocrural and subtalar joints due to the lower impact absorption capacity of the system in that position. This contrasts with the predictions of the musculoskeletal model of Rooney and Derrick (2013) who calculated higher contact forces for FFS runners. The difference is likely to be due to the modeling conditions, where the major source of load in their model was the muscle contraction while, the present simulation, it focus on the impact forces. The plantar fasciitis risk predicted for MFS and FFS is based on two different principles. In FFS, the plantar fascia is stretched due to the bending of the foot; the foot arch compliance is greater, which produces stretch of the fascia. However, in MFS the plantar fasciitis is due to the compressive stress originated at the base of the calcaneus in the plantar fascia insertion. This stress also occurs in RFS at very low impact angles. The excessive strain and the mechanical overload have been pointed out as the main reasons leading to this disease (Wearing et al., 2006). Plantar fasciitis has been correlated with load rate (Pohl et al., 2009), which is associated to RFS, but also was correlated with low arch index (Pohl et al., 2009), which is related to excessive strain. The results show that the control motion function of muscles is affected during impact. In RFS the tibialis anterior presented tensile stresses to control forefoot touchdown. In FFS, the flexor muscle group is firstly more active to prepare a negative angle of impact. Secondly, they are stressed as part of the mechanism of the forefoot to absorb the impact. These findings agree with the electromyography signals reported for RFS and FFS (Yong et al., 2014).

Note that RFS in barefoot running is the harder condition for the foot (De Wit et al., 2000; Nunns et al., 2013; Segal et al., 2004; Nagel et al., 2008; Maiwald et al., 2008; Qiu et al., 2011) (Figure 6.5). Based on this assumption, two additional scenarios were analyzed for runners that do not transition to forward landings when running barefoot. The results suggest that angle of impact plays a more important role in reducing plantar pressure than the surface stiffness. A previous correlation between angle of impact and local pressure under the heel was found in a kinematic study coupled with plantar pressure measurements (De Wit et al.,

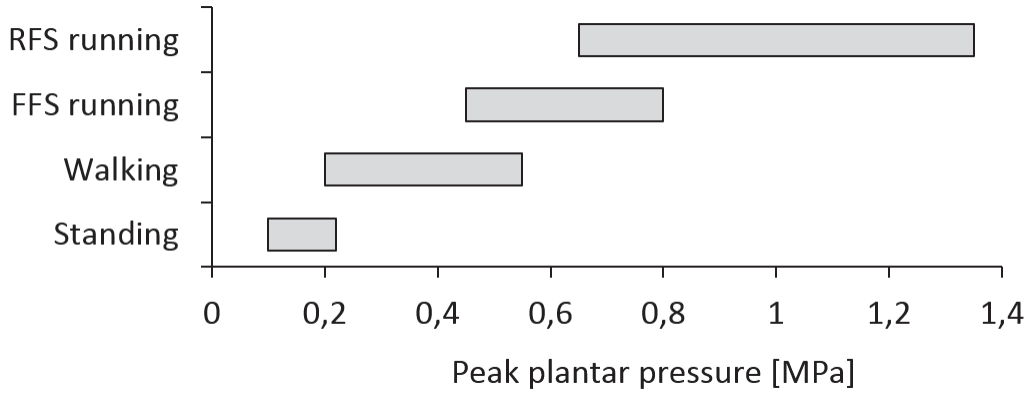

Figure 6.5: Peak plantar pressures in barefoot condition (De Wit et al., 2000; Nunns et al., 2013; Segal et al., 2004; Nagel et al., 2008; Maiwald et al., 2008; Qiu et al., 2011).

2000). It was assumed that barefoot runners strike in flatter positions to avoid high plantar pressure during impact. Our simulation confirmed this reduction of peak plantar pressures from severe (16.4^o) to moderate (8.2^o) impact angles. The slight influence of ground stiffness in stress levels could explain the absence of injury reduction when running on soft surfaces compared with harder surfaces (Nigg, 2001).

One of the limitations of the results is that the simulation is reduced to the impact moment. Hence, the recommendations could vary for a complete analysis of the stance phase. The barefoot simulations and posterior discussion of strike effects can be extended to the minimalist running since the minimalist shoes do not provide any additional cushioning support. Therefore, the mechanics of impact for barefoot and minimalist running can be assumed to be equal. The preference to run minimalist instead of barefoot is due to the protective layer that provides the sole to avoid minor skin injuries such as cuts or abrasions.

It has been demonstrated that runners are able to alter their strike pattern with some practice, achieving similar performance as natural runners (Williams et al., 2000; Samaan et al., 2014). That permits, with a specific training, to adopt the strike pattern more beneficial for the runner. It has been recommended strike with the forefoot when running barefoot (Shih et al., 2013), however that

recommendation does not seems to be appropriate. We suggest landing in flatter position when running barefoot in order to reduce the stiffness of the system choosing a backward or forward initial contact as function of the potential risk of the runner. The decision to adopt one strike pattern or another when transitioned to barefoot running should be evaluated with additional criteria than impact relate injury risks.

In summary, most of the biomechanical studies of barefoot running are focused on kinematic and kinetic measurements (i.e. rigid solid). The present study is intended to analyze the internal stresses (i.e. deformable solid) of the foot components at the impact in function of strike pattern. Two different mechanisms of impact absorption are described and associated to injury risks. It is found that the landing angle has more relevance in reducing impact stresses than the stiffness of the surface. In addition, the model presented in this study is a step forward in the field of foot computational modeling involving a complete three dimensional foot model with real geometry of tendons and muscles, introducing non-linear properties for all soft tissues except plantar fascia and differentiating between rearfoot from forefoot plantar soft tissue responses.

6.6 Model features

The foot FE model developed in Chapter 4 is updated in this chapter. Initially the advances in foot computational modeling field were focused on a detailed representation of the geometry of the internal components. Now the refinement is focused on the material models used to simulate the actual behavior of foot tissues. The improvements incorporated in the model in this line are: non-linear material models for the compressive behavior of muscle tissue, rearfoot and forefoot plantar sole. This, together with the non-linear material model determined in Chapter 3 for tendon tissue traction behavior makes the 70% of the elements of the model have non-linear properties and only the skeleton and the plantar fascia are described with linear material models (Figure 6.6).

This refined characterization of the tissue properties is reflected in the computational cost. The full non-linear model runs in this chapter with different

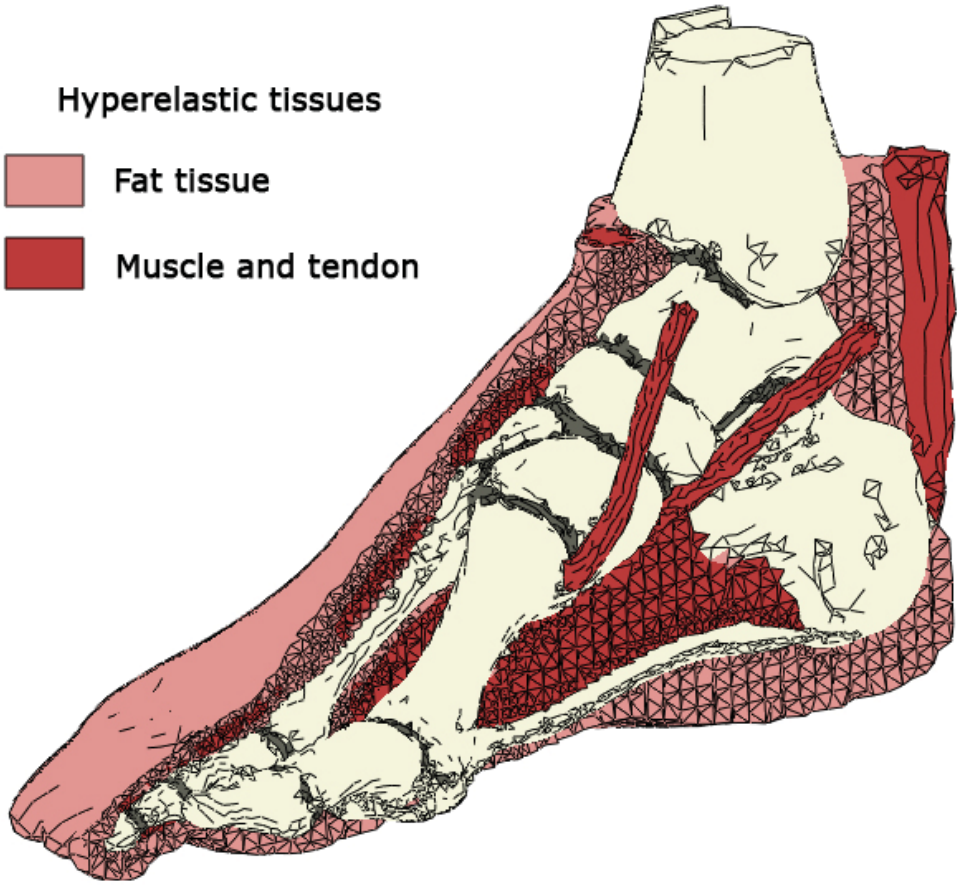

Figure 6.6: Non-linear material models used in the model.

boundary conditions takes around 42h to calculate each case (Intel core i5 3.2GHz processor and 4GB of RAM). This is a 40% time increase when compare to the cases simulated in Chapter 4.

With the improvements introduced in this chapter the model overcomes other of the limitations observed during the in-deep review of the state of the art of foot computational modeling, the inclusion of more refined material models for soft tissues. However, the model presented in this chapter continues with some of the limitations described in Section 4.5, the necessity of improve the loads and boundary conditions of the internal components. Next steps of the model should be oriented in that direction.

CHAPTER

SEVEN

CONCLUSIONS AND ORIGINAL CONTRIBUTIONS

A brief summary of the work developed in this thesis along with the main conclusions, the original contributions and future work lines in computational foot biomechanics are discussed in this chapter.

7.1 Conclusions

The most important conclusions extracted of the work collected in this Thesis, are sorted in three sections. The first section includes the computational modeling aspects of simulating foot biomechanics. The second section covers the experimental aspects of testing foot tendons and plantar soft tissue. Finally, the main clinical aspects extracted from the applications of each foot model are highlighted in the third section.

7.1.1 Computational modeling aspects

- The sophisticated arched bony structure of the foot makes the modeling of its mechanical response extremely challenging. This simulation is more complex when the muscle function is considered.

- Finite element analysis is a complex task with the potential for errors. Thus, every effort must be made to create models that simulate the issue to a suitable degree of accuracy, especially in clinical applications. Assumptions and simplifications at some level are necessary and are dependent on the objective of the study. The reasons for their adoption and their impact on the results have to be clearly explained.

- Skeletal foot modeling is a practical approximation to study bone related issues at low computing cost and with sufficient level of accuracy. Due to the higher stiffness of bone compare with soft tissue, not including soft tissue in the foot model can be a pragmatic way to produce refined solution in much lower times.

- The first order Ogden material model employed to adjust tendon tissue response yield better fit to experimental data of foot tendons under tensile loads than previous linear elastic and Mooney-Rivlin approaches used in the literature.

- The independent characterization of rearfoot and forefoot plantar sole enables to analyze accurately plantar pressure and plantar sole deformation striking forward or backward.

- The complete foot finite element model developed in this Thesis can be used in a wide range of applications in the field of biomechanics and under all rate of loads: standing, walking and running.

- Computational foot simulations expand the knowledge of foot biomechanics, which provides meaningful information for clinical practice. Specifically, the model developed in this Thesis can be used in areas of orthotics, injury, treatment, surgery and sports biomechanics.

7.1.2 Experimental aspects

- Foot tendons, which work at different planes, have been revealed to have different mechanical responses. Flexor/extensor toes tendons have higher

Young's modulus and ultimate tensile stress while inversion/eversion tendons have larger strain failure.

- The criterion proposed to quantify the regions of the tendon stress-strain curve based on the Young's modulus enables an accurate definition of initial strain, toe region and yield point.
- Stress-strain tendon curves exhibit proportionality between regions corresponding to the initial strain, the toe region and the yield point to the 15, 30 and 70% of the strain failure respectively.
- Structural properties are relevant in orthopedic reconstruction surgery and in tendon injuries estimation. The material properties together with the quantitative description of the stress-strain curve will help in the design of synthetic materials and in the development of refined constitutive models.
- The cross-sectional area measurement and the clamping method of the samples to the universal testing machine has been identified as key factors to calculate the material properties in tensile tests.
- The subcalcaneal tissue shows a stiffer response than submetatarsal tissue, while the forefoot is stiffer than the soft tissue in the mid-arch. This differentiation of compressive response is particularly relevant when study the stress distribution in the foot during running barefoot at different strikes.

7.1.3 Clinical aspects

- The geometry of the proximal phalanx of the hallux has the feature of a larger medial compared with lateral side, subjecting it to stresses that could provoke rotation of the proximal phalanx of the hallux toward a more relaxed position. That potential balanced position produced a tendency toward separation of the first metatarsal relative to the original anatomical position, which constituted the beginning of the hallux valgus deformity.
- The geometry of the proximal phalanx of the hallux is a significant factor in the development of hallux valgus, with as much influence as the other

reported skeletal parameters, and should be considered during preoperative evaluation. The clinical assessment of hallux valgus should involve evaluation of the first ray as a whole and not as insolated factors.

- A synergic work of the inversion/eversion tendons is predicted. Pulling from a peroneus or tibialis tendon stressed the antagonist tendons while reducing the stresses in the agonist. This paired action is also predicted for the Achilles tendon with the tibialis anterior. This behavior explains the complex control motion performed by the foot.
- In late-midstance position, higher mechanical response of the foot structure is required. The plantar sole, the fascia, the talocrural joint cartilage and tendons are more stressed in this position.
- Calacaneal stress fracture, cartilage damage, tibialis anterior tendinitis and heel ulceration are more likely to occur running barefoot with heel-to-toe contact pattern, based on the stress level of the internal foot components.
- Metatarsal stress fracture, plantar fasciitis, Achilles tendinitis, submetatarsal ulceration are impact related injuries more prone to develop for forefoot and midfoot strikers in barefoot running. The results show higher levels of stress supported by this components when landing forward.

7.2 Original contributions

The main contribution of this Thesis is the creation of a refined foot FE model which constitutes a step further in foot biomechanics simulation form the continuum mechanics approach. The list of all original contributions carried out during the period of this thesis are exposed below.

- A three-dimensional finite element model of the complete human foot with detailed representation of the internal components and full non-linear properties of the soft tissues. The model has been created from the independent segmentation of every internal component with an optimized mesh size including the detailed geometry of each tendon, muscle, cartilage and bone

of the foot, distinguishing cortical and trabecular properties. The whole foot-ankle complex is embedded in fat tissue. This refined model enables the study of hard and soft tissues biomechanics.

- The mechanical characterization of foot tendon tissue with a hyperelastic model. The first order Ogden material model has been fitted to simulate foot tendon tensile behavior. This characterization provides a more refined fit to experimental data than previous approaches.

- The mechanical characterization of the bilayer plantar sole by regions. The coefficients of the Ogden material model have been fitted with the compressive stress-strain curve of the rearfoot and forefoot plantar sole.

- A complete dataset of the mechanical properties of the balance foot tendons. Structural and material properties of foot tendons has been determined under the same methodology. The mechanical response of inversion/eversion tendons and flexor/extensor toes tendons have been differentiated.

- A criteria to quantify the regions of the tendon stress-strain curve. The criteria takes as reference the Young's modulus of the curve, defining the initial strain as the part of the curve from its beginning to a deviation greater than 20% of the Young's modulus and the linear region is defined as the part of the curve with the curvature less than 20% of the Young's modulus.

- The analysis of the compressive response of plantar soft tissue as function of the location. The stress-strain curves of the subcalcaneal, mid-arch, submetatarsal and toes soft tissue were compared.

- An investigation of a skeletal parameter as etiology factor of the hallux valgus. The size and shape of the proximal phalanx of the hallux have been identify as an etiological factor of the hallux valgus and should be taken into account during clinical assessment.

- A tendon force sensitivity study of the five major stabilizer tendons. A coupled work between peroneus and tibialis tendons and Achilles and tibialis

anterior tendons has been predicted which explains the complex control motion response of the foot.

- A quasi-static analysis of the midstance phase of walking. Higher mechanical requirements of the foot structure have been predicted for late-midstance position with respect to early-midstance.

- A study of the impact absorption mechanism of the foot during running barefoot at different strike patterns. The impact related injuries more prone to occur in barefoot and minimalist runners as function of the strike pattern have been identified.

7.2.1 Publications

The following papers written during the development of this Thesis have been already published or will be published in peer-reviewed scientific journals:

1. **Morales-Orcajo, E.**, Bayod, J., and Las Casas, E.B. (2015). Computational Foot Modeling: Scope and Applications. *Archives of Computational Methods in Engineering*, Published online.

2. **Morales-Orcajo, E.**, Bayod, J., Becerro-de Bengoa-Vallejo, R., Losa-Iglesias, M., and Doblare, M. (2015). Influence of first proximal phalanx geometry on hallux valgus deformity: a finite element analysis. *Medical & Biological Engineering & Computing*, 53(7):645-653.

3. **Morales-Orcajo, E.**, Becerro de Bengoa Vallejo, R., Losa Iglesias, M., and Bayod, J. Structural and material properties of human foot tendons. *Clinical Biomechanics*, Under review.

4. **Morales-Orcajo, E.**, Souza, T.R., Bayod, J., and Las Casas, E.B. Non-Linear finite element model to assess the effect of tendon forces on the foot-ankle complex. *Journal of Biomechanics*, Under review.

5. **Morales-Orcajo, E.**, Becerro de Bengoa Vallejo, R., Losa Iglesias, M., Bayod, J., and Las Casas, E.B. Foot injuries in barefoot

running as function of strike pattern - A finite element study. *Journal of Sport Science*, Under review.

7.2.2 Conferences

The following communications have been presented during the development of this Thesis:

1. **Morales-Orcajo, E.**, 3D Muscle detailed ankle-foot model for finite element analysis. *II Reunión Jóvenes Investiagadores del Instituto de Investigación en Ingeniería de Aragón*, Zaragoza, (Spain), 2013.

2. **Morales-Orcajo, E.**, Bayod, J., Becerro-de Bengoa-Vallejo, R., Losa-Iglesias, M., and Doblare, M., Influencia de la geometría de la falange proximal del primer dedo del pie en la formación de juanetes. *Congress on Numerical Methods in Engineering (CMN 2013)*, Bilbao, (Spain), 2013.

3. **Morales-Orcajo, E.**, Becerro de Bengoa Vallejo, R., Losa Iglesias, M., and Bayod, J., Mechanical properties of foot tendons - In vitro study. 1^st *Pan American Congress on Computational Mechanics (PANACM 2015)*, Buenos Aires, (Argentina), 2015.

4. **Morales-Orcajo, E.**, Bayod, J., and Las Casas, E.B., Developing a proper biomechanical computational model. *VI International Conference on Computational Bioengineering (ICCB 2015)*, Barcelona, (Spain), 2015.

7.3 Future work

The applications of foot finite element models will continue to increase with the increased of power of computing, which doubles its computational capacity every 18 months since the invention of computing, halving costs (known as Moore's law). However, computer power will never be sufficient considering that the number of detailed geometries, complex formulations and demanding conditions will

also increase. The direction of better and faster solutions is promising with vast potential for improvement.

Keeping in mind that the main objective of the Thesis is to advance towards a more refined computational simulation of the foot to clinical assessment, the progress made during this Thesis has been oriented to refine the geometry and the tissue characterization of the internal foot components. Therefore, the future advances should be oriented to refine the loads and boundary conditions. Future works in that direction are listed here:

- Include contact between internal foot components. Within foot many components overlap, limiting the displacement of one component respect to its surrounding. A slipping interaction between these components when a force is applied to a tendon will provide a more accurate transmission of forces within the foot. Contact interaction should be also applied to the joints.

- Simulate active behavior of muscles. The model created in this Thesis is fed by kinetic data which is difficult to measure experimentally and it is usually estimated by kinematic or mathematical models. Hence, introduce loads in model through the active behavior muscle will expand the possibilities of the model.

- Perform dynamic simulations. Physicians and physiotherapists have become increasingly interested in dynamically exploring the entire gait rather than discrete positions. Dynamics simulations include the variable of time and dynamic effects with allows the study of the complete movement.

- Combine multibody and finite element models. The integration of both types of models can be a good approach to face the dynamics simulation driven by the muscle activation.

- Simulate mechano-chemical process. The detailed geometry of the model can be exploited by the formulation of chemical processes governed by mechanical stimulus as in the case of ulcerations or bone regeneration.

- Reduce time for model generation. Create a subject-specific model of the foot is a time-consuming task. Investigations in the automation of the process will be decisive for the implementation of patient-specific studies.
- Reduce time of calculus. In order to orient the model predictions to help in the decision making process of a subject-specific clinical treatment the time of computing should be much faster.

BIBLIOGRAPHY

Abrahams, M. (1967). Mechanical behaviour of tendon In vitro. *Medical and Biological Engineering*, 5:433–443.

Actis, R. L., Ventura, L. B., Lott, D. J., Smith, K. E., Commean, P. K., Hastings, M. K., and Mueller, M. J. (2008). Multi-plug insole design to reduce peak plantar pressure on the diabetic foot during walking. *Medical & biological engineering & computing*, 46(4):363–71.

Actis, R. L., Ventura, L. B., Smith, K. E., Commean, P. K., Lott, D. J., Pilgram, T. K., and Mueller, M. J. (2006). Numerical simulation of the plantar pressure distribution in the diabetic foot during the push-off stance. *Medical & biological engineering & computing*, 44(8):653–63.

Altman, A. R. and Davis, I. S. (2012). Barefoot running: Biomechanics and implications for running injuries. *Current Sports Medicine Reports*, 11(5):244–250.

Anderson, A. E., Ellis, B. J., and Weiss, J. a. (2007). Verification, validation and sensitivity studies in computational biomechanics. *Computer methods in biomechanics and biomedical engineering*, 10(3):171–84.

Andrea, S. E. D., Thompson, D., Cao, D., and Davis, B. (1999). Finite Element Modeling of Load Transmission Through the Calcaneus. In *23rd annual meeting of the American Society of Bio- mechanics*, pages 1–2.

Antunes, P. J., Dias, G. R., Coelho, A. T., Rebelo, F., and Pereira, T. (2007). Non-Linear Finite Element Modelling of Anatomically Detailed 3D Foot Model. In *1st ECCOMAS Thematic Conference on Computational Vision and Medical Image Processing*, Oporto.

Arinci Incel, N., Genç, H., Erdem, H. R., and Yorgancioglu, Z. R. (2003). Muscle imbalance in hallux valgus: an electromyographic study. *American journal of physical medicine & rehabilitation / Association of Academic Physiatrists*, 82(5):345–9.

Arya, S. and Kulig, K. (2010). Tendinopathy alters mechanical and material properties of the Achilles tendon. *Journal of applied physiology (Bethesda, Md. : 1985)*, 108(3):670–675.

Athanasiou, K. a., Liu, G. T., Lavery, L. a., Lanctot, D. R., and Schenck, R. C. (1998). Biomechanical topography of human articular cartilage in the first metatarsophalangeal joint. *Clinical orthopaedics and related research*, 348:269–81.

Babuska, I. and Oden, J. (2004). Verification and validation in computational engineering and science: basic concepts. *Computer Methods in Applied Mechanics and Engineering*, 193(36-38):4057–4066.

Bandak, F. A., Tannous, R. E., and Toridis, T. (2001). On the development of an osseo-ligamentous finite element model of the human ankle joint. *International Journal of Solids and Structures*, 38(10-13):1681–1697.

Barela, A. M. F., Freitas, P. B. D., Celestino, M. L., Camargo, M. R., and Barela, J. A. (2014). Ground reaction forces during level ground walking with body weight unloading. *Brazilian Journal of Physical Therapy*, 18(6):572–579.

Barnicott, N. A. and Hardy, R. H. (1955). The position of the hallux in West Africans. *Journal of Anatomy*, 89:355–361.

Bates, K. T., Savage, R., Pataky, T. C., Morse, S. a., Webster, E., Falkingham, P. L., Ren, L., Qian, Z., Collins, D., Bennett, M. R., McClymont, J., and

Crompton, R. H. (2013). Does footprint depth correlate with foot motion and pressure? *Journal of the Royal Society, Interface*, 10(83).

Bayod, J., Becerro-de Bengoa-Vallejo, R., Losa-Iglesias, M. E., and Doblaré, M. (2012). Mechanical stress redistribution in the calcaneus after autologous bone harvesting. *Journal of biomechanics*, 45(7):1219–26.

Bayod, J., Becerro de Bengoa Vallejo, R., Losa Iglesias, M. E., and Doblaré, M. (2013). Stress at the second metatarsal bone after correction of hammertoe and claw toe deformity: a finite element analysis using an anatomical model. *Journal of the American Podiatric Medical Association*, 103(4):260–73.

Bayod, J., Losa-Iglesias, M., Becerro de Bengoa-Vallejo, R., Prados-Frutos, J. C., Jules, K. T., and Doblare, M. (2010). Advantages and Drawbacks of Proximal Interphalangeal Joint Fusion Versus Flexor Tendon Transfer in the Correction of Hammer and Claw Toe Deformity. A Finite-Element Study. *Journal of Biomechanical Engineering*, 132 (5):51002–51007.

Beaugonin, M., Haug, E., and Cesari, D. (1996). A numerical model of the human ankle/foot under impact loading in inversion and eversion. *Proceedings: Stapp Car Crash Conference*, 40:239–249.

Beaugonin, M., Haug, E., and Cesari, D. (1997). Improvement of numerical ankle/foot model: modeling of deformable bone. *Proceedings: Stapp Car Crash Conference*, 41:225–237.

Beillas, P., Lavaste, F., Nicolopoulos, D., Kayventash, K., Yang, K. H., and Robin, S. (1999). Foot and ankle finite element modeling using ct-scan data. In *43rd Stapp Car Crash Conference*, pages 217–42, San Diego (CA).

Beillas, P., Papaioannou, G., Tashman, S., and Yang, K. H. (2004). A new method to investigate in vivo knee behavior using a finite element model of the lower limb. *Journal of biomechanics*, 37(7):1019–30.

Benedict, J. V., Walker, L. B., and Harris, E. H. (1968). Stress-strain characteristics and tensile strength of unembalmed human tendon. *Journal of Biomechanics*, 1(1):53–63.

Bennett, M. B. and Ker, R. F. (1990). The mechanical properties of the human subcalcaneal fat pad in compression. *Journal of anatomy*, 171:131–138.

Berntsen, G. K. R., Fonnebo, V., Tollan, A., Sogaard, A. J., and Magnus, J. H. (2001). Forearm Bone Mineral Density by Age in 7 , 620 Men and Women The TromsøStudy , a Population-based Study. *American Journal of Epidemiology*, 153(5):465–473.

Blanton, P. L. and Biggs, N. L. (1970). Ultimate tensile strength of fetal and adult human tendons. *Journal of biomechanics*, 3(2):181–9.

Bowles, J. E. (1996). *Foundation Analysis and Design Fifth Edition*, volume 20. McGraw-Hill.

Brilakis, E., Kaselouris, E., Xypnitos, F., Provatidis, C. G., and Efstathopoulos, N. (2012). Effects of foot posture on fifth metatarsal fracture healing: a finite element study. *The Journal of foot and ankle surgery*, 51(6):720–8.

Bryant, a., Tinley, P., and Singer, K. (2000). A comparison of radiographic measurements in normal, hallux valgus, and hallux limitus feet. *The Journal of Foot and Ankle Surgery*, 39(1):39–43.

Budhabhatti, S. P., Erdemir, A., Petre, M., Sferra, J., Donley, B., and Cavanagh, P. R. (2007). Finite element modeling of the first ray of the foot: a tool for the design of interventions. *Journal of biomechanical engineering*, 129(5):750–6.

Burg, J., Peeters, K., Natsakis, T., Dereymaeker, G., Vander Sloten, J., and Jonkers, I. (2013). In vitro analysis of muscle activity illustrates mediolateral decoupling of hind and mid foot bone motion. *Gait & posture*, 38(1):56–61.

Burkhart, T. a., Andrews, D. M., and Dunning, C. E. (2013). Finite element modeling mesh quality, energy balance and validation methods: a review with recommendations associated with the modeling of bone tissue. *Journal of biomechanics*, 46(9):1477–88.

Butler, D., Grood, E., Noyes, F., and Brackett, K. (1984). Effects of structure and strain measurement technique on the material properties of young human tendons and fascia. *Journal of Biomechanics*, 1(8):579–596.

Butz, K. D., Merrell, G., and Nauman, E. a. (2012). A biomechanical analysis of finger joint forces and stresses developed during common daily activities. *Computer methods in biomechanics and biomedical engineering*, 15(2):131–40.

Calhoun, J. H., Li, F., Ledbetter, B. R., and Viegas, S. F. (1994). A Comprehensive Study of Pressure Distribution in the Ankle Joint with Inversion and Eversion. *Foot & Ankle International*, 15(3):125–133.

Cavanagh, P., Erdemir, A., and Petre, M. (2008). A finite element approach to examine the relationship between plantar pressure and internal stress in the foot. *54th Annual Meeting of the Orthopaedic Research Society*, (104).

Chang, R., Rodrigues, P. a., Van Emmerik, R. E. a., and Hamill, J. (2014). Multisegment foot kinematics and ground reaction forces during gait of individuals with plantar fasciitis. *Journal of biomechanics*, 47(11):2571–7.

Chao, C. Y. L., Zheng, Y. P., Huang, Y. P., and Cheing, G. L. Y. (2010). Biomechanical properties of the forefoot plantar soft tissue as measured by an optical coherence tomography-based air-jet indentation system and tissue ultrasound palpation system. *Clinical Biomechanics*, 25(6):594–600.

Chen, W.-M. and Lee, P. V.-S. (2015). Explicit finite element modelling of heel pad mechanics in running: inclusion of body dynamics and application of physiological impact loads. *Computer Methods in Biomechanics and Biomedical Engineering*, 18(14):1582–1595.

Chen, W.-M., Lee, S.-J., and Lee, P. V. S. (2014a). The in vivo plantar soft tissue mechanical property under the metatarsal head: implications of tissues joint-angle dependent response in foot finite element modeling. *Journal of the mechanical behavior of biomedical materials*, 40:264–74.

Chen, W.-M., Lee, S.-J., and Lee, P. V. S. (2015). Plantar pressure relief under the metatarsal heads - Therapeutic insole design using three-dimensional finite element model of the foot. *Journal of biomechanics*, 48(4):659–65.

Chen, W.-M., Lee, T., Lee, P. V.-S., Lee, J. W., and Lee, S.-J. (2010a). Effects of internal stress concentrations in plantar soft-tissue–A preliminary three-dimensional finite element analysis. *Medical engineering & physics*, 32(4):324–31.

Chen, W.-M., Park, J., Park, S.-B., Shim, V. P.-W., and Lee, T. (2012). Role of gastrocnemius-soleus muscle in forefoot force transmission at heel rise - A 3D finite element analysis. *Journal of biomechanics*, 45(10):1783–9.

Chen, W.-M., Phyau-Wui Shim, V., Park, S.-B., and Lee, T. (2011). An instrumented tissue tester for measuring soft tissue property under the metatarsal heads in relation to metatarsophalangeal joint angle. *Journal of biomechanics*, 44(9):1801–4.

Chen, W.-M., Vee-Sin Lee, P., Park, S.-B., Lee, S.-J., Phyau Wui Shim, V., and Lee, T. (2010b). A novel gait platform to measure isolated plantar metatarsal forces during walking. *Journal of biomechanics*, 43(10):2017–21.

Chen, W.-P., Ju, C.-W., and Tang, F.-T. (2003). Effects of total contact insoles on the plantar stress redistribution: a finite element analysis. *Clinical Biomechanics*, 18(6):S17–S24.

Chen, W.-p., Tang, F.-t., and Ju, C.-W. (2001). Stress distribution of the foot during mid-stance to push-off in barefoot gait : a 3-D finite element analysis. *Clinical Biomechanics*, 16(7):614–620.

Chen, Y.-N., Chang, C.-W., Li, C.-T., Chang, C.-H., and Lin, C.-F. (2014b). Finite Element Analysis of Plantar Fascia During Walking: A Quasi-static Simulation. *Foot & Ankle International*, 36(1):90–97.

Cheng, H.-Y. K., Lin, C.-L., Wang, H.-W., and Chou, S.-W. (2008). Finite element analysis of plantar fascia under stretch-the relative contribution of wind-

lass mechanism and Achilles tendon force. *Journal of biomechanics*, 41(9):1937–44.

Cheung, J. T., An, K. N., and Zhang, M. (2006a). Consequences of partial and total plantar fascia release: a finite element study. *Foot & ankle international / American Orthopaedic Foot and Ankle Society [and] Swiss Foot and Ankle Society*, 27(2):125–132.

Cheung, J. T.-M. and Nigg, B. M. (2008). Clinical Applications of Computational Simulation of Foot and Ankle. *Sport-Orthopädie - Sport-Traumatologie - Sports Orthopaedics and Traumatology*, 23(4):264–271.

Cheung, J. T.-M., Yu, J., Wong, D. W.-C., and Zhang, M. (2009). Current methods in computer-aided engineering for footwear design. *Footwear Science*, 1(1):31–46.

Cheung, J. T.-M. and Zhang, M. (2005). A 3-dimensional finite element model of the human foot and ankle for insole design. *Archives of Physical Medicine and Rehabilitation*, 86(2):353–358.

Cheung, J. T.-m. and Zhang, M. (2006). Finite Element Modeling of the Human Foot and Footwear. In *ABAQUS Users' conference*, pages 145–159.

Cheung, J. T.-M. and Zhang, M. (2008). Parametric design of pressure-relieving foot orthosis using statistics-based finite element method. *Medical Engineering & Physics*, 30(3):269–277.

Cheung, J. T.-M., Zhang, M., and An, K.-N. (2004). Effects of plantar fascia stiffness on the biomechanical responses of the ankle-foot complex. *Clinical Biomechanics*, 19(8):839–846.

Cheung, J. T.-M., Zhang, M., and An, K.-N. (2006b). Effect of Achilles tendon loading on plantar fascia tension in the standing foot. *Clinical Biomechanics*, 21(2):194–203.

Cheung, J. T.-M., Zhang, M., Leung, A. K.-L., and Fan, Y.-B. (2005). Three-dimensional finite element analysis of the foot during standing - a material sensitivity study. *Journal of Biomechanics*, 38(5):1045–1054.

Cho, J.-R., Park, S.-B., Ryu, S.-H., Kim, S.-H., and Lee, S.-B. (2009). Landing impact analysis of sports shoes using 3-D coupled foot-shoe finite element model. *Journal of Mechanical Science and Technology*, 23(10):2583–2591.

Chockalingam, N., Healy, A., Naemi, R., Burgess-Walker, P., Abdul Razak, A. H., Zayegh, A., Begg, R. K., and Wahab, Y. (2013). Comments and reply to: Foot plantar pressure measurement system: a review. *Sensors*, 13(3):3527–3529.

Chokhandre, S., Halloran, J. P., van den Bogert, A. J., and Erdemir, A. (2012). A three-dimensional inverse finite element analysis of the heel pad. *Journal of biomechanical engineering*, 134(3):031002.

Chu, T., Reddy, N., and Padovan, J. (1995). Three-dimensional finite element stress analysis of the polypropylene, ankle-foot orthosis: static analysis. *Medical engineering & physics*, 17(5):372–379.

Chu, T. M. and Reddy, N. P. (1995). Stress distribution in the ankle-foot orthosis used to correct pathological gait. *Journal of rehabilitation research and development*, 32(4):349–60.

Clift, S. E. (1992). Finite-element analysis in cartilage biomechanics. *Journal of Biomedical Engineering*, 14(3):217–221.

Cook, D., Julias, M., and Nauman, E. (2014). Biological variability in biomechanical engineering research: Significance and meta-analysis of current modeling practices. *Journal of Biomechanics*, 47(6):1241–1250.

Coughlin, M. J. (1984). Hallux Valgus - causes, evaluation, and treatment. *Postgraduate Medicine*, 75(5):174–&.

Cowin, S., Van Buskirk, W., and Ashman, R. (1987). The properties of bone. In *Handbook of bioengineering*, chapter 2. McGraw-Hill, New York.

Cowin, S. C. (1979). On the Strength Anisotropy of Bone and Wood. *Journal of Applied Mechanics*, 46(4):832–838.

Cowin, S. C. (1985). The relationship between the elasticity tensor and the fabric tensor. *Mechanics of Materials*, 4(2):137–147.

Cronkite, A. E. (1936). The tensile strength of human tendons. *The Anatomical Record*, 64(2):173–186.

Currey, J. (1984). What Should Bones Be Designed to Do? *Calcified Tissue International*, 36:7–8.

Currey, J. (2003). The many adaptations of bone. *Journal of Biomechanics*, 36(10):1487–1495.

Dai, X.-Q., Li, Y., Zhang, M., and Cheung, J. T.-M. (2006). Effect of sock on biomechanical responses of foot during walking. *Clinical Biomechanics*, 21(3):314–321.

Daoud, A. I., Geissler, G. J., Wang, F., Saretsky, J., Daoud, Y. a., and Lieberman, D. E. (2012). Foot strike and injury rates in endurance runners: A retrospective study. *Medicine and Science in Sports and Exercise*, 44(7):1325–1334.

Datta, B., Salleh, R., Mafulli, N., Neil, M., Butler, A., and Walsh, W. (2006). Mechanical properties of human flexor hallucis longus, peroneus brevis and tendo achilles tendons. In *52nd Annual Meeting of the Orthopaedic Research Society Paper No : 1889*, page 1889.

de Almeida, M. O., Saragiotto, B. T., Yamato, T. P., and Lopes, A. D. (2014). Is the rearfoot pattern the most frequently foot strike pattern among recreational shod distance runners? *Physical Therapy in Sport*, 16(1):29–33.

De Clercq, D., Aerts, P., and Kunnen, M. (1994). The mechanical characteristics of the human heel pad during foot strike in running: An in vivo cineradiographic study. *Journal of Biomechanics*, 27(10):1213–1222.

De Wit, B., De Clercq, D., and Aerts, P. (2000). Biomechanical analysis of the stance phase during barefoot and shod running. *Journal of Biomechanics*, 33(3):269–278.

Demir, F. (2005). A new way of prediction elastic modulus of normal and high strength concrete-fuzzy logic. *Cement and Concrete Research*, 35(8):1531–1538.

Devkota, A. C. and Weinhold, P. S. (2003). Mechanical response of tendon subsequent to ramp loading to varying strain limits. *Clinical Biomechanics*, 18(10):969–974.

Divert, C., Mornieux, G., Freychat, P., Baly, L., Mayer, F., and Belli, a. (2008). Barefoot-shod running differences: Shoe or mass effect? *International Journal of Sports Medicine*, 29(6):512–518.

Duda, G. N., Mandruzzato, F., Heller, M., Goldhahn, J., Moser, R., Hehli, M., Claes, L., and Haas, N. P. (2001). Mechanical boundary conditions of fracture healing: borderline indications in the treatment of unreamed tibial nailing. *Journal of Biomechanics*, 34(5):639–650.

Erdemir, A., Guess, T. M., Halloran, J., Tadepalli, S. C., and Morrison, T. M. (2012). Considerations for reporting finite element analysis studies in biomechanics. *Journal of biomechanics*, 45(4):625–33.

Erdemir, A., Hamel, A. J., Fauth, A. R., Piazza, S. J., and Sharkey, N. a. (2004). Dynamic loading of the plantar aponeurosis in walking. *The Journal of bone and joint surgery. American volume*, 86-A(3):546–52.

Erdemir, A., McLean, S., Herzog, W., and van den Bogert, A. J. (2007). Model-based estimation of muscle forces exerted during movements. *Clinical biomechanics (Bristol, Avon)*, 22(2):131–54.

Erdemir, A., Saucerman, J. J., Lemmon, D., Loppnow, B., Turso, B., Ulbrecht, J. S., and Cavanagh, P. R. (2005). Local plantar pressure relief in therapeutic footwear: design guidelines from finite element models. *Journal of biomechanics*, 38(9):1798–806.

Erdemir, A., Viveiros, M. L., Ulbrecht, J. S., and Cavanagh, P. R. (2006). An inverse finite-element model of heel-pad indentation. *Journal of biomechanics*, 39(7):1279–86.

Evans, F. (1973). *Mechanical Properties of Bone*. Springfield, IL, thomas c.c edition.

Even-Tzur, N., Weisz, E., Hirsch-Falk, Y., and Gefen, A. (2006). Role of EVA viscoelastic properties in the protective performance of a sport shoe: computational studies. *Bio-medical materials and engineering*, 16(5):289–99.

Fernandez, J. W., Ul Haque, M. Z., Hunter, P. J., and Mithraratne, K. (2012). Mechanics of the foot Part 1: a continuum framework for evaluating soft tissue stiffening in the pathologic foot. *International journal for numerical methods in biomedical engineering*, 28(10):1056–70.

Ferrari, J., Hopkinson, D. a., and Linney, A. D. (2004). Size and shape differences between male and female foot bones: is the female foot predisposed to hallux abducto valgus deformity? *Journal of the American Podiatric Medical Association*, 94(5):434–52.

Finni, T., Komi, P., and Lukkariniemi, J. (1998). Achilles tendon loading during walking: application of a novel optic fiber technique. *European journal of applied physiology*, 77:289–291.

Flavin, R., Halpin, T., O'Sullivan, R., FitzPatrick, D., Ivankovic, A., and Stephens, M. M. (2008). A finite-element analysis study of the metatarsophalangeal joint of the hallux rigidus. *The Journal of bone and joint surgery. British volume*, 90(10):1334–40.

Fontanella, C. G., Carniel, E. L., Forestiero, A., and Natali, a. N. (2014). Investigation of the mechanical behaviour of the foot skin. *Skin research and technology : official journal of International Society for Bioengineering and the Skin (ISBS) [and] International Society for Digital Imaging of Skin (ISDIS) [and] International Society for Skin Imaging (ISSI)*, 20(4):445–452.

Fontanella, C. G., Forestiero, A., Carniel, E. L., and Natali, a. N. (2013). Analysis of heel pad tissues mechanics at the heel strike in bare and shod conditions. *Medical engineering & physics*, 35(4):441–7.

Fontanella, C. G., Matteoli, S., Carniel, E. L., Wilhjelm, J. E., Virga, A., Corvi, A., and Natali, a. N. (2012). Investigation on the load-displacement curves of a human healthy heel pad: In vivo compression data compared to numerical results. *Medical engineering & physics*, 34(9):1253–9.

Forestiero, A., Carniel, E. L., and Natali, A. N. (2014). Biomechanical behaviour of ankle ligaments: constitutive formulation and numerical modelling. *Computer methods in biomechanics and biomedical engineering*, 17(4):395–404.

Forestiero, A., Carniel, E. L., Venturato, C., and Natali, A. N. (2013). Investigation of the biomechanical behaviour of hindfoot ligaments. *Proceedings of the Institution of Mechanical Engineers. Part H, Journal of engineering in medicine*, 227(6):683–92.

García-Aznar, J. M., Bayod, J., Rosas, A., Larrainzar, R., García-Bógalo, R., Doblaré, M., and Llanos, L. F. (2009). Load transfer mechanism for different metatarsal geometries: a finite element study. *Journal of biomechanical engineering*, 131(2):021011.

García-González, A., Bayod, J., Prados-Frutos, J. C., Losa-Iglesias, M., Jules, K. T., Becerro de Bengoa-Vallejo, R., and Doblaré, M. (2009). Finite-element simulation of flexor digitorum longus or flexor digitorum brevis tendon transfer for the treatment of claw toe deformity. *Journal of biomechanics*, 42(11):1697–704.

Gefen, A. (2002). Stress analysis of the standing foot following surgical plantar fascia release. *Journal of Biomechanics*, 35(5):629–637.

Gefen, A. (2003). Plantar soft tissue loading under the medial metatarsals in the standing diabetic foot. *Medical Engineering & Physics*, 25(6):491–499.

Gefen, a., Megido-Ravid, M., and Itzchak, Y. (2001). In vivo biomechanical behavior of the human heel pad during the stance phase of gait. *Journal of biomechanics*, 34(12):1661–5.

Gefen, A., Megido-Ravid, M., Itzchak, Y., and Arcan, M. (1998). Biomechanical Evaluation of Surgical Plantar Fascia Release Effects. In *Proc. VIII Mediterranean Conf. on Med. & Biol. Eng. & Comput.*

Gefen, A., Megido-Ravid, M., Itzchak, Y., and Arcan, M. (2000). Biomechanical analysis of the three-dimensional foot structure during gait: a basic tool for clinical applications. *J Biomech Eng*, 122(6):630–639.

Gerlo, J., Segers, V., and DeClercq, D. (2013). The frequency content of plantar pressure measurements during barefoot running. *Footwear Science*, 5(sup1):S138–S139.

Giannini, S., Buda, R., Di Caprio, F., Agati, P., Bigi, A., De Pasquale, V., and Ruggeri, A. (2008). Effects of freezing on the biomechanical and structural properties of human posterior tibial tendons. *International Orthopaedics*, 32(2):145–151.

Giddings, V., Beaupre, G., Whalen, R., and Carter, D. (2000). Calcaneal loading during walking and running. *Medicine and science in sports and exercise*, 32:627–634.

Giuliani, J., Masini, B., Alitz, C., and Owens, B. D. (2011). Barefoot-simulating footwear associated with metatarsal stress injury in 2 runners. *Orthopedics*, 34(7):e320–3.

Goldstein, S. A. (1987). The mechanical properties of trabecular bone: Dependence on anatomic location and function. *Journal of biomechanics*, 20(11-12):1055–1061.

Goske, S., Erdemir, A., Petre, M., Budhabhatti, S., and Cavanagh, P. R. (2006). Reduction of plantar heel pressures: Insole design using finite element analysis. *Journal of biomechanics*, 39(13):2363–70.

Gu, Y. and Li, J. (2005). Finite element analysis of the instep fatigue trauma in the high-heeled gait. *World Journal Modelling and Simulation*, 1(2):117–122.

Gu, Y., Li, J., Ren, X., Lake, M. J., and Zeng, Y. (2010a). Heel skin stiffness effect on the hind foot biomechanics during heel strike. *Skin research and technology*, 16(3):291–6.

Gu, Y. D., Li, J. S., Lake, M. J., Ren, X. J., and Zeng, Y. J. (2008). The mechanical response of Achilles tendon during different kinds of sports. *Communications in numerical methods in engineering*, 24(12):2077–2085.

Gu, Y. D., Li, J. S., Lake, M. J., Zeng, Y. J., Ren, X. J., and Li, Z. Y. (2011). Image-based midsole insert design and the material effects on heel plantar pressure distribution during simulated walking loads. *Computer methods in biomechanics and biomedical engineering*, 14(8):747–53.

Gu, Y. D., Ren, X. J., Li, J. S., Lake, M. J., Zhang, Q. Y., and Zeng, Y. J. (2010b). Computer simulation of stress distribution in the metatarsals at different inversion landing angles using the finite element method. *International orthopaedics*, 34(5):669–76.

Guiotto, A., Sawacha, Z., Guarneri, G., Avogaro, A., and Cobelli, C. (2014). 3D finite element model of the diabetic neuropathic foot: A gait analysis driven approach. *Journal of biomechanics*, 47(12):3064–3071.

Guo, Y., Zhang, X., and Chen, W. (2009). Three-Dimensional Finite Element Simulation of Total Knee Joint in Gait Cycle. *Acta Mechanica Solida Sinica*, 22(4):347–351.

Halloran, J. P., Ackermann, M., Erdemir, A., and van den Bogert, A. J. (2010). Concurrent musculoskeletal dynamics and finite element analysis predicts altered gait patterns to reduce foot tissue loading. *Journal of biomechanics*, 43(14):2810–5.

Halloran, J. P., Erdemir, A., and van den Bogert, A. J. (2009). Adaptive surrogate modeling for efficient coupling of musculoskeletal control and tissue deformation models. *Journal of biomechanical engineering*, 131(1):011014.

Hansen, P., Kovanen, V., Hölmich, P., Krogsgaard, M., Hansson, P., Dahl, M., Hald, M., Aagaard, P., Kjaer, M., and Magnusson, S. P. (2013). Micromechanical properties and collagen composition of ruptured human achilles tendon. *The American journal of sports medicine*, 41(2):437–43.

Hardy, R. H. and Clapham, J. C. R. (1951). Observations on Hallux Valgus. *Journal of Bone & Joint Surgery, British Volume*, 33-B(3):376–391.

Hasegawa, H., Yamauchi, T., and Kraemer, W. J. (2007). Foot strike patterns of runners at the 15-km point during an elite-level half marathon. *Journal of strength and conditioning research / National Strength & Conditioning Association*, 21(3):888–93.

Heden, R. I. and Sorto, L. A. (1981). The Buckle point and the metatarsal protrusion's relationship to hallux valgus. *Journal of the American Podiatry Association*, 71(4):200–208.

Hein, T. and Grau, S. (2014). Can minimal running shoes imitate barefoot heel-toe running patterns? Acomparison of lower leg kinematics. *Journal of Sport and Health Science*, 3(2):67–73.

Helal, B. (1981). Surgery for adolescent Hallux Valgus. *Clinical Orthopaedics and Related Research*, (157):50–63.

Helgason, B., Perilli, E., Schileo, E., Taddei, F., Brynjólfsson, S., and Viceconti, M. (2008). Mathematical relationships between bone density and mechanical properties: a literature review. *Clinical biomechanics (Bristol, Avon)*, 23(2):135–46.

Henninger, H. B., Reese, S. P., Anderson, a. E., and Weiss, J. a. (2010). Validation of computational models in biomechanics. *Proceedings of the Institution of Mechanical Engineers, Part H: Journal of Engineering in Medicine*, 224(7):801–812.

Hing, W. a., Rome, K., and Cameron, A. F. (2009). Reliability of measuring abductor hallucis muscle parameters using two different diagnostic ultrasound machines. *Journal of foot and ankle research*, 2:33.

Ho, N. and Meng, C. (2002). The effect of post mortem freezing storage on the tensile properties of tendon. In *Proceedings of the IEEE 28th Annual*, pages 53–54.

Hsu, C. C., Tsai, W. C., Chen, C. P. C., Shau, Y. W., Wang, C. L., Chen, M. J. L., and Chang, K. J. (2005). Effects of aging on the plantar soft tissue properties under the metatarsal heads at different impact velocities. *Ultrasound in Medicine and Biology*, 31(10):1423–1429.

Hsu, Y.-C., Gung, Y.-W., Shih, S.-L., Feng, C.-K., Wei, S.-H., Yu, C.-H., and Chen, C.-S. (2008). Using an optimization approach to design an insole for lowering plantar fascia stress–a finite element study. *Annals of biomedical engineering*, 36(8):1345–52.

Huang, H., Zhang, J., Sun, K., Zhang, X., and Tian, S. (2011). Effects of repetitive multiple freeze-thaw cycles on the biomechanical properties of human flexor digitorum superficialis and flexor pollicis longus tendons. *Clinical biomechanics (Bristol, Avon)*, 26(4):419–23.

Huiskes, R. (1982). On the modelling of long bones in structural analyses. *Journal of Biomechanics*, 15(1):65–69.

Iaquinto, J. M. and Wayne, J. S. (2010). Computational model of the lower leg and foot/ankle complex: application to arch stability. *Journal of biomechanical engineering*, 132(2):021009.

Iida, M. and Basmajian, J. V. (1974). Electromyography of Hallux Valgus. *Clinical Orthopaedics and Related Research*, 101.

Imhauser, C. W., Siegler, S., Abidi, N. a., and Frankel, D. Z. (2004). The effect of posterior tibialis tendon dysfunction on the plantar pressure characteristics and the kinematics of the arch and the hindfoot. *Clinical biomechanics (Bristol, Avon)*, 19(2):161–9.

Ishii, H., Sakurai, Y., and Maruyama, T. (2014). Effect of soccer shoe upper on ball behaviour in curve kicks. *Scientific Reports*, 4:1–8.

Isvilanonda, V., Dengler, E., Iaquinto, J. M., Sangeorzan, B. J., and Ledoux, W. R. (2012). Finite element analysis of the foot: model validation and comparison between two common treatments of the clawed hallux deformity. *Clinical biomechanics (Bristol, Avon)*, 27(8):837–44.

Iwamoto, M., Mikki, K., and Tanaka, E. (2005). Ankle skeletal injury predictions using anisotropic inelastic constitutive model of cortical bone taking into account damage evolution. *Stapp car crash journal.*, 49:133–156.

Jacob, S., Patil, K., Braak, L., and Huson, A. (1996). Stresses in a 3D two arch model of a normal human foot. *Mechanics research communications*, 23(4):387–393.

Jacob, S. and Patil, M. K. (1999). Three-dimensional Foot Modeling and Analysis of Stresses in Normal and Early Stage Hansen's Disease with Muscle Paralysis. *Journal of Rehabilitation Research & Development*, 36(3):252–63.

Jenkins, D. W. and Cauthon, D. J. (2011). Barefoot running claims and controversies: a review of the literature. *Journal of the American Podiatric Medical Association*, 101(3):231–246.

Johnston, O. (1959). Further studies of the inheritance of hand and foot anomalies. *Clinical Orthopedics*, 8:146–159.

Jordan, C. and Bartlett, R. (1995). Pressure distribution and perceived comfort in casual footwear. *Gait & Posture*, 3:215–220.

Jung, H.-J., Vangipuram, G., Fisher, M. B., Yang, G., Hsu, S., Bianchi, J., Ronholdt, C., and Woo, S. L.-Y. (2011). The effects of multiple freeze-thaw cycles on the biomechanical properties of the human bone-patellar tendon-bone allograft. *Journal of orthopaedic research : official publication of the Orthopaedic Research Society*, 29(8):1193–1198.

Kao, P. F., Davis, B. L., and Hardy, P. a. (1999). Characterization of the calcaneal fat pad in diabetic and non-diabetic patients using magnetic resonance imaging. *Magnetic resonance imaging*, 17(6):851–857.

Kasmer, M. E., Liu, X. C., Roberts, K. G., and Valadao, J. M. (2013). Foot-strike pattern and performance in a marathon. *International Journal of Sports Physiology and Performance*, 8(3):286–292.

Kato, T. and Watanabe, S. (1981). The Etiology of Hallux Valgus in Japan. *Clinical Orthopaedics and Related Research*, 157:78–81.

Keaveny, T. M., Guo, X., Wachtel, E. F., McMahon, T. A., and Hayes, W. C. (1994). Trabecular bone exhibits fully linear elastic behavior and yields at low strains. *Journal of Biomechanics*, 27(9):1127–1136.

Ker, R. (2007). Mechanics of tendon, from an engineering perspective. *International Journal of Fatigue*, 29(6):1001–1009.

Kim, J.-E., Li, Z., Ito, Y., Huber, C. D., Shih, A. M., Eberhardt, A. W., Yang, K. H., King, A. I., and Soni, B. K. (2009). Finite element model development of a child pelvis with optimization-based material identification. *Journal of biomechanics*, 42(13):2191–5.

Kim, W. and Voloshin, A. S. (1995). Role of plantar fascia in the load bearing capacity of the human foot. *Journal of biomechanics*, 28(9):1025–1033.

Kirby, K. A. (2001). What future direction should podiatric biomechanics take? *Clinics in podiatric medicine and surgery*, 18(4):719–23, vii.

Kitagawa, Y., Ichikawa, H., King, A., and Begeman, P. (2000). Development of A Human Ankle/Foot Model. In Kajzer, J., Tanaka, E., and Yamada, H., editors, *Human Biomechanics and Injury Prevention*, pages 117–122. Springer Japan.

Kitagawa, Y., Ichikawa, H., King, A. I., and Levine, R. S. (1998). A severe ankle and foot injury in frontal crashes and its mechanism. *SAE Technical Paper*.

Kitaoka, H., Luo, Z., and An, K. (1997). Effect of the posterior tibial tendon on the arch of the foot during simulated weightbearing: Biomechanical analysis. *Foot & ankle international*, 18(1):43–6.

Kitaoka, H. B., Luo, Z. P., Growney, E. S., Berglund, L. J., and An, K.-N. (1994). Material Properties of the Plantar Aponeurosis. *Foot & Ankle International*, 15(10):557–560.

Komi, P. (1990). Relevance of in vivo force measurements to human biomechanics. *Journal of Biomechanics*, 23:23–34.

Kongsgaard, M. and Aagaard, P. (2005). Structural Achilles tendon properties in athletes subjected to different exercise modes and in Achilles tendon rupture patients. *Journal of Applied Physiology*, 99:1965–1971.

Kongsgaard, M., Nielsen, C. H., Hegnsvad, S., Aagaard, P., and Magnusson, S. P. (2011). Mechanical properties of the human Achilles tendon, in vivo. *Clinical biomechanics (Bristol, Avon)*, 26(7):772–7.

Kwan, R. L. C., Zheng, Y. P., and Cheing, G. L. Y. (2010). The effect of aging on the biomechanical properties of plantar soft tissues. *Clinical Biomechanics*, 25(6):601–605.

Lamur, K. S., Huson, A., Snijders, C. J., and Stoeckart, R. (1996). Geometric data of hallux valgus feet. *Foot & Ankle International*, 17(9):548–554.

Laporta, G., Melillo, T., and Olinsky, D. (1974). X-ray evaluation of hallux abducto valgus deformity. *Journal of the American Podiatry Association*, 64(8):544–66.

Larson, P. (2014). Comparison of foot strike patterns of barefoot and minimally shod runners in a recreational road race. *Journal of Sport and Health Science*, 3(2):137–142.

Larson, P., Higgins, E., Kaminski, J., Decker, T., Preble, J., Lyons, D., McIntyre, K., and Normile, A. (2011). Foot strike patterns of recreational and sub-elite runners in a long-distance road race. *Journal of Sports Sciences*, 29(15):1665–1673.

Ledoux, W. R. and Blevins, J. J. (2007). The compressive material properties of the plantar soft tissue. *Journal of biomechanics*, 40(13):2975–2981.

Lemmon, D., Shiang, T. Y., Hashmi, A., Ulbrecht, J. S., and Cavanagh, P. R. (1997). The effect of insoles in therapeutic footwear - A finite element approach. *Journal of Biomechanics*, 30(6):615–620.

Liacouras, P. C. and Wayne, J. S. (2007). Computational modeling to predict mechanical function of joints: application to the lower leg with simulation of two cadaver studies. *Journal of biomechanical engineering*, 129(6):811–17.

Liang, J., Yang, Y., Yu, G., Niu, W., and Wang, Y. (2011). Deformation and stress distribution of the human foot after plantar ligaments release: a cadaveric study and finite element analysis. *Science China. Life sciences*, 54(3):267–71.

Lichtwark, G. a. and Wilson, a. M. (2005). In vivo mechanical properties of the human Achilles tendon during one-legged hopping. *The Journal of experimental biology*, 208(Pt 24):4715–25.

Lieberman, D. E., Venkadesan, M., Werbel, W. a., Daoud, A. I., D'Andrea, S., Davis, I. S., Mang'eni, R. O., and Pitsiladis, Y. (2010). Foot strike patterns and collision forces in habitually barefoot versus shod runners. *Nature*, 463(7280):531–5.

Lievers, W. B. and Kent, R. W. (2013). Patient-specific modelling of the foot: automated hexahedral meshing of the bones. *Computer Methods in Biomechanics and Biomedical Engineering*, 16(12):1287–1297.

Lin, S., Lin, C., Tang, F., and Chen, W. (2007). Combining experimental material property test and finite element analysis to investigate the plantar foot pressure distribution during standing. In *XXI ISB Congress*, number July, pages 337–338.

Lin, S.-C., Chen, C. P.-C., Tang, S. F.-T., Chen, C.-W., Wang, J.-J., Hsu, C.-C., Hsieh, J.-H., and Chen, W.-P. (2014). Stress Distribution Within the Plantar Aponeurosis During Walking - a Dynamic Finite Element Analysis. *Journal of Mechanics in Medicine and Biology*, 14(04):1450053.

Lin, S.-Y., Su, K.-C., and Chang, C.-H. (2013). Reverse engineering of CT-based rocker sole model-Finite element analysis. *1st International Conference on Orange Technologies (ICOT)*, pages 35–38.

Liu, Q., Zhang, K., Zhuang, Y., Li, Z., Yu, B., and Pei, G. (2013). Analysis of the stress and displacement distribution of inferior tibiofibular syndesmosis injuries repaired with screw fixation: a finite element study. *PloS one*, 8(12):e80236.

Liu, X. and Zhang, M. (2013). Redistribution of knee stress using laterally wedged insole intervention: Finite element analysis of knee-ankle-foot complex. *Clinical biomechanics (Bristol, Avon)*, 28(1):61–7.

Lohman, E. B., Balan Sackiriyas, K. S., and Swen, R. W. (2011). A comparison of the spatiotemporal parameters, kinematics, and biomechanics between shod, unshod, and minimally supported running as compared to walking. *Physical therapy in sport : official journal of the Association of Chartered Physiotherapists in Sports Medicine*, 12(4):151–63.

Louis-Ugbo, J., Leeson, B., and Hutton, W. C. (2004). Tensile properties of fresh human calcaneal (Achilles) tendons. *Clinical anatomy*, 17(1):30–5.

Lundberg, B. J. and Sulja, T. (1972). Skeletal Parameters in the Hallux Valgus Foot. *Acta Orthopaedica*, 43(6):576–582.

Luo, G., Houston, V. L., Garbarini, M. A., Beattie, A. C., and Thongpop, C. (2011). Finite element analysis of heel pad with insoles. *Journal of biomechanics*, 44(8):1559–65.

Luximon, Y., Luximon, A., Yu, J., and Zhang, M. (2012). Biomechanical evaluation of heel elevation on load transfer - experimental measurement and finite element analysis. *Acta Mechanica Sinica*, 28(1):232–240.

Mackerle, J. (2006). Finite element modeling and simulations in orthopedics: a bibliography 1998-2005. *Computer methods in biomechanics and biomedical engineering*, 9(3):149–99.

Maganaris, C. N., Narici, M. V., and Maffulli, N. (2008). Biomechanics of the Achilles tendon. *Disability and rehabilitation*, 30(20-22):1542–7.

Maganaris, C. N. and Paul, J. P. (1999). In vivo human tendon mechanical properties. *Journal of Physiology-London*, 521(1):307–313.

Maganaris, C. N. and Paul, J. P. (2002). Tensile properties of the in vivo human gastrocnemius tendon. *Journal of biomechanics*, 35(12):1639–46.

Maiwald, C., Grau, S., Krauss, I., Mauch, M., Axmann, D., and Horstmann, T. (2008). Reproducibility of plantar pressure distribution data in barefoot running. *Journal of Applied Biomechanics*, 24(1):14–23.

Mak, A. F., Lai, W. M., and Mow, V. C. (1987). Biphasic indentation of articular cartilage-I. Theoretical analysis. *Journal of Biomechanics*, 20(7):703–714.

Mancuso, J. E., Abramow, S. P., Landsman, M. J., Waldman, M., and Carioscia, M. (2003). The zero-plus first metatarsal and its relationship to bunion deformity. *The Journal of foot and ankle surgery : official publication of the American College of Foot and Ankle Surgeons*, 42(6):319–26.

Mann, R. A. and Coughlin, M. J. (1981). Hallux valgus–etiology, anatomy, treatment and surgical considerations. *Clinical Orthopaedics and Related Research*, 157:31–41.

Matzaroglou, C., Bougas, P., Panagiotopoulos, E., Saridis, A., Karanikolas, M., and Kouzoudis, D. (2010). Ninety-Degree Chevron Osteotomy for Correction of Hallux Valgus Deformity: Clinical Data and Finite Element Analysis. *The open orthopaedics journal*, 4:152–156.

Mickle, K. J., Nester, C. J., Crofts, G., and Steele, J. R. (2013). Reliability of ultrasound to measure morphology of the toe flexor muscles. *Journal of foot and ankle research*, 6(1):12.

Miller-Young, J. E., Duncan, N. a., and Baroud, G. (2002). Material properties of the human calcaneal fat pad in compression: experiment and theory. *Journal of biomechanics*, 35(12):1523–31.

Moglo, K. and Shirazi-Adl, A. (2003). On the coupling between anterior and posterior cruciate ligaments, and knee joint response under anterior femoral drawer in flexion: a finite element study. *Clinical Biomechanics*, 18(8):751–759.

Moon, D. K., Woo, S. L.-Y., Takakura, Y., Gabriel, M. T., and Abramowitch, S. D. (2006). The effects of refreezing on the viscoelastic and tensile properties of ligaments. *Journal of biomechanics*, 39(6):1153–7.

Morales-Orcajo, E., Bayod, J., and Barbosa de Las Casas, E. (2015a). Computational Foot Modeling: Scope and Applications. *Archives of Computational Methods in Engineering*.

Morales-Orcajo, E., Bayod, J., Becerro-de Bengoa-Vallejo, R., Losa-Iglesias, M., and Doblare, M. (2015b). Influence of first proximal phalanx geometry on hallux valgus deformity: a finite element analysis. *Medical & Biological Engineering & Computing*, 53(7):645–653.

Morgan, E. F., Bayraktar, H. H., and Keaveny, T. M. (2003). Trabecular bone modulus-density relationships depend on anatomic site. *Journal of Biomechanics*, 36(7):897–904.

Munuera, P., Polo, J., and Rebollo, J. (2008). Length of the first metatarsal and hallux in hallux valgus in the initial stage. *International Orthopaedics*, 32(4):489–495.

Nagel, A., Fernholz, F., Kibele, C., and Rosenbaum, D. (2008). Long distance running increases plantar pressures beneath the metatarsal heads. A barefoot walking investigation of 200 marathon runners. *Gait and Posture*, 27(1):152–155.

Nakamura, S., Crowninshield, R. D., and Cooper, R. R. (1981). An analysis of soft tissue loading in the Foot - A preliminary report. *Bulletin of Prosthetics Research*, 18(1):27–34.

Natali, A. N., Fontanella, C. G., and Carniel, E. L. (2010a). Constitutive formulation and analysis of heel pad tissues mechanics. *Medical Engineering & Physics*, 32(5):516–522.

Natali, a. N., Fontanella, C. G., and Carniel, E. L. (2012). Constitutive formulation and numerical analysis of the heel pad region. *Computer methods in biomechanics and biomedical engineering*, 15(4):401–9.

Natali, a. N., Forestiero, A., Carniel, E. L., Pavan, P. G., and Dal Zovo, C. (2010b). Investigation of foot plantar pressure: experimental and numerical analysis. *Medical & biological engineering & computing*, 48(12):1167–74.

Natsakis, T., Burg, J., Dereymaeker, G., Vander Sloten, J., and Jonkers, I. (2015). Extrinsic Muscle Forces Affect Ankle Loading Before and After Total Ankle Arthroplasty. *Clinical Orthopaedics and Related Research®*.

Neal, B. S., Griffiths, I. B., Dowling, G. J., Murley, G. S., Munteanu, S. E., Franettovich Smith, M. M., Collins, N. J., and Barton, C. J. (2014). Foot posture as a risk factor for lower limb overuse injury: a systematic review and meta-analysis. *Journal of Foot and Ankle Research*, 7(1):1–13.

Nguyen, T. C. (2005). *Mathematical modelling of the biomechanical properties of articular cartilage*. PhD thesis, University of Queensland, Australia.

Nigg, B. M. (2001). The role of impact forces and foot pronation: a new paradigm. *Clinical journal of sport medicine : official journal of the Canadian Academy of Sport Medicine*, 11(1):2–9.

Niu, W. X., Wang, L. J., Feng, T. N., Jiang, C. H., Fan, Y. B., and Zhang, M. (2013). Effects of bone Young's modulus on finite element analysis in the lateral ankle biomechanics. *Applied Bionics and Biomechanics*, 10:189–195.

Nix, S., Smith, M., and Vicenzino, B. (2010). Prevalence of hallux valgus in the general population: a systematic review and meta-analysis. *Journal of Foot and Ankle Research*, 3.

Novacheck, T. F. (1998). The biomechanics of running: Review Paper. *Gait and Posture*, 7:77–95.

Novitskaya, E., Chen, P.-Y., Hamed, E., Jun, L., Lubarda, V., Jasiuk, I., and Mckittrick, J. (2011). Recent advances on the measurement and calculation of the elastic moduli of cortical and trabecular bone: A review. *Theoretical and Applied Mechanics*, 38(3):209–297.

Noyes, F. R., DeLucas, J. L., and Torvik, P. J. (1974). Biomechanics of anterior cruciate ligament failure: an analysis of strain-rate sensitivity and mechanisms of failure in primates. *The Journal of bone and joint surgery. American volume*, 56(2):236–253.

Nunns, M., House, C., Fallow, J., Allsopp, A., and Dixon, S. (2013). Biomechanical characteristics of barefoot footstrike modalities. *Journal of biomechanics*, 46:2603–2610.

Oberkampf, W. L., Trucano, T. G., and Hirsch, C. (2002). Verification , Validation , and Predictive Capability in Computational Engineering and Physics. In *Foundations for Verification and Validation in the 21st Century Workshop*, pages 1–74.

Oreskes, N., Shrader-Frechette, K., and Belitz, K. (1994). Verification, Validation, and Confirmation of Numerical Models in the Earth Sciences. *Science*, 263(5147):641–646.

Pai, S. and Ledoux, W. R. (2010). The compressive mechanical properties of diabetic and non-diabetic plantar soft tissue. *Journal of biomechanics*, 43(9):1754–60.

Patil, K., Braak, L., and Huson, A. (1993a). A two dimensional model of a normal foot with cartilages and ligaments for stress analysis. *Innovation et technologie en biologie et médecine*, 14(2):152–162.

Patil, K., Braak, L., and Huson, A. (1996). Analysis of stresses in two-dimensional models of normal and neuropathic feet. *Medical and biological engineering and computing*, 34(4):280–284.

Patil, K. M., Braak, L. H., and Huson, A. (1993b). Stresses in simplified two dimensional model of a normal foot - A preliminary analysis. *Mechanics research communications*, 20(1):1–7.

Pavan, P. G., Pachera, P., Stecco, C., and Natali, a. N. (2014). Constitutive modeling of time-dependent response of human plantar aponeurosis. *Computational and mathematical methods in medicine*, 2014:1–8.

Pavan, P. G., Stecco, C., Darwish, S., Natali, a. N., and De Caro, R. (2011). Investigation of the mechanical properties of the plantar aponeurosis. *Surgical and radiologic anatomy*, 33(10):905–11.

Peña, E., Calvo, B., Martínez, M. a., and Doblaré, M. (2006). A three-dimensional finite element analysis of the combined behavior of ligaments and menisci in the healthy human knee joint. *Journal of biomechanics*, 39(9):1686–701.

Peña, E., Peña, J. a., and Doblaré, M. (2008). On modelling nonlinear viscoelastic effects in ligaments. *Journal of biomechanics*, 41(12):2659–66.

Peltonen, J., Cronin, N. J., Avela, J., and Finni, T. (2010). In vivo mechanical response of human Achilles tendon to a single bout of hopping exercise. *The Journal of experimental biology*, 213(Pt 8):1259–65.

Peltonen, J., Cronin, N. J., Stenroth, L., Finni, T., and Avela, J. (2012). Achilles tendon stiffness is unchanged one hour after a marathon. *The Journal of experimental biology*, 215(Pt 20):3665–71.

Petre, M., Erdemir, A., Panoskaltsis, V. P., Spirka, T. a., and Cavanagh, P. R. (2013). Optimization of nonlinear hyperelastic coefficients for foot tissues using a magnetic resonance imaging deformation experiment. *Journal of biomechanical engineering*, 135(6):61001–12.

Pohl, M. B., Hamill, J., and Davis, I. S. (2009). Biomechanical and Anatomic Factors Associated with a History of Plantar Fasciitis in Female Runners. *Clinical Journal of Sport Medicine*, 19(5).

Potthast, W., Lersch, C., Segesser, B., Koebke, J., and Brüggemann, G. P. (2008). Intraarticular pressure distribution in the talocrural joint is related to lower leg muscle forces. *Clinical Biomechanics*, 23(5):632–639.

Prendergast, P. J. (1997). Finite element models in tissue mechanics and orthopaedic implant design. *Clinical Biomechanics*, 12(6):343–366.

Provenzano, P., Lakes, R., Keenan, T., and Vanderby, Jr., R. (2001). Nonlinear Ligament Viscoelasticity. *Annals of Biomedical Engineering*, 29(10):908–914.

Qian, Z., Ren, L., Ding, Y., Hutchinson, J. R., and Ren, L. (2013). A dynamic finite element analysis of human foot complex in the sagittal plane during level walking. *PloS one*, 8(11):e79424.

Qian, Z., Ren, L., and Ren, L. (2010a). A Coupling Analysis of the Biomechanical Functions of Human Foot Complex during Locomotion. *Journal of Bionic Engineering*, 7:S150–S157.

Qian, Z., Ren, L., Ren, L.-q., and Boonpratatong, A. (2010b). A Three-Dimensional Finite Element Musculoskeletal Model of the Human Foot Complex. In *IFMBE Proceedings*, volume 31, pages 297–300.

Qiu, T.-X., Teo, E.-C., Yan, Y.-B., and Lei, W. (2011). Finite element modeling of a 3D coupled foot-boot model. *Medical engineering & physics*, 33(10):1228–33.

Ramos, a. and Simões, J. a. (2006). Tetrahedral versus hexahedral finite elements in numerical modelling of the proximal femur. *Medical engineering & physics*, 28(9):916–24.

Razak, A. H. A., Zayegh, A., Begg, R. K., and Wahab, Y. (2012). Foot plantar pressure measurement system: a review. *Sensors*, 12(7):9884–912.

Rho, J. Y., Ashman, R. B., and Turner, C. H. (1993). Young's modulus of trabecular and cortical bone material: Ultrasonic and microtensile measurements. *Journal of Biomechanics*, 26(2):111–119.

Richards, C. E., Magin, P. J., and Callister, R. (2009). Is your prescription of distance running shoes evidence-based? *British journal of sports medicine*, 43(3):159–162.

Rixe, J. a., Gallo, R. a., and Silvis, M. L. (2012). The barefoot debate: Can minimalist shoes reduce running-related injuries? *Current Sports Medicine Reports*, 11(3):160–165.

Roache, P. J. (1998). *Verification and Validation in Computational Science and Engineering*. Hermosa Publishers, Albuquerque.

Rome, K. (1998). Mechanical properties of the heel pad: current theory and review of the literature. *The Foot*, 8(4):179–185.

Rome, K., Webb, P., Unsworth, A., and Haslock, I. (2001). Heel pad stiffness in runners with plantar heel pain. *Clinical Biomechanics*, 16:901–905.

Rooney, B. D. and Derrick, T. R. (2013). Joint contact loading in forefoot and rearfoot strike patterns during running. *Journal of Biomechanics*, 46(13):2201–2206.

Root, M. L., Orien, W. P., and H., W. J. (1977). Normal and abnormal function of the foot. *Los Angeles: Clinical Biomechanics Corp.*, II.

Rothschild, C. E. (2012). Primitive Running: A Survey Analysis of Runners' Interest, Participation, and Implementation. *The Journal of Strength & Conditioning Research*, 26(8).

Salathe, E. and Arangio, G. (2002). A Biomechanical Model of the Foot: The Role of Muscles, Tendons, and Ligaments. *Journal of Biomechanical Engineering*, 124(3):281.

Saltzman, C. and Nawoczenski, D. (1995). Complexities of foot architecture as a base of support. *The Journal of Orthopaedic and Sports Physical Therapy*, 21(6):354–360.

Samaan, C. D., Rainbow, M. J., and Davis, I. S. (2014). Reduction in ground reaction force variables with instructed barefoot running. *Journal of Sport and Health Science*, 3(2):143–151.

Sarrafian, S. K. (1987). Functional Characteristics of the Foot and Plantar Aponeurosis under Tibiotalar Loading. *Foot & Ankle International*, 8(1):4–18.

Schechtman, H. and Bader, D. (1997). In vitro fatigue of human tendons. *Journal of biomechanics*, 30(8):829–835.

Schileo, E., Taddei, F., Cristofolini, L., and Viceconti, M. (2008). Subject-specific finite element models implementing a maximum principal strain criterion are able to estimate failure risk and fracture location on human femurs tested in vitro. *Journal of biomechanics*, 41(2):356–67.

Schreppers, G. J., Sauren, a. a., and Huson, A. (1990). A numerical model of the load transmission in the tibio-femoral contact area. *Proceedings of the Institution of Mechanical Engineers. Part H, Journal of engineering in medicine*, 204(1):53–9.

Sciumè, G., Boso, D. P., Gray, W. G., Cobelli, C., and Schrefler, B. a. (2014). A two-phase model of plantar tissue: a step toward prediction of diabetic foot ulceration. *International journal for numerical methods in biomedical engineering*, 30(11).

Sebastian, H., Datta, B., Maffulli, N., Neil, M., and Walsh, W. R. (2007). Mechanical properties of reconstructed achilles tendon with transfer of peroneus brevis or flexor hallucis longus tendon. *The Journal of foot and ankle surgery : official publication of the American College of Foot and Ankle Surgeons*, 46(6):424–8.

Segal, A., Rohr, E., Orendurff, M., Shofer, J., O'Brien, M., and Sangeorzan, B. (2004). The Effect of Walking Speed on Peak Plantar Pressure. *Foot & Ankle International*, 25(12):926–933.

Severinsen, K. and Andersen, H. (2007). Evaluation of atrophy of foot muscles in diabetic neuropathy – a comparative study of nerve conduction studies and

ultrasonography. *Clinical neurophysiology : official journal of the International Federation of Clinical Neurophysiology*, 118(10):2172–5.

Sharkey, N., Ferris, L., Smith, T., and Matthews, D. (1995). Strain and loading of the second metatarsal during heel-lift. *The Journal of Bone & Joint ...*, 77A(7):1050–57.

Sharkey, N. a. and Hamel, A. J. (1998). A dynamic cadaver model of the stance phase of gait: performance characteristics and kinetic validation. *Clinical biomechanics (Bristol, Avon)*, 13(6):420–433.

Shih, Y., Lin, K. L., and Shiang, T. Y. (2013). Is the foot striking pattern more important than barefoot or shod conditions in running? *Gait and Posture*, 38(3):490–494.

Shimazaki, K. and Takebe, K. (1981). Investigations on the origin of hallux valgus by electromyographic analysis. *Kobe J Med Sci*, 27(4):139–158.

Shin, J., Yue, N., and Untaroiu, C. D. (2012). A finite element model of the foot and ankle for automotive impact applications. *Annals of biomedical engineering*, 40(12):2519–31.

Siegler, S., Block, J., and Schneck, C. D. (1988). The Mechanical Characteristics of the Collateral Ligaments of the Human Ankle Joint. *Foot & Ankle International*, 8(5):234–242.

Sim-Fook, L. A. M. and Hodgson, A. R. (1958). A Comparison of Foot Forms Among the Non-Shoe and Shoe-Wearing Chinese Population. *The Journal of Bone and Joint Surgery (American)*, 40(5):1058–1062.

Smith, C. W., Young, I. S., and Kearney, J. N. (1996). Mechanical properties of tendons: changes with sterilization and preservation. *Journal of biomechanical engineering*, 118(1):56–61.

Sopher, R., Nixon, J., McGinnis, E., and Gefen, A. (2011). The influence of foot posture, support stiffness, heel pad loading and tissue mechanical properties on

biomechanical factors associated with a risk of heel ulceration. *Journal of the mechanical behavior of biomedical materials*, 4(4):572–82.

Souza, T. R., Mancini, M. C., Araújo, V. L., Carvalhais, V. O. C., Ocarino, J. M., Silva, P. L., and Fonseca, S. T. (2014). Clinical measures of hip and foot-ankle mechanics as predictors of rearfoot motion and posture. *Manual Therapy*, 19(5):379–385.

Souza, T. R., Pinto, R. Z., Trede, R. G., Kirkwood, R. N., and Fonseca, S. T. (2010). Temporal couplings between rearfoot-shank complex and hip joint during walking. *Clinical Biomechanics*, 25(7):745–748.

Spears, I., Miller-Young, J., Waters, M., and Rome, K. (2005). The effect of loading conditions on stress in the barefooted heel pad. *Medicine and science in sports and exercise*, 37(6):1030–1036.

Spears, I. R. and Miller-Young, J. E. (2006). The effect of heel-pad thickness and loading protocol on measured heel-pad stiffness and a standardized protocol for inter-subject comparability. *Clinical biomechanics (Bristol, Avon)*, 21(2):204–12.

Spears, I. R., Miller-Young, J. E., Sharma, J., Ker, R. F., and Smith, F. W. (2007). The potential influence of the heel counter on internal stress during static standing: a combined finite element and positional MRI investigation. *Journal of biomechanics*, 40(12):2774–80.

Spyrou, L. A. (2009). *Muscle and tendon tissues : constitutive modeling, numerical implementation and applications*. PhD thesis, University of Thessaly, Greece.

Spyrou, L. a. and Aravas, N. (2011). Muscle and Tendon Tissues: Constitutive Modeling and Computational Issues. *Journal of Applied Mechanics*, 78(4):041015.

Spyrou, L. A. and Aravas, N. (2012). Muscle-driven finite element simulation of human foot movements. *Computer Methods in Biomechanics and Biomedical Engineering*, 15(9):925–934.

Squadrone, R., Rodano, R., Hamill, J., and Preatoni, E. (2015). Acute effect of different minimalist shoes on foot strike pattern and kinematics in rearfoot strikers during running. *Journal of Sports Sciences*, 33(11):1–9.

Sun, P.-C., Shih, S.-L., Chen, Y.-L., Hsu, Y.-C., Yang, R.-C., and Chen, C.-S. (2012). Biomechanical analysis of foot with different foot arch heights: a finite element analysis. *Computer methods in biomechanics and biomedical engineering*, 15(6):563–9.

Tadepalli, S. C., Erdemir, A., and Cavanagh, P. R. (2011). Comparison of hexahedral and tetrahedral elements in finite element analysis of the foot and footwear. *Journal of biomechanics*, 44(12):2337–43.

Takahashi, A., Suzuki, J., and Takemura, H. (2012). Finite Element Modeling and Simulation of Human Gait with a Spontaneous Plantar Flexion. *International Journal of Aerospace and Lightweight Structures (IJALS)* -, 02(02):171–185.

Tanaka, Y., Takakura, Y., Kumai, T., Samoto, N., and Tamai, S. (1995). Radiographic analysis of hallux valgus. A two-dimensional coordinate system. *The Journal of Bone & Joint Surgery*, 77(2):205–213.

Tannous, R. E., Bandak, F. A., Toridis, T. G., and Eppinger, R. H. (1996). Three-Dimensional Finite Element Model of the Human Ankle: Development and Preliminary Application to Axial Impulsive Loading. *Proceedings: Stapp Car Crash Conference*, 40:219–236.

Tao, K., Ji, W.-T., Wang, D.-M., Wang, C.-T., and Wang, X. (2010). Relative contributions of plantar fascia and ligaments on the arch static stability: a finite element study. *Biomedizinische Technik. Biomedical engineering*, 55(5):265–71.

Tao, K., Wang, C.-T., Wang, D.-M., and Wang, X. (2005). Primary analysis of the first ray using a 3-dimension finite element foot model. In *Conference proceedings : ... Annual International Conference of the IEEE Engineering in Medicine and Biology Society. IEEE Engineering in Medicine and Biology Society. Conference*, volume 3, pages 2946–9, Shanghai, China.

Tao, K., Wang, D., Wang, C., Wang, X., Liu, A., Nester, C. J., and Howard, D. (2009). An In Vivo Experimental Validation of a Computational Model of Human Foot. *Journal of Bionic Engineering*, 6(4):387–397.

Telfer, S., Woodburn, J., and Cavanagh, P. R. (2015). Footwear embedded ultrasonography to determine plantar soft tissue properties for finite element simulations. *Footwear Science*, 7:9424280.

Thomas, V. J., Patil, K. M., and Radhakrishnan, S. (2004). Three-dimensional stress analysis for the mechanics of plantar ulcers in diabetic neuropathy. *Medical & biological engineering & computing*, 42(2):230–5.

Thordarson, D. B., Schmotzer, H., Chon, J., and Peters, J. (1995). Dynamic Support of the Human Longitudinal Arch - A Biomechanical Evaluation. *Clinical Orthopaedics and Related Research*, (316):165–172.

Tong, J., Lim, C., and Goh, O. (2003). Technique to study the biomechanical properties of the human calcaneal heel pad. *The Foot*, 13(2):83–91.

Trabelsi, N., Milgrom, C., and Yosibash, Z. (2014). Patient-specific FE analyses of metatarsal bones with inhomogeneous isotropic material properties. *Journal of the mechanical behavior of biomedical materials*, 29:177–89.

Urry, S. (1999). Plantar pressure-measurement sensors. *Measurement Science and Technology*, 10:16–32.

Van Buskirk, W. C. and Ashman, R. B. (1981). The elastic moduli of bone. In *Mech. Properties Bone ASME AMD*, pages 45,131.

Vanbrocklin, J. D. and Ellis, D. G. (1965). A Study of the Mechanical Behavior of Toe Extensor Tendons Under Applied Stress. *Archives of physical medicine and rehabilitation*, 46:369–373.

Verdejo, R. and Mills, N. J. (2004). Heel-shoe interactions and the durability of EVA foam running-shoe midsoles. *Journal of biomechanics*, 37(9):1379–86.

Vergari, C., Pourcelot, P., Holden, L., Ravary-Plumioën, B., Gerard, G., Laugier, P., Mitton, D., and Crevier-Denoix, N. (2011). True stress and Poisson's ratio of tendons during loading. *Journal of Biomechanics*, 44(4):719–724.

Vergari, C., Pourcelot, P., Holden, L., Ravary-Plumioën, B., Laugier, P., Mitton, D., and Crevier-Denoix, N. (2010). A linear laser scanner to measure cross-sectional shape and area of biological specimens during mechanical testing. *Journal of biomechanical engineering*, 132(10):105001.

Viceconti, M., Olsen, S., Nolte, L.-P., and Burton, K. (2005). Extracting clinically relevant data from finite element simulations. *Clinical biomechanics (Bristol, Avon)*, 20(5):451–4.

Viidik, A. and Lewin, T. (1966). Changes in tensile strength characteristics and histology of rabbit ligaments induced by different modes of postmortal storage. *Acta orthopaedica Scandinavica*, 37(2):141–55.

Viladot, A. (1973). Metatarsalgia due to biomechanical alterations of the forefoot. *The Orthopedic clinics of North America*, 4(1):165–78.

Wai-Chi Wong, D., Wang, Y., Zhang, M., and Kam-Lun Leung, A. (2015). Functional Restoration and Risk of Non-union of the First Metatarsocuneiform Arthrodesis for Hallux Valgus: A Finite Element Approach. *Journal of Biomechanics*.

Wakabayashi, I., Itoi, E., Sano, H., Shibuya, Y., Sashi, R., Minagawa, H., and Kobayashi, M. (2003). Mechanical environment of the supraspinatus tendon: a two-dimensional finite element model analysis. *Journal of Shoulder and Elbow Surgery*, 12(6):612–617.

Wang, J. H.-C. (2006). Mechanobiology of tendon. *Journal of biomechanics*, 39(9):1563–82.

Wang, Y., Li, Z., and Zhang, M. (2014a). Biomechanical study of tarsometatarsal joint fusion using finite element analysis. *Medical engineering & physics*, 36(11):1394–1400.

Wang, Z., Imai, K., Kido, M., Ikoma, K., and Hirai, S. (2014b). A finite element model of flatfoot (Pes Planus) for improving surgical plan. *Conference proceedings : ... Annual International Conference of the IEEE Engineering in Medicine and Biology Society. IEEE Engineering in Medicine and Biology Society. Annual Conference*, 2014:844–7.

Watanabe, K., Kitaoka, H. B., Fujii, T., Crevoisier, X., Berglund, L. J., Zhao, K. D., Kaufman, K. R., and An, K.-N. (2013). Posterior tibial tendon dysfunction and flatfoot: analysis with simulated walking. *Gait & posture*, 37(2):264–8.

Wearing, S. C., Smeathers, J. E., Urry, S. R., Hennig, E. M., and Hills, A. P. (2006). The pathomechanics of plantar fasciitis. *Sports Medicine*, 36(7):585–611.

Wei, F., Braman, J. E., Weaver, B. T., and Haut, R. C. (2011a). Determination of dynamic ankle ligament strains from a computational model driven by motion analysis based kinematic data. *Journal of biomechanics*, 44(15):2636–41.

Wei, F., Hunley, S. C., Powell, J. W., and Haut, R. C. (2011b). Development and validation of a computational model to study the effect of foot constraint on ankle injury due to external rotation. *Annals of biomedical engineering*, 39(2):756–65.

Weiss, J. a. and Gardiner, J. C. (2001). Computational modeling of ligament mechanics. *Critical reviews in biomedical engineering*, 29(3):303–71.

Williams, D., McClay, I., and Manal, K. (2000). Lower extremity mechanics in runners with a converted forefoot strike pattern. *Journal of applied Biomechanics*, 16:210–218.

Willing, R. T., Lalone, E. a., Shannon, H., Johnson, J. a., and King, G. J. W. (2013). Validation of a finite element model of the human elbow for determining cartilage contact mechanics. *Journal of biomechanics*, 46(10):1767–71.

Wirtz, D., Schiffers, N., and Pandorf, T. (2000). Critical evaluation of known bone material properties to realize anisotropic FE-simulation of the proximal femur. *Journal of Biomechanics*, 33:1325–1330.

Witana, C. P., Goonetilleke, R. S., Xiong, S., and Au, E. Y. L. (2009). Effects of surface characteristics on the plantar shape of feet and subjects' perceived sensations. *Applied ergonomics*, 40(2):267–79.

Wong, D. W.-C., Zhang, M., Yu, J., and Leung, A. K.-L. (2014). Biomechanics of first ray hypermobility: An investigation on joint force during walking using finite element analysis. *Medical engineering & physics*, 36(11):1388–1393.

Wren, T. a., Yerby, S. a., Beaupré, G. S., and Carter, D. R. (2001). Mechanical properties of the human achilles tendon. *Clinical Biomechanics*, 16(3):245–51.

Wright, D. G. and Rennels, D. C. (1964). A Study of the Elastic Properties of Plantar Fascia. *The Journal of bone and joint surgery. American volume*, 46:482–92.

Wu, K. K. (1987). Mitchell bunionectomy: an analysis of four hundred and thirty personal cases. *Journal of foot surgery*, 26:277–292.

Wu, L. (2007). Nonlinear finite element analysis for musculoskeletal biomechanics of medial and lateral plantar longitudinal arch of Virtual Chinese Human after plantar ligamentous structure failures. *Clinical Biomechanics*, 22(2):221–229.

Wu, L., Zhong, S., Zheng, R., Qu, J., Ding, Z., Tang, M., Wang, X., Hong, J., Zheng, X., and Wang, X. (2007). Clinical significance of musculoskeletal finite element model of the second and the fifth foot ray with metatarsal cavities and calcaneal sinus. *Surgical and radiologic anatomy : SRA*, 29(7):561–7.

Wunderlich, R. E. and Cavanagh, P. R. (2001). Gender differences in adult foot shape: implications for shoe design. *Medicine and science in sports and exercise*, 33(4):605–611.

Yamada, H. (1970). *Strength of Biological Materials*. The Williams &Wilkins Company, Baltimore.

Yong, J. R., Silder, A., and Delp, S. L. (2014). Differences in muscle activity between natural forefoot and rearfoot strikers during running. *Journal of Biomechanics*, 47(15):3593–3597.

Yu, J., Cheung, J. T.-M., Fan, Y., Zhang, Y., Leung, A. K.-L., and Zhang, M. (2008). Development of a finite element model of female foot for high-heeled shoe design. *Clinical Biomechanics*, 23, Supple(0):S31–S38.

Yu, J., Cheung, J. T.-M., Wong, D. W.-C., Cong, Y., and Zhang, M. (2013). Biomechanical simulation of high-heeled shoe donning and walking. *Journal of biomechanics*, 46(12):2067–74.

Zhang, R., Haibao, X., Zhang, S., Zeng, G., and Li, J. (2014). Finite Element Analysis in the Characteristics of Ostrich Foot Toenail Traveling on Sand. *Applied Mechanics and Materials*, 461:213–219.

Zhao, H., Ren, Y., Wu, Y.-N., Liu, S. Q., and Zhang, L.-Q. (2009). Ultrasonic evaluations of Achilles tendon mechanical properties poststroke. *Journal of applied physiology (Bethesda, Md. : 1985)*, 106(3):843–849.

Zhao, J. and Huangfu, X. (2012). The biomechanical and clinical application of using the anterior half of the peroneus longus tendon as an autograft source. *The American journal of sports medicine*, 40(3):662–71.

Zheng, Y. P., Choi, Y. K. C., Wong, K., and Mak, A. F. T. (1999). Indentation Assessment of Plantar Foot Tissue in Diabetic Patients. In *Serving Humanity, Advancing Technology*, volume 43, page 634.

In this Thesis, a complete detailed three-dimensional finite element model of the human foot is described to advance towards a more refined computational simulation which provides realistic and meaningful information for clinical practice. The research is structured by chapters where small steps towards the main objective are developed and the potential of these advances are applied to particular cases. These partial contributions in the area of the experimental testing are: the determination of a complete dataset of the mechanical properties of the balance foot tendons, the definition of a criteria to quantify the regions of the tendon stress-strain curve and the analysis of the compressive response of plantar soft tissue as function of the location. And, in the area of clinical biomechanics the contributions are: the investigation of a skeletal parameter as etiology factor of the hallux valgus, the tendon force sensitivity study of the five major stabilizer tendons, the quasi-static analysis of the midstance phase of walking and the study of the impact absorption mechanism of the foot during barefoot running at different strike patterns.

Universidad Zaragoza
1542
UNIVERSIDADE FEDERAL DE MINAS GERAIS
UFMG